Fiber-Optic SPR bioassays for detection of bacteria and viruses

Karel KNEZ

Jury:
Prof. dr. ir. P. Jacobs, chair
Prof. dr. ir. J. Lammertyn, promotor
Prof. dr. ir. A. Aertsen
Prof. dr. ir. L. Lagae
Prof. dr. T. Verbiest
Prof. dr. A. Gils
Dr. F. Frederix

Dissertation presented in partial fulfilment of the requirements for the degree of Doctor in Bioscience Engineering

November 2013

Uitgegeven in eigen beheer, Karel Knez, Oud-Heverlee

ISBN 978-90-8826-332-3
D/2013/11.109/69

Preface

Four years have passed since I started my PhD. During these years numerous people have helped and inspired me to successfully reach the end. Therefore I would like to thank some of the closest involved.

First of all, my gratitude goes out to my promotor Jeroen for giving me the chance to deploy my scientific creativity. As I started my PhD, the both of us did not now where this PhD would start let alone where it would end. I think we both would have signed immediately for this result.
Collaborations allowed me to apply the biosensing concepts to many biological relevant topics. Therefore I have to thank Nick, Wim and Prof. Deckmyn for bringing me in contact with their bacteriophages. Priscilla and Louise supported me with the bacterial work on *L. Pneumophila*. Thank you very much for all the support and ideas.

Another indispensable factor were my colleagues. All those great moments when we shared luck, joy, ideas that possibly could lead to a Nobel Prize, anger, and disappointment. Especially the desk buddies being Bert, Daan, Nicolas, Kris and Filip. But also all other colleagues among which Jeroen, Dinh, Federica, Elena, Karen, Steven, Phalghuni, Iulia, Evgeny, Jiadi … Some of you guys even have written articles with me, which was not always the easiest process, therefore Kris and Dragana, thank you for

engaging yourself fully in the brainstorming and writing of all my articles.
During these four years 3 thesis students helped me out, Deborah, Jeroen and Bjorn, you were great!
Daarnaast wil ik hier ook mijn vrienden bedanken, die altijd klaar stonden voor de meer serieuze zaken van deze wereld. Willem, Ruben, Dries[2], Jakke, Wouter, Evert, Anneleen, merci voor het feestgedruis!

Maar de meeste steun heb ik gedurende mijn gehele studie periode gekregen van mijn ouders. Beste ouders, dit doctoraat is in grote mate jullie verdienste, bedankt om altijd in mij te geloven. Daarnaast kan ik mijn broer Filip en zijn vriendin Astrid, natuurlijk niet vergeten. Filip, ik ben eindelijk klaar voor de vele vragen die je mij altijd al wou stellen over de '*neogenetic recombinator*'.
Dan rest er mij nog 1 iemand om te bedanken. Evelien, je was er bij mijn eerste succesjes bij, je was er in Mexico bij, maar je was er vooral toen we midden in de nacht de laatste verbeteringen aan dit doctoraat waren aan het aanbrengen. Je bent de beste, dat we nog vele successen samen mogen bereiken.

Karel

Abstract

In food quality, healthcare and biotechnology the presence of bacteria and viruses can have considerable consequences both willing and unwilling. Accurate identification and quantification of the bacteria and virusses is key in this context. Currently, there are only a limited number of truly fast and reliable methods available. Sensitive diagnostic tests could have a large impact on several crucial healthcare problems such as antibiotic resistance or could further improve food quality control. Therefore the aim of this disseration was to develop innovative, fast and highly sensitive bioassays on a compact fiber optic SPR biosensor platform (FO-SPR), that can be used to identify and quantify bacteria and viruses in a multiplexed way.

First, the FO-SPR sensor was used to study the affinity and binding kinetics of small viral particles. These so-called bacteriophages, can display peptide libraries with affinity for almost any target molecule. The target molecule, in this case eGFP, was immobilized on the FO-SPR biosensor surface and afterwards exposed to the bacteriophage library, allowing real-time monitoring of their interactions. Although the bioassay based on the detection of the entire viruses showed limited sensitivity, it proved to be a valuable tool for comparing binding kinetics of different viral particles, which expressed affinity peptides in different densities on the surface.

Following, keeping in mind the need for both detecting and identifying pathogens within the same test, a more universal bioassay was created using the genetic material of micro-organisms. The thermal denaturation of DNA complexes was measured using the FO-SPR technology. Here, the target DNA was used to form complexes between

two hybridization probes, each complementary to one half of the target molecule and immobilized both on the gold nanoparticles (Au NPs) and the sensor surface. Amplification with gold nanoparticle labels resulted in a clear signal, which superimposed the SPR signal caused by temperature changes during DNA melting analysis.

This assay was then validated by measuring genetic variability in two genes of *L. pneumophila,* which is a common human pathogen responsible for atypical pneumonia. Although the two selected genes are frequently used for the quantification of these bacteria, one of them is well documented as highly variable and therefore prone to introducing amplification bias in PCR based molecular diagnostic tests. The FO-SPR biosensor proved to be reliable for detecting mutations in those samples that previously displayed ambiguous qPCR quantification results. Moreover, it showed advantages as a high resolution and fast genetic screening tool that can compete with the current standard techniques for single point mutation (SNP) detection.

Next, the possibilities of the FO-SPR DNA biosensor were explored for target quantification. The FO-SPR biosensor was able to monitor in real-time quantitative ligation. The gradual increase in signal over multiple DNA ligation cycles was used to determine DNA concentrations in a broad dynamic range with a detection limit of 100 fM. Even more importantly, the obtained melting signal during each cycle of the ligation was sufficiently accurate to discriminate an SNP in the amplified target molecule.

Finally, the FO-SPR melting assay was applied to directly detect two bacterial species in one sample. To allow multiplex detection on FO-SPR, hybridization probes complementary to two regions of interest in different bacteria were immobilized on a single FO-SPR sensor and Au NPs. By choosing target regions with non-overlapping melting curves in each bacteria, the presence of one or both bacteria could easily be identified. Even DNA targets with SNPs could be differentiated from the wild type targets. This achievement is a significant step towards a FO-SPR biosensor for pathogenic bacteria. Further development of this platform concerning both the FO-SPR biosensor hardware and the implemented bioassays could make this technology an ideal candidate for the next generation point of care biosensors.

Samenvatting

Bacteriën en virussen spelen een cruciale rol in de voedselveiligheid, de gezondheidszorg en de biotechnologische industrie. Deze rol kan zowel gewenst als ongewenst zijn. In beide gevallen is het belangrijk om over snelle meettechnieken te beschikken om de virale en bacteriële aanwezigheid nauwkeurig te bepalen. Tot op heden bestaan er slechts een beperkt aantal snelle en betrouwbare methodes om dit te doen. Nochtans kunnen dergelijke testen een grote impact hebben op problemen in de gezondheidszorg zoals antibioticaresistentie, of een verdere vooruitgang betekenen in de context van voedselveiligheid. Het doel van deze doctoraatsthesis was om een innovatieve biosensor te onwikkelen die toelaat om snel en betrouwbaar virussen en bacteriën te identificeren en te detecteren. Hierbij wordt gebruikt gemaakt van een detectieplatform gebaseerd op optische vezeltechnologie en het concept van oppervlakte plasmon resonantie (FO-SPR).

In een eerste deel werd een FO-SPR biosensor ontwikkeld om de affiniteit en bindingskinetiek van kleine virale partikels te bepalen. Deze virale partikels, bacteriofagen genoemd, kunnen peptidebibliotheken tot expressie brengen met een affiniteit voor bijna eender welk molecule. Het doelmolecule, in dit geval eGFP werd op het FO-SPR biosensor oppervlak geïmmobiliseerd en vervolgens blootgesteld aan de bacteriofaagbibliotheek, wat toeliet om de interacties rechtstreeks op te volgen. Hoewel deze biologische test, gebasseerd op detectie van volledige virale partikels, een beperkte gevoeligheid vertoonde, was het toch een waardevol hulpmiddel voor het vergelijken van bindingskinetieken van verschillende virale partikels die

affiniteitspeptiden tot expressie brengen met een verschillende densiteit.

Daaropvolgend, in een tweede deel, werd een meer universele biologische test ontwikkeld voor de gelijktijdige identificatie en kwantificering van bacteriën gebaseerd op de detectie van het genetische materiaal van de micro-organismen. De thermische denaturatie van DNA complexen werd gemeten met behulp van de FO-SPR technologie. Hierbij werd het doelwit DNA gebruikt om complexen te vormen tussen twee hybridizatieprobes, die elk complementair zijn aan een helft van het doelwitmolecule en geïmmobiliseerd werden op de gouden nanopartikels en op het sensoroppervlak. Singaalversterking met gouden nanopartikels resulteerde in een duidelijk signaal, dat sterker was dan het signaal veroorzaakt door de temperatuursverandering die gepaard gaat met het smelten van het DNA.

In een derde hoofdstuk werd deze test gevalideerd via het meten van de genetische variabiliteit in twee genen van *L. pneumophilia*, een vaak voorkomende humane pathogeen die verantwoordelijk is voor atypische longontstekingen. Hoewel de geselecteerde genen vaak gebruikt worden voor kwantificering van deze bacterie, is één van beide toch zeer variabel en dus voorbestemd om amplificatiefouten te veroorzaken in PCR gebaseerde moleculaire diagnostische testen. Er werd hier aangetoond dat de FO-SPR sensor een snel en betrouwbaar alternatief biedt voor de huidige standaardtechnieken met betrekking tot de detectie van puntmutaties in DNA.

Vervolgens werden de mogelijkheden van de FO-SPR DNA biosensor onderzocht voor wat betreft kwantificering van een doelwit. De FO-SPR biosensor was in staat om kwantitatieve ligatie rechstreeks in kaart te brengen. De graduele toename van het signaal na verschillende ligatie-cycli werd gebruikt om de DNA concentratie te bepalen met een breed dynamisch bereik en een detectielimiet van 100 fM. Bovendien was het smeltsignaal tijdens elke cyclus voldoende nauwkeurig om een puntmutatie in het doelmolecule te onderscheiden.

Tot slot werd de FO-SPR smelttest toegepast op 2 verschillende bacteriën in 1 staal. Om meervoudige detectie te realiseren, werden hybridizatieprobes, die complementair zijn aan twee geschikte regio's

van het DNA van de verschillende bacteriën, geïmmobiliseerd op één sensor en op Au NP's. Door doelregio's te kiezen met niet-overlappende smeltcurves voor elke bacterie, kon de aanwezigheid van één of beide bacteriën gemakkelijk bepaald worden. Zelfs DNA doelwitten met puntmutaties kunnen gemakkelijk onderscheiden worden van het oorspronkelijke doelwit. Deze verwezenlijking is een belangrijke stap in de richting van een FO-SPR biosensor voor pathogene bacteriën.

In dit werk werd het potentieel van de FO-SPR technologie voor de identificatie en kwantificering van bacteriën en virussen succesvol aangetoond. Een verdere ontwikkeling van dit diagnostisch meetplatform, zowel wat betreft de hardware als de geïmplementeerde biologische tests, is nodig om de stap naar de diagnostische markt te kunnen zetten.

List of abbreviations

a.u.	arbitrary units
AFM	atomic force microscope
aM	attomolar
Au NP	gold nanoparticles
BHQ	black hole quencher
bp	basepair
BSA	bovine serum albumine
CCD	charge coupled device
CCP	cationic conjugated polymer
cDNA	complementary DNA
CED	consumer electronic devices
CEL1	celery juice extract 1
DNA	deoxyribonucleic acid
DTT	dithiothreitol
EDC	1-ethyl-3-(3-dimethylaminopropyl) carbodiimide
eGFP	enhanced green fluorescent protein
ELISA	enzyme linked immunosorbent assay
EW	evanescent wave
FAM	carboxyfluorescein
fM	femtomolar
FO-SPR	fiber optic surface plasmon resonance
FRET	fluorescence resonance energy transfer
HRM	high resolution melting

IgG	immunoglobulin G
ITO	indium thin oxide
kD	dissociation constant
LCR	ligation chain reaction
LOC	lab-on-a-chip
LOD	limit of detection
LRSP	long rang surface plasmon resonance
MAP	*Mycobacterium avium* subspecies *paratuberculosis*
MB	molecular beacon
MES	2(N-morpholino)ethanesulfonic acid
min	minute
mM	millimolar
MM	mismatch
NA	numerical aperture
NaCl	sodium chloride
NaOH	sodium hydroxide
NHS	N-hydroxysuccinimide
nm	nanometer
nM	nanomolar
n	refractive index
NTC	no template control
OD	optical density
PBS	phosphate buffered saline
PCR	polymerase chain reaction
PEG	polyethylene glycol
PEO	polyethylene oxide
pM	picomolar
POC	point-of-care
qPCR	quantitative PCR
RCA	rolling circle amplification
RD	regions of difference
RIU	refractive index units

RNA	ribonucleic acid
SAM	self-assembling-monolayer
SDS	sodium dodecyl sulphate
SERS	surface enhanced raman spectroscopy
SNA	spherical nucleic acid
SNP	single nucleotide polymorphism
SPR	surface plasmon resonance
SPR_i	surface plasmon resonance imaging
SPW	surface plasmon wave
ssDNA	single stranded DNA
T	temperature
Taq	thermus aquaticus
T_m	melting temperature
TTH	thermus thermuphilus
VGA	video graphics array
WT	wild type
YFP	yellow fluorescent protein
µM	micromolar

Table of Contents

Chapter 1

General introduction

The discovery of bacteria and viruses in the 17th and late 19th century, respectively, has been ever since a catalyst for the evolution of modern-day medicine, food production, biotechnology and many other fields. However, the detection of these organisms has never been easy. Since the introduction of bacterial colony identification, only limited number of truly fast and reliable methods for bacterial detection have been developed. Nonetheless, there is a great need for such tools, mainly in medicine, to prevent overuse of antibiotics, but also for further improvement of food quality control or for environmental monitoring.

The aim of this chapter is to give the reader an introduction to the different aspects, used in the framework of this thesis, for developing *in vitro* diagnostic tools for detecting bacteria and viruses. First, a concise overview of diagnostic applications and their specific needs is provided, then the field of biosensors and their current strengths and limitations are discussed, followed by a more detailed introduction into a specific biosensing technique for DNA, DNA melting analysis. Next the Surface Plasmon Resonance (SPR) technology is introduced and its fiber-optic implementation which will be used to create a new biosensing platform in combination with DNA melting analysis. Finally a brief overview of

gold nanoparticle labels and surface functionalization strategies is given. To conclude, in the last section of this chapter, a clear scheme of the objectives and the outline of the complete manuscript is given.

1.1 Diagnostics

'Medical diagnosis' is defined according to the Longman English dictionary as: '*the process of discovering exactly what is wrong with someone or something, by examining them closely'*. However, merely examining is in most cases not enough to identify a medical problem. Therefore, various diagnostic tests have been and are still being developed as a crucial tool for caretakers to make a correct diagnosis. Diagnostic tests exist in all sorts and range - from a simple predictor test for pregnancy to complex histopathology analysis of tissue to confirm presence of cancer during an actual operation. Unfortunately, quick and easy diagnostic tests are not available for every disease, especially lacking for confirming presence or absence of viral and bacterial pathogens. At the moment, their occurrence can only be measured in a specialized clinical laboratory environment as a result of rather complex assays, requiring days to weeks for positive identification. Therefore, practitioners often start with a non-specific treatment using broad-spectrum antibiotic agents, which are active against multiple bacteria. Although in the beginning this strategy was proven to be successful for patients treatment, it has boosted the antibiotic resistance in bacteria leading to the appearance of so called 'super' bacteria, which can hardly be treated with any of the existing antibiotics[1]. Fast diagnostic tests, applicable at the POC could thereby become a valuable tool in the prevention of a further aggravation of antibiotic resistance.[2]

In recent years, so called POC diagnostics have seen a rapid evolution, mainly spurred by a new approach in treating patients, known as *personalized medicine*. The idea originated from findings that substantially different genetic makeup exists in a patient population, requiring thus different treatments for patients with similar disease patterns[3]. This discovery made both medical research and pharmaceutical industry change their approach in medical treatments towards a tailor-made therapy for each patient. Famous examples of personalized medicine are mostly found in oncology. For instance,

although only 20 percent of breast cancer cases occur due to the mutations in BRCA gene, these mutations raise a hereditary risk for breast cancer to almost 80 percent, justifying a mastectomy in women carrying these mutations as a preventive step[4]. Another example is overexpression of the HER-2 receptor occurring in 30 percent of breast cancer patients, which are recognized as susceptible to the treatment with drug Herceptin[5,6]. As a result, personalized medicine has boosted developments in molecular diagnostics towards POC sensors, which are not exclusively applicable for cancer screening but can also be applied in other medical fields such as antibiotic susceptibility in the case of a bacterial infection[7]. When bacterial resistance genes are found in a patient sample, the antibiotic treatment can be adopted to circumvent resistance, leading to the improvement of patient outcome[8].

Although personalized medicine has a great potential to improve present day patients treatments, only a handful of personalized medicine tests have been adopted in the clinic so far. Several factors are limiting the introduction of this new approach to medicine:

- Scientific challenges – unknown markers, poor understanding of molecular mechanisms
- Economic challenges – poor incentives
- Operational issues – privacy concerns, data management.

From these three challenges, the economic challenge is considered to be the most troublesome for POC tests, as personalized medicine can be a great creator of cost[8,9]. However, recently pharmaceutical companies started to use diagnostics as a screening/monitoring tool in the development process of new drugs. This new type of diagnostics is called *companion diagnostics*, as the diagnostic test and biomarker are used as an aid, not only during drug development but also in the follow up phase to prove drug efficacy and to optimize drug dosage for individual patients[10]. Furthermore, these companion diagnostics could cut costs in drug development by reducing clinical trial sizes and decrease the time to market. Not every companion diagnostics is economically or technologically achievable[9]. This is dependent on the disease area, as can be seen in Figure 1.1: oncology and anti-infectives are fields, which are interesting targets for development of companion diagnostics, as they are both scientifically and economically attractive.

Therefore, taking into account the impact fast diagnostic tests could have in solving the problem of multiresistant 'super' bacteria by (1) steering the administration of existing antibiotics and (2) reducing the cost of clinical trials for the development of new antibiotics, the focus of this manuscript is on developing fast molecular detection assays for bacteria and viruses that could be integrated in those diagnostic tests. The resulting diagnostic test will not only be of value for medical diagnostics but could also be used as a monitoring tool for food quality both at production facility and along the distribution chain. Here the convenience and speed of a POC test could drastically improve the response time in case of contamination both reducing the losses in production and preventing possible safety hazards[11]. Finally in environmental monitoring, similar tools could improve follow up of changes in environmental bacterial and viral populations. Especially in the light of monitoring the effect of climate changes but also to asses the impact of increasing amounts of antibiotic residues in the environment, new sensitive molecular tools are in urgent need[12-15].

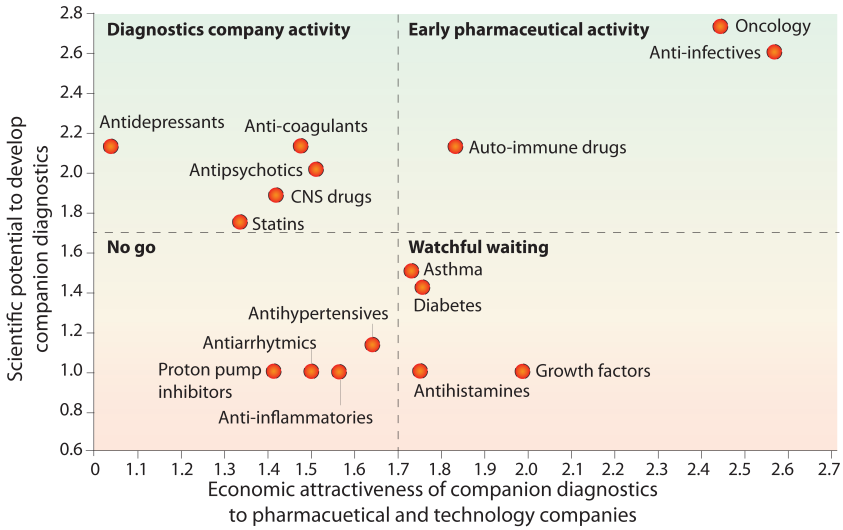

Figure 1.1: Scientific potential and economic attractiveness of companion diagnostics across different fields in medicine. The scaling on the x and y axis represent respectively the scientific potential and economic attractiveness of the development of companion diagnostics in various therapeutic areas and are based on both qualitative factors (such as expert interviews) and quantitative factors (such as data on price premiums for drugs launched in the same therapeutic class). (According to Davis et al.[9])

1.2 Biosensors

Biosensors are a particular class of analytical instruments used in diagnostics, which are distinguished by the incorporation of a biological sensing element[16]. As a result, every biosensor is composed of two major elements, a biorecognition and a transducing element[17]. Biorecognition elements are responsible for the specific recognition of the target analyte and mainly consist of antibodies and DNA, although in recent years new types have been developed, such as aptamers, affinity peptides, molecular imprinted polymers, antibody mimetics, etc.[16] This specific sensing of the biorecognition element is further translated into a measurable signal by transducers, which can be divided in four main categories according to the generated signal: electrochemical, optical, calorimetric and acoustic transducers[18]. Electrochemical and optical transducers are by far the most popular biosensor transducers, with electrochemical biosensors being mostly applied in commercial devices due to their ease of use, miniaturization possibilities and cost of production[19].

Development of biosensors achieved a breakthrough in the 60's with the creation of the glucose sensor. This sensor was a big step forward in the treatment of diabetes, resulting in an increased lifetime and improved quality of life for diabetes patients[20]. Even today, the glucose sensor remains the most sold biosensor[16]. However, despite this, the classic biosensor blueprint seen in the glucose sensor[21] (shown in Figure 1.2A) is no longer applicable for the next generation biosensors, such as the bacterial and viral POC tests. These biosensors require the integration of complex molecular assays and sample preparation steps (Figure 1.2B), with the latter emerging as one of the most crucial aspects of the assay. The ideal sample preparation allows using the assay on multiple sample matrices (e.g., sputum, tissue, faeces, blood) and prevents the dissemination of sample matrix inhibitors to downstream DNA analysis[22]. Another added complexity lies in the actual transducer, as molecular diagnostics support detection of multiple targets in one sample. Finally, management of the obtained test results and their distribution introduces new concepts, such as remote patient monitoring, which can further increase patient quality of life[23].

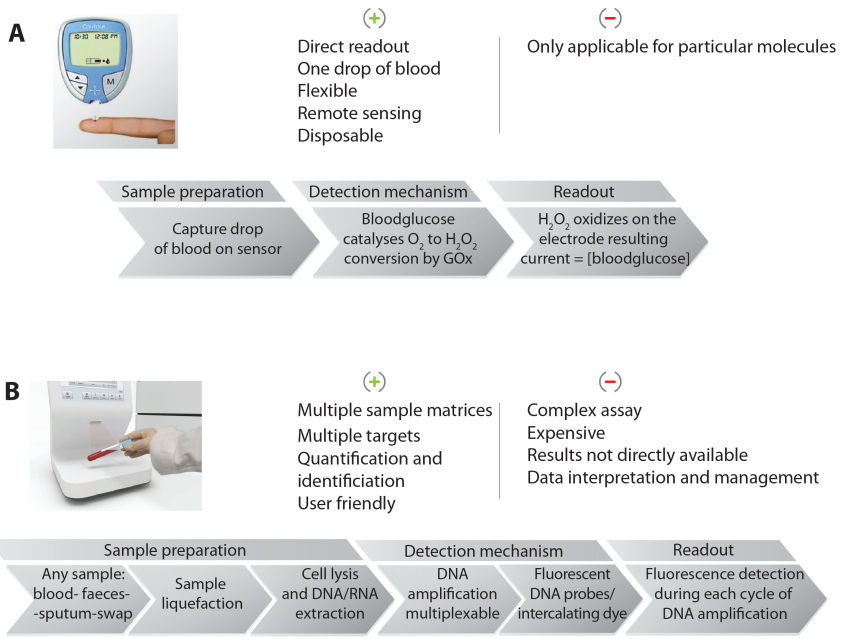

Figure 1.2: A) Overview of the working principal of a classic glucose sensor, from sample to result. (Bayer glucose biosensor) B) Overview of the working principal of a next generation POC biosensor, from sample to result. (Picture: Biocartis POC biosensor)

Sample preparation methods have been succesfully developed, which allow automated extraction of DNA from complex sample matrices ranging from sputum, to blood, to even stool. These techniques have been integrated in POC biosensors which are currently being commercialized[24]. The technologies are often based on lab-on-a-chip (LOC) systems that either used micro-fabricated structures, silica membranes, magenetic nano- or microparticles or a combination thereof. These techniques have enabled extraction of high quality DNA and other biomarkers that can be used for downstream analysis[22]. Nonetheless further improvements in sample prep for POC biosensors are necessary, especially regarding the cost and complexity of these systems, another essential problem preventing next generation POC biosensors from making molecular diagnostics available outside specialized labs, lies in the classic principals used for target detection, such as fluorescence[7,8,25]. However, new technologies are being exploited to enable development of biosensors with potentially lower

costs, short time to result and minimal interpretation whilst still reaching the required detection limits[8]. One of these technologies with great potential to fulfill the mentioned criteria is DNA melting analysis.

1.3 DNA melting

DNA is considered to be the blueprint of life and is therefore a very interesting target molecule in diagnostics, particularly for the detection of bacteria and viruses where a short sequence of DNA carries much more information on the type of these organisms than any protein[26]. Moreover, numerous genes and mutations have been related to various human diseases. Mutations can either cause a predisposition for the particular disease or be the direct cause of the disease. In this regard mutations in both coding and regulating genes have been connected to most known diseases ranging from different types of cancer[27] to neurodegenerative diseases[28,29], autoimmune diseases[30] and many more[31]. In viruses mutations are even more omnipresent as these unicellular organisms lack some of the specialized mutation prevention systems unique to eukaryote and prokaryote organisms[32]. These organisms use mutations to acquire new traits, leading in some cases to new viral strains. Mechanisms linked to virulence[33] such as drug resistance and zoogenesis are acquired by genetic alterations[34] such as mutations. Although in bacteria antibiotic resistance might be acquired by genetic mutations, a major part of antibiotic resistance is spread by horizontal gene transfer between bacteria[35].

Excellent tools for researchers such as sequencing have allowed scientists to gain valuable insights in the mechanisms underlying bacterial and viral evolution. Especially a recent evolution towards 'deep sequencing' where the number of sequencing reads is increased to reduce the number of sequencing errors has enabled the discovery of rare mutations, which allow a better understanding of bacterial and viral evolutionary processes[36]. However currently these technologies are to complex and costley to be applied to routine clinical care or food safety.

The presence of a mutation in a DNA double helix , can be detected using different methods. One of the most popular methods utilizes hybridization probes either on microarrays[37,38] or with *in situ* fluorescence monitoring[39]. These hybridization probes are complementary DNA sequences, carrying a fluorescent label, a radiolabel, an electrochemical label or even a nanoparticle, which are used to generate a signal. In the case of a perfect match between the target strand and the labeled probe, hybridization efficiency is maximal. The presence of a mutation lowers the hybridization efficiency, which can be detected using different transducers. However, this strategy is only useful in the case of very short oligonucleotides as the impact of single mutation on hybridization efficiency diminishes with increasing length of DNA targets[40]. This is demonstrated by plotting the hybridization yield (χ), which denotes the fraction of the limiting reagent (DNA target) that exists in duplex form (with a DNA hybridization probe), against free energy under stqndqrd conditions ($\Delta G'$), which reveals that the binding of the mutated target and the wild type target to the hybridization probe are both thermodynamically favorable and practically indistinguishable at room temperature (Figure 1.3). However, when the assay is performed at the melting temperature, the hybridization yield of the wild type DNA is reduced with 50% while the mutated DNA hybridisation yield is almost 0. Thus, in order to enable a better mutation discrimination, particularly in longer DNA targets, one can study the dissociation of the DNA duplex rather than the association[41].

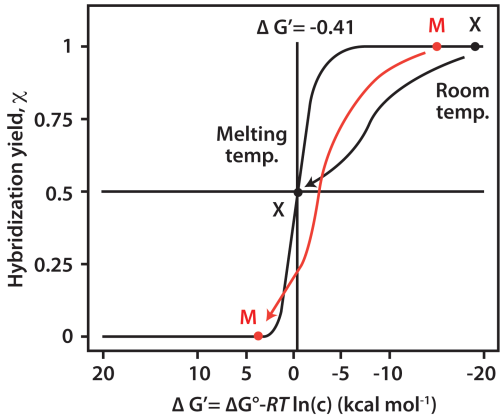

Figure 1.3: Hybridization yield (x-axis) plotted against the free energy at standard environmental conditions being a temperature of 20 °C and an absolute pressure of 101.325 kPa (y-axis) where c is the concentration of the limiting species for a standard bimolecular hybridization reaction. At room temperature, the binding of both the correct target (black dot X) and the mutation-bearing target (red dot M) are thermodynamically favorable and practically indistinguishable. In contrast, at the melting temperature, the hybridization yield of the correct target is 50%, and much lower for the mutated target (according to Zhang *et al.*[42])

This method is called DNA melting analysis. The melting temperature (T_m) of the DNA double helix is defined as, the temperature at which 50% of the probe–target hybrids have dissociated. Practical implementations of DNA melting analysis use often fluorescence to monitor hybridization yield as a function of temperature (T). The T_m can in this case be determined from the inflection point in a plot of the fluorescence intensity (F) and T, or from the peak value of a curve with the derivative of fluorescence and temperature (-dF/dT) plotted as a function of T[43].

Although DNA melting can be achieved with extreme values of pH, increasing dielectric constant, exposure to amides, urea and other solvents, or by applying external force, the focus in this thesis will be on thermal denaturation. During thermal denaturation the temperature is gradually increased leading to the break up of hydrogen bonded base pairs between complementary strands, resulting in an opening up and unwinding of the DNA double strand. The opening of the base pairs occurs in a cooperative manner causing the strands to completely separate. When DNA strands longer than 130bp are analyzed, melting

can occur in different steps, resulting in multiple melting transitions along one melting curve.

During melting analysis, the fraction of DNA in the double stranded state (dsDNA) is determined, which is a function of 4 variables: enthalpy (ΔH°), entropy (ΔS°), temperature, and concentration of the ssDNA species, where enthalpy is the total energy in a thermodynamic system in a particular volume and under a particular pressure, whereas entropy is the progression of the thermodynamic system towards thermodynamic equilibrium. Theoretically, the melting behavior of an oligonucleotide can be expressed with the equilibrium state, which is dependent on the total free energy in the system. The total free energy is a measure for the relative stability of the DNA duplex. Research has been conducted to characterize thermodynamically all 10 possible nearest neighbor interactions (being AA, AT, AC,…) in a Watson and Crick DNA double helix[44,45]. When the enthalpy and entropy obtained in these experiments is used to calculate the free energy using the standard thermodynamic relationship (Equation 1), it is observed that the base sequence rather than base composition determines the free energy and thus relative stabilities. In short, this means that even if two sequences consist of identical nucleotides, but the order of the nucleotides is different between them, their melting temperatures is different as well. This finding forms the basis of all melting analyses.

$$\Delta G^\circ = \Delta H^\circ - T\Delta S^\circ \quad (1)$$

The introduction of the intercalating dye, a molecule with high affinity for double stranded DNA, increased the application of DNA melting in DNA analysis[46]. Initially, the technology was used to evaluate the presence of the correct amplification product after DNA amplification with Polymerase Chain Reaction (PCR). The PCR is an enzyme-based reaction where DNA is amplified with the help of a thermophilic enzyme, which elongates short strands of DNA (primers) complementary to a target region in the DNA (Figure 1.4A). However, the first generation of intercalating dyes was inhibiting the Taq enzyme and thus the PCR reaction, unless used at relative low concentrations. On the other hand, lower concentrations of intercalating dyes were reducing the sensitivity, because the dye was rebinding during the dissociation process, resulting in a very broad melting signal (Figure

1.4B). A new generation of intercalating dyes, named saturating dyes, resolved this problem and introduced high resolution melting (HRM)[47]. This post PCR technique enables fast and accurate DNA T_m determination allowing single nucleotide polymorphisms (SNP) detection even in DNA targets of more than 100bp.

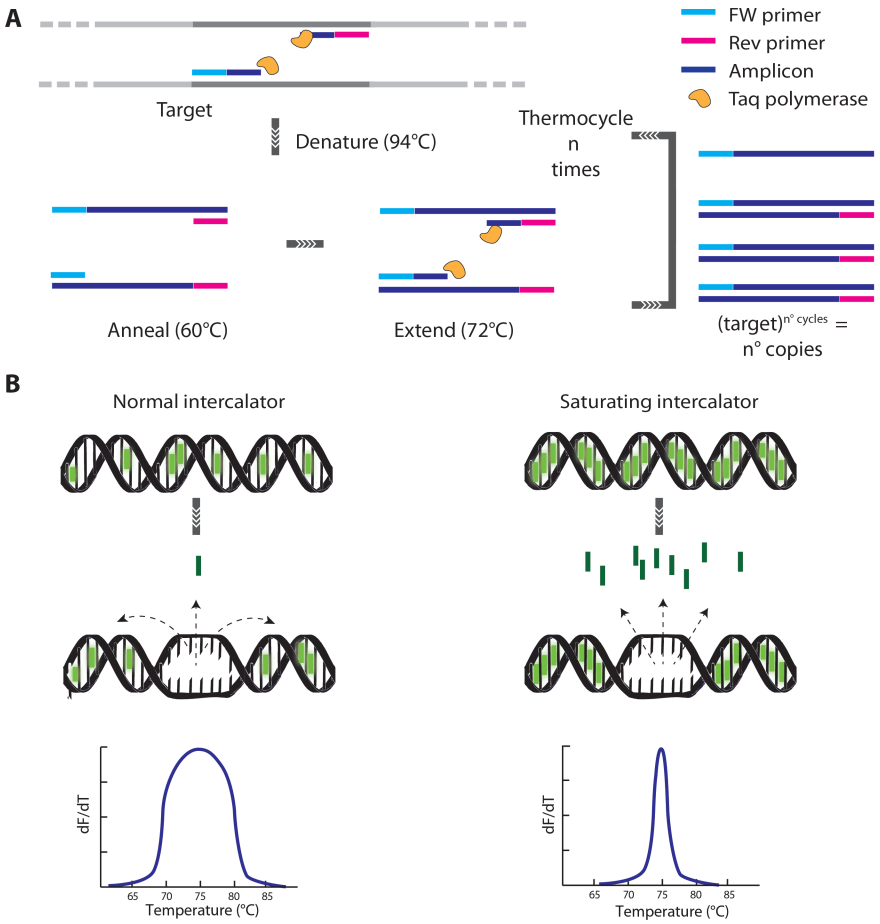

Figure 1.4: A) The basic principles of PCR, where a target region is amplified using a thermophilic polymerase enzyme (Taq) that is used to elongate primers complementary to the target (forward primer) and its amplicon (reverse primer). The different temperatures, necessary to denature the amplicon from the target and to allow the primers to bind (annealing temperature) are cycled in a repetitive manner, allowing exponential amplification of the target DNA. B) Working mechanism of an intercalating dye (green square), where the dye emits a fluorescent signal upon binding with double stranded DNA. Standard intercalating dyes, which cannot be used under saturating conditions, result in 'dye

displacement' upon melting, reducing the resolution of the melting analysis in comparison with saturating dyes.

Nonetheless, the method still possesses some downsides, as it requires optimization to detect particular mutations such as base pair neutral mutations[48], and can only detect a limited number of targets at the same time. Therefore, we aim to improve the sensitivity of DNA melting by combining it with a real-time biosensor (fiber optic surface plasmon resonance, FO-SPR) and gold nanoparticle labels (Au NP).

1.4 Surface plasmon resonance

1.4.1 General concept

While a detailed description of the physical principles behind the Surface Plasmon Resonance phenomenon is outside the scope of this PhD thesis and can be found in excellent review papers and textbooks[49-51], a brief overview of the general concepts is given to allow a better insight in the following chapters.

Surface plasmon resonance (SPR) is a type of biosensor transducer that provides label-free and real-time monitoring of biomolecular interactions. Therefore biomolecules, such as for example an antibody, are immobilized on the SPR sensor surface, which is than exposed to the analyte containing sample. The biomolecular interactions will lead to a local upconcentration of the analyte on the sensor surface and thus a change of refractive index which can be measured by the SPR biosensor.

The SPR biosensor working mechanism is based on the excitation of an electromagnetic wave at the sensor surface, which is sensitive to refractive index changes in the bulk medium[52] (such as a sample matrix). These electromagnetic waves can be excited in a metal when exposed to a light beam. At the atomic level metals are built of positively charged nuclei surrounded by a cloud of electrons. When exposed to the the light beam, the electrons start to move along this external electromagnetic field of the light, increasing their distance from the positive nuclei until counteracted by an external electromagnetic field generated by the charge difference between nucleus and electrons. At this point the electrons start moving back to the nuclei, creating oscilllations of the electron density at the metal surface, also called

plasmons. The light beam used to excite plasmons needs to have the correct frequency (wavelength) in order to generate plasmons at the metal surface. This optimal plasmon frequency differs from one metal to another, below this frequency, light is reflected, whereas above this frequency it is transmitted. Gold and silver are two of the few metals with a plasma frequency in the visible range, with silver having slightly better optical properties for the excitation of SPR. However since gold is inert, it is more suited for biosensing and therefore more often found in SPR biosensors.

The plasmons, occuring in the metal, will also be present at the interface of the metal with a dielectric, such as for example a sample matrix. These surface plasmon waves are evanescent waves (EW), meaning that the waves decay exponentially as a function of the distance from the interface at which they were formed. The size of the decaying SPR wave is related to its energy, wich depends on the wavelength at which it was excited. Therefore the most sensitive SPR region is determined as one third of the excitation wavelength (in general the penetration depth is 200-300 nm). To generate an SPR signal, light not only needs to have the right energy (wavelength), the photons of the light also need to be coupled to the surface plasmons. To achieve this energy coupling, the light needs the right momentum.

The most frequently applied method to increase the momentum of the photons is by passing the light through a prism (Figure 1.5). The light will undergo a change of speed and dispersion while entering the prism (because the permittivity of the prism, ε_P, is higher than the permittivity of the air, ε_a). This allows the photons to fulfill the requirements for total internal reflection (Snells law) resulting in an evanescent wave at the interface. Depending on the SPR configuration chosen, the evanescent wave can make its way through the sample dielectricum and couple with the plasmon wave on the metal-dielectricum interface to generate a surface plasmon wave (SPW) (Otto configuration[53], Figure 1.5A). The Otto configuration has some drawbacks, mainly due to the fact that the prism and gold layer are being separated by the sample. The evanescent wave has to pass through the sample before reaching the metal surface, leading to a low coupling efficiency of the evanescent wave with the gold and thus to a lower efficiency in general. Alternatively, the metal can be coated

directly on the prism (Kretschmann configuration[54], Figure 1.5B). Here, the evanescent wave penetrates through the metal film, creating a plasmonic propagating electron wave on the outside of the metal layer. This configuration is predominantly used for SPR signal excitation in many commercial SPR devices.

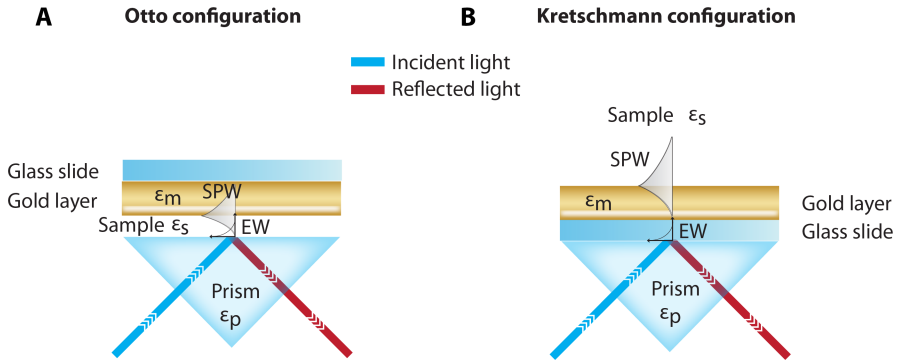

Figure 1.5: A) Scheme showing the Otto and B) the Kretschmann SPR configuration. In the Otto configuration, prism and gold layer are divided by the sample. In the Kretschmann configuration the prism is directly coupled to the gold layer, allowing plasmon resonance wave (SPW) excitation at the opposite side of the gold layer. (EW: evanescent wave, ε_P: permittivity prism, ε_S: permittivity sample, ε_m permittivity gold)

The resonance frequency of the evanescent surface plasmon wave is influenced by the composition of the medium close to the metal surface. SPR biosensors can interrogate changes in the resonance frequency using two different approaches. The first approach is based on Snells law, stating that light of a particular frequency will excite an evanescent wave when it strikes the refractive boundary with an angle of incidence above the critical angle. This approach is called angle resolved SPR and utilizes a laser at a fixed wavelength or another type of monochromatic light source (having a single frequency) to irradiate the sensor surface. Light with an angle of incidence below or above the critical angle will not be adsorbed by the metal, but instead, is reflected and captured with a diode array detector fixed on a motorized goniometer. The SPR wave is visible as a dip in light intensity at a particular reflection angle. Changes in the local refractive index at the sensor surface will slightly change the critical angle, necesseray to excite the SPW, therefore the detector on the goniometer continually measures the intensity of the reflected light at different angles and thus can detect any change in

refractive index. This angle interrogation is very accurate and can register changes up to 0.001°.

The second approach allows the frequency (wavelength) of the light to vary while the angle of incidence is kept constant, only lightwaves with the right frequency for the set critical angle will excite SPWs[55]. For this SPR configuration a polychromatic light source is used in combination with a spectrophotometer, the wavelength at which resonance occurs will have a lower intensity. In the same way as angle interrogation, the wavelength at which the SPR is excited changes when molecules are bound to the metal surface, which enables real-time monitoring of biomolecular interactions (Figure 1.6). This approach does not reach the same sensitivity as angle interrogation, because a spectrophotometer does not allow the same level of accuracy as a goniometer[56].

In Figure 1.6A a typical maesurement of a wavelength interrogation SPR device is shown. As described in the previous paragraph, the spectrophotometer registers the SPR phenomena as a decrease in signal intensity at a particular wavelength, when the local refrative index (n_s) at the sensor surface changes ($n_s+\Delta n_s$), the wavelength at which the intensity dip is found will shift. By monitoring continuously the local refractive index at the sensor surface, biomolecular interactions can be monitored over time. This principal is displayed in Figure 1.6B, where different phases in a bioreceptor analyte interaction tracked with SPR are plotted. Such a plot is called a sensorgram.

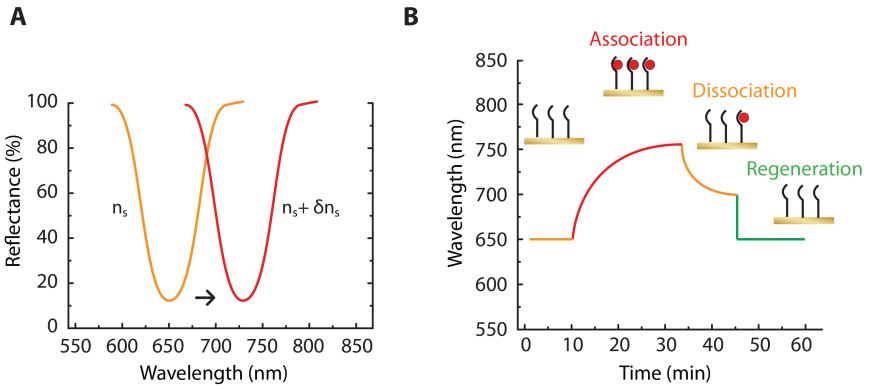

Figure 1.6: A) Typical SPR wave as detected by a spectrophotometer. The SPR wave generates an intensity dip at a particular wavelength, this wavelength depends on the local refractive index at the sensor surface (n_s) and shifts with changes in this refractive index (n_s+Δn_s) B) Sensorgram of an SPR measurement, where shifts in signal are plotted versus time allowing to track biomolecular itneractions at the sensor surface.

Although, most commercial SPR devices are based on angle interrogation, they are very expensive and non-flexible due to some characteristics of this method:

- requirement for complex optical instruments, which are bulky, sensitive and need complex maintenance.
- requirement for microfluidic channels in order to bring the sample to the sensor surface in a controlled way. The most general layout is shown in figure 1.9B, where the prism-gold sensors surface assembly is pressed on a microfluidic channel layout to create different sensing zones.

Nonetheless, this SPR configuration has been recognized as reliable and sensitive becoming thus very popular for various laboratory applications, such as selection of high affinity monoclonal antibodies during their production[57], monoclonal antibody therapy optimization [58] and, drug-target interaction analysis[59]. All these applications are commonly being performed in large research laboratories or in pharmaceutical companies, which have the means to invest in these highly functional but pricey devices. On the other hand, many advantages of the SPR technique, being accuracy in measurements,

automation and the wealth of information generated from even a single SPR measurement, are almost a guarantee for success in point of care testing. Therefore, new implementations of SPR technology should strive to make these devices more simple and affordable. One such implementation is the combination of SPR with optical fibers, which has several advantages as will be discussed in the next section of this chapter.

1.4.2 SPR and optical fibers

Optical fibers (also known as fiber optics: FO) function as waveguides for light[60] and are therefore very popular in high-speed data connections, as data can be transmitted by means of light with minimal loss in quality. In general, FOs consist of a glass or plastic core surrounded by a transparent cladding material (polymer) with a lower index of refraction. The cladding is necessary to keep light in the fiber core by means of the same total internal reflection used to excite SPWs. When light travels trough the FO, it bounces back and forth off the boundary between the core and the cladding. Only light with an angle of incidence below the critical angle, is reflected and, thus able to travel along the FO. Light capable of traveling through a particular FO is said to have an angle of incidence, within the acceptance angle θ_a of the FO. The range of incident angels a particular FO can transport is expressed with the Numerical Aperture (NA).

In general, FOs can be divided in two types, multimode and single mode FOs. Multimode FOs typically have a diameter larger than 10 μM and thus a larger NA, which results in a higher light gathering capacity. Because of the larger NA (and thus θ_a), multimode FOs can suffer from modal dispersion, which is a spread of a light signal in time due to propagation with different modes[61]. Therefore multimode FOs have a limited transport distance in comparison with single mode fibers, which can only support a single light mode (Figure 1.7).

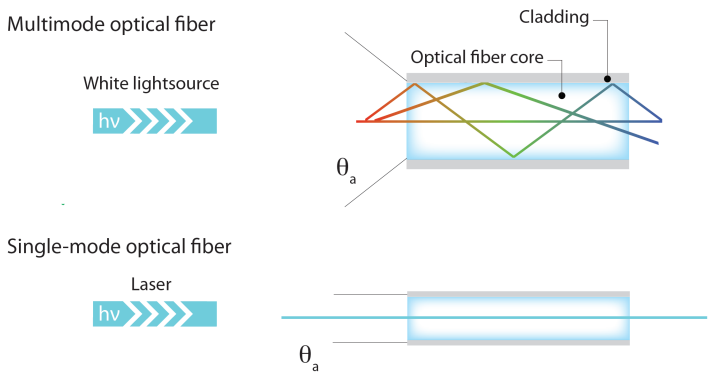

Figure 1.7: Illustration of the numeric aperture in a multimode fiber and a single mode fiber. Because a multimode fiber supports different modes, it can propagate light with different incident angles (θ_a). Therefore, it is often used in combination with a white light source. A single mode fiber, only accepts a very limited number of incident angels and is therefore used in combination with laser light sources.

As described in paragraph 1.4.1 for a two dimensional surface, a prism is necessary to generate total internal reflection of the incident light and excite the surface plasmons in the metal layer of the sensor. Because a multimode fiber-optic cable uses total internal reflection to propagate light, the FOs can be modified to allow SPR sensing without a prism[62]. Like prism based SPR sensing, fiber-optic SPR can be found in various configurations[63] with different FO core materials, geometries and diameters. Here, only the two most popular fiber-optic SPR configurations are discussed (Figure 1.8). The first configuration, known as transmission FO-SPR configuration, is mostly used, mainly because in usage, it resembles many of the prism based SPR configurations[64]. Here, both the protective jacket and the cladding are removed in the middle of a piece of FO. The bare fiber, i.e. fiber core, is directly coated with an SPR suitable metal such as gold. When light is transmitted in the FOs, the light will excite an SPR wave at the gold-coated sensing region. However, only the light with the exact wavelength and mode is converted in SPR waves while the remaining light is reflected and captured on the other end of the FO using a spectrophotometer. This light will have a decreased intensity at the exact wavelength at which the SPR is excited (Figure 1.6A). Alternatively, the fiber-optic cable can also be stripped from its cladding at one end (reflection optical fiber SPR configuration, Figure 1.8)[65]. When this fiber-optic 'pig tail' is coated with gold, it can also be used for SPR sensing, requiring however very

accurate cutting and creating a perfect perpendicular angle that will reflect the incident light at the distal fiber end.

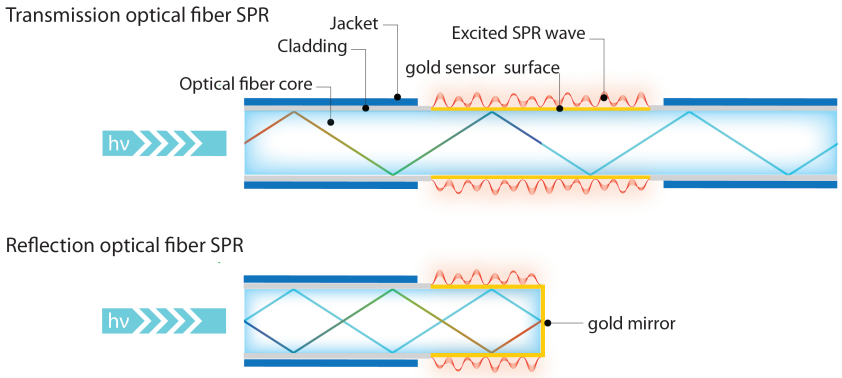

Figure 1.8: Schematic drawing of the two most popular fiber-optic SPR configurations. In the transmission FO-SPR configuration (top) light is directed into one end of the fiber and captured at the other end. In the reflection optic fiber SPR configuration (bottom) light is emitted and captured at the same end of the optical fiber. Both configurations do not require a prism, as evanescent waves arise due to the total internal reflection in the optical fiber .

There are several advantages of the reflection fiber-optic SPR (FO-SPR) sensor configuration (Figure 1.9A). Firstly, it can be used as a dip probe, which is transferred from one sample to another, rendering microfluidic flow cells, commonly used in commercial SPR devices like e.g., BIACORE, obsolete (Figure 1.9B). Secondly, because complex optical equipment including prisms and expensive angle interrogation detectors are not necessary, the FO-SPR sensor is much more compact than a Kretschmann configured sensor (Figure 1.9). This opens new possible applications for SPR, for example as a tool to perform remote sensing at difficult accesible locations. Finally, the reduced cost of an FO-SPR sensor (compared to current commercial SPR devices) could even promote the technology towards disposable sensors.

All these advantages of FO-SPR come however at a price of lower sensitivity compared to their commercial counterparts. Nevertheless, although FO-SPR sensors are in general 10 times less sensitive[66], their sensitivity can be improved to match or even outperform classic SPR devices by using smart labeling techniques, such as gold nanoparticles.

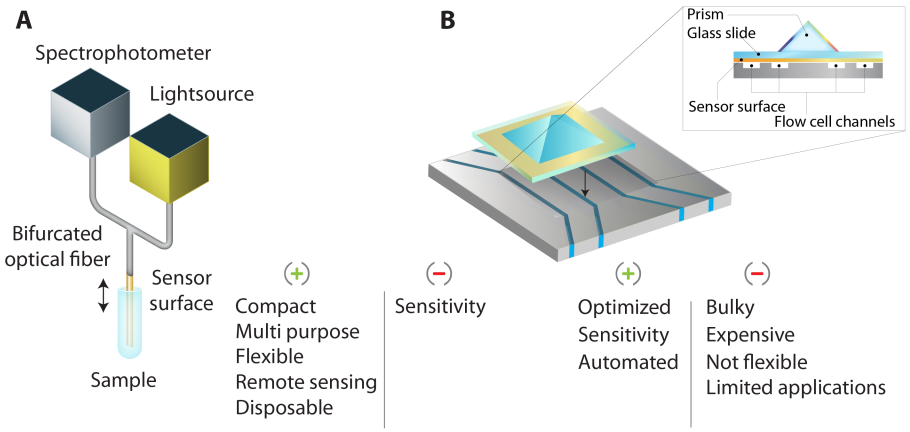

Figure 1.9: A) Layout of a fiber-optic SPR dip probe sensor. B) Layout of a kretschmann SPR sensor as can be found in most commercial SPR devices such as the popular Biacore devices.

1.5 Gold nanoparticles

Gold nanoparticles (Au NPs) are versatile nanometer scale particles that are used in many applications. Because of their special properties (e.g. plasmonic, catalytic, scattering, quenching), they have a great potental as transducers and signal amplification labels in biosensor design[67]. Furthermore, they are also widely used outside the biosensor field as drug carriers[68] or therapeutic agents in medicine[69,70]. Depending on the apllication, Au NPs can have various shapes and have to be functionalized with diverse bioreceptors[71]. In this dissertation, spherical Au NPs coated with DNA molecules will be used.

Spherical Au NPs have, as a consequence of their nanosize, distinct physical properties compared to gold. The optical effect of Au NPs is a result of interactions between light and free electrons of gold, causing a concerted oscillation of electron charge, which is in resonance with the frequency of visible light. Similar to the earlier described SPR phenomena in bulk gold, the localized SPR of Au NPs is also sensitive to its local environment, with however particle size also playing a crucial role. This is directly reflected into the change of Au NPs solution color from intense red to blue when particle size increases. Even more interesting is that Au NPs, when used as SPR signal amplification labels,

improve sensitivity not only due to an increased binding mass and refractive index, but also due to the increased perturbation of the evanescent field[72].

1.6 Surface functionalization

In order to use the SPR biosensors and gold nanoparticle labels their respective surfaces have to be functionalized with the desired biomolecules. A wide range of chemical reactions are available to coat almost any surface with any kind of biomolecule[73]. The best functionalization method depends on the surface, biomolecule and application. In this dissertation only one surface material is used (gold) in combination with a small number of biomolecules, of which DNA is used the most. Three types of chemical bonds are often used for DNA immobilization, surface adsorption[74], semi-covalent[75] bond and the covalent bond[76].

The easiest way of DNA immobilization on a gold surface is by direct adsorption of the ssDNA (Figure 1.10A). This approach allows high density immobilization through hydrophobic interactions between the ssDNA and the gold surface[77]. However, because the affinity of the DNA for the gold surface is lowered when ssDNA hybridizes into dsDNA, it is released from the surface[78]. Therefore this method is not applicable for our intended assay.

Another often used strategy is direct DNA immobilization with a semi-covalent bond (Figure 1.10B), here DNA is functionalized at either the 5' or 3' end with a thiol group, which has a high affinity for gold (homolytic bond strength of 44 kcal/mol)[75]. This method also allows immobilizing high densities of DNA with excellent stability[79].

Lastly DNA can also be imobilized indirectly on a gold surface by means of a self assembling monolayer (SAM). SAM layers are spontaneously formed, highly structured monolayers of organic molecules. Molecules capable of forming SAM layers consist of a head group, a chain and a functional group. The molecules attach first on the gold surface with a thiol head group, which is followed by a slow organization process mediated by alkanechains. The alkanechains tigthly pack together through van der Waals interactions, until they

reach the conformation with the lowest free energy[80]. The functional group is assembled far from the substrate and is used to attach DNA or another biomolecule on the surface. In the SAM layer, vizualized in Figure 1.10C, this functional group is a carboxyl group which can be used to covalently bind 5' or 3' amine functional DNA or it can be used to bind the protein streptavidin which has high affinity for the molecule biotin which also can be attached to either end of a DNA strand. The alkanechains in the SAM can be equiped with polyethyleneoxide repeats, known for their protein repelling properties. As a result the sensor surface will have a less or non-fouling functionalization layer. The indirect SAM approach of DNA immobilization results in a highly organized DNA layer, but at a lower density and at a larger distance from the sensor surface, and, hence, this approach will not result in the highest SPR sensitivity.

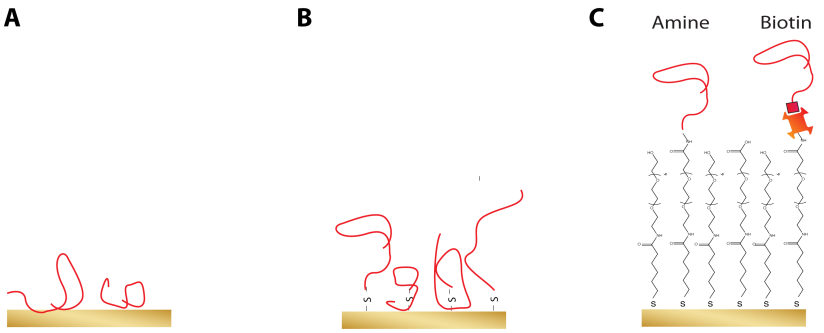

Figure 1.10: A) Direct adsorption of ssDNA on a gold surface. B) Immobilization of thiol functionalized ssDNA on a gold surface. C) Indirect immobilization of amine and biotin functionalized DNA on a Self Assembling Monolayer of alkanethiols with a carboxyl functional end group.

From the previous paragraphs, we conclude that direct immobilization of DNA is the best suited DNA immobilization strategy for a sensitive SPR DNA biosensor as it will allow the highest density of DNA, closest to the sensor surface. In this regard it has to be noted that hybridization reactions between a surface immobilized probe and solution target sequence are subject to greater complexity than bulk hybridization and are therefore less well understood. However the vast number of applications in modern microarray and biosensing technology have made the interest grow, leading to some excellent

reviews on this topic[81-83]. In comparison with bulk hybridization, a target sequence encounters locally higher charges and nucleic acid concentrations, which are not present in solution. Probe density[84] and ionic strength[85], allow to control surface DNA hybridization reactions. After DNA immobilization, the densely packed DNA is not ideally oriented on the surface to allow easy hybridization. Depending on the sequence of the immobilized DNA it can fold back to the surface, due to affinity of particular nucleotides for the surface[86]. Exposure of the gold surface after DNA immobilization to SAM forming agents such as the alkanethiols discussed in the previous paragraph, allows to orient the ssDNA on the gold surfaces[87] (Figure 1.11A).

In addition, these reagents also render the surface protein repellant which is very important for bio-sensing applications[88]. In Figure 1.11B an SPR sensorgram in a complex matrix (PCR mixture) is shown, measured with a backfilled (light blue) and non-backfilled (dark blue) DNA coated SPR sensor. The backfilled sensor does not bind any of the components in the PCR mixture, keeping a steady baseline signal, while the non-backfilled sensor has an increasing signal in the PCR mixture, which not returns to baseline level when the sensor is exposed to buffer. These results prove that when the biosensor is applied outside the optimized buffer conditions, on real seal samples, complex matrices of proteins and other compounds can be encountered which disturb the biosensor performance[89] (Figure 1.11B). Furthermore, this non-specific interaction is not only of danger for the sensor performance, but can also lead to inactivation of enzymes used in some DNA detection assays[90].

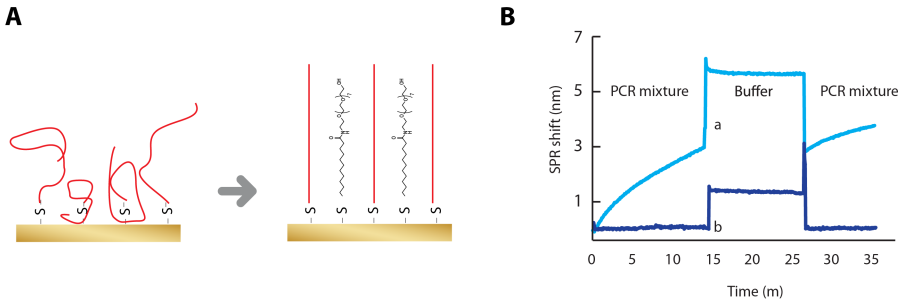

Figure 1.11: A) Conceptual drawing of backfilling a ssDNA functionalized gold surface. B) Actual SPR measurement in a PCR mixture (complex matrix) with (dark blue) and without PEO alkane thiol backfiller (from Janssen et al.[89])

For Au NPs the same functionalization strategies can be applied as for planar gold surfaces. However, these functionalized nanostructures, also called Spherical Nucleic Acid (SNA)[91], acquire through the high density of the DNA monolayer very unique characteristics. The most peculiar characteristics of SNAs are: (1) resistance to nuclease degradation[92], (2) capability to transfect cell lines without ancillary physical or chemical transfection[93] and finally (3) higher binding constants for their complementary DNA than single stranded probes[94]. Especially this last trait is used in the assays described in this dissertation to improve DNA detection. For instance, Au NPs can be linked together through hybridization of complementary DNA molecules on their surface. In this process, the highly specific DNA-DNA interactions hold the Au NPs together without their cores interacting. As a result, either lowering the salt concentration of the solution or increasing the temperature can easily reverse the particle aggregation. When these DNA interlinked Au NP microstructures are melted, the melting occurs over a much smaller temperature range compared to particle-free oligonucleotides[95]. Furthermore, the actual melting temperature for the AuNP DNA microstructures will be considerably higher than for the same particle-free oligonucleotides. Both effects can be attributed to multiple inter-particle connections, creating a much stronger bond between interlinked nanoparticles than between particle-free oligonucleotides. Additionally, Au NPs have high local salt concentrations in their immediate surroundings, which further stabilizes the DNA duplexes and increase the melting temperature. These features make Au NPs ideal candidates for labeling molecules in DNA mutation assays. Multiple Au NP aggregation assays have already proven that this method is highly sensitive, even in the case of a single nucleotide polymorphism[96-98].

In this research project we will apply SNAs as signal enhancement nanostructures in FO-SPR based bioassays, as these nanolabels can both improve the sensor as well as the assay performance, leading to unmet mutation detection capabilities.

1.7 Objectives and outline of this thesis

Bacteria and viruses influence everyday human life, both in a positive and negative way. Recently, they have even been transformed into living 'factories', capable of producing consumer products, such as plastics and gasoline. Nonetheless, some micro-organisms remain a threat to human health, e.g. pathogenic viruses and bacteria, especially with increasing resistance of bacteria towards existing antibiotic agents. As a result there is a strong need to accurately identify and quantify micro-organisms in a short period of time, allowing a physician to make the right treatment decisions and follow up on treatment success. Current detection techniques still consist mainly of culturing the bacteria or virus before identifying them, a process that lasts for most bacteria days to even weeks. This method has certain advantages such as a clear discrimination of life versus death bacteria, and a clear overview of the full spectrum of bacteria present, thoughthe detection speed in culturing assays is low. As discussed earlier the 'time' issue has been resolved by the introduction of the PCR technology However, this detection method is, due to its complexity, not always easily applicable outside a specialized lab environment. Therefore, new means of detection, quantification and identification of bacteria and viruses are a necessity to improve not only healthcare but also food safety, limit antibiotic overuse and enable a better tracking of bacterial evolution.

A very interesting technology in this aspect is SPR, which allows real time monitoring of biological interaction processes, such as binding and denaturing of DNA. Until recently, SPR has never been applied widely for DNA analysis because the assay resulted often in false results, if not extensively optimized for each new DNA target[99]. Furthermore, commercial SPR devices enable the monitoring of biomolecular reactions under equilibrium conditions, i.e. a constant temperature, allowing only hybridization to be monitored. Because single mutation has very limited effect on the hybridization of DNA duplex that consists of multiple basepairs, detecting mutations is challenging with the commercial SPR devices. Contrary to this, the impact a single base pair change can have on thermal denaturation of hybridized DNA is substantially higher, which allows easy discrimination of sequences

containing a mutation. Despite the original sensitivity of SPR technology being limited the potential of FO-SPR to be combined with Au NPs[72] and thermal denaturation has a large potential to improve sensitivity considerably for DNA analysis.

The aim of this work is to develop innovative, fast and highly sensitive bioassays on a compact fiber optic SPR biosensor platform, that can be used to identify and quantify bacteria and viruses in a multiplexed way. Bacteria and viruses are detected either directly or by means of their DNA using DNA melting analysis. This unique combination of techniques will open up new opportunities in the development of POC biosensors for bacteria and viral detection. A schematic overview of the thesis and the correlation between the different chapters can be found in Figure 1.12.

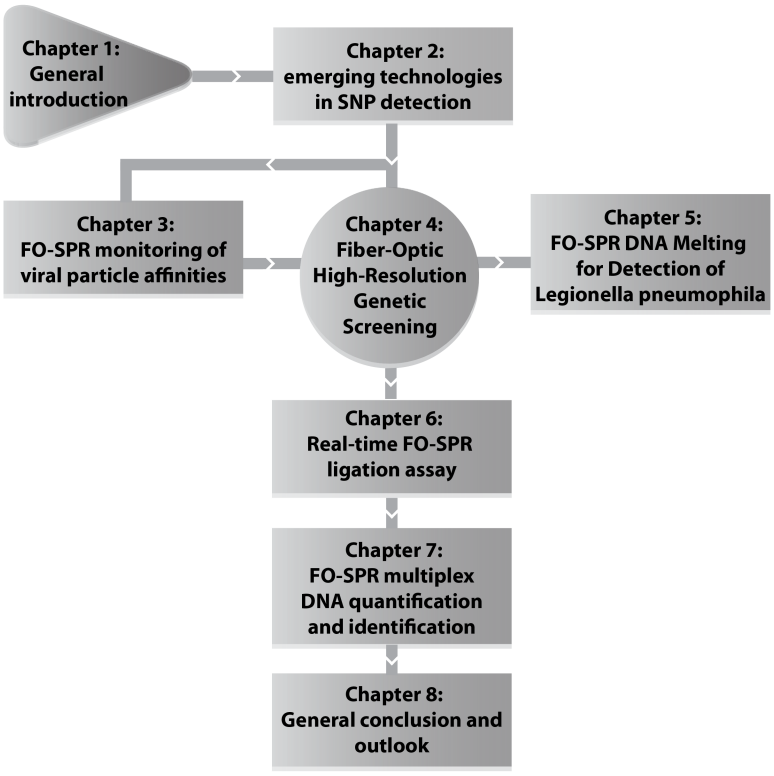

Figure 1.12: Visualization of PhD structure showing the connections between different chapters.

In **Chapter 2** a literature review is made of new molecular diagnostic methods capable of detecting the smallest possible alteration in DNA, a single nucleotide polymorphism (SNP). The focus of this chapter is on fast and robust technologies for sensitive and specific target detection that could potentially be used in POC tests. The chapter is limited to assay design and largely excludes detection methods as most of these assays can be applied on multiple detection platforms with optical, electrochemical and mass sensitive transducers amongst which the FO-SPR biosensor.

The first experimental chapter, **Chapter 3**, deals with development of a biosensor for direct detection of micro-organisms. Because viral particles are substantially smaller than bacteria (low nanometer range versus low micrometer range), they are a good benchmark for the FO-SPR biosensor sensitivity towards small particulate organisms. For this proof of concept, bacteria specific viral particles, named bacteriophages, are used. These bacteriophages can express short peptides on their coat proteins, transforming them in affinity labels. Although, affinities of individual peptides are normally characterized, a new trend is shifting towards usage of the entire phage as affinity label because of increased receptor density, stability and functionality. Therefore, bioassays are needed that can characterize binding kinetics of the entire phage particle. FO-SPR is used to this extent, since one SPR measurement can capture all kinetic binding parameters of the phage affinity label. The FO-SPR phage assay is applied on the selection of a phage affinity label for the fluorescent protein eGFP. Although, FO-SPR is a true asset in the determination of binding constants for non-conventional affinity labels, the limitations of the FO-SPR measuring principal is revealed when using label-free assays.

In **Chapter 4** a new assay is developed, not based on detection of the complete micro-organism, but on the presence of its genetic material. DNA can be used both to quantify and identify micro-organisms, as each micro-organism contains genetic codes, which are unique to the particular micro-organisms. In this proof-of-concept research, a new biosensor is developed combining FO-SPR with DNA melting analysis. The detection of single nucleotide alterations in target DNA strands of variable length is addressed.

In **Chapter 5,** the FO-SPR DNA melting assay is further advanced, in order to allow high resolution DNA melting directly in a PCR amplification mix. Subsequently, the assay is applied on a real test case using a common human pathogen, *Legionella pneumophila* bacteria. Usually, the PCR assay is applied on sputum samples to detect this bacteria. However, the assay was found to be unable to detect some subspecies when they contain a particular mutation. In this chapter, the performance of the FO-SPR melting DNA assay is validated against current state-of-the-art DNA screening assays.

In **Chapter 6**, the FO-SPR DNA melting assay is improved towards simultaneous DNA quantification and multiplex target identification. This will require several changes to the original FO-SPR DNA melting assay, with special attention for the speed of the original FO-SPR melting assay, which will be increased, while safeguarding the resolution in order to detect SNP containing samples. This chapter will capture the full potential of the FO-SPR melting assay as it will allow detection and quantification of bacteria in a single assay, resulting in considerable reduction of the total assay time compared to other, more conventional techniques.

In **Chapter 7,** the througput of the biosensor is further increased by simultaneously detecting two bacteria using the FO-SPR biosensor. The FO-SPR sensor tip and the Au NP labeles are therefore functionalized with two different sets of hybridization probes, each targeting a region of interest in a different bacterial species. To improve the sensitivity of this assay, a multiplex PCR will be used to amplify the target DNA. This also allows the FO-SPR to monitor in real-time the PCR reaction, which makes this multiplex FO-SPR also a quantitative assay. The assay will be able to resolve the presence of one or both bacteria and could even detect mutations in the target sequences.

Finally, in **Chapter 8** the most important achievements in the development of the FO-SPR DNA biosensor are summarized. These milestones are put in perspective of the entire development process, necessary to integrate the FO-SPR platform in a POC biosensor capable of micro-organism detection. In this regard suggestions are made for future improvements to both the biosensor and the presented bioassays. This overview will not only focus on detection of micro-

organisms but also on opportunities for the FO-SPR biosensor in other fields.

References

1. J. Davies, *Science*, 1994, **264**, 375-382.
2. I. N. Okeke*, et al.*, *Drug Resist. Updates*, 2011, **14**, 95-106.
3. P. C. Ng, J. C. Venter, S. S. Murray and S. Levy, *Nature*, 2009, **461**, 724-726.
4. R. Scully and D. M. Livingston, *Nature*, 2000, **408**, 429-432.
5. H. S. Cho, K. Mason, K. X. Ramyar, A. M. Stanley, S. B. Gabelli, D. W. Denney and D. J. Leahy, *Nature*, 2003, **421**, 756-760.
6. Y. Izumi, L. Xu, E. di Tomaso, D. Fukumura and R. K. Jain, *Nature*, 2002, **416**, 279-280.
7. C. C. Boehme*, et al.*, *N. Engl. J. Med.*, 2010, **363**, 1005-1015.
8. S. D. Lawn*, et al.*, *Lancet Infect. Dis.*, 2013, **13**, 349-361.
9. J. C. Davis, L. Furstenthal, A. A. Desai, T. Norris, S. Sutaria, E. Fleming and P. Ma, *Nat. Rev. Drug Discovery*, 2009, **8**, 279-286.
10. J. August, *Nat. Rev. Drug Discovery*, 2010, **9**, 351-351.
11. V. Gubala, L. F. Harris, A. J. Ricco, M. X. Tan and D. E. Williams, *Anal. Chem.*, 2012, **84**, 487-515.
12. C. L. Mitchelmore and J. K. Chipman, *Mutat. Res.*, 1998, **399**, 135-147.
13. L. Guardabassi, A. Petersen, J. E. Olsen and A. Dalsgaard, *Appl. Environ. Microbiol.*, 1998, **64**, 3499-3502.
14. J. C. Chee-Sanford*, et al.*, *J. Environ. Qual.*, 2009, **38**, 1086-1108.
15. K. R. Rogers, *Anal. Chim. Acta*, 2006, **568**, 222-231.
16. A. P. F. Turner, *Chem. Soc. Rev.*, 2013, **42**, 3184-3196.
17. I. E. Tothill, *Semin. Cell Dev. Biol.*, 2009, **20**, 55-62.
18. R. S. Sethi, *Biosens. Bioelectron.*, 1994, **9**, 243-264.
19. N. J. Ronkainen, H. B. Halsall and W. R. Heineman, *Chem. Soc. Rev.*, 2010, **39**, 1747-1763.
20. T. Battelino, M. Phillip, N. Bratina, R. Nimri, P. Oskarsson and J. Bolinder, *Diabetes Care*, 2011, **34**, 795-800.
21. N. S. Oliver, C. Toumazou, A. E. G. Cass and D. G. Johnston, *Diabetic Medicine*, 2009, **26**, 197-210.
22. L. Gervais, N. de Rooij and E. Delamarche, *Adv Mater*, 2011, **23**, H151-176.
23. S. Park and S. Jayaraman, *Ieee Engineering in Medicine and Biology Magazine*, 2003, **22**, 41-48.
24. C. D. Chin, V. Linder and S. K. Sia, *Lab Chip*, 2012, **12**, 2118-2134.
25. A. Niemz, T. M. Ferguson and D. S. Boyle, *Trends Biotechnol.*, 2011, **29**, 240-250.
26. U. Landegren, R. Kaiser, C. T. Caskey and L. Hood, *Science*, 1988, **242**, 229-237.
27. D. Liaw*, et al.*, *Nat. Genet.*, 1997, **16**, 64-67.

28. H. A. Lashuel, D. Hartley, B. M. Petre, T. Walz and P. T. Lansbury, Jr., *Nature*, 2002, **418**, 291.
29. A. Goate*, et al.*, *Nature*, 1991, **349**, 704-706.
30. Y. Ogura*, et al.*, *Nature*, 2001, **411**, 603-606.
31. A. Brooks-Wilson*, et al.*, *Nat. Genet.*, 1999, **22**, 336-345.
32. J. H. Hoeijmakers, *Mech. Ageing Dev.*, 2007, **128**, 460-462.
33. M. J. Mahan, J. M. Slauch and J. J. Mekalanos, *Science*, 1993, **259**, 686-688.
34. R. Benveniste and J. Davies, *Annu. Rev. Biochem.*, 1973, **42**, 471-506.
35. A. C. Palmer and R. Kishony, *Nat. Rev. Genet.*, 2013, **14**, 243-248.
36. V. M. D'Costa*, et al.*, *Nature*, 2011, **477**, 457-461.
37. K. L. Gunderson, F. J. Steemers, G. Lee, L. G. Mendoza and M. S. Chee, *Nat. Genet.*, 2005, **37**, 549-554.
38. M. Schena, D. Shalon, R. W. Davis and P. O. Brown, *Science*, 1995, **270**, 467-470.
39. R. I. Amann, L. Krumholz and D. A. Stahl, *J. Bacteriol.*, 1990, **172**, 762-770.
40. G. Bonnet, S. Tyagi, A. Libchaber and F. R. Kramer, *Proc. Natl. Acad. Sci. U. S. A.*, 1999, **96**, 6171-6176.
41. K. S. J. Elenitoba-Johnson, S. D. Bohling, C. T. Wittwer and T. C. King, *Nat. Med. (N. Y., NY, U. S.)*, 2001, **7**, 249-253.
42. D. Y. Zhang, S. X. Chen and P. Yin, *Nature Chem.*, 2012, **4**, 208-214.
43. C. T. Wittwer, *Hum. Mutat.*, 2009, **30**, 857-859.
44. K. J. Breslauer, R. Frank, H. Blocker and L. A. Marky, *Proc. Natl. Acad. Sci. U. S. A.*, 1986, **83**, 3746-3750.
45. J. SantaLucia, Jr., H. T. Allawi and P. A. Seneviratne, *Biochemistry*, 1996, **35**, 3555-3562.
46. K. M. Ririe, R. P. Rasmussen and C. T. Wittwer, *Anal. Biochem.*, 1997, **245**, 154-160.
47. L. Zhou, A. N. Myers, J. G. Vandersteen, L. Wang and C. T. Wittwer, *Clin. Chem.*, 2004, **50**, 1328-1335.
48. C. N. Gundry*, et al.*, *Nucleic Acids Res.*, 2008, **36**, 3401-3408.
49. B. Liedberg, C. Nylander and I. Lundstrom, *Biosens. Bioelectron.*, 1995, **10**, i-ix.
50. R. B. R. B. M. Schasfoort and A. J. Tudos, *Handbook Of Surface Plasmon Resonance*, Royal Society of Chemistry, 2008.
51. J. Homola, *Chem. Rev.*, 2008, **108**, 462-493.
52. J. Homola, S. S. Yee and G. Gauglitz, *Sens. Actuators, B*, 1999, **54**, 3-15.
53. A. Otto, *Zeitschrift für Physik*, 1968, **216**, 398-410.

54. E. Kretschmann and H. Raether, *Zeitschrift Fur Naturforschung Part a-Astrophysik Physik Und Physikalische Chemie*, 1968, **A 23**, 2135-2141.
55. U. Aldinger, P. Pfeifer, G. Schwotzer and P. Steinrucke, *Sens. Actuators, B*, 1998, **51**, 298-304.
56. J. Homola, I. Koudela and S. S. Yee, *Sens. Actuators, B*, 1999, **54**, 16-24.
57. A. C. Malmborg and C. A. K. Borrebaeck, *J. Immunol. Methods*, 1995, **183**, 7-13.
58. A. P. Chapman, P. Antoniw, M. Spitali, S. West, S. Stephens and D. J. King, *Nat. Biotechnol.*, 1999, **17**, 780-783.
59. A. Koul*, et al.*, *Nat. Chem. Biol.*, 2007, **3**, 323-324.
60. K. S. Thyagarajan and A. Ghatak, *Fiber Optic Essentials*, Wiley, 2007.
61. B. E. A. Saleh and M. C. Teich, *Fundamentals of photonics*, Wiley, 1991.
62. L. L. Obando and K. S. Booksh, *Anal. Chem.*, 1999, **71**, 5116-5122.
63. B. D. Gupta and R. K. Verma, *Journal of Sensors*, 2009, **2009**.
64. A. K. Sharma, R. Jha and B. D. Gupta, *Ieee Sensors Journal*, 2007, **7**, 1118-1129.
65. L. A. Obando, D. J. Gentleman, J. R. Holloway and K. S. Booksh, *Sens. Actuators, B*, 2004, **100**, 439-449.
66. J. Pollet*, et al.*, *Biosens. Bioelectron.*, 2009, **25**, 864-869.
67. H. Jans and Q. Huo, *Chem. Soc. Rev.*, 2012, **41**, 2849-2866.
68. D. Zheng*, et al.*, *Proc. Natl. Acad. Sci. U. S. A.*, 2012, **109**, 11975-11980.
69. K. Zhang, L. L. Hao, S. J. Hurst and C. A. Mirkin, *J. Am. Chem. Soc.*, 2012, **134**, 16488-16491.
70. B. Van de Broek*, et al.*, *ACS Nano*, 2011, **5**, 4319-4328.
71. E. Boisselier and D. Astruc, *Chem. Soc. Rev.*, 2009, **38**, 1759-1782.
72. L. He, M. D. Musick, S. R. Nicewarner, F. G. Salinas, S. J. Benkovic, M. J. Natan and C. D. Keating*, J. Am. Chem. Soc.*, 2000, **122**, 9071-9077.
73. G. T. Hermanson, *Bioconjugate Techniques*, Elsevier Science, 2010.
74. X. Zhang, B. Liu, M. R. Servos and J. Liu, *Langmuir*, 2013, **29**, 6091-6098.
75. L. H. Dubois and R. G. Nuzzo, *Annu. Rev. Phys. Chem.*, 1992, **43**, 437-463.
76. J. I. Cutler, D. Zheng, X. Xu, D. A. Giljohann and C. A. Mirkin, *Nano Lett.*, 2010, **10**, 1477-1480.
77. X. Zhang, B. Liu, N. Dave, M. R. Servos and J. Liu, *Langmuir*, 2012, **28**, 17053-17060.

78. E. M. Nelson and L. J. Rothberg, *Langmuir*, 2011, **27**, 1770-1777.
79. S. J. Hurst, A. K. Lytton-Jean and C. A. Mirkin, *Anal. Chem.*, 2006, **78**, 8313-8318.
80. J. C. Love, L. A. Estroff, J. K. Kriebel, R. G. Nuzzo and G. M. Whitesides, *Chem. Rev.*, 2005, **105**, 1103-1169.
81. L. Moiseev, M. S. Unlu, A. K. Swan, B. B. Goldberg and C. R. Cantor, *Proc. Natl. Acad. Sci. U. S. A.*, 2006, **103**, 2623-2628.
82. S. Draghici, P. Khatri, A. C. Eklund and Z. Szallasi, *Trends Genet.*, 2006, **22**, 101-109.
83. P. Gong and R. Levicky, *Proc. Natl. Acad. Sci. U. S. A.*, 2008, **105**, 5301-5306.
84. A. W. Peterson, R. J. Heaton and R. M. Georgiadis, *Nucleic Acids Res.*, 2001, **29**, 5163-5168.
85. T. Springer, H. Sipova, H. Vaisocherova, J. Stepanek and J. Homola, *Nucleic Acids Res.*, 2010, **38**, 7343-7351.
86. H. Kimura-Suda, D. Y. Petrovykh, M. J. Tarlov and L. J. Whitman, *J. Am. Chem. Soc.*, 2003, **125**, 9014-9015.
87. C. Y. Lee, P. Gong, G. M. Harbers, D. W. Grainger, D. G. Castner and L. J. Gamble, *Anal. Chem.*, 2006, **78**, 3316-3325.
88. A. R. Lokanathan, *et al.*, *Biointerphases*, 2011, **6**, 180-188.
89. K. P. Janssen, K. Knez, L. Vanysacker, J. Schrooten, D. Spasic and J. Lammertyn, *Nanotechnology*, 2012, **23**, 235503.
90. J. Pollet, K. P. Janssen, K. Knez and J. Lammertyn, *Small*, 2011, **7**, 1003-1006.
91. J. I. Cutler, E. Auyeung and C. A. Mirkin, *J. Am. Chem. Soc.*, 2012, **134**, 1376-1391.
92. D. S. Seferos, A. E. Prigodich, D. A. Giljohann, P. C. Patel and C. A. Mirkin, *Nano Lett.*, 2009, **9**, 308-311.
93. N. L. Rosi, D. A. Giljohann, C. S. Thaxton, A. K. R. Lytton-Jean, M. S. Han and C. A. Mirkin, *Science*, 2006, **312**, 1027-1030.
94. A. K. R. Lytton-Jean and C. A. Mirkin, *J. Am. Chem. Soc.*, 2005, **127**, 12754-12755.
95. R. C. Jin, G. S. Wu, Z. Li, C. A. Mirkin and G. C. Schatz, *J. Am. Chem. Soc.*, 2003, **125**, 1643-1654.
96. W. J. Qin and L. Y. L. Yung, *Nucleic Acids Res.*, 2007, **35**.
97. H. Wang, J. S. Li, Y. X. Wang, J. Y. Jin, R. H. Yang, K. M. Wang and W. H. Tan, *Anal. Chem.*, 2010, **82**, 7684-7690.
98. J. S. Li, T. Deng, X. Chu, R. H. Yang, J. H. Jiang, G. L. Shen and R. Q. Yu, *Anal. Chem.*, 2010, **82**, 2811-2816.
99. E. Milkani, S. Morais, C. R. Lambert and W. G. McGimpsey, *Biosens. Bioelectron.*, 2010, **25**, 1217-1220.

Chapter 2

Emerging technologies for Single Nucleotide Polymorphism detection

Part of this chapter has been published in:

Knez K., Spasic D., Janssen K., Lammertyn J. (2013). Emerging technologies for Single Nucleotide Polymorphism detection. *Analyst*, (in press).

2.1 Introduction

Recent advances in the field of molecular biology have created opportunities for the development of novel diagnostic methods, which are becoming irreplaceable not only in the detection and typing of diseases, but as well in steering the drug therapy, being either with antibiotics or novel cancer drugs. For instance, numerous genes have been related to various human diseases[1] promoting thus genetic screening to become applicable in prenatal diagnostics,[2] detection of cancer,[3] cardiovascular disease[4] and many other pathologies[5,6].

Moreover, molecular diagnostics can even be used to enhance cancer therapy through assessing a patient's susceptibility for certain treatments[7-9]. These so called 'companion diagnostics' are increasingly becoming an essential guide for the successful application of a number of treatments[10]. Furthermore, molecular diagnostic methods are used in microbiology[11] for identifying pathogens and their antibiotic resistance genes, hence guiding treatments towards correct antibiotic type/dose and preventing further growth in global antibiotic resistance of bacterial pathogens[12].

Currently, however, the molecular diagnostics field is still limited to laborious and costly methods that require significant infrastructure and skills, only available at specialized laboratory facilities. For human genetic screening the preferable method is sequencing because it can capture the complete spectrum of genetic variation in an individual[13]. Although in recent years sequencing technologies have experienced a dramatic drop in price and time to result,[14,15] some hurdles still severely limit its direct application in routine diagnostics[13]: (1) reliable sequencing results depend in first place on careful construction of a sequence library and sample preparation[16] and (2) the amount of data generated by sequencing and the complexity of their processing is not compatible with routine applications[17,18].

In microbiological applications, the preferred method for pathogen detection and evaluation of antibiotic resistance still relies on actual selective bacterial growth, limiting the speed of these assays to 48h.[19] Molecular diagnostics such as PCR are able to improve the sample throughput, time to detection and sensitivity for non-cultivable bacteria but are introducing new problems such as sample preparation, expertise and facility requirements[20].

Recently, the trend in developing rapid and cost-effective point-of-care (POC) diagnostics has increased tremendously. Devices that allow detection of genetic changes, such as point mutations, with minimal user intervention and laboratory requirements and which could even be deployed in resource limited regions are being developed[21,22]. Although this next generation of molecular diagnostic devices presents a large improvement compared to classical methods, they remain linked to the intrinsic limitations of the PCR method such as total analysis time and

high sensitivity towards sample contamination. Furthermore the cost per test remains too high for the intended markets such as developing countries[23].

In recent years, several new methods for detection of genetic mutations have become available that are, currently, at least comparable to PCR in their performance. These new developments have been promoted to drastically improve and simplify present-day POC tools, enabling sensitive detection in minutes' time and at a fraction of the cost of current methods. However not a lot of these new concepts have found their way to commercial applications due to numerous obstacles such as performance, price and applicability[24], allowing classic PCR to remain the method of choice for molecular diagnostics.

2.2 Aim of this chapter

In this chapter a selection is made of new molecular diagnostic methods that could break this spell and live up to the promises of improving molecular diagnostics. There will be a particular focus on single nucleotide polymorphism (SNP) detection for two reasons: one, SNP mutation detection can be taken as a benchmark and two, the impact of a SNP on the overall double strand is limited and strongly depends on multiple factors, making this one of the most challenging mutations to detect. The chapter is limited to assay design and largely excludes detection methods as most of these assays can be applied on multiple detection platforms (i.e. optical, electrochemical, mass based, etc.).

New assays are categorized in the following three fields based on the applied methodology:

1 Hybridization mediated SNP detection
2 Protein mediated SNP detection
3 SNP detection through thermal denaturation of hybrids.

Each of these topics will be discussed elaborately in the following paragraphs, with a particular focus on sensitivity and applicability of the methods.

2.3 Hybridization mediated SNP detection

2.3.1 Single hybridization probes

Detection of SNPs through direct hybridization remains one of the most popular methods for genotyping. However, the greatest challenge in these assays is the specificity of the hybridization,[25] because the impact of a single variable nucleotide on the overall double strand stability is rather limited (Figure 2.1). For example, the influence of a SNP on a 20bp DNA double helix target comprises only 5% of the total number of basepairs. Several factors can improve the selectivity of hybridization, all being related to the mass transport and kinetics involved in the hybridization process[26]. Therefore, parameters such as temperature, ionic strength, sequence and oligonucleotide concentration, which all have a direct influence on mass transport and kinetics, need to be precisely controlled ensuring optimal hybridization efficiency[27]. However, for every new target, new optimal parameters need to be defined, requiring a substantial investment in assay optimization and making the detection of multiple DNA targets very complex.

Figure 2.1: Basic concept of hybridization based strategies for SNP detection. In this direct hybridization of two complementary strands detection of a mutation is difficult, as the mutation only gives lower hybridization yields in short target sequences. Detection platforms can be of any kind: fluorescent, electrochemical, SPR.

These limitations have pushed SNP detection towards a new generation of assays where, the influence of specific conditions on the hybridization process are being eliminated as much as possible. By introducing a better control over hybridization, new assays have

become more sensitive and robust. One example of improved specificity of the hybridization process is the introduction of secondary structures (e.g. stem-loop) in reporter oligonucleotides. These reporter molecules can hybridize to a target sequence, only after the target strand has displaced the secondary structure through a process called branch migration[28,29]. Branch migration can happen between any single stranded DNA and a double stranded molecule when they share a homologous region for binding the single strand to the duplex. As a result of the homologous regions, the single strand can attack the existing duplex resulting in three-stranded structure where all strands compete for binding their complementary strands. In the presence of a SNP, the thermodynamic driving force towards breaking up the secondary structure in the reporter sequence and hybridization to the target molecule will be lowered explaining why these structured probes possess increased specificity and robustness in comparison with simple complementary strands[30]. One of the first implementations of the branch migration process in molecular diagnostics was Molecular Beacons (MB).

2.3.2 Molecular beacons

MBs are a particular class of branch migrating molecules, as they use a self-complementary region as the competing DNA duplex in the process of SNP identification (Figure 2.2)[31]. The MBs internal structure forms an oligonucleotide hairpin probe with a fluorophore and a quencher conjugated to the opposite ends of the oligomer. When the complement of the MB is not present, they form a stem-loop structure that brings the quencher in close proximity to the fluorophore, resulting in a low fluorescent signal. From the moment the target sequence is present, the hairpin unfolds in favour of target hybridization, resulting in an increased fluorescence signal.

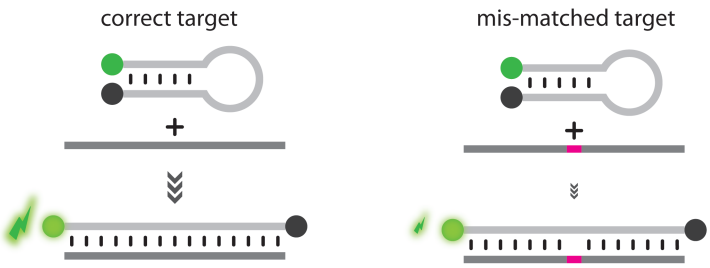

Figure 2.2: Molecular beacon strategy for SNP detection. Mutation discrimination is improved by introducing a secondary structure (hairpin) in the DNA reporter strand which drastically lowers the hybridization yield in case of a mutation, resulting in lower fluorescence. The hairpin also brings together quencher and fluorophore when the MB is not bound to the DNA target.

Although the new generation of point of care (POC) biosensors is making molecular diagnostics available outside specialized labs, the technology makes use of classic principals such as fluorescence and quantitative PCR to detect a sample[32-34]. This technology limits the abilities of the molecular diagnostic POC test, as it cannot reach the strongpoints such as ease of interpretation, time to results and assay cost[35] that made the initial generation of biosensors so successful. However new technologies can be developed, which could enable development of biosensors with potentially lower costs, time to result and require minimal interpretation whilst still reaching the required detection limits[32]. One of these high potential technologies is DNA melting analysis.

2.3.3 Binary DNA probes

An alternative for molecular beacons, known as binary probe, is based on a simple division of the probe into two individual parts (Figure 2.3), where the individual, shorter probes, also known as the analyte binding arms, are used to bind to the target. The individual binding arms can be labelled with any kind of reporter molecule that only gives a signal when both are bound to the target, resulting in a remarkable increase in both specificity and sensitivity towards SNP detection. The improvements in performance can be explained by the relatively short

length of the individual fragments of the binary probe, which consist each of 7-10 bases, emphasizing considerably the effect of a single variable base on the DNA hybrid.

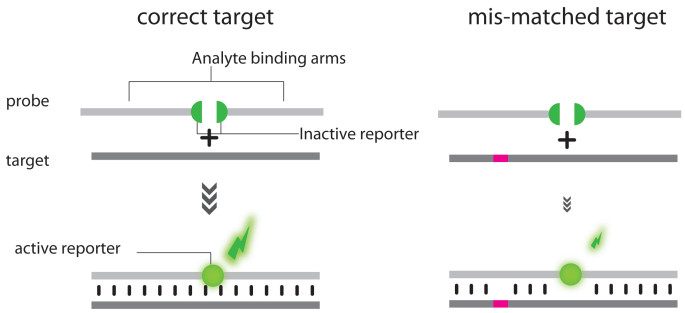

Figure 2.3: General concept of binary probes where a probe is split into two halves to increase the impact of a mutation on the hybridization yield. Binary probes use always reporters, which require the presence of the two probes hybridized to the target in order to activate a reporter molecule or reaction.

Initially, binary probes were mainly used in combination with fluorescence resonance energy transfer detection (FRET). Kolpashchikov *et al*. have recently made improvements on the binary probe concept, through integration of an RNA aptamer. Aptamers are RNA or DNA oligonucleotides selected for their binding capacity towards a particular molecule, being in this case the fluorescent dye malachite green (Figure 2.4). The aptamer was integrated into the binary probe concept by splitting its sequence in two parts, each linked to a target-binding probe. The aptamer only becomes functional when its two target-binding probes are bound to the target DNA strand, which brings the individual aptamer parts in each other's vicinity. Once functional, the aptamer can bind the malachite green dye stabilizing it in a more fluorescent conformation, which results in a 2000 fold increase in the fluorescence signal[36]. The assay is able to detect 41 out of the possible 42 mutations in a 14bp nucleotide target strand[37]. However the assay is limited in sensitivity by the affinity of the aptamer for the target dye.

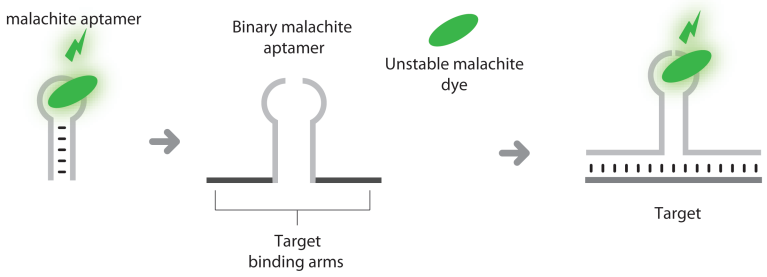

Figure 2.4: Design of the binary malachite aptamer. On the left, the structure of the parent malachite aptamer is shown, which stabilizes the dye resulting in an increased fluorescence. This aptamer is split in two halves, each extended with a target binding arm, resulting in the binary malachite aptamer. When the target DNA strand is present, the functional malachite aptamer is formed. Reproduced after Kolpashchikov *et al.*[37]

Binary probe assays can be further improved with the integration of a ribozyme (Figure 2.5)[38] which are DNA/RNA sequences with an enzymatic activity. In the first application of this concept, the assay was designed to integrate a deoxyribozyme in DNA probes that bind specifically to a 20bp target. When bound to this target, the two fragments form the functional ribozyme, which then cleaves a phosphodiester bond in a DNA reporter molecule, resulting in separation of a fluorescent FAM at the 5' end from a black hole quencher at the 3' end. Mutations can in this way be discriminated but not identified, by calculating the ratios between probe fluorescence. This is done by registration of fluorescence intensities, after subtraction of the background fluorescence, at 517 nm in the presence of the true target and in the presence of each mismatched oligonucleotide. The resulting fluorescent signal can easily discriminate 11 of 20 tested SNPs in the target strand with a high signal to noise ratio compared to MBs. Furthermore, integration of a ribozyme in a binary probe has the advantage that the formation of one functional ribozyme can be used to activate multiple reporter molecules, which results in a strong signal amplification. As a result, the detection limit of this ribozyme-based assay is 1 nM, which is two orders of magnitude lower than the previously described malachite based assay. Use of more efficient DNAzymes in similar assays has shown to further improve the detection

limit, with the theoretical detection limit being 10^{-15} M due to the general limitations of enzyme catalysed reactions[39].

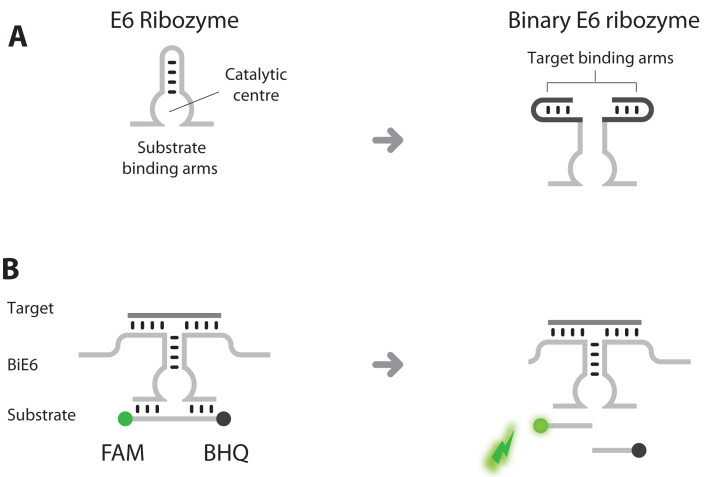

Figure 2.5: Design of the binary deoxyribozyme probe. A) Structure of the parent deoxyribozyme E6, which is transformed into the binary deoxyribozyme biE6 with hairpin forming target binding arms to reduce non-specific binding. B) Scheme for fluorescent detection of the analyte-dependent catalytic activity of biE6. FAM indicates fluorescein, BHQ is black hole quencher. Reproduced after Kolpashchikov *et al*.[38]

Further improvements in detection limit are possible with catalytic cascades, where a specific recognition event results in the activation of multiple DNAzymes and thus even stronger signal amplification. The group of Willner proved this concept for the detection of a SNP involved in the Tay-Sachse genetic disorder[40]. They made a combination of a Zn^{2+} dependent ligation DNAzyme and an Mg^{2+} dependent DNAzyme that cuts a fluorophore/quencher DNA substrate, resulting in fluorescence. Both DNAzymes are integrated in the binary probes, and thus depend on highly specific hybridization events before activation. In short, presence of the target strand opens a loop in the inactive Zn^{2+} ligation enzyme, which catalyses the ligation of a 5' imidazole modified DNA strand with a 3' hydroxylated DNA strand. This ligation product assembles the functional Mg^{2+} dependent DNAzyme, which cleaves another sequence, releasing a fluorescent reporter strand from its

quencher. Main advantage of this enzyme cascade is that the presence of one target molecule results in activation of multiple DNAzymes, allowing activation of multiple reporter molecules and thus enabling lower detection limits. With the most optimal assay design it is possible to detect the mutant with an SNP from the wild type 25bp DNA target at concentrations up to 10 pM.

Similar assays have also been performed with peroxidase like DNAzymes, which are more suited for POC diagnostics, as the colorimetric reaction does not require specialized readout equipment. Peroxidase DNAzymes are characterized by a high density of G triplet repeats, which bind with high affinity to hemine. The hemine is responsible for the catalytic activity of the DNAzyme as it can catalyze the oxidation of either 3,3'-Diaminobenzidine (DAB) or 2,2-azino-bus(3ethylbenzyiothiozoline-6-sulfonic acid) (ABTS2-) by means of H_2O_2 into their respective blue and brown coloured radicals. The first attempt to use this DNAzyme in a binary probe resulted in a somewhat poor detection limit of 1 μM.[41] The assay was further improved by splitting the DNAzyme asymmetrically, leading to a lower background signal due to a decreased tendency of the DNAzyme to self-assemble without the target strand. This method has also been applied for longer targets (up to 44bp), by the introduction of competing probes for the target sequence with a detection limit of 5 nM[42].

Combining DNAzymes with bimolecular beacons leads to even further improvements in assay detection limit[43]. Bimolecular beacons are two molecular beacons, which have complementary regions. When a target strand is present, it will bind to one of the molecular beacons (MB1), opening the stem-loop of MB1, which can then bind the second MB (MB2). Binding of MB2 with MB1 liberates the target, making it available for opening up another MB1. This process is called 'catalysed hairpin assembly' and will result in a self-propagating chain reaction of molecular beacon hybridization events.[44] The method as such can be also used in combination with DNAzymes to construct nanowires consisting of functional DNAzymes. The first configuration of this method had a detection limit of 10^{-9} M of target molecules[45] when combined with a magnesium DNAzyme that could cut a reporter oligonucleotide, releasing a fluorophore from a quencher. When this concept was combined with repeating horseradish like DNAzymes that

can catalyse the formation of a colorimetric substrate, an even more sensitive assay was created, capable of detecting SNPs in a 19bp target derived from the BRCA1 oncogene at concentrations of 10^{-13} M[46]. Although this assay is extremely sensitive, the long assay time of 4-6 hours necessary to reach this sensitivity is not suited for a POC diagnostic test. Therefore, it is currently combined with PCR for achieving better sensitivity in a shorter time period[47].

2.3.4 DNA junction forming probes

As an extension to the principles of binary probes, a combination is made between them and MBs, resulting in several advantages over both traditional strategies, foremost in an increased sensitivity and specificity. In general, the assay consists of 4 oligonucleotides that can only assemble in a DNA four-way junction in the presence of the analyte and a molecular beacon. Both binary probes have complementary regions to the analyte and at the same time have binding arms that are complementary to the MB separating the quencher from the fluorophore at the MB ends upon hybridization. However, the binary probes need sufficient conformational freedom to bind both the target oligonucleotide and the MB at the same time, which is ensured through connection of these binding domains by triethylene glycol linkers. In the absence of analyte, both the molecular beacon and the binary probes are in a stable hairpin form, limiting chances of non-specific hybridization. These junction probes are able to discriminate a SNP at any position in a 20bp target with a more clear discrimination than a conventional MB.[48] Moreover, the junction probes can be applied on analytes with strong secondary structures directly at room temperature without any loss of sensitivity towards the SNP,[49] showing a clear advantage over MBs on that aspect. The highly specific analytical power of junction probes[50] can also be used to analyse the presence of multiple interesting genetic markers in one target. In recent research, junction probes are applied to detect the presence of both a *Mycobacterium* specific sequence and an antibiotic resistance mutation (towards Rifampin) (Figure 2.6).

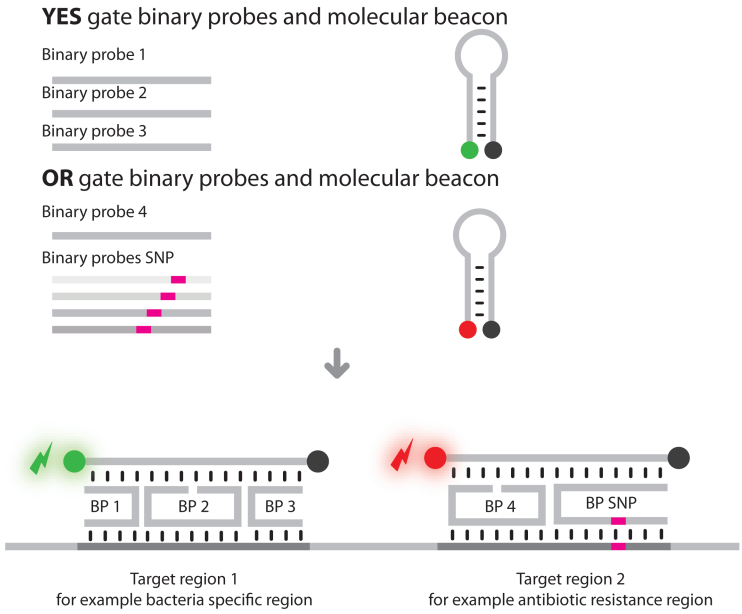

Figure 2.6: Design of the logic gate binary probe, designed to detect multiple regions in one target. The Yes gate is made of a first molecular beacon (MB1), that is combined with 3 different probes that only activate MB1 in the presence of the target DNA by hybridizing both with the target and the molecular beacon resulting in a highly specific detection. A next logic gate, is used to locate mutations in a particular locus, and is therefore named OR as its activation can be the result of multiple mutations. This logic gate uses a different molecular beacon (MB2) labelled with another fluorescent label. Activations is done by only two binary probes, one present in different versions, for all possible target mutations. Adapted from Cornett *et al.* [51]

This application used two junction probe designs to detect both a general locus present in all *Mycobacteria tuberculosis* and a SNP present only in Rifampin resistant strains of the *M. tuberculosis*. The combination of these junction probes results in a DNA 'Logic Gate'[52,53] meaning that the presence of none, one or two junction probe signals results in an NO, YES, OR, AND answer to two questions: 'Is there any *M. tuberculosis* present in the sample?' and 'Is this *M. tuberculosis* Rifampin resistant?'[51].

A variant of the initial junction probe, known as the three-way junction (Figure 2.7), is designed in such a way that the analyte binds

together with an assistant probe, probe B to a reporter sequence, probe A, containing both a quencher and fluorophores, forming thus a three-way motif. In the initial assay design the junction allowed the formation of a double stranded restriction enzyme recognition site in the reporter probe (probe A), resulting in the separation of the fluorescent label from the quencher and a detectable fluorescent signal[54]. The same process is repeated with a MB resulting in a sensitive self-recycling assay that can detect SNPs in short oligonucleotides at low concentrations[55]. This concept is applied successfully using different detection concepts, such as colorimetric, electrochemical and fluorescence detection[56-60].

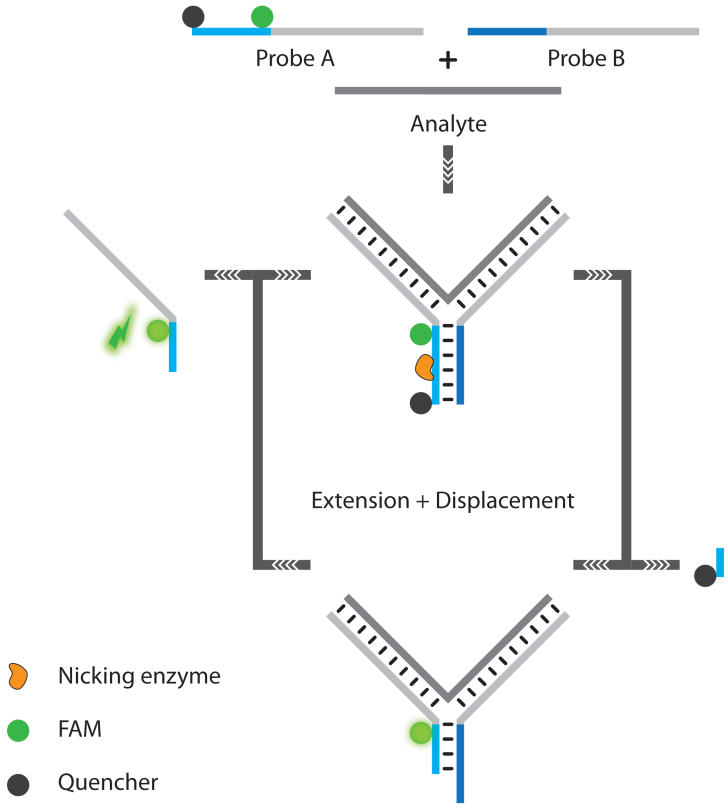

Figure 2.7: Three-way junction concept where the target strand and a reporter strand (probe A) can hybridize with the help of an assistant probe (probe B) into a 3-way structure. Only when this structure is formed, a restriction site is generated that liberates the quencher from the reporter. Afterwards the analyte can be recycled by denaturing the 3-way structure to activate a next reporter strand, resulting in signal amplification. Adapted from Nakayama *et al.*[54]

Werner and coworkers combined the three-way junction with silver nanoclusters, creating an assay that can identify the exact basepair substitution in the SNP. The assay is based on earlier research of the group, which states that a silver nanocluster can emit a fluorescent signal in the presence of particular basepairs and that the emission wavelength changes when these basepairs are altered. To apply this in a real assay, they labelled a reporter strand with silver nanoclusters (consisting of ± 30 silver atoms) and combined this with a complementary 'enhancer' strand, which formed a three-way junction in the presence of the target sequence[61]. Hybridization of both reporter and enhancer strand to the target moves the enhancer sequence in close proximity of the nanocluster, which results in a fluorescent signal. When a mutation is present in the target sequence, the enhancer sequence will be shifted, resulting in a change of the sequence in the local vicinity of the silver nanocluster leading to a corresponding shift of the fluorescence emission band of the silver nanocluster of up to 60 nm. The assay proved to be highly sensitive and can even discriminate easily between 3 out of 4 possible base variations for one SNP position. Furthermore the assay is applicable on both short (20bp) and long oligonucleotides (120bp). Although no LOD has been determined, the lowest concentration estimated from the calibration curve at which SNPs can be clearly discriminated is 2 μM.

2.3.5 Toehold mediated hybridization

Even though the above mentioned 'next generation' hybridization probes can be applied on complex targets harnessing secondary structures and are able to discriminate all types of SNPs in a target, they still rely in general on complex designs and require optimization for performance under particular conditions, such as ionic strength and temperature. Another type of structured probe, namely the toehold probe tackles these limitations[62]. Toehold probes are DNA duplexes where the reporter strand has a short extension, which is used as a nucleation site for hybridization with a complementary target strand (Figure 2.8).

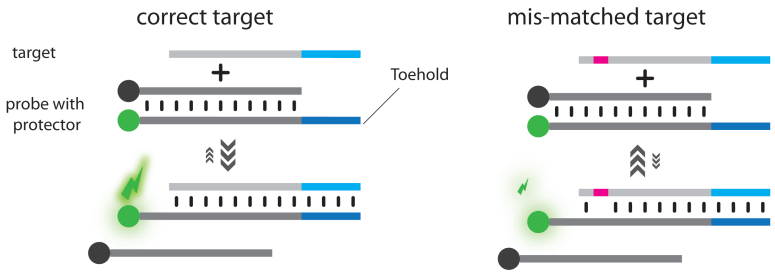

Figure 2.8: Toehold concept, where the reporter, is extended with a non-overlapping region, complementary to a region on the DNA target, which drastically increases hybridization speed and specificity when the reporter is hybridized to a protector containing strand (the protector is a fluorophore quenching molecule).

Toeholds were first applied for SNP detection by Z. Zhang *et al.* [63] and improved by Subramanian *et al.*[64] where they were used to initiate the formation of a DNA origami structure. The presence of a SNP in the target sequence inhibits the strand displacement of the toehold, resulting in the absence of the DNA origami complex. Each of the four possible A, C, G or T base pair substitutions results in the formation of a different DNA origami that corresponds to the letter of the displaced nucleotide. The origami structure itself is read out using an Atomic Force microscope.

Zhang *et al.* redesigned the original toehold probe into a SNP detection method, which is almost completely insensitive towards changes in temperature, salinity and target concentration[65]. This SNP detection consists of a fluorescently labelled reporter strand and its reverse compliment labelled with a quencher (Figure 2.9). The toehold reporter probe is designed in such a way that hybridization to both the quencher sequence and the complementary DNA target sequence are not fully overlapping, resulting in ssDNA toehold domain. In contrast with an original toehold, in this assay both hybridization events are catalysed with a toehold reporter probe. Without the reverse toehold, probes would discriminate nucleic acids on a single-base level using initial association kinetics, rather than thermodynamics, which would drastically limit the SNP discrimination power.

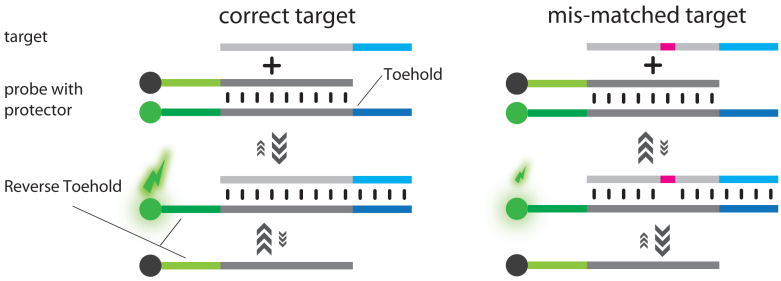

Figure 2.9: Toehold exchange assay according to D. Zang *et al.*[65]. In this assay, the reporter oligonucleotide contains a toehold domain that speeds up hybridization both to the target strand and the protector strand, resulting in a hybridization assay that is subject to equilibrium hybridization even under stringent conditions, such as high salinity, temperature variability and high DNA concentrations.

The presence of the toehold increases the kinetics of the displacement reaction, normally having a half-life of months under typical conditions to a half-life of 10s. This equilibrium-based toehold design is able to discriminate SNPs at any position in target sequences with a concentration of up to 1 nM even when secondary structures are present in the target. The hybridization yield does not change when excessive target is added (200x), when the temperature is varied over more than 20°C or if Mg^{2+} concentration is increased with several µmoles. However, a downside to this highly robust assay with the increased specificity is much slower reaction kinetics similar to all assays that rely on conformational constrained probes[66].

Table 2.1: Comparison of different hybridization probe based assays

Hybridization Mediated SNP Detection	Transducer	Optimization required	bp	LOD	Number and /or Position of Detected Mutation	Differentiation of Mutations	Assay Time
Single Hybridization probes							
Urakawa *et al.*[26]	Fluorescence (microarray)	For every Target	39	500 nM	All positions	Hybridization spot on the array	1 h
Milkani *et al.*[27]	SPR	For every target	21	100 pM	3' end - Middle - 5' end	Hybridization speed and yield	10 min
Molecular Beacons							
Tyagi *et al.*[67]	Fluorescence	No	26	100 nM	4 different alleles	Fluorophore emission spectrum	30 min
Binary DNA Probes							
Kolpashchikov[37]	Fluorescence	No	14	2 µM	All 42 possible basepair substitutions	Fluorescence yield	15 min
Kolpashchikov[38]	Fluorescence	No	20	80 nM	19 of 20 possible SNP positions	Fluorescence yield	2 h
Lu *et al.*[40]	Fluorescence	No	25	10 pM	1 SNP	Fluorescence yield	2 h
Kolpashchikov[41]	Colorimetric	No	29	1 µM	2 SNPs	Optical density	5 min
Deng *et al.*[42]	Colorimetric	No	40	20nM	SNPs at different positions	Optical density	5 min
Li *et al.*[44]	Colorimetric	No	25	1 nM	1 SNP	Optical density	30 min
Wang *et al.*[45]	Fluorescence	No	47	10 fM	No SNP tested	No differentiation	4-6 h
Shimron *et al.*[46]	Colorimetric	No	19	100 fM	1 SNP	Optical density	4-6 h
Dong *et al.*[47]	Colorimetric	No	29	100 zM	1 SNP	Optical density	40 min

Junction Forming Probes							
Grimes *et al.*[49]	Fluorescence	No	20	2.5 nM	9 different SNPs in a secondary structure containing target	Fluorescence yield	15 min
Cornett *et al.*[51]	Fluorescence	No	80	250 nM	4 SNPs discriminated in 2 loci	Fluorescence color/yield	15 min
Nakayama *et al.*[54]	Fluorescence	No	24	2 µM	3 SNPs containing targets	No differentiation	5 h
Kong *et al.*[55]	Fluorescence	No	23	5 pM	3 SNPs containing targets	No differentiation	30 min
Zhang *et al.*[59]	Electrochemical	No	24	760 fM	3 SNPs containing targets	Cyclic voltammetry	1 h
Yeh *et al.*[61]	Fluorescence	No	120	2 µM	11 positions with each 4 bp substitutions	Fluorescence emission shift	1 h
Toehold Mediated Hybridization							
Zhang *et al.*[63]	Atomic Force Microscopy	No	24	/	4 positions with different bp substitution	Change in origami structure	1-3 h
Subramanian *et al.*[64]	Atomic Force Microscopy	No	15	5µM	1 position with all 3 possible bp substitutions	Change in origami structure	3h
Zhang *et al.*[65]	Fluorescence	No	25	1 nM	16 positions with different substitutions	Fluorescence yield	20 min

2.4 Protein mediated SNP detection

Hybridization based assays have clearly evolved in the last 5 years both in specificity and sensitivity reaching a level where these assays can compete with other means of detection. However, they are still mainly applied to detection of SNPs in short oligonucleotides. Contrary to this, protein enzymes and mismatch binding ligands are not limited to the target oligonucleotide length. This can be explained by the fact that both protein enzymes and protein ligands recognize specifically the uncomplimentary base pairs, thereby not being constrained to hybridization processes for recognition of the SNP and as such have no limitation in target length.

2.4.1 Mismatch binding ligands

Mismatch binding ligands are a class of reporters that specifically recognize mismatched base pairs and bind to them with high affinity. One of the best-known mismatch binding ligands is the protein MutS, which is a part of the post replicative mismatch repair system of the *E. coli* bacterium. Recognition of a mismatch triggers structural conformational change of this protein, which results in MutS strongly binding mismatched base pairs. MutS can be applied for identifying a mismatch in a target directly on microarrays[68]. Another application for MutS can be to enhance the discriminative power of polymerase based assays. For example, Tan and co-workers showed that binding of MutS to a mismatch in a target-primer complex assisted in inhibition of the polymerase reaction upon the presence of a mutation[69]. Furthermore, MutS, in combination with a hairpin probe, is used in electrochemical assays for detection of SNPs. Here, the hairpin is used to detect the target DNA, by opening up in the presence of the target DNA, while in case of a mutation the electrical resistance is further increased upon binding of MutS to a SNP allowing sensitive and discriminative detection up to 100 pM of the target DNA[70]. The main limitation in use of MutS is the disability to discriminate among different mutations and to identify multiple mutations in one strand. These limitations can be prevailed by combining MutS with gold nanoparticles (Au NPs) labelled oligonucleotides complementary to the target sequence. When a

mismatch is present in the target strand, MutS binds to this Au NP-DNA complex. This influences the melting temperature resulting in a shift to higher values in the presence of MutS. The various nucleotide mismatches influence the melting temperature differently allowing to discriminate among base pair substitutions[71].

Another group of non-protein molecules, known as intercalators, with affinity for particular mismatches,[72] can also be used as mismatch binding ligands. Although some of these intercalating molecules have been applied for SNP detection,[73-75] they are not widely used because in general they can detect only a particular subset of base pair substitutions.

2.4.2 Ligation based SNP detection

Ligation enzymes catalyse covalent joining of two adjacent oligonucleotides in one strand. Strands can only be joined when the nick is located between fully adjacent nucleotides and if there is a perfect match between the template and the oligonucleotides at the nick. Landegren and coworkers were the first to exploit these properties of the enzyme in an assay where oligonucleotides were joined in the presence of a SNP[76]. Since then, the ligase enzyme is a popular tool for SNP detection as the combination of short oligonucleotide hybridization and the selective enzymatic activity ensures high assay specificity[77]. Ligase enzymes can be used in simple assays for SNP detection when combined with Au NPs[78,79]. One of these assays is based on the feature of DNA having a strong tendency to bind to the Au NP surface when in the single stranded form, a feature that is strongly diminished after hybridization into double stranded DNA. In the presence of a 24bp wild type strand, two ssDNA strands, of which one has a fluorophore, are ligated, allowing the target and the ligated product to form a stable double stranded helix. On the other hand, the presence of a SNP in the target molecule prevents ligation of the two ssDNA oligonucleotides. Because these two oligonucleotides are individually too short to form a stable double helix with the target molecule, they remain in ssDNA form and thus bind to the Au NP, which results in fluorescence quenching. Not only is this assay highly sensitive towards SNPs, it also has a fairly low LOD of 0.3 nM of target DNA.

In another ligation assay combined with Au NPs, different SNP mutations are discriminated in a 24bp target sequence using a colorimetric approach[79]. The assay relies on the hybridization of Au NPs to a glass slide surface, which are both modified with oligonucleotides complementary to the target strand. In the absence of a SNP in the target molecule, the Au NPs are ligated to the surface, followed by a signal enhancement through a silver deposition on the Au NPs. This assay allows even discrimination of SNP position in the target molecule because presence of mutations at increasing distance from the ligation site decreases the inhibitory influence on the ligation reaction. As a result, a gradual increase in ligation yield is visible with each shift in mutation position.

In a similar approach, ligation of Au NPs to a surface is measured in real-time with Surface Plasmon Resonance Imaging (SPRi). Surface plasmon resonance uses a partial coupling of the energy of a light wave with a noble metal, in order to measure refractive index changes at the noble metal surface[80], thereby enabling detection of surface events such as the binding of biomolecules. In SPRi, a Charge Coupled Device (CCD) camera is used to image the noble metal surface, which is prepared in an array format where each active spot is used as an SPR active measuring point. This layout greatly increases the measurement throughput. For SNP detection, each spot of the array is functionalized with different short oligonucleotides complementary to half of the target strand. The other half of the target strand is complementary to the oligonucleotide immobilized on the Au NPs surface. These capture oligonucleotides bare a different base at a known mutation site (A-T-C-G) of the target strand. Hybridization of target strands to the capture oligonucleotides on the SPRi spot triggers further hybridization with an oligonucleotide attached to Au NPs. Next, the Au NP-oligonucleotide and the capture oligonucleotide are ligated, but ligation will only occur on spots where a perfect sequence match is present at the ligation site, resulting thus in a covalent coupling of Au NPs to the corresponding array spot. Subsequent chemical denaturation, removes all non-ligated Au NPs, which results in a very specific signal present only at the patch of the array where a 100% complementary capture oligonucleotide is hybridized[81]. Although this method is innovative as mutations can be

detected at the nucleotide level, its applicability is limited as it is only applicable for known mutation sites.

Even more interesting is a POC concept that results in a highly sensitive assay, requiring only a couple of minutes without the need for any specialized instruments. Here, the highly specific ligation reaction is integrated in a lateral flow test and combined with the colorimetric properties of Au NPs[82,83]. As in the previous assay, presence of the target DNA results in the ligation of two oligonucleotides. However this assay uses oligonucleotides labeled with digoxin and the other one labeled with biotin. Antibodies specific for digoxin are immobilized on a detector zone of a nitrocellulose membrane (test zone), while molecules with high affinity towards biotin (being either an antibody or streptavidin) are immobilized on Au NPs. In the presence of the target strand, the nanoparticles are captured on the test zone, resulting in a colored band that can be seen with the bare eye.

The detection limit of ligation assays for SNP detection can be further improved when used to create padlock probes, which are circular templates for an isothermal amplification reaction known as rolling circle amplification (RCA) (Figure 2.10).

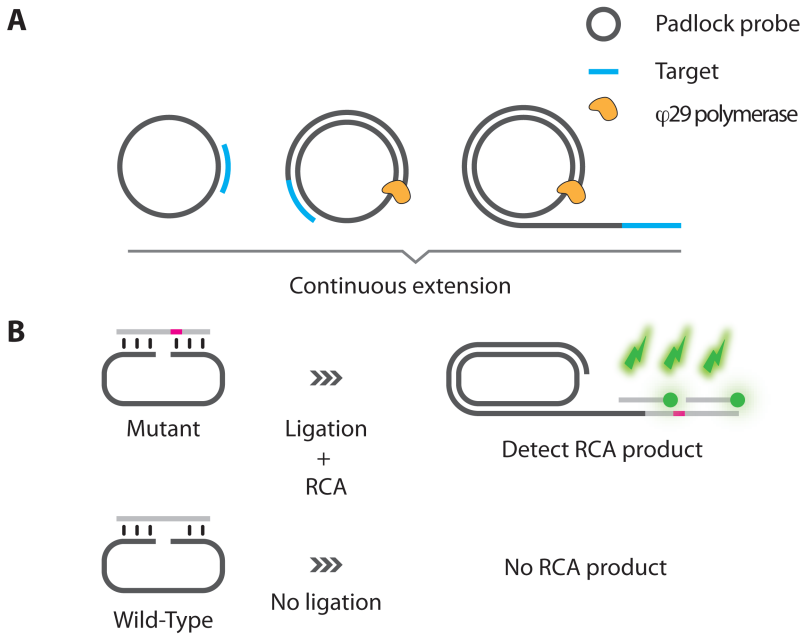

Figure 2.10: Rolling circle SNP detection concept: A) The rolling circle concept where a circular primer is used to repetitively extend a target sequence; B) the integration of SNP detection in rolling circle reaction: a padlock probe becomes circular only in the presence of a particular mutation (as indicated on the figure), or alternatively in the absence of SNP, depending on the assay design (not shown). The circular padlock is further extended and detected with a reporter oligonucleotide.

This reaction requires a special polymerase enzyme, phi29, which creates a ssDNA ribbon of repeating padlock sequences. RCA combines the specificity introduced by the ligation step with a strong signal amplification resulting from the high template copy numbers.[84] When further combined with Au NPs, a very sensitive colorimetric assay can be developed for SNP detection. The ligation of a circular primer into a padlock probe is initiated in the presence of the target strand. After the target has been amplified with RCA, its multiple copies can be cut out of the ssDNA ribbon using a restriction enzyme. These cut fragments interlink specifically Au NPs, resulting in a characteristic color shift of the gold solution, which is visible with the bare eye. Because of the high amplification efficiency of the RCA polymerase, the assay can reach a detection limit of 70 fM even in the presence of high copy numbers of wild type DNA.[85] A similar combination of RCA and Au NPs, but without

the restriction step, also allows sensitive surface enhanced raman spectroscopy (SERS) detection of SNPs in a target strand. This SERS based assay even outperformed PCR for SNP detection[86].

Zang and co-workers[87] further exploited the circular ligation concept, for developing an ultrasensitive SNP detection assay[88]. Here, the presence of a SNP in the target strand triggers formation of a circular ligation product on which multiple other circular templates can interlock by means of a complementary sequence. The interlocking circular primers contain DNAzymes, which are amplified with an RCA amplification, resulting in thousands of copies of the DNAzyme. This strategy allows creation of 1000 active enzymes, even if only a single SNP containing target strand is present, resulting in an ultrasensitive assay also when SNP expression is low. The assay was applied to detect the K-ras SNP and reached a detection limit of 71 aM even when applied directly on blood serum.

Although RCA offers an elegant target amplification strategy for ligation products, the ligase reaction on its own can also be used to amplify the target sequence. In a process called ligation chain reaction (LCR), a thermophilic ligase from *Thermus thermophilus* is used (tth ligase[89]) that enables multiple sequential ligation cycles. After each ligation reaction, the temperature is increased to denature the ligation product from the target sequence, making place for two new oligonucleotides to be ligated. The main advantage of this strategy is the high specificity of the reaction due to the ligation enzyme catalyzing the reaction only if the sequences at the nick are perfectly complementary and because hybridization at elevated temperatures is more specific. Nonetheless, this technology has never been very popular because the LCR products cannot be easily detected, except for laborious methods such as gel-electrophoresis[90,91]. However, recent developments have implemented the LCR reaction on new platforms allowing more straightforward detection of LCR products. For instance, Cheng *et al.* designed an assay to fluorescently detect LCR products by using a cationic conjugated polymer (CCP)[92]. The assay uses two sets of probes, one complementary to the target DNA and another one to the reverse complement. In the presence of the target, the first set of probes, complementary to the WT target, is ligated creating a new template for the ligation reaction of the second set of probes. This enables an

exponential amplification of the target sequence. Subsequently, the CCP is added and binds electrostatically to the negatively charged DNA. Because CCP has unique light absorbing properties[93], it is used to transfer excitation energy to a 5' FAM label on the ligation probes, resulting in a strong fluorescence of LCR products. Non-ligated products are degraded with exonuclease I and exonuclease III. Resulting FAM labelled monomer by-products have only a very weak affinity for CCP leading to a low background signal. The assay allowed detection of targets up to 1 fM and could be applied on mixtures of WT and mutated DNA.

Trau and co-workers used a somewhat similar approach to allow electrochemical detection of LCR products[94]. In short, they showed that a successful LCR could both be detected by the intercalator methylene blue that changes the redox current or by a HRP labelled probe through electrocatalytic reduction of hydrogen peroxide. The second approach proved to be more useful as it was able to detect the target strand at 100 times lower concentrations and with higher specificity than the methylene blue approach. Albeit, HRP remains a bit unpractical for POC integration as the reaction requires a continuous stream of H_2O_2, which is not a stable component.

Finally, a method was developed to monitor LCR in real-time[95,96] ligating, in the presence of a target sequence, probes immobilized on Au NPs. Therefore, in every cycle of the LCR reaction, an increasing fraction of the Au NPs is ligated, leading to an increasing amount of closely linked Au NPs. Their interlinking results in a characteristic shift in the absorption band of the Au NPs solution, which is monitored in real time using a standard spectrophotometer. The resulting assay has a very wide dynamic range spanning 6 orders of magnitude with a detection limit of 20 aM and strong discriminative power, even in the presence of 1500x excess of mutant target DNA.

Next to ligases, another class of enzymes, so called nicking enzymes, can be used for recognition of specific sequences, which is followed by cutting one of the strands in the double stranded DNA. Although they can only recognize a particular subset of sequence motives, which is limiting their universal use, they can be used in combination with a three-way junction for specific target recycling[97,98]. This strategy was

applied for developing an ultrasensitive and specific assay in combination with MBs[99]. In this assay, a MB is nicked when forming an Y junction, which can only be created in the presence of a target molecule. The opened MB serves afterwards as a primer for an RCA reaction, while the target molecule is recycled. The RCA product allows specific hybridization of multiple quantum dots, which are measured with voltammetry after being dissolved in acid. The assay has a dynamic range of 6 orders and a detection limit of 11 aM. Similar strategies for target recycling using nicking enzymes but without RCA are applied and can also reach sub-femtomolar detection limits without losing specificity, thus proving the versatility of the method[100-102].

Target recycling can also be achieved with exonucleases, which independently catalyse the degradation of the target reporter duplex starting at the single stranded part of a blunt or recessed 3' end. They were first used in combination with MBs in order to digest the MBs that get opened upon target binding, freeing thus the target-sequence (Figure 2.11)[103]. This strategy has two advantages, the target is released from the MB and can bind another one, while the fluorophore is separated permanently from the quencher of the degraded MB. This approach allows reaching a much lower detection limit than a classic MB assay with the same amount of target DNA without any loss in specificity. A similar target recycling strategy is applied for SNP detection by Xuan *et al*. on an electrochemical detection platform[104]. In their assay, target binding opens the stem of a MB resulting in its enzymatic digestion and release of a methylene blue labelled nucleotide. This nucleotide can bind with a much higher efficiency to a negatively charged indium thin oxide (ITO) electrode than the MB, because the repulsive negative charges between ITO and the single nucleotide are lower than the ones between ITO and MB. The assay can detect label free, pM concentrations of the target sequence while differentiating SNPs with a high specificity. The sensitivity of this strategy is further improved by Tang and co-workers, who used the liberation of a DNAzyme upon exonuclease III digestion[105] instead of a labelled nucleotide. This led to an improvement of one order of magnitude in detection limit to 10 fM, while specificity towards SNP detection was unaffected.

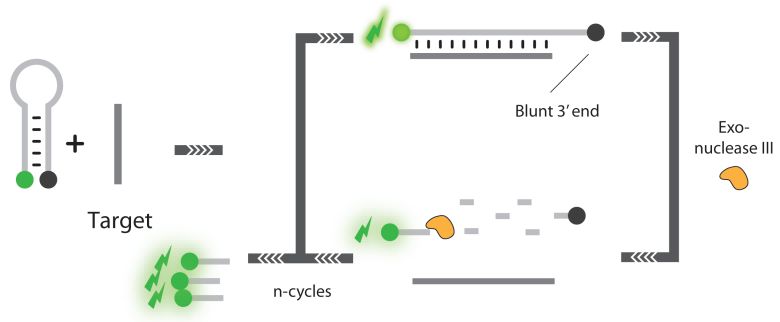

Figure 2.11: Target recycling concept combining a MB with exonuclease III to liberate the target after bound with the MB. Because a blunt end is created at the 3' end of the MB, only the MB will be degraded, separating the quencher from the fluorophore, while the target can open a new MB in a next round of exonuclease III degradation. According to Zuo *et al.*[103]

A new type of nuclease, known as CEL1 endonuclease, combines the mismatch specificity of mismatch binding enzymes with exonuclease activity. The enzyme is therefore used to increase the sensitivity of SNP analysis on a microarray, as the enzyme can detect mismatches, inserts and deletions of up to 12bp initiating degradation of mismatched oligonucleotides. Performing SNP analysis on a microarray requires highly specific hybridization, which can be achieved by lowering the salt concentrations and adjusting the hybridization temperature close to the target melting temperature. Because this approach lowers the sensitivity of the assay severely, CEL1 endonuclease is used to digest all mismatched DNA on the microarray before readout of the fluorescent signal. One of the first applications of CEL1 endonuclease was improving microarray screening for antibiotic resistance in *Klebsiella pneumoniae*[106]. The same strategy can be used on DNA biosensor platforms to increase the specificity and sensitivity towards a DNA target of interest as shown recently[107].

Table 2.2: Comparison of different protein mediated hybridization assays

Protein Mediated SNP Detection	Transducer	Optimization required	bp	LOD	Number and /or Position of Detected Mutation	Discriminate Between Mutations	Assay Time
Mismatch Binding Ligands							
Jiao *et al.*[69]	Fluorescence	No	21	20 nM	2 SNPs	No discrimination	30 min
Cho *et al.*[71]	Colorimetric	No	21	1 μM	4 SNPs	Shift in melting temperature	80 min
Ligation Based SNP detection							
Wang *et al.*[78]	Colorimetric	No	24	300 pM	1 SNP	No discrimination	30 min
Xue *et al.*[79]	Colorimetric	No	24	1 nM	5 positions with different SNPs	Grayscale	10 min
Li *et al.*[81]	SPRi	No	36	1 pM	1 position with all 3 basepair substitutions	Location of SPRi spot	15 min
Toubanaki *et al.*[82]	Colorimetric LFA	No	40	12.5 fM (after PCR)	1 SNP	Position LFA membrane	20 min
Li et *al.*[85]	Colorimetric	No	30	70 fM	1 SNP	No discrimination	3.5 h
Hu *et al.*[86]	Raman spectroscopy	No	32	10 pM	1 SNP	No discrimination	2 h
Bi *et al.*[88]	Chemiluminiscence	No	39	71 aM	1 SNP	No discrimination	1.5 h
Cheng *et al.*[92]	Electrochemical	No	51	1 fM	1 SNP	No discrimination	3 h
Shen *et al.*[96]	Colorimetric	No	45	20 aM	2 SNPs	No discrimination	1.5 h
Nicking Enzymes							
Ji *et al.*[99]	Electrochemical	No	23	11 aM	1 SNP	No discrimination	2.5 h
Xu *et al.*[108]	Colorimetric	No	27	500 aM	3 SNPs	No discrimination	30 min
Exonuclease							
Zuo *et al.*[103]	Fluorescence	No	27	7.8 nM	1 SNP	Fluorescence yield	30 min
Liu *et al.*[105]	Electrochemical	No	15	10 fM	1 SNP	Current	2.5 h
Gao *et al.*[107]	Electrochemical	No	/	1 fM	1 SNP	/	2h

2.5 SNP detection through thermal denaturation of hybrids

Enzymes are effective tools for detection of SNPs even in the presence of complex media such as blood. However, most of the enzymatic SNP assays are only applicable on known mutations, which is just a fraction of those causing diseases[109]. Moreover, the capability of detecting unknown mutations allows following up on acquisition of new mutations[110,111]. Therefore, methods, such as DNA melting that allow screening of mutations in a much more generic way, are appreciated alternatives.

When a DNA duplex is thermally denatured, the temperature at which half of the strands are in the fully hybridized state, while the other half is in the single stranded state, is known as the melting point (T_m) and is highly sequence dependent. Changes in the DNA sequence have a direct effect on the thermodynamic stability of the DNA duplex resulting in a predictable change in T_m[112-114]. However, DNA melting was initially not easily applicable for identifying SNPs routinely as the minimal thermodynamic effect of a SNP on a DNA double strand could not be detected with then standard fluorescent intercalating dyes. These intercalating dyes are fluorescent molecules that increase their fluorescence upon binding double stranded DNA. However, because intercalating dyes inhibit PCR, they are used at non-saturating concentrations, at which the dye can redistribute during the DNA melting process to the remaining double stranded part of the DNA complex, resulting in a hampered resolution of the melting curve. Initially, this problem was solved using specially designed fluoresence resonance energy transfer (FRET) hybridization probes, which even allowed multiplex melting analysis of different targets using multiple fluorescent dye molecules[115]. Later on, the technology was made generally applicable by introducing saturating dyes. These dyes can be used at a much higher concentration without PCR inhibition. As a result, monitoring of DNA melting is made available at unmet resolution without the use of labelled detection probes, providing a universal SNP detection platform.[116] The technology has been commercialized and is gaining popularity as a worthy alternative for differential gel electrophoresis,[117] the golden standard technique for mutation

detection, which is based on gel separation of PCR products with mutations.

DNA melting, is also being applied as a first line fast mutation screening tool to identify possible mutational hotspots[118,119]. Nonetheless, the technology is not perfect and requires optimization for detection of some types of mutations such as base pair neutral mutations, where for example a G:C from C:G is mutated or A:T from T:A base-pair[120]. Recently, new developments have been made in the field of DNA melting technology increasing both sensitivity and applicability of the method. In general, one can distinguish two approaches in DNA melting analysis, liquid and solid phase DNA melting methods.

2.5.1 Liquid phase DNA melting

Liquid phase DNA melting monitors the denaturation of DNA free in solution and, in comparison with solid surface melting, the DNA does not need to be chemically modified for surface immobilization. Furthermore, the method can be applied immediately after PCR as the saturating intercalating dye does not inhibit amplification, which even allows monitoring the amplification process, thereby resulting in both quantification and direct identification of amplicons. As the technology has mostly been used in combination with a traditional PCR sample preparation and on bulky high resolution melting (HRM) enabled qPCR devices, the technology was for a long time considered as not being fit for POC concepts. In an attempt to solve this problem, Crews *et al.* integrated DNA melting analysis in a microfluidic chip[121]. Here, the liquid flows through a microfluidic channel over a temperature gradient. While the sample is slowly heated along this gradient, the DNA double strand is melted, which is visible by a decrease in the fluorescence intensity of the intercalating dye. As the position along the microfluidic channel, where the fluorescence signal is switched off, represents the melting point, this method is called spatial DNA melting. Spatial DNA melting allows monitoring both DNA denaturation and renaturation along the temperature gradient since the fluorescence intensity increases when leaving the temperature gradient in the opposite direction as a result of gradual re-annealing of the DNA duplex. The method proved to be highly sensitive towards SNPs and allowed to discriminate heterozygous mixtures of WT and mutant DNA in real

clinical samples even when targets exceeded 150bp. The concept was further developed and integrated in a chip for direct genotyping from a human saliva sample[122] proving the applicability of the concept.

Another label free DNA melting approach is to monitor the change in movement of the molecule rather than the change in fluorescence. This method is called thermophoresis and has some particular advantages over traditional DNA melting. The movement of molecules in a temperature gradient depends on their size, charge, ionic shielding and hydration, implying that change in any of these parameters can be monitored by the changes in thermophoresis. Using this method, Wienken *et al.* were able to detect SNPs of target sequences in very low sample volumes (250 nl). Although thermophoresis has only been applied on short oligonucleotides (22bp) at high concentrations (1 μM), the method is very sensitive towards secondary structures and nucleotide modifications such as methylation[123].

Currently, one of the major limitations of DNA melting is that the small free energy difference caused by the polymorphisms results in only a minimal variation of the melting profile measured as a function of change in fluorescence intensity, requiring careful experimental design and data analysis. Lee *et al*. designed a strategy to amplify the thermal dynamic difference allowing easy discrimination of mutations. By monitoring DNA melting inside an optofluidic cavity that is excited with a laser, a gain in laser signal intensity is realized that is dependent on the hybridization state of the DNA in the cavity[124]. As can be noted in this assay, the generated laser output of the optical cavity is monitored instead of fluorescence, which results in a strong amplification of the signal. The method is highly sensitive and can detect a SNP in a 100bp target with 25x signal intensity difference between the WT and the mutant DNA, allowing more easy discrimination of SNPs in comparison with standard HRM. However the method is only proven to work at very high DNA concentration (250 μM), limiting this technique to post PCR DNA melting analysis.

DNA melting technologies are also limited in their ability to detect multiple targets in parallel in one sample. This is due to the fact that only one intercalating dye can be used at a time, resulting in the detection of only a single target. In recent work, Li and co-workers,

increased the potential for multiplexing both DNA melting assays and PCR by combining different fluorescent labels with T_m labels, creating a two-dimensional label (Figure 2.12)[125]. The assay uses two different oligonucleotides that are ligated together in the presence of the specific target sequence. The two oligonucleotides consist of different domains necessary for multiplexing.

Both right and left ligating probe have a genomic DNA-specific binding site and primers, whereas the left ligating oligonucleotide also contains a T_m tag. The T_m tag is a sequence not complementary to the target. For each target a unique set of T_m tags is made which are ligated in the presence of particular local SNPs. The specificity of the ligation reaction allows introduction of a different tag if the target contains a particular SNP. Because each T_m tag comes with a different sequence variation, their melting temperatures are diverse. After the tag is ligated, the ligation product containing the temperature tag is amplified with an asymmetric PCR and probes are used to hybridize to the amplified tags. Finally a melting analysis is performed to identify the amplified tags. Performing simultaneous genotyping of 48 forensic SNPs occurring on 23 different human chromosomes proved the usefulness of the assay.

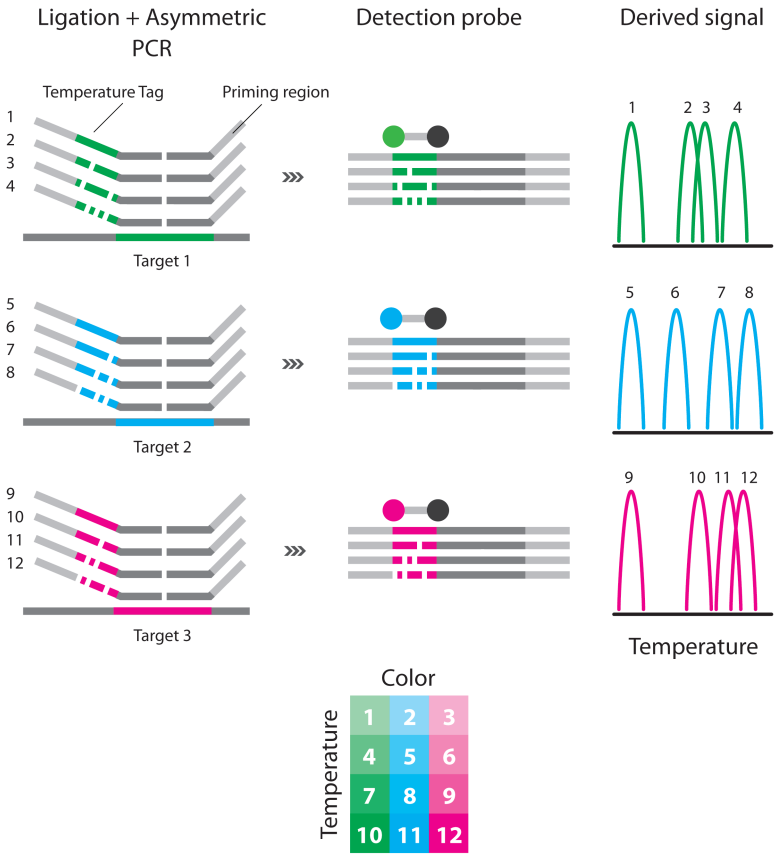

Figure 2.12: Combination of fluorescent labels and ligation labels that affect melting temperature in order to increase multiplexibility of SNP assays. Each target has its own fluorescent label, while internal target variation (SNPs) results in ligation of an extra tag (T_m tag), which is incorporated in the asymmetric PCR product. The amplified tags are used to identify the target and the resulting change of melting temperature is used to generate a 2D label. Figure reproduced according to Liao *et al.*[125]

Therefore three different reactions using each a unique T_m tag, allowed identifying 32 possible alleles per reaction, resulting in a total of 96 identified alleles. The robustness of the method was proven by its direct application on clinical samples.

2.5.2 Surface-immobilized DNA melting

DNA melting performed on a surface has some advantages over liquid phase melting, such as extra options to increase sensitivity and

parallelization of DNA analysis[126,127] that compensate for the possible downsides, mostly being slow hybridization kinetics due to steric hindrance and electrostatic repulsion,[128,129] as well as the need for labeled oligonucleotides for surface immobilization[130]. To overcome the first limitation, extensive research has been done on surface immobilization methods. It has become clear that the density and conformation of the DNA on the sensor surface are critical for hybridization efficiency[131-133]. These two parameters can be carefully controlled using small alkane thiol molecules or extending the oligonucleotides with adenine repeats, known to have high affinity for gold surfaces. Both approaches help organizing the DNA strands on the sensor surface while also diluting the strands on the surface, which results in better accessibility of the target strands and improved hybridization kinetics[134-138]. Other options include the use of small internal complementary DNA strands that can boost hybridization kinetics on surfaces by assisting in DNA organization and presentation, a strategy that can result in a 5-fold increase in hybridization rate[139]. Moreover, new strategies allow DNA surface immobilization within minutes[140], making it an easy procedure. Lastly, it has been even shown that labeling is not a necessity for surface immobilization[141].

Mirkin and co-workers were the first to show the great potential for DNA melting assays on surfaces[142]. They discovered enhanced resolution in melting analysis when DNA is immobilized on Au NPs, the so-called spherical nucleic acids. In comparison with DNA melting in solution, where the melting phase occurs over a range of approximately 20 °C, gold labeled DNA has a melting transition over a very narrow temperature range (ca. 2-8°C) which is shifted to a higher temperature range. One explanation for this melting behavior is the number of inter-particle connections at the nanoparticle surface, which results in a collectively stronger bond that melts at higher temperatures. Together with a higher local salt concentration at the NP surface, this cooperative binding results in a more narrow melting transition. This was proven by a broader melting transition when the number of strands, and consequently the number of inter-particle connections on the nanoparticle surface, were diluted[142,143]. Using this enhanced melting resolution, Stehr *et al.*, designed a SNP detection assay, in which Au NPs acted both as carriers of reporters for the target DNA and local heating

elements[144,145]. As stated earlier, Au NPs have a strong light adsorption wavelength, which varies with the size of the nanoparticle. When a pulsed laser source is used at this specific adsorption band of the Au NPs, an optothermal conversion can be realized. Au NPs transform light into thermal energy, resulting in a fast temperature increase in the local nanoparticle surrounding. This highly sensitive and fast SNP assay is capable of performing DNA melting analysis for SNPs in a 30bp target strand in less than a millisecond.

Although DNA melting on nanoparticle surfaces allows better melting transitions, their monitoring is limited to either use of laser absorption or scattering techniques such as dynamic light scattering (DLS) or classic spectrometry based methods[146]. These techniques are all somewhat limited in sensitivity as they measure a bulk effect and do not support easy real-time monitoring of the melting process. Other options include electrochemical sensors such as the one recently described to monitor the transition from single stranded to double stranded DNA[147]. By immobilizing the complementary DNA strand of a 29bp target on a diamond surface, which allows excellent thermal conduction, the biosensor is used to monitor DNA binding during temperature cycling. Because the solution was heated from below the diamond sensor surface, the authors observed a strong heat transfer resistance when DNA was single stranded, while the resistance was not present when the DNA was in a double stranded state. Using this principal of heat resistance, the authors can derive the melting point of the DNA duplex from the temperature measurement at the sensor surface corrected for the heating power input. This method made SNP detection readily available on a cheap platform, with a sub nanomolar (600 pM) sensitivity, although the concept was only able to detect SNPs in short oligonucleotides.

As discussed earlier, SPRi allows direct measuring of DNA behaviour at a surface in real-time and with high precision, making this technology ideally suited for DNA melting. Fiche *et al.*, were one of the first to implement continuous real-time DNA melting monitoring on an SPRi chip[148]. This strategy allowed detection of SNPs in short oligonucleotides, albeit at high DNA concentrations (1 µM). The assay was further optimized towards a universal HRM protocol on microarrays for detection of low abundant DNA with mutations[149]. By

using temperature cycling, they were able to concentrate the target DNA on the array surface. Hybridization at the optimal temperature of the target sequence allowed a 10-fold increase in hybridization of mutated DNA on the surface in comparison with the sample content. This approach lead to ultrasensitive detection of mutated DNA in heterozygous mixtures even when the DNA of interest was present at a fraction (1%) of total DNA concentration. Nonetheless, in general, these melting transitions did not show the same narrow melting transitions as observed on the nanoparticles surfaces (<10°C) because the assay monitors melting behavior of unlabeled DNA strands.

These limitations will be addressed in the next chapters of this dissertation, where the narrow melting transitions of Au NPs will be combined with SPR real-time monitoring of the melting process, enabling great possibilities for SNP detection. The combination of SPR and gold nanoparticle melting analysis is only possible due to an in-house developed FO-SPR platform integrated in a fiber-optic dipstick (FO-SPR), which can be handled more easily and allows precise temperature control, even at elevated temperatures.

Table 2.3: Comparison of different solid phase hybridization assays

SNP Detection Through Thermal Denaturation of Hybrids	Transducer	Optimi-zation Required	bp	LOD	Number and/or Position of Detected Mutation	Discriminate Between Mutations	Assay Time
Liquid Phase DNA Melting							
Crews *et al.*[121]	Fluorescence	No	190	PCR amplified	Different SNPs, heterozygous	Melt profile	2-90 min
Wienken *et al.*[123]	Thermophoresis	No	22	1 µM	SNPs, but especially sensitive to methylation	No discrimination	1 h
Lee *et al.*[124]	Laser intensity	No	100	250 µM	1 SNP	Laser intensity	/
Liao *et al.*[125]	Fluorescence	No	100	PCR	48 SNPs	2D label	2 h
Solid Phase DNA Melting							
Stehr *et al.*[144]	Colorimetric	No	30	1 µM	1 SNP	Extinction time	Milliseconds
Van grinsven *et al.*[147]	thermal resistance	No	29	600 pM	3 SNPs	Melting temperature	2 h

2.6 Conclusion

The last 3 years have seen a remarkable evolution in SNP detection techniques, leading to unmet resolution by employing albeit simple but clever techniques. This evolution has made classic labor intensive assays such as DGGE, PCR, FISH and others obsolete and allowed the design of simple and fast SNP assays that can be integrated in POC tests. In general, the improvements in SNP detection have been achieved with technological advances in one of the following three domains:

1. Hybridization sensitivity
2. Enzymatic cascades
3. Thermal DNA denaturation

Better understanding of processes that determine the speed and specificity of hybridization have enabled the design of target specific DNA probes for detecting SNPs at room temperature. Employment of specific short hybridization oligonucleotides resulted in more sensitive and robust SNP detection. Furthermore, integration of binary and ternary probes, which rely on independent hybridization events, resulted in both high specificity and sensitivity within the same assay. This was achieved by activation of a label only when all probes are hybridized to the target strand. Although these advanced hybridization probes are ideally suited for SNP detection, they still rely on complex DNA binding probe designs. This problem has been addressed by the reversible toehold, a universally applicable concept that allows to make hybridization probes insensitive to external factors, such as temperature and ionic concentration, for their specificity and sensitivity. This enabled SNP identification under almost any condition.

A lot of efforts have been made to make SNP assays work at low target concentrations. Therefore several strategies have been employed to strongly amplify SNP detection signals, such as use of multiple enzymes for SNP detection. Also, some enzymes only work in case of a perfect sequence match, so enzymes not only increase sensitivity but can also be used to enhance reaction specificity. One of the most important findings in the last decade are so-called enzymatic cascades, which rely on the activation of multiple enzymes in the presence of the

target sequence resulting in detection limits that can compete or even outperform PCR DNA amplification. This is very important, as PCR is known to introduce errors while amplifying target sequences, which decreases the sensitivity of the method[150]. Another important concept introduced through this approach is enzymatic target recycling. In this concept specific enzymes degrade the reporter probe while bound to the target sequence allowing the next reporter to bind to the target. These self-amplifying strategies result in highly sensitive assays, whilst maintaining specificity.

Lastly, a lot of research has been done on the improvement of DNA analysis by monitoring thermal denaturation, as this assay allows screening for unknown mutations. Of all new techniques, HRM is the only one that is becoming a standard procedure both in research and in clinical laboratories[151]. New developments have made the technology even more versatile, especially the application of the technology on Au NP supports, resulting in improved SNP sensitivity. Furthermore the first microfluidic integrated POC test based on the DNA melting assays has seen the light, proving that bulky thermocyclers are not a necessity for HRM.

In light of these conclusions, the following chapters of this dissertation will describe the implementation of novel bioassays for SNP detection on a FO-SPR biosensor. This miniaturized and robust, real-time biosensor will allow us to evaluate directly some of the above-mentioned assays for the detection of micro-organisms. Because the FO-SPR biosensor will be particularly suited for solid phase melting analysis, the focus will be on this assay in combination with enzyme based target amplification, to allow both specific identification and sensitive detection within a reasonable time period.

References

1. K. A. Frazer, S. S. Murray, N. J. Schork and E. J. Topol, *Nat. Rev. Genet.*, 2009, **10**, 241-251.
2. D. W. Bianchi, *Nat. Med.*, 2012, **18**, 1041-1051.
3. C. Lerman, J. Seay, A. Balshem and J. Audrain, *Am. J. Med. Genet.*, 1995, **57**, 385-392.
4. R. S. Vasan, *Circulation*, 2006, **113**, 2335-2362.
5. P. M. Farrell*, et al.*, *Pediatrics*, 2001, **107**, 1-13.
6. M. W. Leigh*, et al.*, *Genet. Med.*, 2009, **11**, 473-487.
7. E. Van Cutsem*, et al.*, *J Clin Oncol*, 2011, **29**, 2011-2019.
8. R. Rosell*, et al.*, *Lancet Oncology*, 2012, **13**, 239-246.
9. D. Gonzalez de Castro, P. A. Clarke, B. Al-Lazikani and P. Workman, *Clin. Pharmacol. Ther.*, 2013, **93**, 252-259.
10. N. Papadopoulos, K. W. Kinzler and B. Vogelstein, *Nat. Biotechnol.*, 2006, **24**, 985-995.
11. L. B. Rice, *Clin. Infect. Dis.*, 2011, **52**, S357-S360.
12. M. S. Dryden, J. Cooke and P. Davey, *J. Antimicrob. Chemother.*, 2009, **64**, 885-888.
13. P. C. Ng, S. S. Murray, S. Levy and J. C. Venter, *Nature*, 2009, **461**, 724-726.
14. M. L. Metzker, *Nat. Rev. Genet.*, 2010, **11**, 31-46.
15. N. J. Loman, R. V. Misra, T. J. Dallman, C. Constantinidou, S. E. Gharbia, J. Wain and M. J. Pallen, *Nat. Biotechnol.*, 2012, **30**, 562-562.
16. L. Mamanova*, et al.*, *Nat. Meth.*, 2010, **7**, 479-479.
17. P. M. Milos, *Expert Rev Mol Diagn*, 2009, **9**, 659-666.
18. T. J. Treangen and S. L. Salzberg, *Nat. Rev. Genet.*, 2012, **13**, 36-46.
19. I. N. Okeke*, et al.*, *Drug Resist. Updates*, 2011, **14**, 95-106.
20. J. C. Palomino, *FEMS Immunol. Med. Microbiol.*, 2009, **56**, 103-111.
21. C. C. Boehme*, et al.*, *N. Engl. J. Med.*, 2010, **363**, 1005-1015.
22. J. D. Roberts*, et al.*, *Lancet*, 2012, **379**, 1705-1711.
23. C. A. Evans, *PLoS Med*, 2011, **8**, e1001064.
24. J. C. Davis, L. Furstenthal, A. A. Desai, T. Norris, S. Sutaria, E. Fleming and P. Ma, *Nat Rev Drug Discov*, 2009, **8**, 279-286.
25. V. V. Demidov and M. D. Frank-Kamenetskii, *Trends Biochem. Sci.*, 2004, **29**, 62-71.
26. H. Urakawa*, et al.*, *Appl. Environ. Microbiol.*, 2003, **69**, 2848-2856.

27. E. Milkani, S. Morais, C. R. Lambert and W. G. McGimpsey, *Biosens Bioelectron*, 2010, **25**, 1217-1220.
28. G. Bonnet, S. Tyagi, A. Libchaber and F. R. Kramer, *Proc. Natl. Acad. Sci. U. S. A.*, 1999, **96**, 6171-6176.
29. I. G. Panyutin and P. Hsieh, *Proc. Natl. Acad. Sci. U. S. A.*, 1994, **91**, 2021-2025.
30. Y. Krishnan and F. C. Simmel, *Angew Chem Int Edit*, 2011, **50**, 3124-3156.
31. S. Tyagi and F. R. Kramer, *Nat. Biotechnol.*, 1996, **14**, 303-308.
32. S. D. Lawn*, et al.*, *Lancet Infect. Dis.*, 2013, **13**, 349-361.
33. C. C. Boehme*, et al.*, *N. Engl. J. Med.*, 2010, **363**, 1005-1015.
34. A. Niemz, T. M. Ferguson and D. S. Boyle, *Trends Biotechnol.*, 2011, **29**, 240-250.
35. C. D. Chin, V. Linder and S. K. Sia, *Lab Chip*, 2012, **12**, 2118-2134.
36. J. R. Babendure, S. R. Adams and R. Y. Tsien, *J. Am. Chem. Soc.*, 2003, **125**, 14716-14717.
37. D. M. Kolpashchikov, *J. Am. Chem. Soc.*, 2005, **127**, 12442-12443.
38. D. M. Kolpashchikov, *ChemBioChem*, 2007, **8**, 2039-2042.
39. Y. V. Gerasimova, E. Cornett and D. M. Kolpashchikov, *ChemBioChem*, 2010, **11**, 811-817, 729.
40. C. H. Lu, F. A. Wang and I. Willner, *J. Am. Chem. Soc.*, 2012, **134**, 10651-10658.
41. D. M. Kolpashchikov, *J. Am. Chem. Soc.*, 2008, **130**, 2934-2935.
42. M. G. Deng, D. Zhang, Y. Y. Zhou and X. Zhou, *J. Am. Chem. Soc.*, 2008, **130**, 13095-13102.
43. P. Yin, H. M. Choi, C. R. Calvert and N. A. Pierce, *Nature*, 2008, **451**, 318-322.
44. B. Li, A. D. Ellington and X. Chen, *Nucleic Acids Res.*, 2011, **39**, e110.
45. F. Wang, J. Elbaz, R. Orbach, N. Magen and I. Willner, *J. Am. Chem. Soc.*, 2011, **133**, 17149-17151.
46. S. Shimron, F. Wang, R. Orbach and I. Willner, *Anal. Chem.*, 2012, **84**, 1042-1048.
47. J. Dong, X. Cui, Y. Deng and Z. Tang, *Biosens. Bioelectron.*, 2012, **38**, 258-263.
48. D. M. Kolpashchikov, *J. Am. Chem. Soc.*, 2006, **128**, 10625-10628.
49. J. Grimes, Y. V. Gerasimova and D. M. Kolpashchikov, *Angew Chem Int Ed Engl*, 2010, **49**, 8950-8953.
50. D. M. Kolpashchikov, Y. V. Gerasimova and M. S. Khan, *ChemBioChem*, 2011, **12**, 2564-2567.

51. E. M. Cornett, E. A. Campbell, G. Gulenay, E. Peterson, N. Bhaskar and D. M. Kolpashchikov, *Angew Chem Int Ed Engl*, 2012, **51**, 9075-9077.
52. Y. V. Gerasimova and D. M. Kolpashchikov, *Chem.--Asian J.*, 2012, **7**, 534-540.
53. G. Seelig, D. Soloveichik, D. Y. Zhang and E. Winfree, *Science*, 2006, **314**, 1585-1588.
54. S. Nakayama, L. Yan and H. O. Sintim, *J. Am. Chem. Soc.*, 2008, **130**, 12560-12561.
55. R. M. Kong*, et al.*, *Anal. Chem.*, 2011, **83**, 14-17.
56. J. Li, X. J. Qi, Y. Y. Du, H. E. Fu, G. N. Chen and H. H. Yang, *Biosens. Bioelectron.*, 2012, **36**, 142-146.
57. Z. Shen, S. Nakayama, S. Semancik and H. O. Sintim, *Chem Commun (Camb)*, 2012, **48**, 7580-7582.
58. S. Tang, P. Tong, H. Li, F. Gu and L. Zhang, *Biosens. Bioelectron.*, 2013, **41**, 397-402.
59. J. Zhang, X. Wu, P. Chen, N. Lin, J. Chen, G. Chen and F. Fu, *Chem Commun (Camb)*, 2010, **46**, 6986-6988.
60. J. Zhang, J. H. Chen, R. C. Chen, G. N. Chen and F. F. Fu, *Biosens. Bioelectron.*, 2009, **25**, 815-819.
61. H. C. Yeh, J. Sharma, I. M. Shih, D. M. Vu, J. S. Martinez and J. H. Werner, *J. Am. Chem. Soc.*, 2012, **134**, 11550-11558.
62. B. Yurke, A. J. Turberfield, A. P. Mills, Jr., F. C. Simmel and J. L. Neumann, *Nature*, 2000, **406**, 605-608.
63. Z. Zhang*, et al.*, *Small*, 2010, **6**, 1854-1858.
64. H. K. K. Subramanian, B. Chakraborty, R. Sha and N. C. Seeman, *Nano Lett.*, 2011, **11**, 910-913.
65. D. Y. Zhang, S. X. Chen and P. Yin, *Nat Chem*, 2012, **4**, 208-214.
66. G. Altan-Bonnet and F. R. Kramer, *Nat Chem*, 2012, **4**, 155-157.
67. S. Tyagi, S. A. Marras and F. R. Kramer, *Nat. Biotechnol.*, 2000, **18**, 1191-1196.
68. H. A. Behrensdorf, M. Pignot, N. Windhab and A. Kappel, *Nucleic Acids Res.*, 2002, **30**.
69. A. Jiao*, et al.*, *Chem Commun (Camb)*, 2012, **48**, 5659-5661.
70. H. Gong, T. Y. Zhong, L. Gao, X. H. Li, L. J. Bi and H. B. Kraatz, *Anal. Chem.*, 2009, **81**, 8639-8643.
71. M. Cho, M. S. Han and C. Ban, *Chem Commun (Camb)*, 2008, 4573-4575.
72. B. M. Zeglis, V. C. Pierre and J. K. Barton, *Chem Commun (Camb)*, 2007, 4565-4579.

73. Z. H. Jiang, Y. H. Zhang, Y. Yu, Z. Q. Wang, X. Zhang, X. R. Duan and S. Wang, *Langmuir*, 2010, **26**, 13773-13777.
74. S. Miura, S. Nishizawa, A. Suzuki, Y. Fujimoto, K. Ono, Q. Gao and N. Teramae, *Chemistry*, 2011, **17**, 14104-14110.
75. N. B. Sankaran*, et al.*, *J. Phys. Chem. B*, 2009, **113**, 1522-1529.
76. U. Landegren, R. Kaiser, J. Sanders and L. Hood, *Science*, 1988, **241**, 1077-1080.
77. C. Shi, C. Zhao, Q. Guo and C. Ma, *Chem Commun (Camb)*, 2011, **47**, 2895-2897.
78. H. Wang, J. S. Li, Y. X. Wang, J. Y. Jin, R. H. Yang, K. M. Wang and W. H. Tan, *Anal. Chem.*, 2010, **82**, 7684-7690.
79. X. Xue, W. Xu, F. Wang and X. Liu, *J. Am. Chem. Soc.*, 2009, **131**, 11668-11669.
80. J. Homola, *Chem Rev*, 2008, **108**, 462-493.
81. Y. Li, A. W. Wark, H. J. Lee and R. M. Corn, *Anal. Chem.*, 2006, **78**, 3158-3164.
82. D. K. Toubanaki, T. K. Christopoulos, P. C. Ioannou and C. S. Flordellis, *Anal. Chem.*, 2009, **81**, 218-224.
83. Z. Xiao*, et al.*, *Chem Commun (Camb)*, 2012, **48**, 8547-8549.
84. K. Sato*, et al.*, *Lab Chip*, 2010, **10**, 1262-1266.
85. J. Li, T. Deng, X. Chu, R. Yang, J. Jiang, G. Shen and R. Yu, *Anal. Chem.*, 2010, **82**, 2811-2816.
86. J. Hu and C. Y. Zhang, *Anal. Chem.*, 2010.
87. M. Nilsson, H. Malmgren, M. Samiotaki, M. Kwiatkowski, B. P. Chowdhary and U. Landegren, *Science*, 1994, **265**, 2085-2088.
88. S. Bi, L. Li and S. Zhang, *Anal. Chem.*, 2010, **82**, 9447-9454.
89. F. Barany and D. H. Gelfand, *Gene*, 1991, **109**, 1-11.
90. I. Kalin, S. Shephard and U. Candrian, *Mutat. Res.*, 1992, **283**, 119-123.
91. K. Abravaya, J. J. Carrino, S. Muldoon and H. H. Lee, *Nucleic Acids Res.*, 1995, **23**, 675-682.
92. Y. Q. Cheng, Q. Du, L. Y. Wang, H. L. Jia and Z. P. Li, *Anal. Chem.*, 2012, **84**, 3739-3744.
93. X. R. Duan, L. B. Liu, F. D. Feng and S. Wang, *Acc. Chem. Res.*, 2010, **43**, 260-270.
94. E. J. Wee, M. J. Shiddiky, M. A. Brown and M. Trau, *Chem Commun (Camb)*, 2012, **48**, 12014-12016.
95. W. Shen, H. Deng, A. K. Teo and Z. Gao, *Chem Commun (Camb)*, 2012, **48**, 10225-10227.
96. W. Shen, H. Deng and Z. Gao, *J. Am. Chem. Soc.*, 2012, **134**, 14678-14681.

97. L. Yan, S. Nakayama, S. Yitbarek, I. Greenfield and H. O. Sintim, *Chem Commun (Camb)*, 2011, **47**, 200-202.
98. Q. Wang, L. Yang, X. Yang, K. Wang, L. He, J. Zhu and T. Su, *Chem Commun (Camb)*, 2012, **48**, 2982-2984.
99. H. Ji, F. Yan, J. Lei and H. Ju, *Anal. Chem.*, 2012, **84**, 7166-7171.
100. Y. Chen, Q. Wang, J. Xu, Y. Xiang, R. Yuan and Y. Chai, *Chem Commun (Camb)*, 2013, **49**, 2052-2054.
101. H. Zhou, J. Liu, J. J. Xu and H. Y. Chen, *Anal. Chem.*, 2011, **83**, 8320-8328.
102. W. Xu, X. Xue, T. Li, H. Zeng and X. Liu, *Angew Chem Int Ed Engl*, 2009, **48**, 6849-6852.
103. X. Zuo, F. Xia, Y. Xiao and K. W. Plaxco, *J. Am. Chem. Soc.*, 2010, **132**, 1816-1818.
104. F. Xuan, X. Luo and I. M. Hsing, *Anal. Chem.*, 2012, **84**, 5216-5220.
105. S. Liu, C. Wang, C. Zhang, Y. Wang and B. Tang, *Anal. Chem.*, 2013.
106. H. Schulze*, et al.*, *Anal. Chem.*, 2012, **84**, 5080-5084.
107. Z. Gao, W. Shen, H. Deng and Y. Ren, *Chem Commun (Camb)*, 2013, **49**, 370-372.
108. W. Xu, X. J. Xie, D. W. Li, Z. Q. Yang, T. H. Li and X. G. Liu, *Small*, 2012, **8**, 1846-1850.
109. B. Moore, H. Hu, M. Singleton, M. G. Reese, F. M. De La Vega and M. Yandell, *Genet. Med.*, 2011, **13**, 210-217.
110. D. Hanahan and R. A. Weinberg, *Cell*, 2011, **144**, 646-674.
111. J. Y. Yun*, et al.*, *Science*, 2009, **325**, 1555-1559.
112. J. SantaLucia and D. Hicks, *Annu Rev Bioph Biom*, 2004, **33**, 415-440.
113. R. Owczarzy, P. M. Vallone, F. J. Gallo, T. M. Paner, M. J. Lane and A. S. Benight, *Biopolymers*, 1997, **44**, 217-239.
114. K. M. Ririe, R. P. Rasmussen and C. T. Wittwer, *Anal. Biochem.*, 1997, **245**, 154-160.
115. K. S. Elenitoba-Johnson, S. D. Bohling, C. T. Wittwer and T. C. King, *Nat. Med.*, 2001, **7**, 249-253.
116. C. T. Wittwer, *Hum. Mutat.*, 2009, **30**, 857-859.
117. G. Distefano, M. Caruso, S. La Malfa, A. Gentile and S. B. Wu, *PLoS One*, 2012, **7**, e44202.
118. M. M. Cousins*, et al.*, *J. Clin. Microbiol.*, 2012, **50**, 3054-3059.
119. T. K. Er and J. G. Chang, *Clin. Chim. Acta*, 2012, **414**, 197-201.
120. C. N. Gundry*, et al.*, *Nucleic Acids Res.*, 2008, **36**, 3401-3408.
121. N. Crews, C. T. Wittwer, J. Montgomery, R. Pryor and B. Gale, *Anal. Chem.*, 2009, **81**, 2053-2058.
122. I. Pjescic and N. Crews, *Lab Chip*, 2012, **12**, 2514-2519.

123. C. J. Wienken, P. Baaske, S. Duhr and D. Braun, *Nucleic Acids Res.*, 2011, **39**, e52.
124. W. Lee and X. Fan, *Anal. Chem.*, 2012, **84**, 9558-9563.
125. Y. Liao, X. Wang, C. Sha, Z. Xia, Q. Huang and Q. Li, *Nucleic Acids Res.*, 2013.
126. D. I. Stimpson*, et al.*, *Proc. Natl. Acad. Sci. U. S. A.*, 1995, **92**, 6379-6383.
127. E. G. Hvastkovs and D. A. Buttry, *Analyst*, 2010, **135**, 1817-1829.
128. A. Harrison*, et al.*, *Nucleic Acids Res.*, 2013, **41**, 2779-2796.
129. A. W. Peterson, L. K. Wolf and R. M. Georgiadis, *J. Am. Chem. Soc.*, 2002, **124**, 14601-14607.
130. S. J. Hurst, A. K. Lytton-Jean and C. A. Mirkin, *Anal Chem*, 2006, **78**, 8313-8318.
131. Y. Gao, L. K. Wolf and R. M. Georgiadis, *Nucleic Acids Res.*, 2006, **34**, 3370-3377.
132. A. W. Peterson, R. J. Heaton and R. M. Georgiadis, *Nucleic Acids Res.*, 2001, **29**, 5163-5168.
133. W. Michel, T. Mai, T. Naiser and A. Ott, *Biophys. J.*, 2007, **92**, 999-1004.
134. S. M. Schreiner, D. F. Shudy, A. L. Hatch, A. Opdahl, L. J. Whitman and D. Y. Petrovykh, *Anal. Chem.*, 2010, **82**, 2803-2810.
135. C. Boozer, S. Chen and S. Jiang, *Langmuir*, 2006, **22**, 4694-4698.
136. E. A. Josephs and T. Ye, *ACS Nano*, 2013.
137. H. Pei*, et al.*, *J. Am. Chem. Soc.*, 2012, **134**, 11876-11879.
138. X. Zhang, P. J. Huang, M. R. Servos and J. Liu, *Langmuir*, 2012, **28**, 14330-14337.
139. A. E. Prigodich, O. S. Lee, W. L. Daniel, D. S. Seferos, G. C. Schatz and C. A. Mirkin, *J. Am. Chem. Soc.*, 2010, **132**, 10638-10641.
140. X. Zhang, M. R. Servos and J. Liu, *Chem Commun (Camb)*, 2012, **48**, 10114-10116.
141. X. Zhang, B. Liu, N. Dave, M. R. Servos and J. Liu, *Langmuir*, 2012, **28**, 17053-17060.
142. R. C. Jin, G. S. Wu, Z. Li, C. A. Mirkin and G. C. Schatz, *J. Am. Chem. Soc.*, 2003, **125**, 1643-1654.
143. J. W. Zwanikken, P. J. Guo, C. A. Mirkin and M. O. de la Cruz, *J. Phys. Chem. C*, 2011, **115**, 16368-16373.
144. J. Stehr*, et al.*, *Nano Lett.*, 2008, **8**, 619-623.
145. C. Hrelescu, J. Stehr, M. Ringler, R. A. Sperling, W. J. Parak, T. A. Klar and J. Feldmann, *J. Phys. Chem. C*, 2010, **114**, 7401-7411.
146. A. Buchkremer*, et al.*, *Small*, 2011, **7**, 1397-1402.
147. B. van Grinsven*, et al.*, *ACS Nano*, 2012, **6**, 2712-2721.

148. J. B. Fiche, J. Fuchs, A. Buhot, R. Calemczuk and T. Livache, *Anal Chem*, 2008, **80**, 1049-1057.
149. J. Pingel, A. Buhot, R. Calemczuk and T. Livache, *Biosens. Bioelectron.*, 2012, **31**, 554-557.
150. D. Aird*, et al.*, *Genome Biol*, 2011, **12**, R18.
151. M. P. Audrezet, A. Dabricot, C. Le Marechal and C. Ferec, *J. Mol. Diagnostics*, 2008, **10**, 424-434.

Chapter 3

FO-SPR monitoring of viral particle affinities

Part of this chapter has been published in:

Knez K., Noppe W., Geukens N., Janssen K., Spasic D., Heyligen J., Vriens K., Thevissen K., Cammue B., Petrenko V., Ulens C, Deckmyn H. and Lammertyn J., Affinity comparison of p3 and p8 peptide displaying bacteriophages using surface plasmon resonance. *Analytical Chemistry*, (in press).

3.1 Introduction

The interest in multivalent bioreceptors has been increasing in the last years with applications acknowledged in very diverse research fields, such as cell biology, where their role was studied in the process of cell attachment[1], cell receptor clustering[2,3] and molecular motion[4], but as well in the fields of drug development[5], affinity chromatography[6] and biosensors[7]. The concept of using multivalent bioreceptors due to their

higher selectivity towards a target of interest[8] became especially appealing in the biosensors field, as the ever-increasing demands on the performance of biosensors continuously drives research towards more selective and sensitive receptors. Recently, it was even shown that immobilizing receptors, namely antibodies, at high densities of more than 100.000 receptor copies per magnetic particle, allows to control binding kinetics, resulting in extremely low dissociation constants (K_d) in the femtomolar range[9].

This trend has also been introduced in the field of filamentous phage particles, which can express multiple receptors on their surface through one of their five unique coat proteins, promoting thereby usage of the entire phage as a receptor rather than the individual proteins[10]. The most used coat proteins, as illustrated in Figure 3.1, are the minor coat protein p3, present in 5 copies at the phage distal end and the major coat protein p8, present much more abundantly all over the virus surface with up to 2700 copies[11]. Normally these phages display a library of peptides[12,13], used to select individual high affinity ligands in a procedure called panning. Here, the phage display library[12], consisting of different peptides expressed on the bacteriophage surface as part of their coat proteins, is used to present the peptides to targets of interest with the aim of selecting those peptides with the strongest affinity. Thus, p8 expressing phages were used in the past only to select peptides with lower affinities, as their dense packing on the surface results in a stronger binding due to avidity masking low individual peptide affinity[14-17]. However, with the trend of implementing whole phages as receptors on biosensors[18,19], p8 expressing phages have become valuable due to the advantages of high receptor valence, rivaling high affinities and binding capacity of p3 expressing phages or classic affinity labels such as antibodies. Furthermore, phages can have few clear advantages in such applications compared to nano- and microparticles with high receptor density. Firstly, they can be directly used as a scaffold for the peptide affinity labels[6,7,20,21]. Secondly, phages can be easily produced while the peptides remain confined to their original conformation used during the peptide selection phase, which can be crucial for the peptide function[22,23].

3.2 Aim of this chapter

Despite numerous advantages of using the entire phage as a receptor rather than the individual peptides, binding kinetics of complete phage particles have never been studied in detail. In this chapter, we will use an in house developed fiber-optic surface plasmon resonance (FO-SPR) biosensor[24,25] to study the affinity and binding kinetics of phages. Moreover, we will evaluate if dense packing of the peptides on phage surfaces truly results in increased affinity by means of avidity as has been theorized multiple times[26-28]. As illustrated in Figure 3.1, we will study whether the location of the expressed peptides on the phage p3 or p8 coat protein is influencing the affinity towards a target molecule or whether it is primarily influencing the orientation on the FO-SPR sensor surface. This will be discerned by analyzing different phases of SPR measurements during phage binding. It can be expected that expression of affinity peptides on the p8 coat proteins will result in a phage orientation closer to the biosensor surface and an increase of the sensor signal, which will mainly disturb the initial phase of the SPR measurement, used to determine the association rate (k_{on}). On the other hand, monitoring of the dissociation rate (k_{off}), will give a better insight in the actual influence of high valence on the affinity of the phages, as high valence results in very low dissociation[29].

As a model system, we used phages panned with affinity for enhanced Green Fluorescent Protein (eGFP). This 256 amino acid eGFP is a common protein label for both *in vivo* and *in vitro* experiments[30-32]. Because of the widespread use of eGFP, phages with affinity for this protein can be used for different applications, such as purification and extraction of recombinant eGFP labeled proteins, much in the same way as protein A or G are used as a universal affinity label for antibodies[33,34].

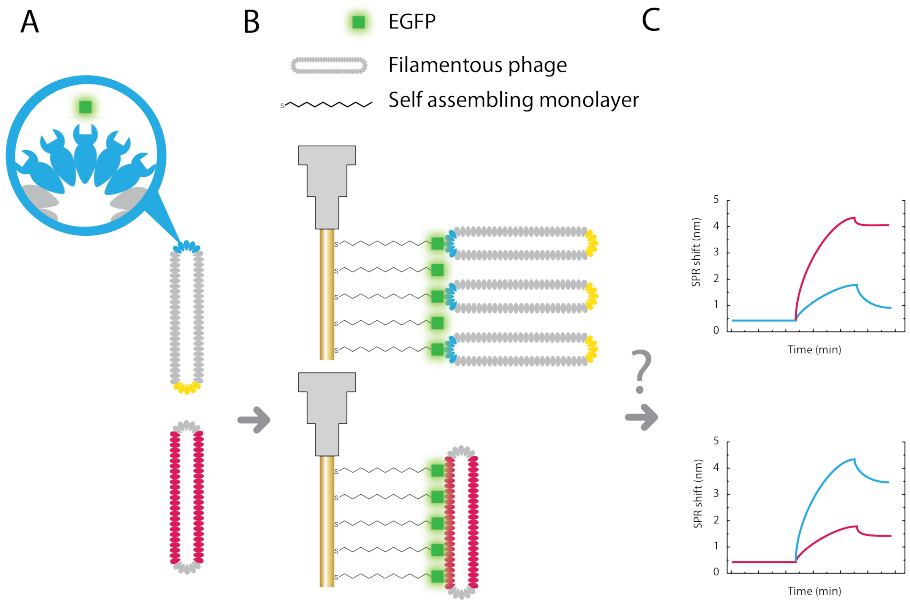

Figure 3.1: Concept of fiber optic SPR based screening for eGFP-binding phages. A) Visualization of the filamentous phages, displaying peptides selective for eGFP either at the N-terminus of the p3 protein (blue) or p8 protein (red). Each individual coat protein expresses one peptide. The p9 protein is marked solely for clarification (yellow); B) Measurement concept with the FO-SPR sensor coated with the eGFP protein (green) and interaction with the two types of phages; the expression of peptides on p3 or p8 proteins can have a strong influence on the affinity of the filamentous phage and consequently their orientation when bound to the FO-SPR sensor surface. C) The two expected sensorgrams are visualized with a red and blue curve, corresponding to the p8 and the p3 peptide, respectively.

3.3 Materials and methods

3.3.1 Phage panning

Depending on the phage library used (Table 3.1), two different panning strategies were followed:

1. For the linear 6-mer (p3L6), 15-mer (p3L15) and cyclic 6-mer (p3C6) phage display libraries, a tube panning procedure was applied as described earlier[35]. Briefly, after coating eGFP (5 µg/mL) in immuno-tubes followed by post coating with 0.4% milk powder in PBS, the phage libraries were incubated overnight at 4°C (or 2.5 hours at room temperature (RT) for the next rounds). Subsequently the tubes were washed to remove unbound phage and eluted with 0.1 M glycine pH 2.0 for 10 min. The eluted phages were neutralized and incubated with *E.coli*-TG1 cells (Stratagene, Diegem, Belgium) cells at 37°C for 30 min. Infected cells were plated on agar-tetracycline plates for phage amplification.

2. The linear 9-mer landscape (p8L9-LS) library was panned as described earlier[36]. The method was identical to the above-described method for p3 phages except for the usage of a microtiter plate instead of immuno-tubes. Furthermore the eluted phages were neutralized and incubated with "starved" *E.coli* K91 BluKan cells at RT. Infected cells were further grown in NZY-tetracycline-medium (Sigma Aldrich, Bornem, Belgium) in an overnight incubation step at 37°C.

For both p3 and p8 phages, three rounds of selection were performed. From the third panning round, single clone phages were isolated, identified (through DNA sequencing) and tested for binding to eGFP using ELISA and FO-SPR technology. All selected phages were finally stored in PBS-5% glycerol (w/v%) at -20°C until further use.

Table 3.1: Phage libraries and phage clones.

Phage library	Properties	Single phage clones	Library Origin
p3 phages			
p3C6	Cyclic 6-mer peptide type 3 library. Peptides are expressed at the N-terminus of the p3 coat protein	1A6; 1B2; 1C3; 1D2; 1F7; 1H3	G. Vlasuk, Corvas, San Diego CA, USA
p3L6	Linear 6-mer peptide type 3 library. Peptides are expressed at the N-terminus of the p3 coat protein	2F7; 2H3	G.P. Smith, University of Missouri, Columbia MO, USA
p3L15	Linear 15-mer peptide type 3 library. Peptides are expressed at the N-terminus of the p3 coat protein	3D6; 3E5; 3F3; 3G2; 3G4; 3G6	G.P. Smith, University of Missouri, Columbia MO, USA
p8 phages			
p8L9-LS	Linear 9-mer peptide library inserted in the p8 coat protein by deleting replacing amino acids 2-5. A so called Landscape Phage Library	4R3.3; 4R3.5; 4R3.6; 4R3.10; 4R3.11; 4R3.12; 4R3.13; 4R3.14; 4R3.15	V.A. Petrenko, Auburn University, Auburn AL, USA
control phages			
	Non-binding eGFP phages	B1	

3.3.2 Expression and purification of eGFP

The cDNA encoding eGFP was cloned into the pFastBac vector (Invitrogen) as a N-terminal His-tagged fusion. Baculovirus was produced using the Bac-to-Bac expression system according to the manufacturer's guidelines (Invitrogen). His-tagged eGFP was expressed in Sf9 insect cells using P2 recombinant baculovirus. eGFP-His was purified from cleared cell lysate using Ni Sepharose beads (GE Healthcare). Impurities were washed out with 40 mM imidazole in PBS buffer and bound protein was eluted with 250 mM imidazole in PBS. eGFP-His was further purified by gel filtration on a Superdex 200 10/300 GL column (GE healthcare) with PBS as a running buffer. Purified protein was concentrated to 2 mg/ml and stored a 4˚C until further use.

3.3.3 SPR device setup

The FO sensors were made of a HL-2000 tungsten halogen lamp (Ocean optics, Dunedin, USA), a miniature UV-VIS spectrophotometer (USB4000, Ocean Optics, Dunedin, USA) and an FO sensor, as previously described in Pollet *et al.*[37] The FO-SPR setup was built in order that replaceable and interchangeable FO-SPR sensors can be coupled with a bifurcated optical fiber to guide white light from the tungsten halogen lamp into the sensor. The light will first pass the SPR sensitive gold zone, afterwards it will reflect back at the tip and travel towards the spectrometer (Figure 3.2). Binding phenomena at the gold surface will result in a shift of the typical spectral resonance SPR-dip recorded by the spectrometer.

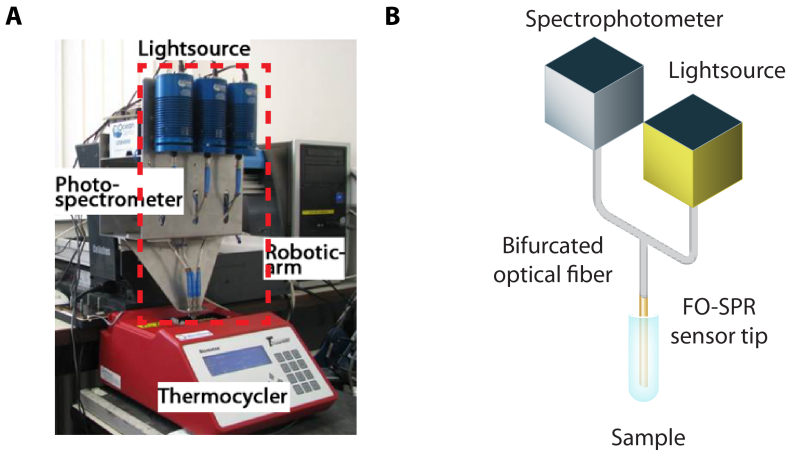

Figure 3.2: A) Picture of the measuring setup with all components. B) Schematic close up of the sensing region with yellow arrows indicating incident light, which excites surface plasmons and red arrows indicating reflected light in the SPR sensor tip which is analyzed with a spectrometer.

All components of the FO-SPR device were mounted on a robotic arm (High-Z S400, CNC-Step, Geldern, Germany) enabling automated handling. The temperature of the samples is controlled using a modified T1 thermocycler (Biometra, Gottingen, Germany). Because temperature can cause SPR signal drift, the temperature was also monitored externally using a NI-DAQ (National instruments, Austin, USA) with three highly responsive T-type WK-200 thermocouple threads (Labfacillity, Leeds, United Kingdom). The interchangeable SPR measurement probes, were easily coupled to the SPR device through a

subminiature version A connector (SMA-type connector, Thorlabs, Munchen, Germany).

3.3.4 FO-SPR sensor tip

FO sensors were designed and manually manufactured as previously described in Pollet *et al.*[38] In short, a 400 µm 0.39 NA multimode TEQS optical fiber (Thorlabs, Germany) was cut consistent to a length of 2.8 cm, next the fiber was assembled into an SMA connector after removal of the protective cladding. Following, the fiber end was placed in acetone for 5 min to loosen the hard polymer cladding. Afterwards, the FO sensor was carefully cleaned with isopropyl ethanol and rinsed with water. Subsequently, the FO sensors were coated with a 50 nm gold layer using a sputter coater (Balzers, Pfäffikon, Switzerland). The freshly prepared fibers were immediately incubated with 1 µM of a biotin self-assembling monolayer (SAM) formation reagent (Dojindo, Japan), which was used as a scaffold to immobilize biotinylated eGFP on the FO-SPR sensor surface (Figure 3.1)

3.3.5 FO-SPR sensor tip preparation

The gold sensing layer of the FO-SPR sensor tip, was functionalized with a self-assembling monolayer (SAM), to couple biomolecules on the sensor tip. The SAM consisted of alkane thiol chains with a biotin functional head group (Dojindo Molecular Technologies, Munich, Germany). During an overnight incubation (1 µM of thiols in ethanol), the thiol groups attached to the gold surface, while the alkane chains oriented themselves into a well-organized monolayer. After 12 h of incubation, the probes were rinsed in ethanol to remove any unbound alkane thiols and were stored at 4°C prior to use. For binding biotinylated eGFP on the sensor tip, 10 µg/mL of streptavidin (Invitrogen, Stockholm, Sweden) was immobilized on the SAM biotin groups in 50 mM MES buffer with pH 6.0. The surface was washed with rinsing solution (50 mM NaOH, 1 M NaCl) to remove all non-specifically bound molecules, followed by binding of biotinylated eGFP (10µg/mL).

3.3.6 FO-SPR measurements of phage binding

For screening, phages were serially diluted twofold starting from 2x1012 phages/mL. Both phage binding and phage dissociation to and from the eGFP coated sensor tip, respectively, were monitored for 15 min in 100 µL volumes. Afterwards, the FO-SPR sensor tip was regenerated for 60 s in phosphate washing buffer (PBS, 0.1% Tween 20, 1 M NaCl) under continuous stirring. In between two measurements the FO-SPR sensor tip was equilibrated in measurement buffer (MES, 0.1% Tween 20, pH 6.0) during 5 min. Dilution series of two different phages were simultaneously analyzed using two different measurement channels of the FO-SPR device. Moreover, the repetition dilution series of the same phage were analyzed on different measurement channels to minimize FO-SPR sensor tip artifacts. Binding of both biotinylated eGFP and filamentous phages (colored with the intercalating dye Sybr gold, Life Technologies, Oslo, Norway) on the probe surface was characterized using an inverted fluorescence microscope.

3.3.7 ELISA

The wells of a streptavidin coated ELISA plate (Thermo scientific, Rockford, USA) were incubated with 100 µl of 5 µg/ml biotin-eGFP in TBS for 1.5 hours at room temperature and subsequently washed. Afterwards, the eGFP-binding phages were added in a concentration of $1x10^{11}$ phages/ml in MES buffer (pH 6.0, 50 mM, 0.1% Tween 20) for 1.5 hours at RT and extensively washed with MES. Next the wells were incubated with rabbit anti-fd bacteriophage antibody (Sigma, Bornem, Belgium) at a concentration of 0.66 µg/ml and a secondary antibody, goat anti rabbit-IgG conjugated with alkaline phosphatase (Jackson ImmunoResearch, West-Grove, USA) at a concentration of 0.24 µg/ml for 1 hour each at RT in following buffer: 50 mM Tris, 150 mM NaCl, 0.1% Tween 20, 1 mg/ml BSA, pH7.5. After extensive washing with MES, the substrate, p-nitrophenylphosphatein in 1 M diethanolamine, 1 mM $MgCl^{2+}$ pH 9.8 was added to each well. Finally the absorbance at 405 nm was monitored during 15 min using a plate reader (Fluostar Optima, Ortenberg, Germany).

3.3.8 Data analysis

The FO-SPR set-up was controlled using an in house developed National Instruments Labview script (National Instruments). This script timed the measurements of the spectrometer by sending trigger signals to the Ocean optics spectrometer enabling exact time control over spectrometer measurements. Data was logged in TDMS compression allowing extended time measurements. The data was extracted from the TDMS files using a Matlab (The Mathworks, Natick, USA) script that recognizes motives in the SPR data, which increased the speed of data processing. Downstream data analysis of the SPR measurements was performed using Excel (Microsoft, Redmond, USA) and Origin (Originlabs, Northampton, USA). The kinetic data of phage binding was derived from the SPR measurements using Prism (Graphpad Software, San Diego, USA), by fitting the SPR binding curves with a 1:1 Langmuir model.

3.4 Results

3.4.1 Optimization of the FO-SPR assay for phage-eGFP interaction

Phage affinity towards the target protein, i.e. eGFP in this study, was evaluated in a direct interaction assay using the FO-SPR biosensor. To establish the assay, immobilization of eGFP onto the FO-SPR sensor tip surface was optimized first. Because the eGFP molecule has a tightly packed barrel structure, which makes functional groups less accessible[39], immobilization was done through biotin and streptavidin. Thus, eGFP was labeled with a small biotin molecule in solution before being bound to a streptavidin molecule on the SPR sensor. This resulted in a higher immobilization efficiency due to use of a modification reaction in free solution rather than directly on the sensor surface, which is known to cause steric hindrance and electrostatic repulsion[40]. Moreover, the tetramer structure of streptavidin[41] holds an extra advantage, as multiple eGFP biotin molecules can be immobilized on one streptavidin molecule.

The streptavidin immobilization was tested in buffered solutions: MES (pH 6), PBS (pH 7.4), Acetic Acid (pH 5.2) in order to achieve optimal protein density on the probe surface (Figure 3.3**,** part A**,** blue bars). According to the SPR signal, the highest streptavidin density was

realized in MES buffer with pH 6.0. This result is in accordance with the pI for both streptavidin (pI= 6.3)[42] and biotin (pI= 3.5)[43], making both molecules oppositely charged at pH 6.0, allowing them to diffuse closely to the surface which increases the chances for a binding event[44]. Although these molecules should be even more oppositely charged at pH 5.2, a lower binding was observed. This can be explained through charges generated on the FO-SPR sensor surface as a result of deprotonated SAM functional groups at this pH, repelling the highly charged streptavidin molecules. In a similar experiment, differences in the immobilization efficiency of biotinylated eGFP appeared to be much more pronounced (Figure 3.3**,** part A, green bars). For instance, at pH 7.4 a shift of less than 1 nm was observed, whereas lowering the pH to 6.0 doubled the amount of eGFP on the probe surface. By introducing extra ions in this buffer, the density on the FO-SPR surface was further improved and a better reproducibility was achieved (Figure 3.3, part A, pH 6.0*).

Subsequently, one of the phage clones panned for eGFP (1B2 - p3 phage) was randomly selected for optimizing phage binding to eGFP on the FO-SPR sensor tip surface (Figure 3.3**,** part A). In a standard PBS buffer with pH 7.4, a minor SPR signal shift was visible at a concentration of $5x10^{13}$ phages/mL, which was only marginally higher than the SPR signal of a non-eGFP selected control phage. In fact, a large part of the FO-SPR signal shift can be attributed to the glycerol matrix of the phage storage buffer, as glycerol has a higher refractive index[45] than the measuring buffer. The low binding signals of phages can be explained by negative charges of eGFP on the probe surface, as well as on the phage surface at pH 7.4, which prevents binding interactions. Knowing that eGFP has a pI around pH 6.0[46], while the filamentous phages have a pI around 4.0[47], buffers with a similar pH were applied (pH 5-7.4) in order to decrease the charges on both surfaces. Results show that by lowering the pH, the SPR signal steadily increased, reaching saturation at pH 5.0 (Figure 3.3**,** part B).

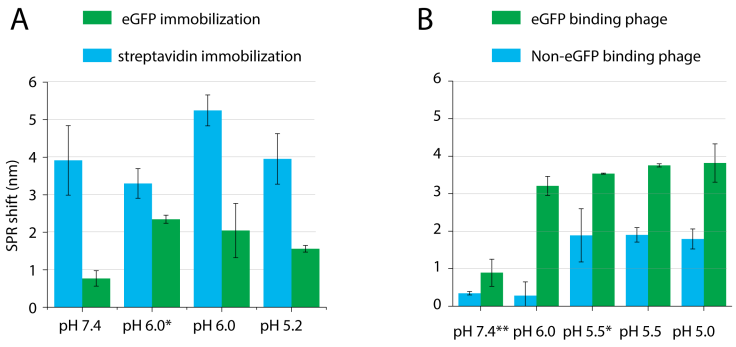

Figure 3.3: Influence of pH and ionic strength on the binding of phages to eGFP using FO-SPR: A) Optimization of streptavidin and eGFP binding at different pH values and in the presence of 300 mM (*) NaCl (n=4); B) Binding of an eGFP-specific or control phage clone at different pH values and in the presence of 137 (**) or 300 mM (*) NaCl (n=4). Error bars indicated are the standard deviations of the mean.

However, the affinity of a non-eGFP selected control phage also increased with decreasing pH, but with a different pH-sensitivity compared to the eGFP binding phages. Based on these experimental results, a pH of 6.0 is chosen since it results in the highest specific binding. Addition of ions such as Na^+ and Cl^-, another often-used strategy to facilitate molecules to reach their targets[48], did not affect binding of selected or control phages considerably (Figure 3.3, part B). An actual sensorgram for the optimized binding of selected phage is shown in Figure 3.4, part A. The SPR signal of phage binding at pH 6.0 increased approximately 10 times compared to pH 7.4, irrespective of a ten-fold lower phage concentration that is applied at pH 6.0 ($1x10^{12}$ phages/mL) in order to prevent sensor saturation. The optimized conditions were further confirmed with fluorescence microscopy (Figure 3.4, part B). Increasing intensity of fluorescence is visible after binding eGFP and fluorescently labeled filamentous phage 1B2 to the sensor surface.

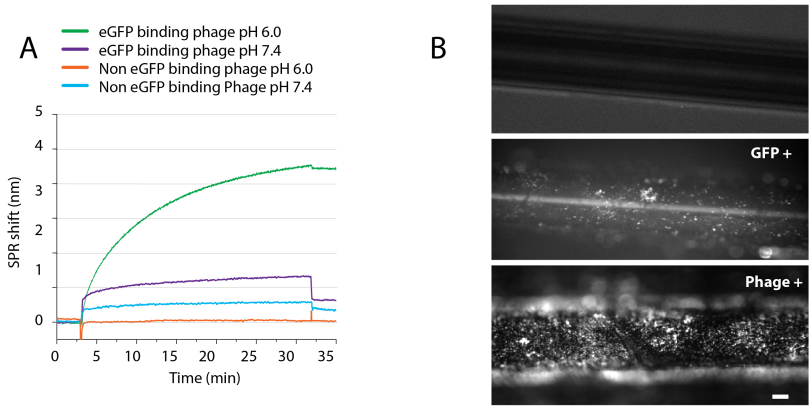

Figure 3.4: A) SPR-binding curves of an eGFP-specific and control phage clone at pH 6.0 and 7.4; B) Microscopy images of the FO-SPR sensor tip with biotin SAM FO-SPR probe (top), after eGFP immobilization (middle) and after phage binding (bottom). Scale bar = 100 µm.

3.4.2 FO-SPR screening of selected phages with affinity for eGFP

Using the above described optimized conditions for binding of phages to the FO-SPR sensor tip surface, both p3 and p8 eGFP panned phages were screened for their affinity towards eGFP. Phage measurements were conducted at 4 different concentrations in a range of 10^{11}-10^{12} phages/mL. The intrinsic non-specific binding of a native non-panned filamentous phage to eGFP was first examined. This interaction appeared to be negligible, even at the highest tested concentration ($2x10^{12}$ phages/mL, Figure 3.5, part A). Next, the binding of eGFP panned p3 phage clones was measured. These p3 phages can be distinguished according to the type of peptide they express, being either a linear peptide or a cyclic peptide (by the introduction of cysteine groups which can form disulfide bonds[49]). Although all linear p3 phages showed a clear difference in interaction with eGFP compared to the native phage (Figure 3.5, part A), substantially higher SPR signal shifts were noted for the p3 cyclic phages (Figure 3.5, part B). Phages expressing cyclic peptides are known to have considerably better affinities than phages expressing linear peptides, because of a structurally more stable binding conformation, with limited structural entropy in the unbound state, favoring higher binding affinities[50].

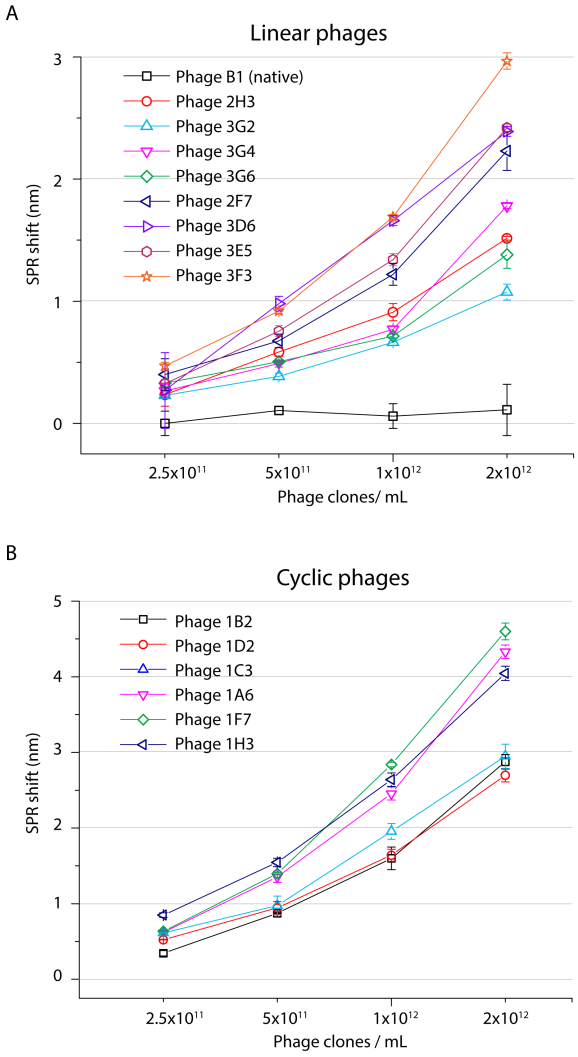

Figure 3.5: Binding of phage clones to eGFP as determined with FO-SPR: A) Non-eGFP panned native phage together with the linear p3 expression phages; B) the p3 phages expressing a cyclic peptide;

Lastly, p8 phages, known as landscape phages, (Figure 3.6) showed a remarkably higher affinity for eGFP compared to all p3 phages, with one of the p8 clones (phage 4R3.12) having an affinity, higher than any of the other landscape clones.

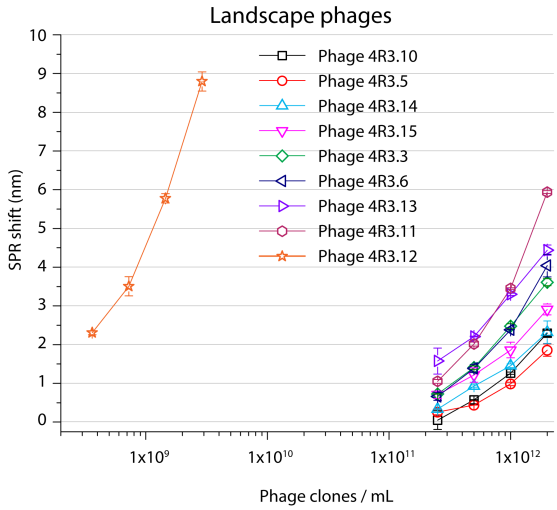

Figure 3.6: Binding of p8 expressing landscape phage clones.

SPR measurements were further validated with an endpoint ELISA test (Figure 3.7), which showed similar trends for individual clones in both assays. Thus, clones 1H3 and 4R3.12 appeared as one of the best binding p3 and p8 phages, respectively, according to both assays. However, a discrepancy was observed in the overall signal intensity for p3 and p8 phages in the two assays. Whereas p3 phages gave a much higher signal in the ELISA assay than p8 phages, SPR binding signals were a mirror image of these results. Here, an explanation can be found with the underlying mechanisms of the two bioassays: FO-SPR measurements monitor phage clones interactions with eGFP label free, while the ELISA measurements are based on a sandwich type of assay. Therefore, in the ELISA, an antibody against the p8 protein (R@fd-IgG) is used to identify phages, after they have bound to eGFP on the microtiter plate surface. As a result, when the p8 coat protein is expressing peptides selective for eGFP, the epitope for the antibody can be modified, resulting in a lower binding efficiency of the antibody.

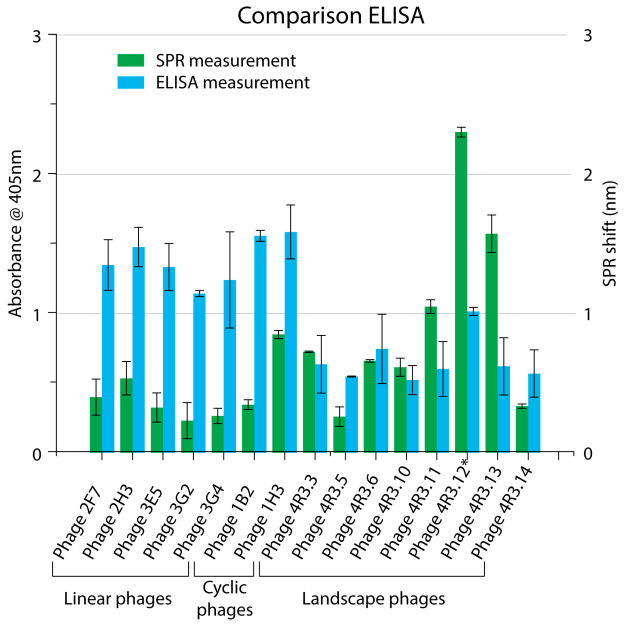

Figure 3.7: Comparison of phage binding (1011 phages/mL) with eGFP as obtained with ELISA and FO-SPR. (*) phage clone measured at lower concentration with FO-SPR (108 phages/mL) (n=4, error bars represent the standard deviation of the mean).

Higher SPR binding signals obtained with p8 phages are not only indicating higher affinity/avidity for the eGFP immobilized on the SPR sensor, but can also be attributed to the orientation of phages on the sensor surface (Figure 3.1). Nonetheless, as the number and density of affinity peptides displayed on the p8 coat protein is much higher than in p3 phages, p8 phages are capable of binding multiple times to different eGFP molecules on the sensor surface. Earlier reports on multivalent antibodies showed that avidity mainly results in a decrease in dissociation constant[51,52]. The same effect should be observed when SPR dissociation kinetics of p8 phages are compared to p3 phages. To evaluate this hypothesis, binding curves of the best binding p3 and p8 phages (being clones 1H3, 1F7, 1A6, 4R.11, 4R.12) were studied in more detail.

3.4.3 Binding kinetics

For each of the 5 selected phage clones, the kinetic binding parameters such as association rate (k_{on}) and dissociation rate (k_{off}) were derived

from the individual SPR measurements (Figure 3.8). The ratio of both constants further determined the dissociation constant (K_d) for each phage (summarized in Table 3.2).

Table 3.2: Kinetic parameters (± std. dev. of 4 measurements) of eGFP-binding phages measured by FO-SPR.

Phage	1H3	1F7	1A6	4R3.12	4R3.11
kon (s^{-1} x M^{-1})	$1.2\pm0.1x10^{8}$	$3.8\pm0.3x10^{8}$	$3.6\pm0.2x10^{8}$	$1.9\pm x0.1x10^{11}$	$2.3\pm1.1x10^{8}$
koff (s^{-1})	$2.7\pm0.1x10^{-3}$	$4.0\pm0.6x10^{-3}$	$6.0\pm0.2x10^{-3}$	$2.2\pm0.1x10^{-3}$	$1.0\pm0.1x10^{-3}$
Kd (M)	$2.3\pm0.3x10^{-11}$	$1.1\pm0.2x10^{-11}$	$1.6\pm0.4x10^{-11}$	$1.2\pm0.1x10^{-14}$	$4.5\pm0.9x10^{-12}$

K_d values for both p8 phages were at least one order of magnitude lower than for the p3 phages, confirming our previous conclusions that p8 phages have a higher affinity for eGFP. Nonetheless, the p3 phages also had a K_d in the pM range (Figure 3.8), which is equivalent to the best performing antibodies[53].

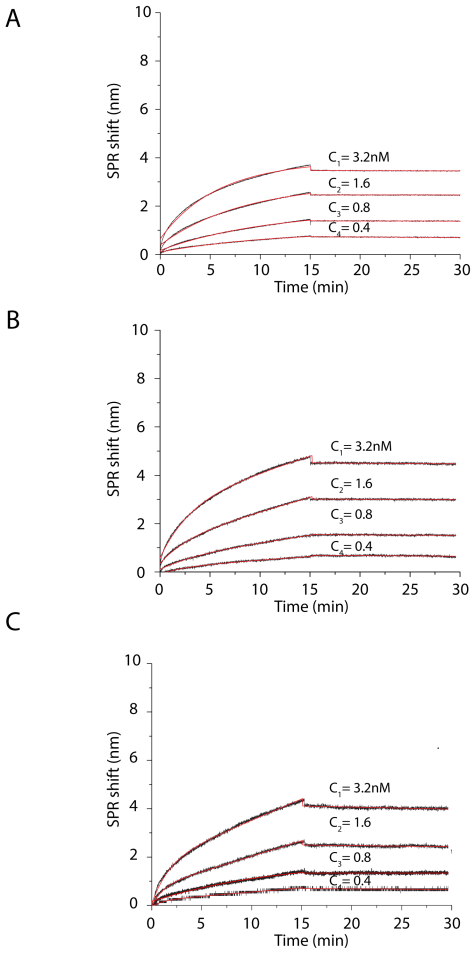

Figure 3.8: Binding curves of 5 eGFP-binding phage clones with the highest interaction signal in the screening experiment: A) p3 phage clone 1H3; B) p3 phage clone 1F7; C) p3 phage clone 1A6; Measured signal is depicted in black while fitted curve values for deriving binding parameters are shown in red.

The actual SPR binding curves revealed that the SPR signal is almost a flat line during the dissociation phase of p8 phages, indicating only a minimal amount of dissociation from the sensor surface (Figure 3.9). This result verified the hypothesis that the increase in affinity of p8 phages is influenced considerably by a change in k_{off}. Surprisingly, p3 phages also displayed a very slow dissociation phase (Figure 3.8), which indicated that even the five-plex multivalence of the p3 protein has a considerable impact on the affinity, as was also found in earlier work[54,55]. In a recent publication, highly valent magnetic particles (1µm diameter), which are comparable to p8 landscape phages, showed very

similar binding kinetics and a similar increase in both k_{on} and k_{off} rates as p8 phages. Moreover, the affinity of these magnetic particles towards a protein immobilized on a flat surface (prostate specific antigen) was comparable to the affinity of the p8 phages for eGFP used in this research with K_d-values in the fM range[9].

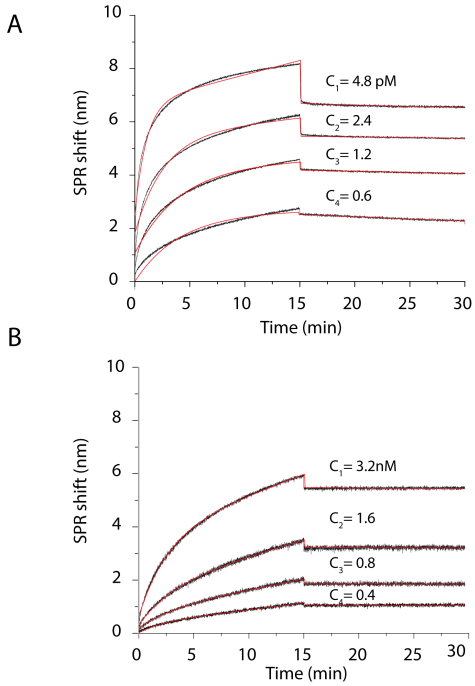

Figure 3.9: Binding curves of 5 eGFP-binding phage clones with the highest interaction signal in the screening experiment: A) p8 phage clone 4R3.12; B) p8 phage clone 4R3.11. The measured signal is depicted in black while fitted curve values for deriving binding parameters are shown in red.

3.4.4 Competitive assays for testing the specificity of the phage-eGFP interactions

The specificity of the highest affinity phages (being clones 1F7, 1A6, 4R3.11 and 4R3.12) towards eGFP was evaluated in two different assays.

In the first assay, eGFP immobilized on the sensor surface was competing for phage binding with free eGFP in solution. Increasing concentrations of free eGFP are likely to decrease the number of phages capable of binding to the sensor, if binding is specific (Figure 3.10, part A). As expected, the high peptide densities of the landscape phages

made them less prone to inhibition of binding with free eGFP. At moderate concentrations of free eGFP, the capacity of the landscape phages to bind multiple eGFP molecules was further exhibited, when the binding signal even surpassed the maximal signal obtained in the previous experiments. At these concentrations the landscape phages very likely did bind both free and FO-SPR bound eGFP increasing thus their mass and consequently resulting in a higher SPR-shift. For phage clone 4R3.12, with the highest affinity for eGFP, no complete inhibition of the binding to the FO-SPR sensor was achieved. Even in the presence of 200 µg/mL of free eGFP, this clone was still at 40 percent of the normal binding signal, indicating that this phage has a high binding capacity. To exclude involvement of any non-specific sensor surface interaction, an extra test was performed with this phage using a non-eGFP coated sensor surface, which resulted in no binding (data not shown).

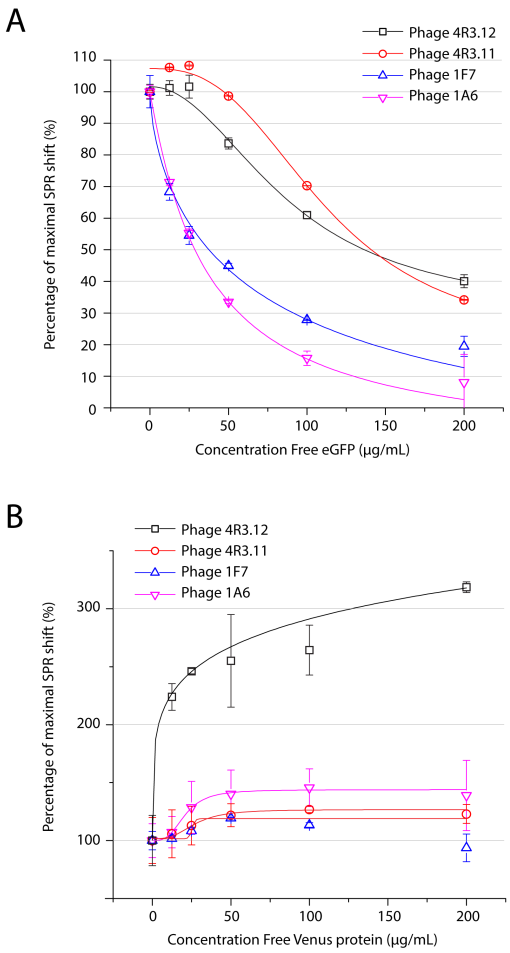

Figure 3.10: A) Free eGFP dose-dependently competes with sensor-bound eGFP for binding to phages; B) The highly homologous Venus protein dose-dependently increases the binding signal of eGFP-binding phages bound to the sensor, indicating low affinity interaction of phages with Venus protein. Symbols represent experimental data, while the lines are a logistic sigmoidal fit. (n=4, error bars represent the standard deviation of the mean)

In a second assay, the specificity towards eGFP was tested using an eGFP homologous protein, namely Venus protein, which differs in only 6 out of 256 amino acids of native GFP, resulting in a red shift in the emission spectrum of the fluorescent protein[56]. Surprisingly, the Venus protein did not inhibit binding with eGFP on the FO-SPR surface for all 4 phages tested, even at Venus concentrations as high as 200 µg/mL, demonstrating that the phages are indeed highly specific for eGFP. Nevertheless, Venus protein did increase the binding signal indicating a

certain degree of cross-reactivity (Figure 3.10, part B). For 3 phages, only a very small shift in SPR binding was recorded above the normal binding signal, suggesting that the phages indeed did bind a small amount of the Venus protein, which increased the density on the sensor surface. In contrast, the signal of clone 4R3.12, increased to 200-300 percent in the presence of 200 µg/mL Venus protein. This signal increase can only result from high amounts of Venus protein binding to the phage that is already bound to the FO-SPR sensor. However, affinity of this phage for eGFP must be higher than for the Venus protein because the phage is not displaced from the FO-SPR sensor, as was the case for free eGFP in the competitive assay. This corresponds with previous reports showing that affinity molecules developed for 'Aequorea victoria'-derived fluorescent proteins, such as eGFP and Venus protein, have affinity for all of these highly homologous proteins[57].

3.5 Conclusion

This paper presents the first FO-SPR based kinetic analysis of bacteriophage affinities, where phages are used as a whole with either the minor coat protein p3 or the major coat protein p8 expressing peptides selective for eGFP. As expected, the higher peptide densities on the p8 coat protein resulted in a better affinity towards the target protein (eGFP) compared to phages expressing peptides through the p3 coat protein, with K_d values being up to 3 orders of magnitude lower for some p8 phage clones. This difference in affinities could be partially explained with the orientation of p8 phages, as the p8 coat protein expresses affinity peptides throughout the entire phage surface, the phages are positioned with the longer side closer to the sensor surface, which increased the SPR signal during the association phase. Another contributing aspect to such high affinities of p8 phages was the observed decrease in dissociation rate, which is exclusively attributable to multivalent interactions. Nonetheless, p3 phages also express the peptides multivalent, having an especially strong effect on the k_{off} of these phages, resulting in little phage dissociation once bound to eGFP on the sensor surface. SPR measurements, together with the ELISA assays, also revealed considerable differences in eGFP-binding

parameters among different p3 and p8 clones, making some phage clones more suited for certain applications than for others.

The application of FO-SPR on viral particles is a useful tool for selection of viral clones with high affinities. For this application the technology can even have a larger added value, when FO-SPR would be applied during the early panning stage of viral clone selection, as the kinetic parameters could guide the phage affinity maturation towards binding parameters optimally suited for the intended application. However the assay is maybe not the best choice for POC biosensor applications, as it lacks sensitivity, with a detection limit of 10^8 viral particles. The needs for clinical applications cannot be met without additional amplification strategies. Furthermore, the assay does not allow to discriminate between different viral particles, any particle with affinity for the receptor on the FO-SPR sensor will result in a signal.

Other options include detection by means of antibodies, however in combination with SPR similar problems as in the above mentioned assay might be encountered. The mass density of bacteria and viruses is low, which does not allow detecting these micro-organisms sensitively using SPR (results not shown). Therefore in the following chapters, not the detection of the micro-organism as a whole will be targeted but instead, the genetic material will be used. This allows more easily to improve the LOD as the genetic material is more abundant and can easily be identified. Furthermore unique regions in the genome of closely related micro-organisms enable straightforward identification.

References

1. E. A. Englund*, et al.*, *Nat. Commun.*, 2012, **3**, 614-621.
2. A. Grochmal, E. Ferrero, L. Milanesi and S. Tomas, *J. Am. Chem. Soc.*, 2013, **135**, 10172-10177.
3. S. Tomas and L. Milanesi, *Nature Chem.*, 2010, **2**, 1077-1083.
4. A. Perl, A. Gomez-Casado, D. Thompson, H. H. Dam, P. Jonkheijm, D. N. Reinhoudt and J. Huskens, *Nature Chem.*, 2011, **3**, 317-322.
5. A. Kecskes, D. K. Tosh, Q. Wei, Z. G. Gao and K. A. Jacobson, *Bioconjugate Chem.*, 2011, **22**, 1115-1127.
6. J. Muzard, M. Platt and G. U. Lee, *Small*, 2012, **8**, 2403-2411.
7. V. Nanduri, I. B. Sorokulova, A. M. Samoylov, A. L. Simonian, V. A. Petrenko and V. Vodyanoy, *Biosens. Bioelectron.*, 2007, **22**, 986-992.
8. F. J. Martinez-Veracoechea and D. Frenkel, *Proc. Natl. Acad. Sci. U. S. A.*, 2011, **108**, 10963-10968.
9. V. Mani, D. P. Wasalathanthri, A. A. Joshi, C. V. Kumar and J. F. Rusling, *Anal. Chem.*, 2012, **84**, 10485-10491.
10. S. Cabilly, *Mol. Biotechnol.*, 1999, **12**, 143-148.
11. S. S. Sidhu, *Biomol. Eng.*, 2001, **18**, 57-63.
12. A. S. Kang, C. F. Barbas, K. D. Janda, S. J. Benkovic and R. A. Lerner, *Proc. Natl. Acad. Sci. U. S. A.*, 1991, **88**, 4363-4366.
13. V. A. Petrenko and V. J. Vodyanoy, *J. Microbiol. Methods*, 2003, **53**, 253-262.
14. H. B. Lowman, *Annu. Rev. Biophys. Biomol. Struct.*, 1997, **26**, 401-424.
15. R. M. de Wildt, I. M. Tomlinson, J. L. Ong and P. Holliger, *Proc. Natl. Acad. Sci. U. S. A.*, 2002, **99**, 8530-8535.
16. J. Speck, K. M. Arndt and K. M. Muller, *Protein Eng. Des. Sel.*, 2011, **24**, 473-484.
17. J. Vrielink, M. S. Heins, R. Setroikromo, E. Szegezdi, M. M. Mullally, A. Samali and W. J. Quax, *FEBS J.*, 2010, **277**, 1653-1665.
18. G. A. W. Penner and M. Reginald, *Anal. Chem.*, 2008, **80**, 3082-3089.
19. L. M. Yang, J. E. Diaz, T. M. McIntire, G. A. Weiss and R. M. Penner, *Anal. Chem.*, 2008, **80**, 933-943.
20. W. Noppe, F. M. Plieva, I. Y. Galaev, K. Vanhoorelbeke, B. Mattiasson and H. Deckmyn, *J. Chromatogr. A*, 2006, **1101**, 79-85.
21. J. A. Arter, J. E. Diaz, K. C. Donavan, T. Yuan, R. M. Penner and G. A. Weiss, *Anal. Chem.*, 2012, **84**, 2776-2783.
22. W. Noppe, K. Vanhoorelbeke, I. Y. Galaev, B. Mattiasson and H. Deckmyn, *J. Dairy Sci.*, 2004, **87**, 3247-3255.

23. K. Murase, K. L. Morrison, P. Y. Tam, R. L. Stafford, F. Jurnak and G. A. Weiss, *Chem. Biol.*, 2003, **10**, 161-168.
24. J. Pollet*, et al.*, *Biosens. Bioelectron.*, 2009, **25**, 864-869.
25. K. Knez, K. P. F. Janssen, J. Pollet, D. Spasic and J. Lammertyn, *Small*, 2012, **8**, 868-872.
26. T. Clackson, H. R. Hoogenboom, A. D. Griffiths and G. Winter, *Nature*, 1991, **352**, 624-628.
27. A. Fagerlund, A. H. Myrset and M. A. Kulseth, *Appl. Microbiol. Biotechnol.*, 2008, **80**, 925-936.
28. S. S. Sidhu, W. J. Fairbrother and K. Deshayes, *ChemBioChem*, 2003, **4**, 14-25.
29. E. M. Munoz, J. Correa, R. Riguera and E. Fernandez-Megia, *J. Am. Chem. Soc.*, 2013, **135**, 5966-5969.
30. S. R. McRae, C. L. Brown and G. R. Bushell, *Protein Expression Purif.*, 2005, **41**, 121-127.
31. D. A. Zacharias, J. D. Violin, A. C. Newton and R. Y. Tsien, *Science*, 2002, **296**, 913-916.
32. J. Livet*, et al.*, *Nature*, 2007, **450**, 56-+.
33. S. Hober, K. Nord and M. Linhult, *J. Chromatogr. B*, 2007, **848**, 40-47.
34. B. Akerstrom, T. Brodin, K. Reis and L. Bjorck, *J. Immunol.*, 1985, **135**, 2589-2592.
35. W. Noppe, F. Plieva, I. Y. Galaev, H. Pottel, H. Deckmyn and B. Mattiasson, *BMC Biotechnol.*, 2009, **9**, 21.
36. J. R. Brigati, T. I. Samoylova, P. K. Jayanna and V. A. Petrenko, *Current Protocols in Protein Science*, 2008, **Chapter 18**, Unit 18 19.
37. J. Pollet*, et al.*, *Biosens Bioelectron*, 2009, **25**, 864-869.
38. J. Pollet, K. P. F. Janssen, K. Knez and J. Lammertyn, *Small*, 2011, **7**, 1003-1006.
39. M. Ormo, A. B. Cubitt, K. Kallio, L. A. Gross, R. Y. Tsien and S. J. Remington, *Science*, 1996, **273**, 1392-1395.
40. B. Lu, M. R. Smyth and R. OKennedy, *Analyst*, 1996, **121**, R29-R32.
41. P. C. Weber, D. H. Ohlendorf, J. J. Wendoloski and F. R. Salemme, *Science*, 1989, **243**, 85-88.
42. S. Burazerovic, J. Gradinaru, J. Pierron and T. R. Ward, *Angewandte Chemie International Edition*, 2007, **46**, 5510-5514.
43. X. Li, J. Qian and S. He, *Nanotechnology*, 2008, **19**, 355501.
44. H. Jans, K. Jans, T. Stakenborg, B. Van de Broek, L. Lagae, G. Maes and G. Borghs, *Nanotechnology*, 2010, **21**, 345102.
45. J. B. Beusink, A. M. Lokate, G. A. Besselink, G. J. Pruijn and R. B. Schasfoort, *Biosens. Bioelectron.*, 2008, **23**, 839-844.

46. J. A. Sniegowski, J. W. Lappe, H. N. Patel, H. A. Huffman and R. M. Wachter, *J. Biol. Chem.*, 2005, **280**, 26248-26255.
47. D. A. Marvin, L. C. Welsh, M. F. Symmons, W. R. Scott and S. K. Straus, *J. Mol. Biol.*, 2006, **355**, 294-309.
48. S. Pasche, J. Voros, H. J. Griesser, N. D. Spencer and M. Textor, *J. Phys. Chem. B*, 2005, **109**, 17545-17552.
49. C. Heinis, T. Rutherford, S. Freund and G. Winter, *Nat. Chem. Biol.*, 2009, **5**, 502-507.
50. L. B. Giebel, R. T. Cass, D. L. Milligan, D. C. Young, R. Arze and C. R. Johnson, *Biochemistry*, 1995, **34**, 15430-15435.
51. U. Iqbal*, et al.*, *Br. J. Pharmacol.*, 2010, **160**, 1016-1028.
52. J. H. Myung, K. A. Gajjar, J. Saric, D. T. Eddington and S. Hong, *Angewandte Chemie-International Edition*, 2011, **50**, 11769-11772.
53. H. R. Hoogenboom, *Trends Biotechnol.*, 1997, **15**, 62-70.
54. E. R. Goldman, M. P. Pazirandeh, P. T. Charles, E. D. Balighian and G. P. Anderson, *Anal. Chim. Acta*, 2002, **457**, 13-19.
55. B. P. Gray, S. Li and K. C. Brown, *Bioconjugate Chem.*, 2013, **24**, 85-96.
56. T. Nagai, K. Ibata, E. S. Park, M. Kubota, K. Mikoshiba and A. Miyawaki, *Nat. Biotechnol.*, 2002, **20**, 87-90.
57. B. Shui*, et al.*, *Nucleic Acids Res.*, 2012, **40**, e39.

`

Chapter 4

FO-SPR high-resolution genetic screening

Part of this chapter has been published in:

Knez K., Janssen K., Pollet J., Spasic D., Lammertyn J. (2012). Fiber optic high-resolution genetic screening using gold-labeled gene probes. *Small, 8*(6), 868-872.

4.1 Introduction

The fast moving field of genetic screening is currently revolutionizing medical diagnostics and life sciences[1,2]. Nevertheless, the accurate detection of a single nucleotide polymorphism (SNP), the smallest possible type of genetic variability, still remains a challenging task. These single base pair alterations at the genetic level can have significant effects at the phenotype level. SNPs are linked with complex pathologies such as cancer[3], cystic fibrosis[4], infectious diseases[5] and many others[6]. Detection and identification of SNPs will allow for more accurate diagnostics, will improve drug development and can simplify treatment decisions. Consequently, there is an increasing demand for screening technologies, which has catalyzed the development of new

methods for SNP analysis[7-9]. Currently, sequencing is the method of choice for SNP screening and discovery. Despite the major advances offered by next-gen-sequencing, the technology is not yet ready to be used in routine point-of-care applications because of labor intensity and cost. To make genetic screening more accessible significant effort has been put in the development of faster and less expensive assays[10,11], yet the design of robust microarrays for genotyping with single nucleotide resolution on a genome-wide scale has proven to be a very difficult task. In this respect, High Resolution Melting (HRM), which is actually an improved embodiment of classical DNA melting analysis, is gaining popularity[11-13]. HRM technology is a post PCR method that characterizes nucleic acid samples based on their dissociation behavior during melting. This approach has a number of distinct advantages such as reduced total assay time and cost. However, there are some issues with fluorescence based HRM. Results are not consistently unambiguous and variations in the wild type melting behavior can hamper reliable SNP detection[14].

4.2 Aim of this chapter

In the search for an improved, highly sensitive and cost effective genetic profiling technique, we present a new HRM method based on DNA probes and gold nanoparticles (Au NPs). Au NPs have proven to be very efficient labeling agents for Surface Plasmon Resonance (SPR) based study of oligonucleotide interactions[15] and offer significant advantages over fluorescent dyes[16-18].

In this proof-of-concept work, we apply Fiber Optic – Surface Plasmon Resonance (FO-SPR) sensors (Figure 4.1) in combination with high-resolution sample heating to monitor the melting behavior of synthetic DNA duplexes, enabling SNP screening. In order to show the power and applicability of this FO sensor we tested different genetic targets of varying length and makeup.

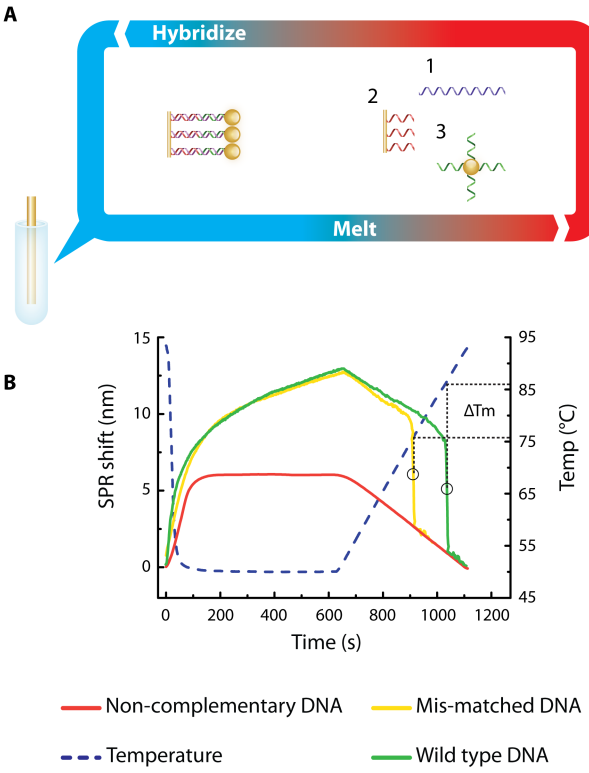

Figure 4.1: A) Schematic representation of an FO genetic screening assay with DNA target (1), DNA probe functionalized FO-SPR sensor (2) and DNA probe functionalized Au NP (3). Gene probes hybridize at the FO surface, and are subsequently melted off by a gradual increase of the temperature. B) Representative sensorgram. DNA targets and DNA Au NP probes were allowed to hybridize for 10min at 50°C, resulting in a shift of the SPR wavelength. Subsequently, the temperature is increased stepwise to accurately determine the melting temperature (Tm). At Tm DNA-Au NP complex melts off, decreasing the SPR signal.

4.3 Materials and methods

4.3.1 Reagents

All synthesized oligonucleotides were purchased from Integrated DNA Technologies (Belgium). All general chemicals were obtained from Sigma-Aldrich (Belgium) unless stated otherwise. Optics and optical components were purchased from Ocean Optics (Dunedin, USA).

4.3.2 Device setup

The FO-SPR device used was identical to the setup described in Chapter 3 Section 3.3.3. When the gold layer is coated with DNA as is in the case the FO-SPR HRM assay, the FO-SPR sensor can be used to monitor interactions of this immobilized DNA with free DNA in a solution. In order to augment assay sensitivity the complementary gene probes are labeled with Au NP. The thermocycler temperature was monitored externally using a NI-DAQ (National instruments, Austin, USA) with three highly responsive T-type WK-200 thermocouple threads (Labfacillity, Leads, United Kingdom). This allowed us to monitor the exact temperature at the FO surface and derive the exact melting temperature by combining temperature data with the SPR sensorgram.

Spectrophotometer data was processed in real-time using Omnidriver software (Ocean optics, Dunedin, USA) and an in house written Matlab script (The Mathworks Inc, Natick, USA). Temperature logging of the NI-DAQ was managed using a custom Labview program (National Instruments, Austin).

4.3.3 FO sensor tips

FO-SPR sensor tips were manufactured as described in Chapter 3 Section 3.3.4. The freshly coated FO sensors were immediately incubated with 1 µM reduced DNA with a 3' thiol endgroup (Table 4.1) to create a dense DNA surface coating. The reduction of the thiol-DNA was done by incubating 50 µM thiol-DNA for 3 h in 0.1 M phosphate buffer (PB) containing 0.18 M Dithiotreithol (DTT, Acros Organics, Geel, Belgium). Afterwards, the DTT was removed from the activated DNA using NAP5 Sephadex columns (GE Healthcare, Pittsburgh, USA). The FO sensors are incubated overnight in the DNA PB solution to get a dense DNA covering. Afterwards the FO sensor was rinsed three times in PB with 0.01% SDS and stored in a fridge. The final DNA density on the FO sensor was estimated 0.40 ± 0.02 strands per nm^2.

4.3.4 Gold nanoparticles

Au NPs with a diameter of approximately 20 nm were produced using the citrate reduction method as described by Frens *et al.*[19]. In order to functionalize the Au NPs with DNA, the citric acid stabilizing

agent was gradually exchanged with DNA oligonucleotides, functionalized with a 5' or 3' thiol endgroup (Table 4.1). Similar to the functionalization of the FO sensor surface, the thiol-DNA was added to the gold nanoparticles in a final concentration of 1 µM. To maximize DNA loading on the Au NPs a fast salt maturation protocol as described in Hurst *et al.*[20] was used. After 5 h, the Au NPs were washed three times in PB with 0.01% SDS, to remove the excess of salt and any unbound DNA. Finally the beads were dissolved in PBS 300 mM NaCl. The final DNA density on the AU NPs was determined using DTT stripping of a fluorescently labeled gene probe. On each Au NP approximately 230 ± 10 strands were counted.

4.3.5 Oligonucleotides

Synthetic DNA oligonucleotides were purchased from IDT (Haasrode, Belgium). The capture probes on the FO-surface and on the Au NPs were attached with a C-3 or C-6 thiol group at concordant the 3' and 5' end of the oligonucleotide sequence. All the oligonucleotide probes were equipped with either a poly A or poly T spacer in order to improve the hybridization efficiency of the DNA[20]. Three target sequences were chosen to demonstrate the measuring principle and the superior sensitivity of the FO-SPR biosensor platform.

In a first proof of principle experiment a short 30bp target was chosen, further referred to as target 1. The sequence was adopted from the literature[21], therefore the spacer differs of the oligonucleotide probes from the other targets. To the best of our knowledge target 1 has no real-life functionality. Target 2 is a part of the coding sequence of the P53 tumor suppressor gene , which is found to be involved in more than 50% of all cancers [22]. The 55bp sequence is known to be a mutational hot spot[23], however screening this target for SNPs is challenging because it has a GC ratio of 59% and is therefore prone to secondary structures. The last target was an 80bp bacterial target comprising a gene of the *Legionella pneumophila* bacteria genome, crucial for the pathogenicity of the *Legionella pneumophila* strain. The sequence is used in routine quantification of bacteria numbers and was first described in a paper by Yanez, *et al.*[24]

For every sequence three random base pair substitutions were chosen, the mutations are located in the middle or either at the 3' or

5'end. We chose these positions to prove that the detection principle is not depending on the position of the mutation and furthermore that the FO sensor can consistently locate the position of the mutation. Sequences of the DNA targets and the DNA probes used in this paper are listed in

Table 4.1.

Table 4.1: Summary of all synthetic DNA sequences used for FO-SPR HRM

Targets

Target 1 (30 bp)	**Target 2: P53 cancer gene locus (56 bp)**
Wild type 5- GAG GGA TTA TTG TTA AAT ATT GAT AAG GAT -3 **Middle MM** 5- GAG GGA TTA TTG TTA AAC ATT GAT AAG GAT -3 **5' MM** 5- GAG GGA TTA TTG TTA AAT ATT GAT AAA GAT -3 **3' MM** 5- GAG AGA TTA TTG TTA AAT ATT GAT AAG GAT -3	**Wild type** 5- TTC CTG CAT GGG CGG CAT GAA CCG GAG GCC CAT CCT CAC CAT CAT CAC ACT GGA AG -3 **Middle MM** 5- TTC CTG CAT GGG CGG CAT GAA CCG GAG ACC CAT CCT CAC CAT CAT CAC ACT GGA AG -3 **5' MM** 5- TTC CTG CAT GGG CGG CAT GAA CCG GAG GCC CAT CCT CAC CAT CAT CAC ACT AGA AG -3 **3' MM** TTC CTG CAT GGA CGG CAT GAA CCG GAG GCC CAT CCT CAC CAT CAT CAC ACT GGA AG -3
Target 3: Legionella P. amplicon dotA gene (80 bp)	
Wild type 5- ATT GTC TCG CGC GAT TGC TAT ACA GCA AAT GTA TGT GAC TTT ATC TAC GGT GGC ACA GGT GAT GGT TAA TAA TGA TCC GG -3 **Middle MM** 5- ATT GTC TCG CGC GAT TGC TAT ACA GCA AAT GTA TGT GAA TTT ATC TAC GGT GGC ACA GGT GAT GGT TAA TAA TGA TCC GG -3 **5' MM** 5- ATT GTC TCG CGC GAT TGC TAT ACA GCA AAT GTA TGT GACTTT ATC TAC GGT GGC ACA GGT GAT GGT TAA TAA TAA TCC GG -3 **3' MM** 5- ATT GTC TCG CGC GAT TGC TCT ACA GCA AAT GTA TGT GACTTT ATC TAC GGT GGC ACA GGT GAT GGT TAA TAA TGA TCC GG -3 **Non-matching DNA template (37 bp)** 5- TTCCCCGGCCTGGGCTCG GGACCCACTCGTGCTGTCC-3	

Probes

FO sensor Oligonucleotide	**Au NP Oligonucleotide**
Target 1 5- TAA CAATAATCC CTC A_{20}/3ThioMC3-D/ -3	5-/5ThioMC6/A_{20} ATC CTT ATC AAT ATT -3
Target 2- P53 target 5- CCT CCG GTT CAT GCC GCC CAT GCA GGA A T_{18} /3ThioMC3-D/ -3	5- /5ThioMC6/T_{18} CTT CCA GTG TGA TGA TGG TGA GGA TGG G -3
Target 3 - Bacterial target	

5- AGT CAC ATA CAT TTG CTG TAT AGC AAT CGC GCG AGA C AAT T_{18}/3ThioMC3-D/ -3	5- /5ThioMC6/T_{18} CCG GAT CAT TAT TAA CCATCA CCT GTG CCA CCG TAG ATA A

4.3.6 Calculation of the probability of ssDNA secondary structure formation in the target sequences (using mFold[25] and DINAfold[25])

Finally we evaluated the probability of the hybridization of our DNA targets into secondary structures (self-hybridization) in comparison to the probability of hybridizing to its complementary sequence (forming a normal dsDNA sequence). This is important because these structures could influence or hamper the T_m measurements.

The chance of secondary structures was calculated using the well-known mFold algorithm to calculate the Gibbs free energy for secondary structures and the theoretical T_m (self-hybridization of the ssDNA of the targets). For the dsDNA of the target and its complementary sequence the DINAmelt model was applied.

The results clearly show that the Gibbs free energy for all the targets is in favor of hybridization with its complementary sequence into dsDNA (Table 4.2). Furthermore the calculated T_m of the secondary structures was much lower than the T_m that was predicted for the targets and the T_m that was measured using both HRM and FO-SPR. We therefore can conclude that the melting analysis was by no means influenced by the secondary structures.

Table 4.2: Summary of the theoretical calculation of the Gibbs free energy and the melting temperature for the secondary structures of the ssDNA of the 3 target sequences as compared to the Gibbs free energy of the formation of the dsDNA structure of target DNA with its complementary sequence. The values were obtained using respectively the mFold model for ssDNA secondary structures and the DINAmelt model for the dsDNA of the targets. The DINAMelt model was not applicable for sequence 3 because of its length. (All models were made using an NaCl concentration of 300mM and a DNA concentration of 10nM).

	Target 1:	Target 2:	Target 3:
DINAMelt			
ΔG (Kcal/mol)	- 43.2	- 115.8	NA
T_m (C°)	59.9	85.1	NA
mFold			
ΔG (Kcal/mol)	0.51	-2.91	-1.26

T_m (C°)	32.0	73.9	61.3

Finally we also evaluated the ssDNA secondary structures of the immobilized probes on both Au NP and FO-SPR surface. (using mFold, data not shown) The Gibbs free energy of these probes was not favorable for the formation of these structures. Due to the length of these sequences as compared to the full length of the targets, their melting points were below the hybridization temperatures applied in the tests described in this article. Therefore we can conclude self-hybridization and secondary structures did not influence our results.

4.3.7 FO sensor high resolution melting assay

The SPR melt analysis uses the binding and release of Au NPs on the SPR surface by means of DNA strands. As described in Figure 4.1, the general measurement procedure uses a single stranded DNA target, which binds simultaneously a NP and the SPR sensors surface, both functionalized with an oligonucleotide complementary to the 5' and the 3' side of the target, respectively. In the case of a mismatch in the sequence, binding of the target to both the NP and the SPR fiber will be hindered. This will result in a lower binding signal. However, previous research showed that depending on the locus of the mutation and the type of single nucleotide polymorphism, detection of these single base variations could become difficult and demands an elaborate assay optimization[26]. Therefore a heating step was introduced. By slowly heating the analyte solution, the bound DNA will melt and the nanoparticles will detach from the sensor surface. Base pair mismatches will affect and cause a shift in the melting temperature (T_m).

All buffer components for the melting experiments were purchased from Sigma Aldrich (Bornem, Belgium) unless stated otherwise. For every melting experiment 15 µL of the DNA target in a concentration ranging from picomolar to nanomolar concentrations was added to 125 µL PBS with 300 mM NaCl and functionalized gold nanoparticles (concentration depended on experiment). In order to prevent evaporation because of the heating cycles, all reaction vials were covered with a thin layer of silicon oil (Bio-Rad, Hercules, USA).

Before each measurement, the samples were very briefly exposed to 94°C for 5 s. Subsequently, the temperature was dropped to the optimal

hybridization temperature of the target to allow the DNA to bind to both the fiber surface and the Au NPs. After 15 min, the temperature was slowly augmented (0.1 °C s^{-1}) to determine the precise T_m. Blank measurements were executed using a non-matching DNA template consisting of a scrambled DNA sequence with a length of 37bp.

4.3.8 HRM reference measurements

Without pre-amplification

The melting points of the oligonucleotide targets were validated using standard HRM analysis on a Qiagen Rotorgene 6000 (Qiagen, Germantown, USA) device in combination with Evagreen saturating dye (Biotium, Hayward, USA). The synthetic reverse complement of every target sequence was ordered to get a double stranded sequence suited for HRM analysis. The melting reactions were performed in the same PBS 300 mM NaCl buffer as the FO melt reactions in order to compare the melting points and the results. The reaction mixture consisted of 1.5 µL Evagreen dye (20 X), 10 µM of the DNA target, 10 µM DNA of the target complement in a final volume of 15 µL. The thermal cycle and heating steps were similar to the thermal sequence of the FO sensor melt reaction and consisted of a quick denaturation step of 1 min at 94°C followed by a hybridization step of 10 min and finally a heating step, with a temperature gradient of 0.1 °C s^{-1}.

Raw melting curves of both HRM and SPR measurements were analyzed in the same way. All melting points were determined using the first derivative of the measurement signal divided by the first derivative of the temperature.

With pre-amplification

Because the bacterial sequence is a PCR target, the sequence was also analyzed using HRM with a pre-amplification step. HRM reaction mixtures were prepared using AccuMelt™ HRM SuperMix (Quanta bioscience, Gaithersburg, USA) according to the manufacturers recommendations. Primers were ordered and used in the amounts asas described by Yanez[24]. The samples were amplified using shuttle PCR. The TAQ enzyme was activated at 95°C for 5 min, afterwards 40 cycles of 60°C annealing/extension for 30 s followed by a denaturing step at

95°C for 5 s were performed. The actual melting analysis was initiated at 60°C and ended at 95°C with a temperature gradient of 0.1°C s^{-1}.

4.4 Results

The SPR melt analysis uses the binding and release of Au NP labeled gene probes on the SPR surface to detect variations in the synthetic DNA sequence. As illustrated in Figure 4.1, a single stranded DNA target (1) will simultaneously bind to an Au NP (3) and the FO sensor surface (2). Both FO sensor and Au NP are functionalized with an oligonucleotide sequence complementary to the 5' and the 3' ends of the target, respectively. In the case of a mismatched sequence, binding of the target to the Au NP and the SPR fiber will be influenced, resulting in slightly altered hybridization kinetics. However, variations in the locus of the mutation and the type of SNP make detection of these small kinetic variations challenging, requiring elaborate assay optimization[26]. Nevertheless, by slowly heating the sample, the surface-bound DNA will melt and the Au NPs will detach from the sensor surface, causing an SPR wavelength shift. FO-SPR based Tm analysis involves hybridization of the target DNA at two distinct sites, the FO-SPR sensor and the Au NP reporter. It is well known that local surface geometry and -functionalization can significantly influence the hybridization behavior of DNA on a support[27,28]. It can therefore be envisioned that FO-SPR analysis offers the intrinsic capability to not only detect SNPs but also offer information on the location of the SNP. Classic HRM cannot offer this advantage. Figure 4.1 shows the shift in SPR signal for a non-matching DNA template (red) and two positive DNA samples (yellow, SNP and green, wild-type). The data clearly show the influence of DNA binding, superimposed on the temperature-induced change in SPR wavelength shift[29,30]. When the T_m is reached, Au NPs will dissociate from the fiber surface, causing a significant signal shift. Above the T_m, the FO will be free of Au NPs and only the temperature induced SPR shift is observed. Because the FO sensor uses the T_m as the only point of differentiation, it holds a clear advantage compared to previously reported SPR SNP sensors, which typically require specific conditions or additional sample manipulations[27,28,31,32].

To validate the use of FO-SPR as an SNP detection platform, three targets, each with specific properties were chosen. Target 1 consists of a 30bp-long random synthetic DNA sequence. Target 2 is a challenging 56bp sequence with a high GC content of 59%. It is a part of the coding sequence of the P53 tumor suppressor gene, which is found to be involved in over 50% of all cancers[22] and known to be a mutational hot spot[23]. Finally, the FO genomic assay was used to detect SNPs in an 80bp sequence (target 3), which is part of a defect in the organelle trafficking gene (dotA) of *L. pneumophila*[27,33]. Target 3 is particularly interesting because it can be expected that practical assay embodiments will involve measurements on samples produced through PCR amplification. Amplicons are typically 80 to 120bp- long, whereas most reports on SNP detection platforms[8,34-36] focus on short oligonucleotide sequences (<30bp) because the impact of an SNP is more apparent at these sequence lengths (more details on the sequences used can be found in the supporting information).

Two important assay parameters were evaluated to optimize the biosensor sensitivity for SNP detection. First, the performance of the FO sensor was tested at different concentrations of target DNA while keeping the Au NP concentration constant at 1 nM. Hybridization increases at higher concentrations of the target DNA, and this will impact T_m up to the moment where the sensor surface is completely saturated, at which point the SPR wavelength shift upon binding can also be expected to level off. Part A in Figure 4.2 clearly shows the concentration-dependent evolution of T_m for target concentrations between 1 pM and 1 µM. The accuracy with which T_m can be determined is excellent, even for sub-nanomolar concentrations of target DNA.

An analogous experiment was conducted with variable Au NP concentrations while keeping the concentration of target DNA constant at 10 nM (Figure 4.2, part B). High Au NP concentrations induced larger SPR shifts, however, the T_m remained constant for all measured NP concentrations. Based on the data presented in Figure 4.2, Au NP concentrations of 1 nM and DNA target concentrations of 10nM were chosen for all further experiments as these conditions allowed for maximal SPR shifts with minimal T_m variability.

For each of the DNA targets three types of mismatches were evaluated respectively at the 3` end, the middle or at the 5` end. Mismatches were chosen at these sites to test whether FO sensor is capable of detecting them, irrespective of their location.

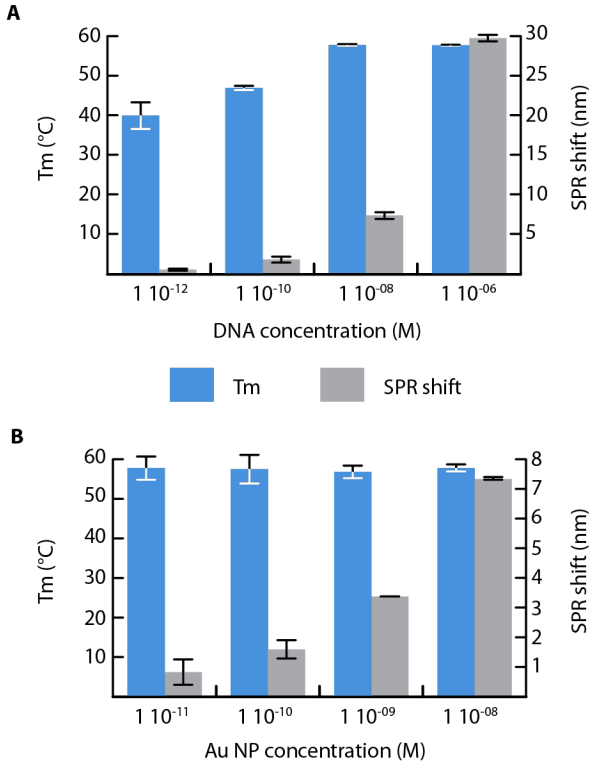

Figure 4.2: A) Effect of synthetic DNA target concentration on the SPR wavelength shift and Tm. B) Effect of the Au NP concentration on the SPR wavelength shift and the concentration dependent evolution of Tm. Results are based on experiments with target 1, other targets showed similar trends. Error bars indicate standard deviations (n=3).

Figure 4.3 shows the first derivative of the melting curves obtained for target 2. As can be seen in the graph, the FO sensor allows for a clear differentiation of single nucleotide mutations. FO-SPR derived T_m is a good indicator for SNP identification.

The FO-SPR measurements were validated using classical fluorescence-based melting analysis on an HRM-ready qPCR device

(Rotorgene 6000, Qiagen, USA). For the HRM assay, relatively high DNA concentrations (10µM) were necessary to get an acceptable readout.

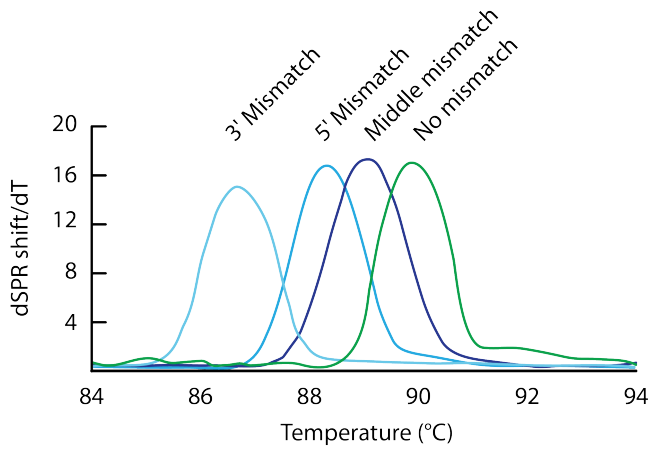

Figure 4.3: First derivative of the melting curves for the p53 target, and three different mutants as obtained with the FO-SPR sensor.

All remaining conditions, such as hybridization temperature, time and melting steps were identical to those used for the FO melting assay. For target 3, a full HRM assay with amplification of the target was also performed, while this was not possible for the first two targets because of their limited length (Figure 4.4).

The results of both the FO- and the HRM assay for the first target show a significant difference in T_m for the SNP sequences versus their wild type counterparts. However, the FO-SPR assay offers the additional benefit of also providing information on the location of the SNP. The 3' mismatch had the most significant impact on the T_m, while the 5' mismatch and middle mismatch were harder to differentiate. Note that classic HRM measurements did not allow for discrimination between the 5' mutant and the wild type sequence. Finally, for target 3, the detection of SNPs was improved with the new FO assay. Both HRM and pre-amplification HRM hardly show any difference in T_m compared to the wild type sequence.

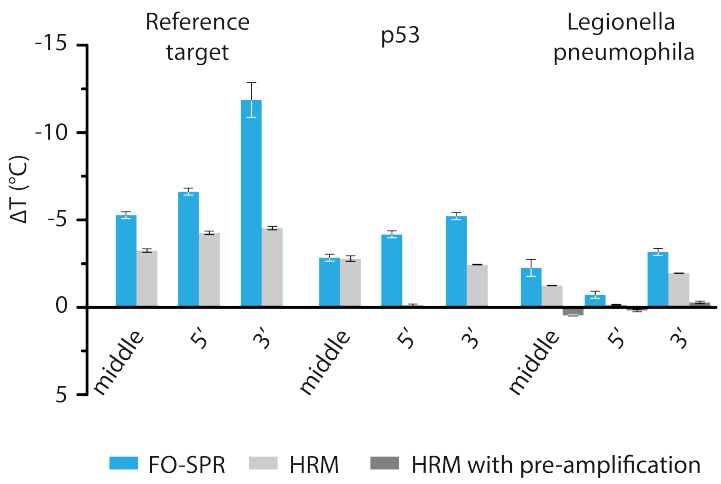

Figure 4.4: General comparison between SNP data obtained by the FO-SPR melting assay and fluorescence based HRM. The bars indicate the difference between the Tm of SNPs relative to the Tm of the wild type sequences. Error bars indicate standard deviations (n=3). Note that pre-amplification HRM can also produce negative ΔT_m values since the analysis relies on the difference in melting behavior of different, yet fully complementary amplicons whereas the other techniques monitor the melting of mis-matched sequences, which will always have lower T_m as opposed to the wild-type sequences. See supporting information for the full data.

In contrast to the other targets, target 3 gave the smallest T_m shift for the 5' mutation. One would expect that mutations close to either the gold surface of the optical fiber or the Au NP would result in a maximal T_m shift because of surface effects [27,28]. However, the results of the HRM reference measurements show that the mutation hardly influences the T_m, which is an indication of the very high duplex stability of this particular sequence and this in turn could explain the behavior observed during the FO-SPR measurement.

As expected, comparison of the relative magnitude of the T_m shift for different targets indicates that the sequence length has an important impact on the sensitivity. One can see that, independent of the detection technique, the signal decreases gradually with increasing target length. For longer sequences such as target 3, the mismatch has only a limited impact on the duplex stability of the 80bp sequence; hence the mutation only minimally disturbs the hybridization.

4.5 Conclusion

In conclusion, we have presented an FO-SPR sensor for real-time monitoring of melting curves using Au NP linked gene probes. We first validated the system using a range of target- and Au NP concentrations for ultra-sensitive SNP detection. Results showed that the combination of thermal cycling and the FO-SPR sensor transforms traditional SPR and its FO counterpart into a fast and highly applicable genetic screening tool. Secondly, we have shown that SNP detection is not limited to short length targets but can be easily extended to longer target sequences, such as those typically produced during PCR. Moreover, sequences with a high G/C content did not negatively impact sensor resolution.

Results were validated using commercially available, fluorescence-based HRM. The FO sensor showed improved resolution and allowed to easily differentiate mutations. Furthermore, we have shown how FO-sensor melting analysis could be used to locate the mismatch to a specific sequential site. This could be an extra advantage if the FO sensor would be used as a routine SNP detection tool prior to sequencing, as it would allow for shorter sequencing domains. The FO-SPR is therefore ideally suited for genetic screening; we showed that in less than 20 minutes mutations in the p53 gene or bacteria could accurately be identified. Even if additional sample preparation, such as post PCR cleanup would be necessary prior to FO-SPR analysis, total assay time can easily be limited to less than 2 hours. These results prove that the FO-SPR sensor can make a difference in the choice for treatment options for cancer or for bacterial infections where fast but accurate diagnostics are crucial for the patient survival[37]. The robust nature of the FO-SPR sensor would also allow for the application in the food and water industry, where detection of pathogenic microorganisms is essential for the public safety.

In order to proof that the FO-SPR melt assay truly can live up to these great promises the assay will be applied in the next chapter on clinical samples and the performance of the assay will be directly compared to routine genetic screening techniques such as sequencing

and fluorescence based HRM. This will allow us to evaluate whether the FO-SPR melt assay is a potential POC candidate.

References

1. W. Burke, *N. Engl. J Med.*, 2002, **347**, 1867-1875.
2. D. Altshuler, M. J. Daly and E. S. Lander, *Science*, 2008, **322**, 881-888.
3. M. D. Bacolod, G. S. Schemmann, S. F. Giardina, P. Paty, D. A. Notterman and F. Barany, *Cancer Res.*, 2009, **69**, 723-727.
4. J. Lamba, V. Lamba, S. Strom, R. Venkataramanan and E. Schuetz, *Drug Metab. Dispos.*, 2008, **36**, 169-181.
5. N. W. Schroder and R. R. Schumann, *Lancet Infect. Dis.*, 2005, **5**, 156-164.
6. C. S. Carlson, M. A. Eberle, L. Kruglyak and D. A. Nickerson, *Nature*, 2004, **429**, 446-452.
7. F. Teles and L. Fonseca, *Talanta*, 2008, **77**, 606-623.
8. Y. Xiao, K. J. Plakos, X. Lou, R. J. White, J. Qian, K. W. Plaxco and H. T. Soh, *Angew. Chem. Int. Ed. Engl.*, 2009, **48**, 4354-4358.
9. D. Kato, N. Sekioka, A. Ueda, R. Kurita, S. Hirono, K. Suzuki and O. Niwa, *Angew. Chem. Int. Ed. Engl.*, 2008, **47**, 6681-6684.
10. A. Sassolas, B. D. Leca-Bouvier and L. J. Blum, *Chem. Rev.*, 2008, **108**, 109-139.
11. A. M. Leconte*, et al.*, *Angew. Chem. Int. Ed. Engl.*, 2010, **49**, 5921-5924.
12. M. Erali and C. T. Wittwer, *Methods*, 2010, **50**, 250-261.
13. G. H. Reed, J. O. Kent and C. T. Wittwer, *Pharmacogenomics*, 2007, **8**, 597-608.
14. J. Jimenez Ide, E. Esteban Cardenosa, S. Palanca Suela, E. B. Gonzalez and P. Bolufer Gilabert, *Clin. Biochem.*, 2009, **42**, 1572-1576.
15. J. Pollet, K. P. Janssen, K. Knez and J. Lammertyn, *Small*, 2011, **7**, 1003-1006.
16. Y. P. Bao, M. Huber, T. F. Wei, S. S. Marla, J. J. Storhoff and U. R. Muller, *Nucleic Acids Res.*, 2005, **33**, e15.
17. D. Kim, W. L. Daniel and C. A. Mirkin, *Anal. Chem.*, 2009, **81**, 9183-9187.
18. H. Q. Wang, W. Y. Liu, Z. Wu, L. J. Tang, X. M. Xu, R. Q. Yu and J. H. Jiang, *Anal Chem*, 2011, **83**, 1883-1889.
19. G. Frens, *Nature-Phys Sci*, 1973, **241**, 20-22.
20. S. J. Hurst, A. K. Lytton-Jean and C. A. Mirkin, *Anal. Chem.*, 2006, **78**, 8313-8318.
21. Y. C. Cao, R. Jin, C. S. Thaxton and C. A. Mirkin, *Talanta*, 2005, **67**, 449-455.

22. G. P. Pfeifer and M. F. Denissenko, *Environ. Mol. Mutagen*, 1998, **31**, 197-205.
23. D. Gerion*, et al.*, *Anal. Chem.*, 2003, **75**, 4766-4772.
24. M. A. Yanez, C. Carrasco-Serrano, V. M. Barbera and V. Catalan, *Appl. Environ Micro.b*, 2005, **71**, 3433-3441.
25. C. Chen, W. Wang, J. Ge and X. S. Zhao, *Nucleic Acids Res.*, 2009, **37**, 3756-3765.
26. E. Milkani, S. Morais, C. R. Lambert and W. G. McGimpsey, *Biosens. Bioelectron.*, 2010, **25**, 1217-1220.
27. R. Jin, G. Wu, Z. Li, C. A. Mirkin and G. C. Schatz, *J. Am. Chem. Soc*,. 2003, **125**, 1643-1654.
28. P. Gong and R. Levicky, *Proc. Natl. Acad. Sci. U S A*, 2008, **105**, 5301-5306.
29. P. Heinz*, et al.*, *Langmuir*, 2008, **24**, 6166-6175.
30. A. Dhawan and J. F. Muth, *Nanotechnology*, 2006, **17**, 2504-2511.
31. K. Nakatani, S. Sando and I. Saito, *Nat. Biotechno.l*, 2001, **19**, 51-55.
32. Y. Li, A. W. Wark, H. J. Lee and R. M. Corn, *Anal. Chem.*, 2006, **78**, 3158-3164.
33. R. R. Isberg, T. J. O'Connor and M. Heidtman, *Nat. Rev. Microbiol*, 2009, **7**, 13-24.
34. J. H. Watterson*, et al.*, *Nucleic Acids Res.*, 2004, **32**, e18.
35. X. Duan, Z. Li, F. He and S. Wang, *J. Am. Chem. Soc.*, 2007, **129**, 4154-4155.
36. B. A. Du, Z. P. Li and C. H. Liu, *Angew. Chem. Int. Ed. Engl.*, 2006, **45**, 8022-8025.
37. R. Etzioni*, et al.*, *Nat. Rev. Cancer*, 2003, **3**, 243-252.

Chapter 5

FO-SPR DNA melting for detection of *Legionella pneumophila*

Part of this chapter has been published in:

Knez K., Janssen K., Spasic D., Declerck P., Vanysacker L., Denis C., Tran T., Lammertyn J. (2013). Spherical Nucleic Acid enhanced FO-SPR DNA melting for detection of mutations in *Legionella pneumophila*. *Analytical Chemistry, 85*(3), 1734-1742.

5.1 Introduction

The development of fast, sensitive and affordable technologies for the detection of DNA in clinical and environmental diagnostics has been the subject of intense research to date[1,2]. Of particular interest is the accurate detection of point mutations, so called single nucleotide polymorphisms (SNPs), in genetic material of various origins. It is well known that these SNPs for example can play a significant role in the onset and development of many, if not all, types of cancer[3,4], cystic fibrosis[5], and antibiotic resistance for bacteria[6]. As such their identification is vitally important for making accurate clinical treatment decisions[7,8].

Likewise, SNPs can also be highly important when dealing with pathogen detection not only in healthcare settings but also for food, environmental and public safety applications. An effective illustration of this is *Legionella pneumophila,* which is one of the most common pathogenic *Legionella* species, accounting for more than 90% of Legionnaires' disease outbreaks[9]. Human infection occurs through inhalation of aerosols generated near man-made water ducts where the bacterium can thrive, particularly in hot water systems such as public showers, or even cooling towers[10]. Bacterial numbers therefore need to be tightly monitored[11]. Moreover, virulence of *L. pneumophila* varies greatly among different serogroups, with serogroup 1 being responsible for a large fraction of all infections[12]. Hence, these bacteria not only need accurate quantification but also classification based on small genetic variations between different serogroups. In this respect, quantitative PCR (qPCR), standalone or in combination with a high resolution melting assay (HRM), is often used for fast identification of pathogenic bacteria in both environmental[13] and clinical samples[14], and is accepted as an alternative for the more time consuming bacterial cultures. The method is generally known for its high sensitivity and specificity[15], but a good assay is highly dependent on the region within the genome that is targeted for amplification. This region needs to be well conserved in order to allow for the design of efficient primers. However, one of the regions often used to quantify *L. pneumophila* - 'the defect in organelle trafficking' gene (*dotA*) - was recently found to be highly variable[16-18]. Mutations in the priming regions can thus cause significant bias in PCR based quantification or even complete inhibition of amplification[19].

Next-generation sequencing could address some of these concerns by providing access to the full genetic make-up of a sample. However, despite rapid advancement of these sequencing technologies, they still remain largely impractical for applications such as mutation analysis of *L. pneumophila* due to the demanding technical requirements as well as the high costs. Moreover, within a particular species, only a relatively small number of sequence variations can be expected across the genome[20] and as such, full sequence availability is not necessary in most cases[21].

The complexities of next-generation sequencing can be avoided by making use of the fact that hybridization of short oligonucleotides with the target genetic material is quantitatively sensitive to the number and position of mismatches[22-24]. These mismatches between target sequence and probe sequence are changing the melting point, which can be detected. When these assays are performed with probes immobilized on solid surfaces, they become amenable to multiplexing[25] and are more sensitive[26] compared to the commonly used qPCR-HRM assays[27-29]. Moreover, if the solid support is a gold nanoparticle (Au NP), the sensitivity of DNA melting can significantly increase[24,30,31] compared to traditional probe based melting analyses. The properties of these DNA functionalized Au NPs are so unique that they warranted the introduction of a new terminology: spherical nucleic acids (SNA)[32]. When SNAs are applied as labeling probes in DNA dehybridization, cooperative effects of the DNA strands near the SNAs surface result in exceptionally sharp transitions between the double- and single stranded state. Therefore, SNAs can increase the resolution in discriminating various types of mutations when implemented in a DNA melting assay.

Surface Plasmon Resonance (SPR) was introduced to monitor DNA melting in real-time by Fiche *et al.*[33] Using this approach, SNPs were directly detected in short oligonucleotides immobilized on a SPR imaging array. As described in the previous chapter, we combined SNAs with Fiber Optic (FO)-SPR, which allowed monitoring of DNA hybridization and melting in real-time with even higher resolution and in longer DNA strands. As SNAs are excellent signal enhancers for SPR which also narrow the width of the melting signal, this biosensor has an outstanding resolution for fast and accurate detection of mutations[24]. Moreover, the assay is able to discriminate SNPs in oligonucleotides of up to 80bp and even with high GC content. By further improvement, the FO-SPR melting assay was made compatible with complex samples such as PCR mixtures, which contain both enzymes and DNA, steering thus its application towards differentiation of highly homologous bacterial serogroups[34].

5.2 Aim of this chapter

In this chapter the FO-SPR melting assay is applied to unravel mutations in the *dotA* gene of *L. pneumophila* PCR samples. Identifying mutations in PCR samples is particularly challenging as mutations in the priming region become low abundant after a few PCR cycles due to the incorporation of the primers in the amplification products. Furthermore additional mutations can be introduced by the polymerase enzyme. However, these mutations are the ones of most importance as they can influence the efficiency of qPCR reaction and result in false negative results. Therefore it is of great importance to asses the genetic variability in genetic regions before implementing them as qPCR target regions. This article focuses on comparing this new approach with current standard technologies routinely applied in genetic testing, such as HRM and Sanger sequencing (Figure 5.1). Results show that FO-SPR solid phase melting in combination with SNA signal enhancement can readily be applied on PCR amplified bacterial targets to assess mutations. Furthermore, the FO-SPR approach surpassed both standard techniques in detecting rare mutations.

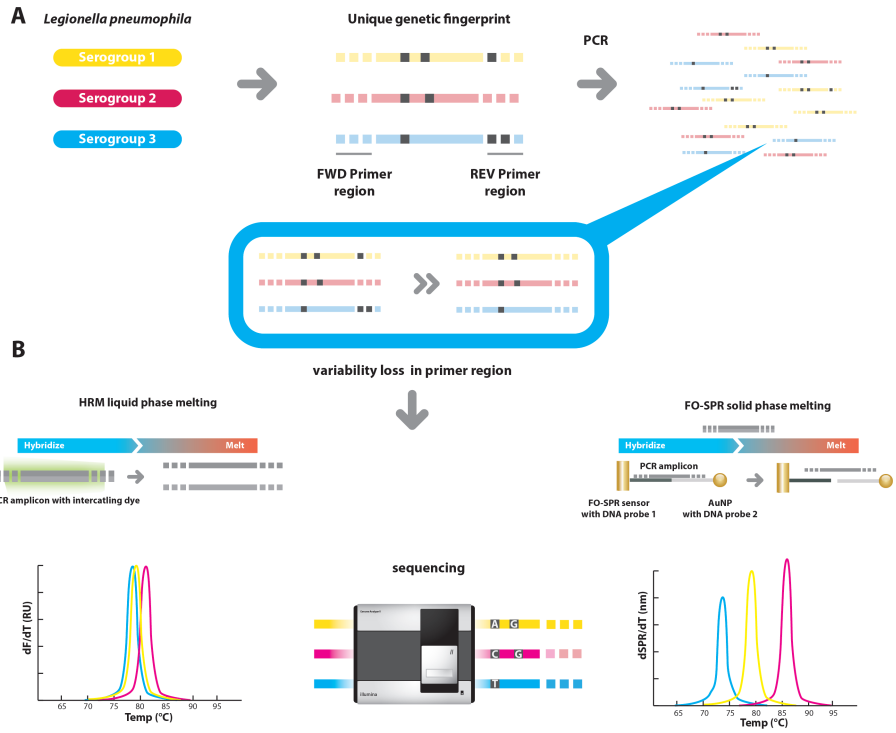

Figure 5.1: Schematic overview of different methods for bacterial serotyping. A) Different serogroups contain distinct versions of the target gene, due to mutations that accumulated in the bacterial genome over time. When the target region of the gene is amplified through PCR, the abundance of mutations in the priming regions can decrease. B) The obtained PCR product is subsequently used for the actual differentiation. This differentiation can be based on traditional HRM, which is known to offer limited resolution in particular cases, especially when mutations occur in close proximity. Full sequencing of the genetic material does not suffer this limitation but is expensive, time-consuming and amplification bias can still occur. FO-SPR offers high-resolution differentiation of sequences because the surface hybridization is inherently location specific, it will either hybridize to the Au NPs or the sensor surface, which affects the melting temperature differently.

5.3 Materials and methods

5.3.1. Reagents

Oligonucleotides were purchased from Integrated DNA Technologies (Haasrode, Belgium). All chemicals were purchased from Sigma-Aldrich (Belgium) unless stated otherwise. Au NPs with a diameter of approximately 20 nm were purchased from BBI international (Cardiff, United Kingdom).

5.3.2 Primers and probe design

For the presented assays, different primer and detection probe sequences were adopted from literature to amplify a region of the Macrophage Infection Progenitor (*MIP*) and the defect in the organelle trafficking A (*dotA*) genes and modified in correspondence with specific assay requirements (Table 5.1). qPCR was based on a Taqman design, which requires two primers and a Taqman probe with a 5' FAM label and a 3' prime minor groove binder. For the HRM assay only the primers were used of the Taqman qPCR assay without modifications. For the FO-SPR assay probes complementary to the full qPCR amplicon were designed and the specificity towards the target sequence and self-complementarity was checked using mFold[7]. The probes were modified with a 5' thiol for the Au NP probe and 3' thiol modification for the FO-SPR sensor tip.

Table 5.1: Overview of the different assays and their corresponding primer-probe combinations. ThioMC6: 5' thiol group coupled at carbon 6 at the 5' end of the phosphate backbone of the oligonucleotide. ThioMC3: thiol at the 3' end of the DNA oligo. FAM: Carboxyfluorescein MGB: minor groove binder.

Assay	Type	Sequence	Ref.
dotA qPCR	Fw Primer*	5'-ATTGTCTCGCGCGATTGC-3'	[35]
	Rev Primer*	5'-CCGGATCATTATTAACCATCACC-3'	
	Taqman probe	FAM 5'-ATACAGCAAATGTATGTGACTT-3' MGB	
MIP qPCR	Fw Primer*	5'- TTCATTTGYTGYTCGGTTAAAGC-3'	[9]
	Rev Primer*	5'- AWTGGCTAAAGGCATGCAAGAC-3'	
	Taqman probe	FAM 5'- AGCGCCACTCATAG-3' MGB	
FO-SPR (dotA)	Fiber probe	5'-AGTCACATACATTTGCTGTATAGCAATCGCGCGAGACAAT - T18 – Thio - 3'	Chapter 4
	Au NP probe	5'-Thio-T18 CCGGATCATTATTAACCATCACCTGTGCCACCGTAGATAA -3'	

*These primers were also used for the HRM assay

5.3.3 Culture analysis and DNA extraction

L. pneumophila serogroups, which are closely related strains of *L. pneumophila* expressing different antigens, were obtained from the American Type Culture Collection (ATCC). Seven clinical isolates of *L. pneumophila* serogroup 1, among which the *L. pneumophila* Corby isolate, originated from different outbreaks of *L. pneumophila*. A list with the ATCC numbers of all serogroups and the origin of the Clinical Isolates can be found in the supporting information (table S1). The *L. pneumophila* strains were cultured at 37°C on buffered charcoal yeast extract supplemented with L-cysteine and ferric pyrophosphate. The grown bacteria were used to spike samples of autoclaved Ringer solution. Cell numbers were first estimated using UV-VIS measurements

of bacterial suspensions at 650 nm, for all experiments 10^6 bacteria were used. The cell suspensions were plated and resulting colonies were counted after 5 days according to the NEN 6265 standard (1991). The culture detection limit was found to be 50 cfu/L.

The DNA of the bacterial suspensions was extracted using a NucleoSpin® Tissue kit (Machery-Nagel, Germany), according to the manufacturer's instructions. Extracted DNA was stored at -20°C in aliquots prior to usage.

5.3.4 FO-SPR setup and sensor manufacturing

The FO-SPR biosensor used was identical to the setup described in Chapter 3 Section 3.3.3. FO-SPR sensor tips were also manufactured according to the protocol described in Chapter 3 Section 3.3.4. Afterwards these FO-SPR sensor tips were functionalized using the protocol described in Chapter 4 Section 4.3.3. Subsequently, the DNA coated FO-SPR tips were backfilled in order to block non-specific binding of proteins to the sensor tip as described earlier[34] (a detailed description of the backfilling concept can be found in Chapter 1 section 1.6, using 10 µM of an hydroxyl terminated alkanethiol with 8 polyethylene oxide repeats (Polypure, Norway). This molecule was dissolved in ethanol and allowed to react for 3 h before rinsing the fiber with ethanol and placing it in phosphate buffer at 4°C for storage. In order to augment the FO-SPR device signal, Au NPs with complementary DNA probes were produced. Thiol-functionalized DNA was immobilized on the Au NPs by adding activated and purified DNA to a concentrated nanoparticle solution. A fast salt maturation protocol was used to maximize the DNA loading on the Au NPs[36]. Afterwards Au NPs were washed three times in phosphate buffer with 0.02% SDS and stored at 4°C prior to use.

5.3.5 Quantitative PCR

Taqman Q-PCR was performed on an ABI Prism 7000 system, in 96-well optical reaction plates (Applied biosystems, USA). The final reaction volume was 25 µl. For the MIP qPCR, 0.56 µl (10 µM) of both primers was used, 1 µl (0.2 µM) of probe, 2.5 µl 2% bovine serum albumin (BSA, Sigma Aldrich, USA), 12.5 µl 1X Taqman® universal master mix (Applied biosystems, USA), and 5 µl of template DNA which

corresponded to a starting volume of 10^6 genome units (GU) of *L. pneumophila* genome DNA. The *dotA* qPCR was obtained from Labaqua (Spain), and used according to the manufacturer's instructions. The following thermal cycling conditions were used for both qPCR reactions: 10 min 95 °C followed by 50 cycles of 15 s at 95°C and 1 min at 60 °C. Fam and respectively Rox dye, were used to monitor the amplification and the background during PCR amplification, these signals were obtained after each thermal cycle. The efficiency of the reaction was very close and in some cases even above 1.

5.3.6 High resolution melting analysis

Post-PCR HRM melting analysis was performed using a commercial HRM kit (Quanta, USA) in a Rotor gene 6000 5-plex HRM device (Qiagen, USA). Before HRM, the samples were amplified using primers for the *MIP* gene as described earlier[9] or the *dotA* gene as reported in Yanez *et al.*[35]. Both *MIP* and *dotA* HRM qPCR used a 15 µl final reaction volume, which contained 7.5 µl of 2X AccuMelt™ HRM SuperMix (Quanta, USA), 0.3 µl (1 µM) of each primer, 6.5 µl PCR H_20 (5PRIME, Gaithersburg, USA) and 1 µl of sample.

5.3.7 FO-SPR Melting analysis

An overview of the FO-SPR assay concept can be seen in Figure 5.1B. The FO-SPR melting analysis was performed in a final volume of 100 µL, which was covered, with 60 µL of Silicon oil (Bio-Rad, Hercules, USA) to prevent evaporation. The samples consisted of 5 µl of the non-purified qPCR product, containing the amplified DNA (final concentration of DNA ≈ 1 µM, which was well above the 1 nM detection limit of the system, as determined in Chapter 4), 80 µL PBS with 300 mM NaCl and 15 µL of 10 nM Au NPs. Before each measurement, the samples were briefly centrifuged to remove air bubbles and were heated to 94°C for 5 s to denature the dsDNA in ssDNA that could interact with the probes on the FO-SPR sensor and on the Au NPs. Subsequently, the temperature was lowered to 50°C to allow hybridization. After 15 min, the temperature was slowly raised (0.1°C s^{-1}) to determine the exact melting temperature (T_m). The total assay time was 18 min. Negative control measurements were performed using the non-template control (NTC) reaction mixture of the qPCR reaction.

5.3.8 Sequencing and sequence alignment

Before sequencing, all samples were amplified using Taq polymerase (Invitrogen) with the *dotA* primers as described earlier. Next, they were cloned into the pGEM-T vector (Promega, Madison, USA) according to manufacturer guidelines. Samples were sequenced with the SP6 primer at the genetic sequencing facility of the VIB (Antwerp, Belgium).

The obtained sequences were compared with sequences of *L. pneumophila* serogroups available in the National Center for Biotechnology (NCBI) database, which can be accessed using the online tool nucleotide BLAST (http://www.ncbi.nlm.nih.gov/BLAST)[37]. The query on Entrez was limited by the keyword: "Bacteria". The sequence of *L. pneumophila* serogroup 1 (ATCC 33152), available under accession number AF9009 in the NCBI database was found and used as base of comparison for all serogroups because the original primers and probes for the Taqman qPCR of *Yanez et al.*[35] were designed using this sequence. The ATCC serogroups analyzed in this research could all be found in the NCBI database except for one serogroup (serogroup 15 - ATCC 35251).

5.3.9 Data analysis

Data were collected and analyzed using the appropriate software. For ABI Prism data the SDS 1.1 software (Applied Biosystems) was used. HRM data was analyzed using the Rotor Gene Q 1.7 build 94 software. The FO-SPR setup was operated using a National instruments Labview program that was developed in-house. Further analyses of the SPR data were performed using Excel (Microsoft, USA), Origin (Originlabs, USA) and Matlab (The Mathworks, USA).

5.4 Results

5.4.1 Mutation detection through sequencing

Recently, it was discovered that the L. pneumophila *dotA* gene has relatively high variability among different serogroups[16]. Because this gene is often used for detection of L. pneumophila by qPCR, it is important to asses the impact this genetic variability has on the outcome of this quantification assay. Therefore, in this paper, an 80bp

region of the *dotA* gene, which is expected to contain different mutations[18], was first screened among 9 American Type Culture Collection (ATCC) *L. pneumophila* serogroups using the standard Sanger sequencing method.

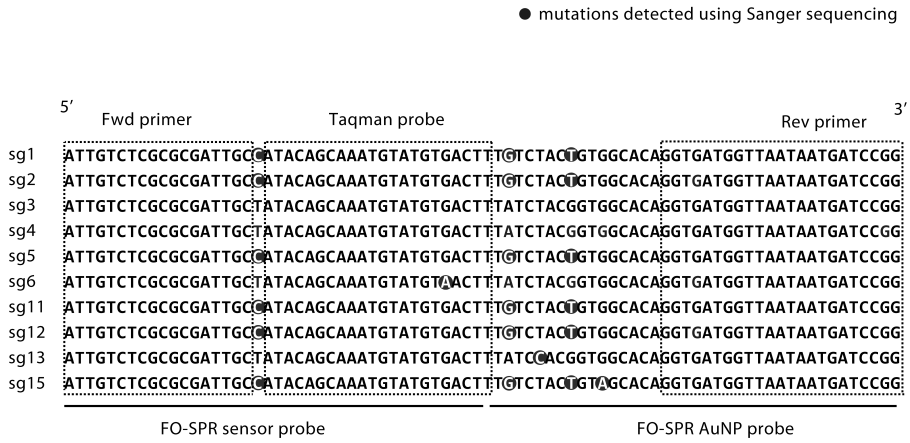

Figure 5.2: Results of sequencing the *dotA* gene of 9 interesting *L. pneumophila* serogroups. The bases marked are mutations detected using sequencing. Primer and Taqman probe regions are marked with a dashed line.

The acquired sequences were compared to those available in the NCBI database (Figure 5.3). Surprisingly, among the 9 sequenced serogroups, only two were found to be completely free of mutations (serogroup 3 and 4). Other serogroups encompassed several mutations each, with some of them being recurrent between different serogroups. However most of these mutations were not present in the NCBI database and only 4 among 9 sequenced serogroups were found to have mutations reported in the NCBI database.

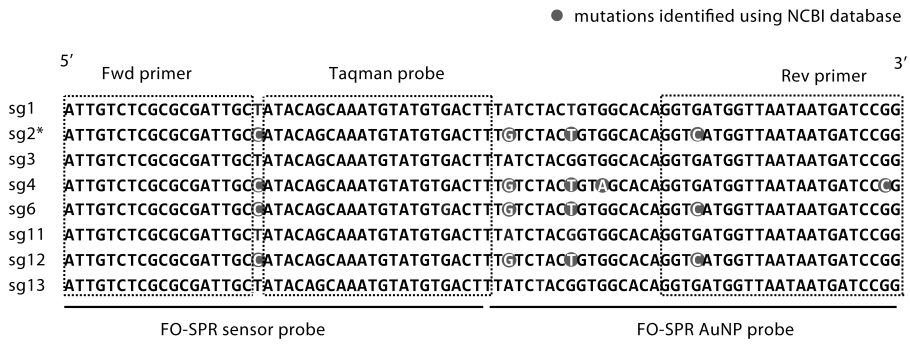

Figure 5.3: Results of analyzing the *dotA* gene of 9 interesting *L. pneumophila* serogroups using the NCBI database. The bases marked are identified mutations using the NCBI database. Primer and Taqman probe regions are marked with a dashed line.

These results show that the *dotA* sequence is highly variable and that most of the serogroups tested have acquired several mutations. It cannot be excluded that these mutations are introduced by Taqman polymerase DNA amplification, although this would be highly coincidently as these mutations are in exact the same positions as can be found in other *L. pneumophilia* serogroups. Unexpectedly, sequencing did not reveal any mutations in the priming regions of serogroups (Figure 5.2), while several mutations were found in the priming regions of different serogroups in the NCBI database. This discrepancy can be explained by the intrinsic limitations of the Sanger sequencing technique. When sequencing is applied directly to a PCR product, chances of detecting mutations in the priming regions are low, because primers are incorporated in the PCR product during amplification, resulting in a irrelevant low number of copied strands with mutations from the original priming region sequence.

To further test this hypothesis, the same 80bp region of the *dotA* gene was used as a target in qPCR to quantify all 15 *L. pneumophila* serogroups available. If mutations are present within the priming or Taqman probe regions, the qPCR based quantification of bacteria will be affected[38], causing thus a clear discrepancy compared to the reference method of bacterial colony counting (Figure 5.4). The results showed that indeed *dotA* qPCR quantification for several serogroups is substantially different from results obtained through counting bacterial

colonies, whereas there is a good correlation between this reference technique and the qPCR quantifications of the more conserved '*Macrophage Infection Potentiator*' (*MIP*) gene[9].

The differences were especially pronounced for serogroups 1, 2, 6, 12 and 15. For some of them (2, 6 and 12) mutations in the priming region are reported in the NCBI database (Figure 5.3). Moreover, they all have the same mutation at base 4 of the 3' end of the reverse primer. It has already been studied extensively that a single mutation at the 3' end of a primer has the largest impact on PCR[39,40 41].

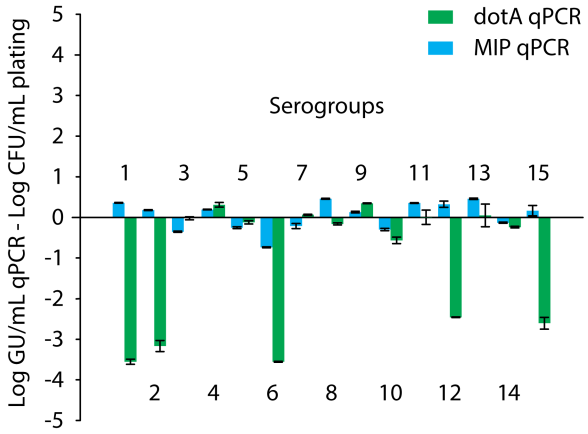

Figure 5.4: Results of quantification of 15 *L. pneumophila* serogroups using qPCR assays based on *MIP* and *dotA* genes. The logarithm of the qPCR genomic counts is subtracted by the logarithm of the standard plating counts and the actual differences in quantification are represented as bar graphs. Variability is expressed as standard deviation (n=4). GU= genomic units, CFU= Colony forming units.

On the other hand serogroup 4 had according to the NCBI database a mutation at base 2 of the 5' end of the reverse primer, explaining thus why this mutation does not affect the qPCR reaction (Figure 5.4). Surprisingly serogroup 1 and 15 had no mutations in the priming region according to the NCBI database although they showed large discrepancies in quantification when using the two methods. However, Sanger sequencing revealed in their non-priming region the same cluster of mutations as in the inhibited serogroups 2 and 12. This suggests that serogroups 1 and 15 might have acquired the same

mutations as serogroup 2 and 12, including the ones in the priming region, which might explain the observed PCR inhibition. To test this hypothesis and to reveal whether serogroups 1, 2, 12 and 15 all have similar mutations a new fast genetic screening technique was applied based on DNA melting.

5.4.2 Mutation detection through high resolution melting

To evaluate the potential merits of DNA melting assays for the identification of mutations in *L. pneumophila,* two high-resolution melting assays were performed (Figure 5.1). The first assay is the routinely applied qPCR - high resolution melting (qPCR-HRM), which uses a saturating intercalating dye to monitor the melting of the DNA double strand in solution directly after qPCR. The other assay is the new, by our group, developed FO-SPR melting assay, which can monitor DNA melting in real time. It is also applied directly after PCR, but the melting process is monitored on a solid surface, which provides a significant resolution gain as has been shown in our previous work[24].

Among several serogroups that showed consistency in quantification (Figure 5.4), only few were included in these experiments (such as serogroup 3, 4, 5 and 11), as no mutations are expected in their priming region. The DNA melting principle was first tested by comparing the general variation in melting temperatures of the *dotA* gene amplicon with those of the *MIP* gene amplicon for the different serogroups. This is a good benchmark, because the sequencing results already have proven that *dotA* is highly variable while *MIP* should be more conserved. Results are visualized as a heat map, which displays the difference in T_m between *L. pneumophila* serogroups but at the same time shows the overall variability within the sequence of interest. The T_m is approximately 79.7°C for all serogroups in the case of *MIP* PCR amplicon with a maximal variation of 0.2°C pointing to low or almost absent genetic variability. Contrary to this, T_m values for the *dotA* qPCR amplicon have a broad span with T_m values measured between 78°C and 81°C for different serogroups. This is represented by the colored pattern of the heat map for the *dotA* amplicon, which indicates pronounced differences in T_m values ranging from -2 to +2 °C and thus sequence variability for the tested serogroups (Figure 5.5 A, top triangle). The same samples were further analyzed with the FO-SPR

HRM assay. The heat map in 5.5 B represents a comparison between qPCR HRM (bottom triangle) and FO-SPR HRM assay (top triangle) for the *dotA* amplicon. Noticeably, the variability in T_m values between different serogroups is even more pronounced with FO-SPR HRM compared to qPCR HRM, further supporting observations from our previous work on higher resolution of the former melting assay.

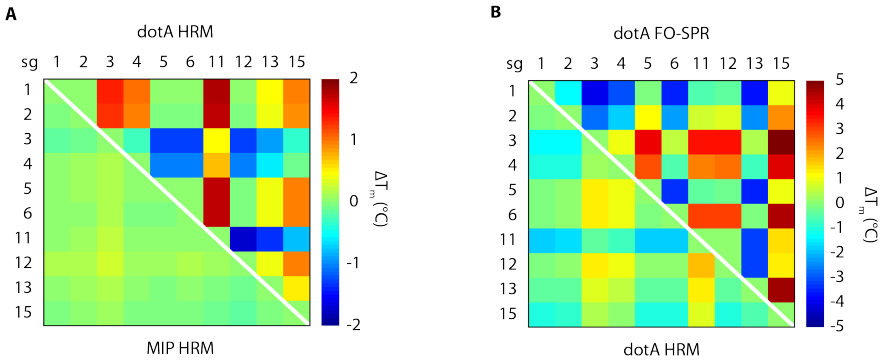

Figure 5.5: A) ΔT_m Heat map of HRM results, showing the difference in genetic variability of the PCR amplified *MIP* locus and the *dotA* locus. The *dotA* locus has a much larger span of T_m values, indicating higher genetic variability. B) Heat map of HRM melting analysis for the *dotA* locus in comparison to FO-SPR determined T_m values. The range of T_m values measured by FO-SPR is larger compared to qPCR-HRM indicating the higher sensitivity towards mutation detection by FO-SPR.

To further link the sequencing results and the results from DNA melting assays, the Tm of the sequences obtained with Sanger sequencing were predicted in silico using µMelt, an algorithm developed for the prediction of HRM melting data[42]. The in silico obtained Tm values were compared to the Tm of every serogroup as measured with qPCR-HRM and FO-SPR HRM. All Tm values were subtracted with the Tm of the original sequence on which the *dotA* primers were based (genebank accession number: AF9009) and the (ΔTm) differences are shown as bar graphs on Figure 5.6. For the *MIP* gene no mutations were found in the amplification region. A first thing to notice is that there is a strong correlation in trend between the µMelt predictions and the actual measured ΔT_m with qPCR HRM (blue and grey bars). For all the serogroups tested ΔT_m is larger than zero, except for serogroup 3 as this serogroup has no mutations. When the mutations in the priming region

from the NCBI database (Figure 5.2, red dots) are included into the Sanger sequencing results, used in the µMelt model, this correlation between qPCR HRM measured ΔT_m and predicted ΔT_m further improved (Figure 5.6, black bars indicated with arrows). For instance serogroup 4 had no mutations according to Sanger sequencing (note the absence of grey bars), though both DNA melting methods detect a ΔT_m. When the sequence was supplemented with the mutations of the NCBI database, the predicted ΔT_m (black bar) was similar to the qPCR-HRM measured one (blue bar). Similar results were obtained for serogroup 6, where a negative value of ΔT_m, predicted with µMelt for Sanger sequencing, changed into positive ΔT_m after NCBI primer corrections were applied. This change again corresponded with the ΔT_m measured with qPCR-HRM. For FO-SPR (green bars) ΔT_m is larger compared to qPCR HRM and µMelt prediction for the *L. pneumophila* serogroups. Nonetheless the trend in the shifts corresponds perfectly with the presence or absence of mutations. These results altogether prove that detecting mutations in the priming region is possible when using melting assays, as opposed to Sanger sequencing.

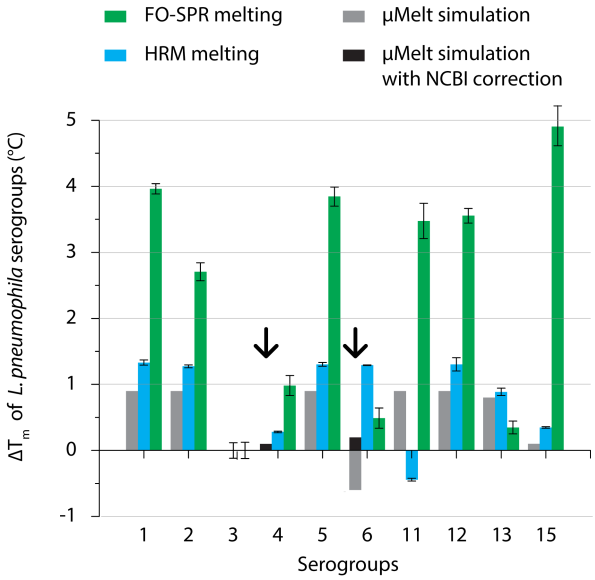

Figure 5.6: ΔT_m for the *dotA* gene among different *L. pneumophila* serogroups as measured with the melting assays in comparison with the *in silico* determined T_m of the sequencing results (visualized in absolute ΔT_m from the T_m of the non mutated sequence). For serogroup 3, no ΔT_m bars are present as this serogroup has no mutations. The error bars correspond to the variability of the qPCR-HRM

melting assay and FO-SPR HRM assay, respectively. The serogroups which had a different Tm after correction for the priming region mutations are marked with an arrow. Variability is expressed as standard deviation (n=4).

From Figure 5.5 it can be seen that serogroups 1, 2, 12 and 15 all have a large ΔT_m, pointing to our initial hypothesis that these four serogroups all have the same cluster of mutations. The same trend was found for all methods except that for serogroup 15 only FO-SPR could detect a ΔT_m indicative of the highest number of mutations. This discrepancy is due to the probe-based design of the FO-SPR HRM assay, which is sensitive to individual mutations while qPCR-HRM, on the other hand, is sensitive to the overall ΔT_m of the qPCR amplicon DNA duplex.

5.4.3 Mutation detection in clinical samples of *L. pneumophilia*

Next, the same approach to identify mutations in the *dotA* sequence was applied on a panel of clinically isolated *L. pneumophila* serogroup1 bacteria. Different isolates were first quantified using both *dotA* qPCR and *MIP* qPCR and the results were compared with plate culture counts. Two of the seven tested isolates (isolate 3 and *Legionella pneumophila* strain Corby) differed in their quantification between the two used methods (Figure 5.7, part A). Especially for the very virulent strain of *L. pneumophila*, known as Corby[43], there was no detectable PCR amplification of the *dotA* gene.

After qPCR, the amplicons were ligated in a vector and sequenced (Figure 5.7, part B). Several mutations were discovered in the clinically isolated *L. pneumophila* that resembled to a great extent the mutations found in the *L. pneumophila* serogroups. A new mutation was found in the Corby isolate, which was located in the middle of the Taqman probe hybridization site on the *dotA* gene. Previously, a similar mutation was also found in serogroup 6 but this mutation did not interfere with the PCR reaction. However, for the Corby strain the PCR reaction was completely inhibited. In order to evaluate whether this inhibition was the result of a mutation within primer or probe a PCR reaction without Taqman probe was performed. This resulted in normal amplification, indicating that the mutation in the probe sequence is responsible for inhibition of the qPCR, which was confirmed with an agarose gel identification of the amplified product (confirmed by a fluorescent band

in the gel at the 80bp DNA ladder marker, data not shown). For another isolate with differences in quantification, isolate 3, no mutations were present in either the probe or priming zones. To further analyze this, all bacterial isolates were subjected to both DNA melting assays. A direct comparison of these results is summarized in Figure 5.7, part C. Using qPCR HRM, small variations in T_m are visible, including the Corby strain. In line with our results on serogroups, FO-SPR HRM assay again revealed more pronounced differences in ΔT_m. Although both techniques were able to sense increased genetic variability to a different extent, there seemed to be no connection with qPCR results.

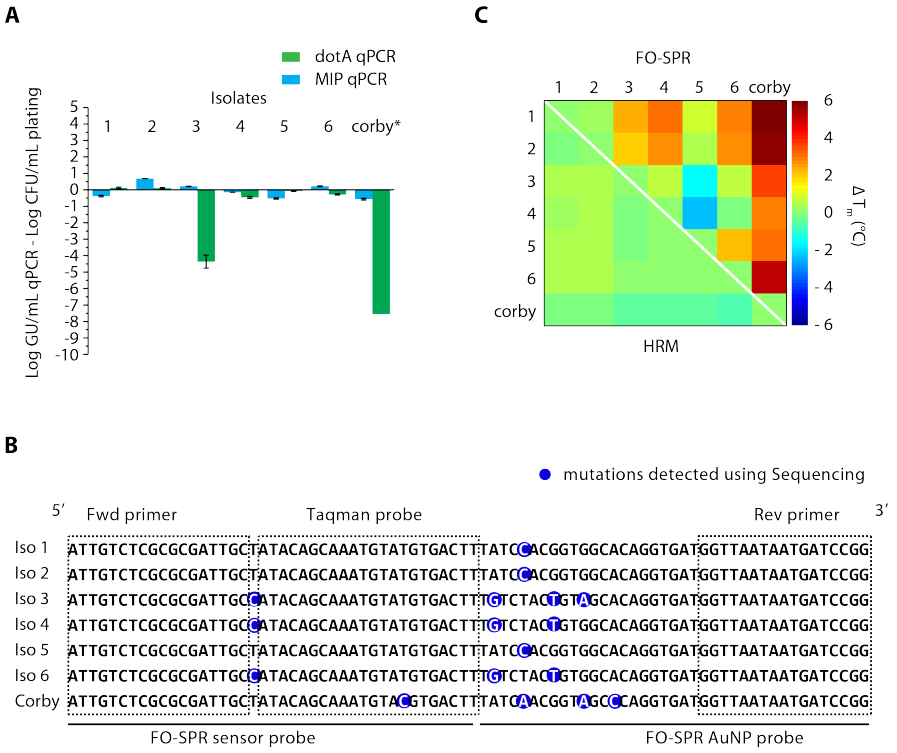

Figure 5.7: A) qPCR quantification of different *L. pneumophila* clinical isolates using the *dotA* and the *MIP* gene expressed as the logarithmic difference with the plating counts. The symbol * marks isolates that showed no amplification for *dotA*. Variability is expressed as standard deviation (n=4). B) Sequencing results of 6 *L. pneumophila* clinical isolates. The bases marked in blue are the mutations detected using sequencing. Primer and probe regions are marked with dashed lines. C) Heat map comparison of the T_m for different *L. pneumophila* isolates as measured with qPCR HRM (bottom) and FO-SPR HRM (top) assay.

Therefore, the sequencing data were linked with the DNA melting data using the same µMelt *in silico* T_m predictions. The ΔT_m of µMelt has a good correlation with the qPCR HRM concerning the height of the signal (compare black and blue bars on the graph, Figure 5.8). On the other hand the discrepancy between FO-SPR HRM is attributable to the sensitivity of the FO-SPR HRM assay towards mutations. As a result, ΔTm is much higher than the µMelt predicted value, which allows easy discrimination of mutated bacterial isolates with the FO-SPR HRM assay.

Most of the mutations in the isolates were at the detection limit of the qPCR-HRM assay and were therefore not always detectable as can be seen in Figure 5.8. Some isolates (isolates 3, 4, 6 and corby) on the other hand had large ΔT_m values, caused by the same cl,n uster of mutations, but those could only be measured with FO-SPR HRM assay. For isolate 3, a particular discrepancy in ΔT_m values was observed between µMelt prediction and both the qPCR HRM and the FO-SPR HRM assay. Unsurprisingly, this is the only isolate where qPCR inhibition was observed and no PCR primer or probe mutation could be found with Sanger sequencing. Mutations in the primer were not detected with sequencing, as was the case for the *Legionella* serogroups.

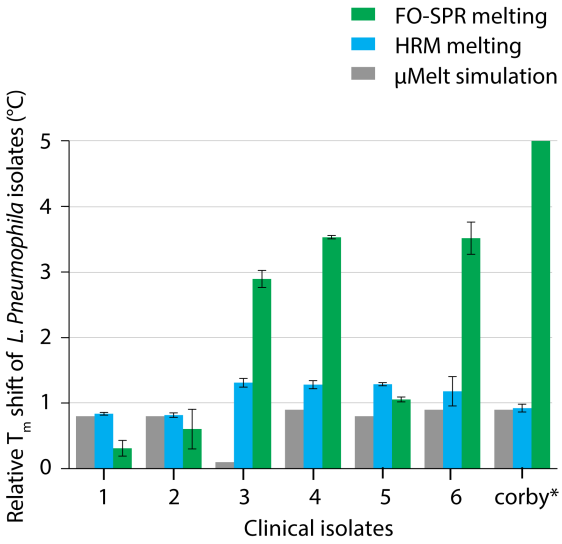

Figure 5.8: Relative ΔT_m for the different *L. pneumophila* clinical isolates as measured with the melting assays in comparison to the *in silico* determined T_m of the sequencing results (visualized in absolute ΔT_m from the T_m of the non mutated

sequence) The symbol * marks that isolate Corby has a higher ΔT_m than 5 (ΔT_m = 7.12 ± 0.28). Variability is expressed as standard deviation (n=4).

Further proof for increased resolution of FO-SPR HRM assay was obtained from the actual melting curves (Figure 5.9). The qPCR HRM melting peaks of mutated *Legionella pneumophila* isolates had neither special features, nor a large shift in ΔT_m. The FO-SPR melting curves showed multiple melting points, which indicated variation in the target sequence. As these variations had very similar melting temperatures, this led only to a widening of the melting curve for qPCR HRM additionally explaining why this assay did not comply with the *in silico* predictions. In the FO-SPR HRM assay Au NP probe hybridization induced a larger ΔT_m with sufficient resolution for identifying SNP mismatches.

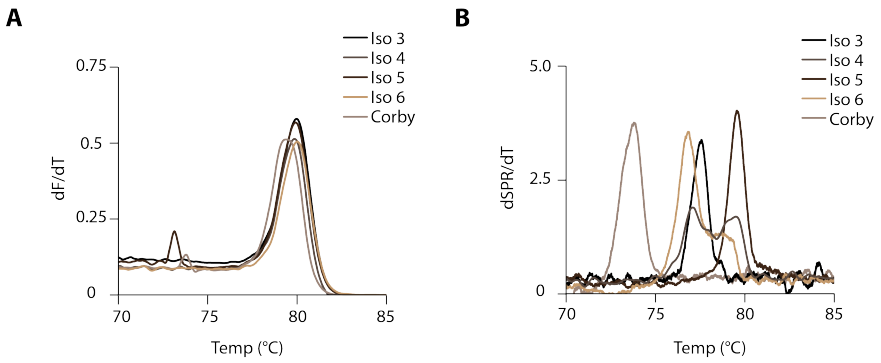

Figure 5.9: A) First derivative of the melting curve measured with qPCR HRM for a selection of 5 clinical isolates. B) First derivative of the measured melting signal with FO-SPR HRM assay for a selection of 5 clinical isolates.

5.5 Conclusion

In this paper we made a direct comparison between DNA high resolution melting assays and Sanger sequencing exposing thus the advantages and disadvantages of both technologies. Sanger sequencing proved not to be suited for fast screening of genomic regions, which are highly variable among different closely related bacteria. This can be explained with the use of this sequencing method post cloning, which

can only reveal the sequence of one selected clone, while different subtypes of a particular sequence present in other non-selected clones cannot be revealed. DNA melting on the other hand, can be applied directly after PCR without any purification or processing of the DNA and when different variations of the target sequence are present in the sample, not only the most abundant type will be detectable[44]. The PCR reaction that precedes the DNA melting holds valuable information on the priming region. However, some mutations in the priming region can have serious impact on the PCR reaction, as was the case for several *L. pneumophila* serogroups, and can cause a complete PCR inhibition.

Previously the merits of solution based DNA melting over solid phase DNA melting were summarized[29], although never compared experimentally. In this paper, both techniques were applied to screen for mutations in *L. pneumophila* and proved to be very sensitive in detecting the mutations present in the *dotA* gene. However, the differences in T_m for FO-SPR were more pronounced than was the case for qPCR HRM and thus resulted in more information on the target sequence. Although the actual resolution of sequencing is unmet, as sequencing delivers the exact base pairs, the FO-SPR melting assay was able to detect low abundant variations in the priming sequence at a fraction of time and cost. Thus for the moment both platforms need to be applied as complementary technologies whereby DNA melting identifies the samples with mutations that need to be sequenced. However, with FO-SPR already a considerable gain in resolution is achieved especially considering that mutations located in the priming region could not be detected with qPCR HRM or sequencing. On the other hand, FO-SPR HRM detected consistently differences in T_m even with the mutations in the priming region. The gain in resolution was particularly pronounced for the analyzed clinical samples where multiple melting peaks were evident with FO-SPR HRM while only a single melting signal was visible for qPCR HRM. These results are a clear testament for the advantages of the solid phase melting approach. However, the technique remains prone to a loss in resolution at the priming regions introduced by the PCR reaction. Therefore future research should be directed at increasing the sensitivity of the FO-SPR assay, while maintaining the sensitivity towards mutations.

In the following chapter, the sensitivity issue of FO-SPR will be addressed by integrating different target amplification strategies. The amplification strategies will be chosen with a particular emphasis on mutation detection and their impact on the FO-SPR melting assay will be evaluated in detail.

References

1. M. J. Heller, *Annu. Rev. Biomed. Eng.*, 2002, **4**, 129-153.
2. B. L. Poe, D. M. Haverstick and J. P. Landers, *Clin. Chem.*, 2012.
3. S. N. Stacey*, et al.*, *Nat. Genet.*, 2011, **43**, 1098-U1085.
4. S. Tuupanen*, et al.*, *Nat. Genet.*, 2009, **41**, 885-U837.
5. W. Dalemans*, et al.*, *Nature*, 1991, **354**, 526-528.
6. D. D. Levy, B. Sharma and T. A. Cebula, *Antimicrob. Agents Chemother.*, 2004, **48**, 2355-2363.
7. P. R. Srinivas, B. S. Kramer and S. Srivastava, *The lancet oncology*, 2001, **2**, 698-704.
8. L. J. Engle, C. L. Simpson and J. E. Landers, *Oncogene*, 2006, **25**, 1594-1601.
9. J. Behets, P. Declerck, Y. Delaedt, B. Creemers and F. Ollevier, *J. Microbiol. Methods*, 2007, **68**, 137-144.
10. F. Martinelli, A. Caruso, L. Moschini, A. Turano, C. Scarcella and F. Speziani, *Current microbiology*, 2000, **41**, 374-376.
11. S. Ditommaso, M. Giacomuzzi, M. Gentile, A. R. Moiraghi and C. M. Zotti, *Am. J. Infect. Control*, 2010.
12. B. S. Fields, R. F. Benson and R. E. Besser, *Clinical microbiology reviews*, 2002, **15**, 506-526.
13. L. Imamovic, E. Balleste, J. Jofre and M. Muniesa, *Appl. Environ. Microbiol.*, 2010, **76**, 5693-5701.
14. E. T. Zemanick, B. D. Wagner, S. D. Sagel, M. J. Stevens, F. J. Accurso and J. K. Harris, *PLoS One*, 2010, **5**, e15101.
15. C. J. Smith and A. M. Osborn, *FEMS Microbiol. Ecol.*, 2009, **67**, 6-20.
16. J. Costa, I. Tiago, M. S. da Costa and A. Verissimo, *Environmental Microbiology*, 2010, **12**, 2711-2729.
17. I. Morozova, X. Y. Qu, S. D. Shi, G. Asamani, J. E. Greenberg, H. A. Shuman and J. J. Russo, *Plasmid*, 2004, **51**, 127-147.
18. K. S. Ko, H. Miyamoto, H. K. Lee, M. Y. Park, K. Fukuda, B. J. Park and Y. H. Kook, *Clin Microbiol Infect*, 2006, **12**, 254-261.
19. B. Suss, G. Flekna, M. Wagner and I. Hein, *J. Microbiol. Methods*, 2009, **76**, 316-319.
20. K. E. Holt*, et al.*, *Nat Genet*, 2008, **40**, 987-993.
21. D. Gresham, D. M. Ruderfer, S. C. Pratt, J. Schacherer, M. J. Dunham, D. Botstein and L. Kruglyak, *Science*, 2006, **311**, 1932-1936.
22. A. W. Peterson, L. K. Wolf and R. M. Georgiadis, *J. Am. Chem. Soc.*, 2002, **124**, 14601-14607.

23. E. Milkani, S. Morais, C. R. Lambert and W. G. McGimpsey, *Biosens. Bioelectron.*, 2010, **25**, 1217-1220.
24. K. Knez, K. P. Janssen, J. Pollet, D. Spasic and J. Lammertyn, *Small*, 2012, **8**, 868-872.
25. H. Du, C. M. Strohsahl, J. Camera, B. L. Miller and T. D. Krauss, *J. Am. Chem. Soc.*, 2005, **127**, 7932-7940.
26. J. Pingel, A. Buhot, R. Calemczuk and T. Livache, *Biosens. Bioelectron.*, 2012, **31**, 554-557.
27. N. Crews, T. Ameel, C. Wittwer and B. Gale, *Lab Chip*, 2008, **8**, 1922-1929.
28. Cisse, II, H. Kim and T. Ha, *Nat. Struct. Mol. Biol.*, 2012, **19**, 623-627.
29. N. Crews, C. T. Wittwer, J. Montgomery, R. Pryor and B. Gale, *Anal. Chem.*, 2009, **81**, 2053-2058.
30. A. K. R. Lytton-Jean and C. A. Mirkin, *J. Am. Chem. Soc.*, 2005, **127**, 12754-12755.
31. J. H. Oh and J. S. Lee, *Anal. Chem.*, 2011, **83**, 7364-7370.
32. J. I. Cutler, E. Auyeung and C. A. Mirkin, *J. Am. Chem. Soc.*, 2012, **134**, 1376-1391.
33. J. B. Fiche, A. Buhot, R. Calemczuk and T. Livache, *Biophys. J.*, 2007, **92**, 935-946.
34. K. P. Janssen, K. Knez, L. Vanysacker, J. Schrooten, D. Spasic and J. Lammertyn, *Nanotechnology*, 2012, **23**, 235503.
35. M. A. Yanez, C. Carrasco-Serrano, V. M. Barbera and V. Catalan, *Appl. Environ. Microbiol.*, 2005, **71**, 3433-3441.
36. S. J. Hurst, M. S. Han, A. K. Lytton-Jean and C. A. Mirkin, *Anal. Chem.*, 2007, **79**, 7201-7205.
37. M. Johnson, I. Zaretskaya, Y. Raytselis, Y. Merezhuk, S. McGinnis and T. L. Madden, *Nucleic Acids Res.*, 2008, **36**, W5-9.
38. D. Bru, F. Martin-Laurent and L. Philippot, *Appl. Environ. Microbiol.*, 2008, **74**, 1660-1663.
39. C. R. Newton*, et al.*, *Nucleic Acids Res.*, 1989, **17**, 2503-2516.
40. D. Y. Wu, L. Ugozzoli, B. K. Pal and R. B. Wallace, *Proc. Natl. Acad. Sci. U. S. A.*, 1989, **86**, 2757-2760.
41. J. H. Wu, P. Y. Hong and W. T. Liu, *J. Microbiol. Methods*, 2009, **77**, 267-275.
42. Z. Dwight, R. Palais and C. T. Wittwer, *Bioinformatics*, 2011, **27**, 1019-1020.
43. R. I. Jepras, R. B. Fitzgeorge and A. Baskerville, *J Hyg (Lond)*, 1985, **95**, 29-38.
44. C. N. Gundry*, et al.*, *Nucleic Acids Res.*, 2008, **36**, 3401-3408.

Chapter 6

Real-time FO-SPR ligation assay for DNA quantification and identification

6.1 Introduction

Nowadays new point-of-care (POC) diagnostic tests in microbiology are expected to deliver fast and sensitive detection of micro-organisms[1]. However, detection on its own is often not sufficient, as both quantification of the micro-organisms and specific identification of particular mutations[2,3] has become essential for various applications. Therefore, many different assays, including quantitative PCR (qPCR)[4] and ligation assays[5] have been developed to meet these requirements. Already, qPCR has shown extensive utility, as it combines extreme sensitivity with real-time detection and multiplexing capacity[6]. Despite this, several characteristics of this assay, among which a high cost, complexity of the assay and fluorescence used to monitor the amplification process in real-time[7], have limited its application towards POC diagnostics. Therefore, in the last decade, numerous efforts have been made to use nanoparticles (NPs), and in particular Au NPs, as transducers for detection of bacteria[8,9]. Au NPs combine colorimetric read-out with high molecular stability and are therefore ideally suited for integration in POC sensors[10]. However, the sensitivity of Au NP assays remained for years inferior to qPCR, as the enzymatic amplification of DNA during PCR strongly boosts the detection limit.

Recently, it was proven that Au NPs could be combined with DNA amplification through the ligation chain reaction (LCR)[11,12]. In the LCR, DNA is amplified exponentially, much in the same way as in the PCR reaction. However, a thermophilic ligation enzyme is used to covalently bind the phosphorylated 5' end of one DNA strand with the 3' end of another strand, these hybridization probes, are only ligated when they are hybridized to a perfectly matching target sequence (Figure 6.1, part B). In this way, multiple DNA probes can be linked together even when only one target strand is present, as the complex formed between ligated probes and target is denatured at a temperature above its melting temperature (T_m), liberating target strands for the multiple subsequent ligation cycles. The reaction results in an exponential amplification, as each ligated target will function as a template for ligation of reverse probes complementary to the original ligation probes. In this way, Shen *et al.*[11] linked together DNA probes immobilized on Au NPs only in the presence of the target sequence. As a result, an increasing amount of Au NPs irreversibly aggregated with increasing number of ligation cycles, causing a gradual shift in the absorbance of the Au NP solution due to LSPR adsorption band coupling. The assay could quantify the initial target concentration by determining the number of ligation cycles necessary to generate a colorimetric change in the Au NP solution. This colorimetric assay had a linear range spanning 6 orders of magnitude and a detection limit of 50 aM.

In this chapter, the Au NP LCR reaction is further improved by replacing the colorimetric read-out of the assay, which is limited in measurement speed and sensitivity, with SPR that directly measures Au NP binding and considerably increases assay sensitivity[13]. In this regard, we redesign the original assay by ligating probes in free solution instead of on Au NPs, which were then binding to complementary probes immobilized on both the Au NP surface and the FO-SPR sensor surface (Figure 6.1). Each cycle of the LCR reaction resulted in more ligated probes, allowing more Au NPs to bind to the FO-SPR, which gradually increased the FO-SPR signal from cycle to cycle. LCR products were quantified by counting the number of cycles necessary to reach the amplification threshold. Moreover, the Au NP-ligated probe complex formed on the FO-SPR surface was melted during each LCR cycle, allowing identification of the amplified strands during the LCR reaction. Hence, in this approach, Au NPs were used to their full potential as labels in melting analysis and identification of the amplified targets[14], contrary to their utilization in the LCR Au NP assay as this assay is based on irreversible aggregation of NPs.

6.2 Aim of this chapter

In this chapter, the FO-SPR melting assay, which was developed and benchmarked in the previous chapters, will be integrated with the LCR reaction. This will enable both quantification and cycle-to-cycle identification of the reaction products. It is important to notice that mutations in close vicinity of the ligation site will inhibit the ligation reaction, therefore every target containing mutations in the ligation site needs a new set of hybridization probes for successful amplification. The ligation reaction improves the detection limit of the FO-SPR melting assay drastically improved while the main advantage of the FO-SPR sensor, namely SNP detection, will be conserved. To this end, the performance of the FO-SPR melt assay must be carefully evaluated, because higher DNA melting speeds are necessary to allow successful implementation of the LCR assay. Integration of DNA quantification is a significant step towards development of a FO-SPR POC biosensor for detection of bacteria and viruses.

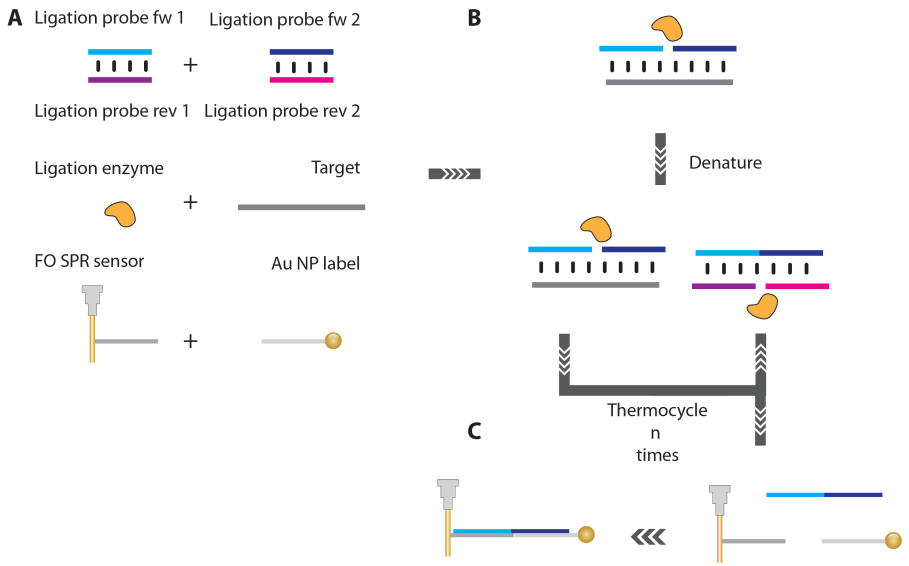

Figure 6.1: Schematic overview of the FO-SPR LCR. A.) Different components of the reaction. B.) LCR reaction where the forward (fw) and reverse (rev) probes are ligated only in the presence of the target sequence, resulting in an exponential amplification during multiple thermal cycles. C.) The forward LCR product can, during the LCR reaction, form a complex with two complementary probes immobilized on the FO-SPR sensor and on Au NPs, allowing real-time monitoring of the reaction by means of its reaction products.

6.3 Materials and methods

6.3.1 Reagents

The chemically synthesized oligonucleotides were purchased from integrated DNA technologies (Haasrode, Belgium) an overview can be found in Table 6.1. Both capture probes, used to capture the target sequence, are modified with a 3' C3 or 5' C6 thiol modifier (-SH) for immobilization of the oligonucleotides on the on the FO-SPR sensor and the Au NPs gold surfaces, respectively. All chemicals were purchased from Sigma-Aldrich (Bornem, Belgium) unless stated otherwise.

Table 6.1: Overview of used oligonucleotides

Targets (5'→3')
Wildtype (WT)
ATC CTT ATC AAT ATT TAA CAA TAA TCC CTC
Mismatch (MM)
ATC CTT ATC AAT **G**TT TAA CAA TAA TCC CTC
Probes (5'→3')
Ligation probe FW 1
/5Phos/AAT ATT GAT AAG GAT
Ligation probe FW 2
GAG GGA TTA TTG TTA
Ligation probe Rev 1
/5Phos/TAA CAA TAA TCC CTC
Ligation probe Rev 2
ATC CTT ATC AAT ATT
Ligation probe FW 2 Mismatch
/5Phos/AA**C** ATT GAT AAG GAT
Ligation probe Rev 1 Mismatch
ATC CTT ATC AAT **G**TT
Probe FO-SPR
TAA CAA TAA TCC CTC A_{20}/3ThioMC3-D/
Probe Au NP
/5ThioMC6-D/ A_{20} ATC CTT ATC AAT ATT

Thiol-functionalized DNA was immobilized on the Au NPs by adding 1 µM of 5' thiol functionalized DNA oligo activated with dithiothreitol (DTT, 0.1 M in PB 0.18 mM, pH 8.3) to break up thiol dimers that could inhibit the DNA functionalization. DNA was first purified using a sephadex column (GE, Oslo, Norway) to remove any traces of active DTT before it was added to the concentrated nanoparticle solution. A fast salt maturation protocol[15] was used to maximize the DNA loading on the Au

NPs. Afterwards, Au NPs were washed three times in phosphate buffer with 0.01 % SDS and stored at 4°C prior to use.

6.3.2 FO-SPR sensor fabrication and Au NP functionalization

The FO-SPR device and sensors were manufactured as described in Chapter 4 Sections 3.3.3 and 3.3.4. Citrate stabilized Au NPs, with a mean diameter of 20 nm, were purchased from BBI international (Cardiff, United Kingdom) and functionalized using the protocol described in Chapter 4 Section 4.3.3.

6.3.3 Gold surface backfilling

Both the FO-SPR sensor and Au NPs were backfilled, prior to use in the LCR assay. Backfilling is a process used to fill in 'empty spots' in between DNA molecules immobilized on a surface, which is often done using alkane thiols with a PEG moiety[16] (a detailed description of the backfilling concept can be found in chapter 1 section 1.6). Here, backfilling is performed in order to make the DNA functionalized gold surfaces more stable at elevated temperatures[17] as well as protein repellant[18], preventing enzyme inhibition during the LCR reaction. Both FO-SPR sensors and Au NPs were incubated for 3 h with a 50 µM alkane thiol PEG (Polypure, Oslo, Norway) dissolved in pure ethanol. Afterwards, the FO-SPR sensor surface and Au NPs were washed 3 times with a 0.01 % SDS phosphate buffer.

6.3.4 Ligation chain reaction

The LCR was performed to link the 5' phosphate-functionalized probe 2 to the 3' end of probe 1. A thermophilic ligation enzyme (9°N™ DNA Ligase, New England Bioscience, Ipswich, USA) was used as it can withstand thermocycling of the reaction solution between different temperatures: the probe hybridization temperature (2 min at 35 °C), the optimal ligation temperature (2 min at 42.5 °C) and the denaturing temperature of the ligation product (5 s at 70 °C). The thermal ramping speed had to be lowered compared to 5 °C/s standardly used in LCR assays to allow a good FO-SPR signal acquisition during DNA melting. It was optimized for achieving reasonable speed and thus safeguarding the total assay timev(1 °C/s, 0.5 °C/s and 0.1 °C/s). Another parameter that was optimized was the ligation buffer, which standardly contains DTT, known to reduce thiol bonds[19]. Therefore, three DTT free buffers with different ionic contents were evaluated for their performance during the LCR reaction (Table 6.2).

Table 6.2: Composition of ligation buffers (10x concentrated) used to evaluate optimal LCR conditions; all buffers were adjusted to pH 7.5 using HCl.

	Standard buffer	Buffer 1	Buffer 2	Buffer 3
Tris-Hcl	100 mM	100 mM	100 mM	100 mM
ATP	6 mM	6 mM	6 mM	6 mM
$MgCl_2$	25 mM	25 mM	50 mM	25 mM
NaCl	0	0	0	600 mM
Triton X-100	1 %	1 %	1 %	1 %
DTT	25 mM	0	0	0

The final ligation reaction mixture used for the FO-SPR LCR calibration curves and sample analysis consisted of 10 µL ligase buffer (10x concentrated), 10 µL of 9°N enzyme (10 u/µL), 2.5 µL Fw ligation probes (10 µM, for each target sequence), 2.5 µL Rev ligation probes (1 µM, for each target sequence), 50 µL Au NPs (0.5 nmol/L in distilled nuclease free H_2O), 10 µL target DNA, 15 µL distilled nuclease free H_2O making a total reaction volume of 100µL. After adding all these components the LCR reaction mixture was mixed very carefully and covered with 60 µL mineral oil (Immobiline DryStrip Cover Fluid, GE healthcare, Diegem, Belgium) to prevent evaporation during thermocycling.

6.3.5 Data processing

Data acquisition on the two spectrometers and NiDaq coupled thermocouples was done with the in-house developed LabView program (National Instruments, Austin, Texas) as described in Chapter 5 Section 5.3.9. Once the SPR data and thermocouple data were combined, a first order derivative was made for each LCR melting cycle. The resulting melting peak was fitted using a Gaussian fit in Matlab (the mathworks, Natick, USA) to determine the melting temperature (T_m) and evaluate the melting peak quality for each LCR cycle.

6.4 Results

6.4.1 LCR buffer optimization

The first step in the implementation of the LCR reaction on the FO-SPR platform was selection of the buffer compatible with both the FO-SPR melting assay and the LCR reaction. The standard ligation buffer supplied by the manufacturer of the ligation enzyme 9°N was not

compatible with FO-SPR assay due to the presence of DTT, which reduces thiol bonds essential for immobilization of DNA molecules on gold surfaces. Furthermore, a buffer with certain ionic strength was needed to stabilize the Au NPs and to speed up their hybridization on the FO-SPR surface during the LCR reaction. Therefore, three different compositions of the standard ligation buffer (Table 6.2) were evaluated for their performance both in the LCR reaction (Figure 6.2, part A) and the FO-SPR melting assay (Figure 6.3). The ligation yield was measured using qPCR High Resolution Melting (HRM) analysis on a ligated product. Here, the size of the melting signal was indicative for the ligation reaction yield. The results suggested that next to the standard buffer, using buffer 1 resulted also in the highest ligation yield (visible from the height of the melting peak), confirming that DTT is not a necessary component for the LCR enzyme. On the other hand, doubling the amount of $MgCl_2$ in buffer 2 drastically lowered the ligation yield, while the yield of LCR in buffer 3 was only a fraction lower than in the standard buffer. Because buffer 3 contains the same components as standard buffer, except for 60 mM NaCl, these results clearly suggested that monovalent salts have a less drastic effect on the ligation yield in comparison with the divalent $MgCl_2$. Based on these results, buffer 2 was already excluded from further tests for selecting a buffer compatible with both assays. It should also be mentioned that buffer 1 and buffer 2 have a small shift in T_m in comparison with the standard buffer provided by the manufacturer of the ligation enzyme (NEB). This is probably the result in a slight deviation of one of the components in the respective buffers (ionic strength, surfactant).

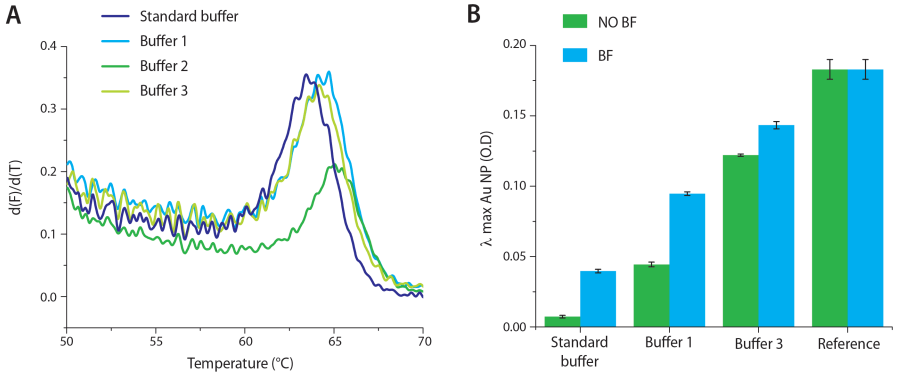

Figure 6.2: A) qPCR HRM following the ligation reaction under different buffering conditions. B) UV-Vis derived maximal absorbance of Au NPs with and without backfilling (BF) after 35 ligation cycles under different buffering conditions. The reference Au NPs did not undergo the ligation reaction.

Next, the stability of Au NPs coated with DNA was tested in the three remaining buffers, i.e. standard buffer, buffer 1 and buffer 3. For

this purpose, Au NPs, prepared both with and without backfilling, were compared in LCR, as it is known that backfilled Au NPs should have an increased stability and performance in hybridization assays[17]. When unstable, Au NPs aggregate, which leads to coupling of the LSPR adsorption band of the individual NPs, resulting in a color change of the Au NP solution. Au NP aggregation could by no means be the result of ligation as they only contain a single probe complementary to the target sequence. Therefore, the stability of Au NPs can be evaluated by measuring the optical density of the solution at the λ max of the Au NP LSPR. As seen part B of Figure 6.2, the increase in absorbance clearly shows that backfilled particles perform better in all buffers, even when DTT is present, such as in the standard buffer. The best Au NP stability was observed in buffer 3, therefore in a final test, buffer 1 was compared with buffer 3 to evaluate the performance of the FO-SPR melting assay in these buffers. Figure 6.3 summarizes results of the FO-SPR melting assay as described in Chapter 4 for the 30bp target sequence in the two selected buffers. Here buffer 3, which already proved to result in the highest Au NP stability, was also the most suited buffer for the FO-SPR melting assay, as it resulted in the highest melting signal.

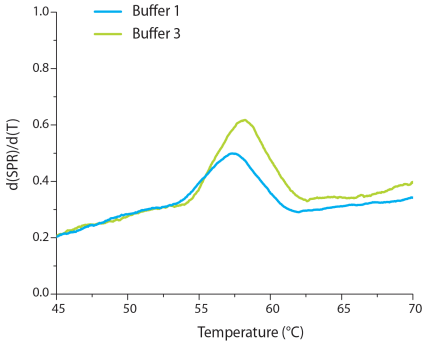

Figure 6.3: FO-SPR melting analysis of BF Au NPs in two different buffers.

6.4.2 DNA Melting optimization

In Chapters 4 and 5, DNA melting analysis was performed at a temperature ramping speed of 0.1 °C/s. However, this ramping speed considerably slows down the LCR reaction and increases the total assay time. Therefore, we evaluated if higher ramping speeds of 0.5 °C/s and 1 °C/s could result in the same melting resolution. To test this, a melting analysis was performed using the same targets as described in Chapter 4. Results are shown in part A of Figure 6.4. As can be expected, the best melting signal was obtained at the slowest ramping speed with almost 2 fold and 3 fold decrease in signal at 0.5 °C/s and 1 °C/s ramping speeds, respectively. Moreover, at the slowest cycling speed, the inter

measurement variability was the lowest (standard deviation obtained on the mean T_m is 0.01 °C for n=4), while with increasing ramping speed this variability increased to 0.1 °C and 0.16 °C for 0.5 °C/s and 1.0 °C/s ramping speeds, respectively. Furthermore, at 1.0 °C/s ramping speed, the melting temperature also shifted to a higher value (from 56.8 °C at 0.5 and 0.1 °C/s to 59.5 °C at 1.0°C/s) and the width of the fitted peak of the melting signal considerably increased (from 2.5 °C at 0.5 and 0.1 °C/s to 4.2°C at 1.0 °C/s), which could potentially lower the sensitivity of the FO-SPR melting assay and compromise SNP detection. To evaluate this, 30bp target sequences carrying two SNPs at different positions were compared to the wild type (WT) target of the same size as previously described (Chapter 4, Table 4.1). The acquired melting signal, visualized in part B of Figure 6.4, confirmed that even at a 10 fold increased ramping speed, all mutations could clearly be resolved, justifying the choice for 1.0 °C/s ramping speed in further experiments. For each FO-SPR melting experiment, 35 consecutive repetitions were performed on the same FO-SPR sensor, to evaluate assay variability. Each cycle consisted of two steps, a first step where the target was allowed to bind for 10 min. followed by a melting step, this resulted in 35 individual melt peaks that had very low variability confirming a good assay performance (Figure 6.4, part B).

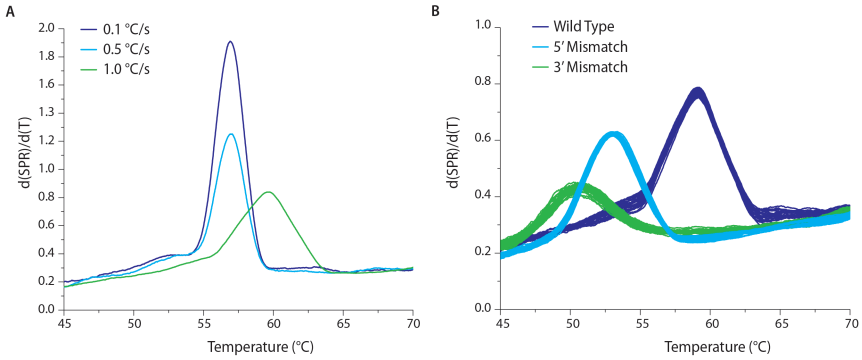

Figure 6.4: A) Performance of the FO-SPR melting assay at different temperature ramping speeds. B) FO-SPR melting analysis in the LCR optimal buffer 3 of the wild type (WT) target in comparison with two targets containing a mutation at the 5' or 3' end of the target. The graph represents an overlay of 35 consecutive melting cycles, proving the low variation between assays even after extensive thermocycling.

6.4.3 FO-SPR LCR assay

As described in Figure 6.1, the FO-SPR LCR reaction consists of multiple ligation cycles, which are enabled by heating up and cooling down the reaction mixture. Because the heating of a fluid expands its volume, it also decreases the refractive index of the LCR reaction mixture, resulting in the SPR signal that is the exact inverse of the temperature signal (Figure 6.5). This temperature effect is clearly visible in the FO-SPR signals on both measurement channels and allows easy processing of the data, as the refractive index changes can be used to determine the reaction cycle boundaries. Each reaction cycle is split in 3 phases, namely the hybridization phase where the DNA target strands can hybridize with the ligation probes, the ligation phase where the ligation enzyme covalently links perfectly hybridized probes and finally the melting phase where ligated products are melted from the target liberating it for the next round of ligation. The essential part of the LCR DNA amplification is the reverse ligation probe set as the exponential amplification and thus a high detection limit (10^{-9} M of target DNA) are not attainable without them. During the hybridization step of each LCR cycle, the forward ligation products can hybridize to detection probes on the FO-SPR surface and Au NPs, forming a complex that is melted of in the melting phase of each reaction cycle.

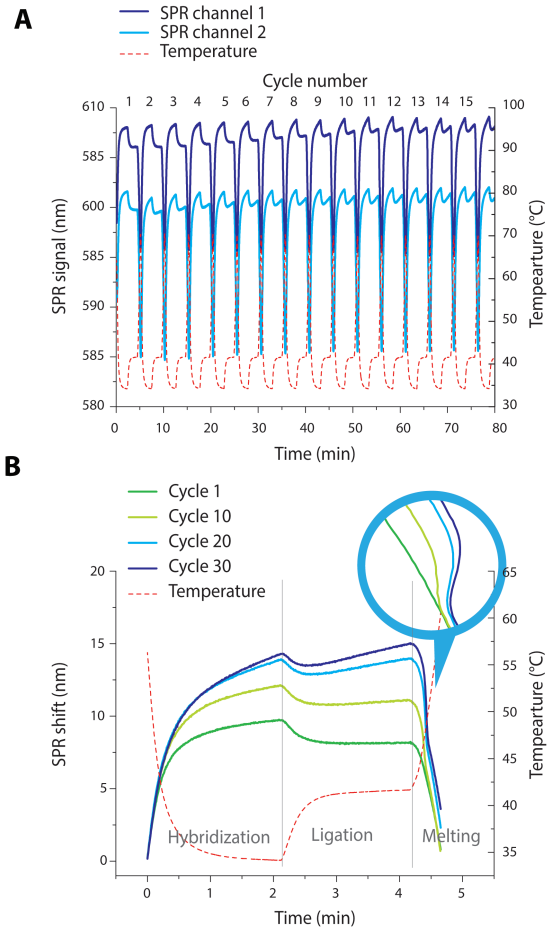

Figure 6.5: Overview of typical FO-SPR LCR measurements and data processing performed on the WT target DNA. A) The flow diagram shows the raw signal as measured with the FO-SPR device. B) This diagram is further cut in individual reaction cycles.

Therefore, the acquired melting signal in the melting phase is uniquely attributable to the acquired LCR products and can thus be used to both identify and quantify the LCR product (Figure 6.6). Importantly, Au NP and FO-SPR probes cannot be ligated because they do not have a phosphate group necessary for the formation of a phosphodiester bond between the 3' hydroxyl group of probe 1 and the 5' phosphate group of probe 2.

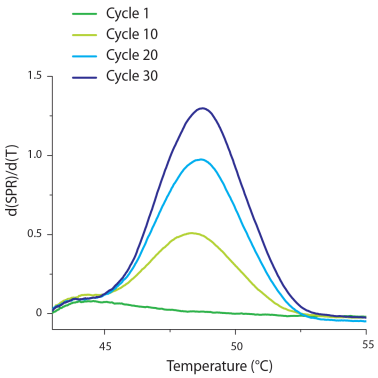

Figure 6.6: The melting signal of each cycle is obtained by plotting the derivative of the FO-SPR signal and thermocouple signal during the melting phase as a function of temperature.

6.4.4 Quantification of DNA targets using FO-SPR LCR assay

Next, the FO-SPR LCR assay was used to determine the target concentration by examining the number of LCR cycles necessary to obtain a FO-SPR melting point of the corresponding DNA target. In Figure 6.7 (part A), the concept is shown for a WT DNA target concentration of 100 fM. Out of 40 LCR cycles performed, no clear melting point was observed for this target in the first 27 cycles. In the subsequent cycles, a melting point appeared first at 51 °C followed by gradual increase towards 52.3 °C. This shift in T_m is expected and can be attributed to the dependence of T_m on the increasing target concentration through LCR cycles[20]. In comparison with the T_m obtained during the DNA melting optimization experiments described in paragraph 6.4.2, the T_m has shifted almost 7 °C, this is both a result from shorter hybridization times in the actual LCR assay and slight differences in ionic makeup of the reaction mixture in comparison with the pure buffer used during the optimization experiments.

Similar FO-SPR LCR reactions were then performed for 7 different target concentrations (100 nM, 10 nM, 1 nM, 100 pM, 10 pM, 1 pM and 100 fM) including a negative control without DNA target (no template control, NTC). For each concentration, the height of melting peaks were derived from all 40 LCR cycles and normalized to 1. These values, represented in Figure 6.7, part B as a function of the total number of reaction cycles, pointed out that an increasing number of LCR reaction cycles is necessary for lower target concentrations. At approximately the 35th cycle, a positive melting signal became evident also for the NTC, suggesting either contamination of the reaction mixture with target DNA or the occurrence of non-specific amplification in the LCR assay at these later cycles. Next the cycle threshold was chosen -this is the

minimal SPR shift above baseline- that is indicative of successful LCR amplification. By using a cycle threshold of 0.25 (horizontal red line in part B of Figure 6.7), Ct values for each target concentration were derived and plotted as a function of the concentration, resulting in a calibration curve for the FO-SPR LCR assay (Figure 6.7, part C). The assay had a linear range spanning 7 orders of magnitude, which is only 1 order less than a conventional qPCR assay. The lowest detectable concentration was 100 fM, at lower concentrations, the Ct was indistinguishable from the Non template control signal. Thus, the LCR reaction improved the detection limit with 4 orders of magnitude in comparison with results from previous chapters on the FO-SPR melting assay (e.g. Chapter 4). Although still far from the detection limit of qPCR[21], a considerable improvement in detection limit is possible. For instance, the ligation was not performed at the optimal ligation temperature of the enzyme (45-90°C) because of the low hybridization temperature (35 °C), resulting in less than optimal assay[22]. Better probe design and selection of targets would allow the LCR assay to be performed at higher hybridization temperatures, which can improve ligase performance and eliminate non-specific binding, thus further decreasing the detection limit.

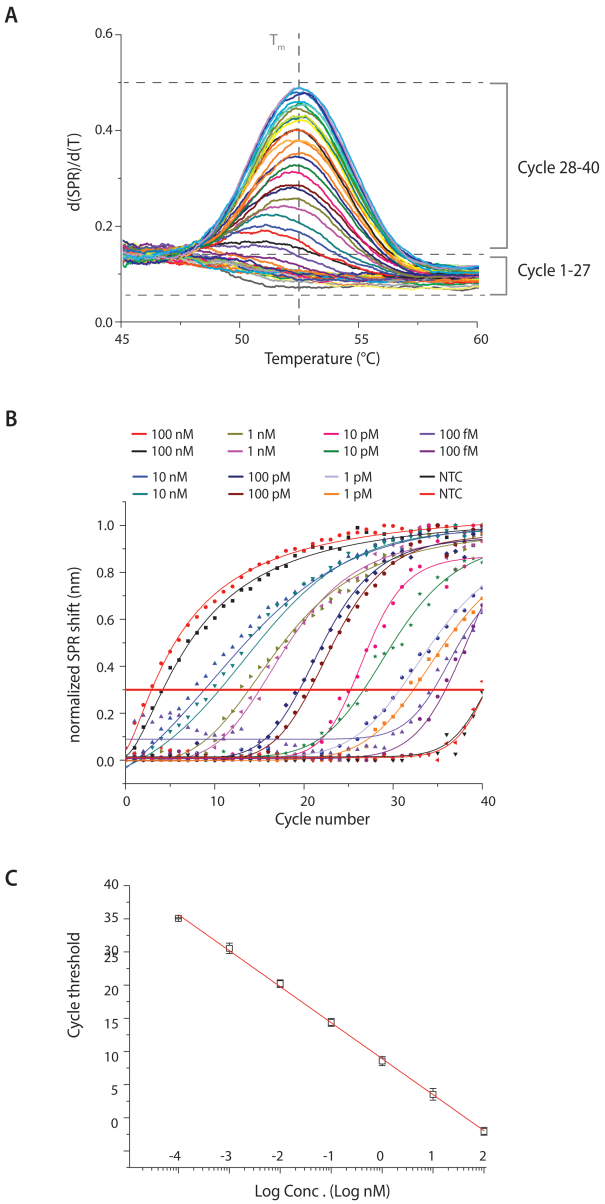

Figure 6.7: A) FO-SPR LCR reaction results for one concentration of target DNA (100 fM). The results are an overlay of the derived melting signal obtained from 40 thermal cycles. Starting from cycle 27 the melting peak height gradually increases. B) The increase in melting peak signal for different target concentrations (100 nm, 10 nm, 1 nm, 100 pM, 10 pM, 1 pM, 100 fM and NTC, each with a repetition) is represented as sigmoidal second order fit of the corresponding points. The red horizontal line indicates the cycle threshold (C_t) used to derive a calibration curve. C) The derived calibration curve of C_t values, with a linear range spanning 7 orders of magnitude for DNA concentrations. Red line is a logarithmic fit of the Ct values for each measured concentration (R^2=0.99). Variability is expressed as standard deviation (n=2).

6.4.5 Target identification using FO-SPR LCR assay

A final experiment was done to evaluate the performance of the FO-SPR LCR reaction for SNP detection. In order to detect a SNP within the target DNA strand using LCR assay, two new ligation probes, matching the SNP in the target, needed to be introduced in the assay. This adjustment was necessary to fulfill the requirement of the ligation enzyme for perfect sequence complementarity between target strand and two ligation probes. The FO-SPR assay allows to discriminate the different LCR products because even a single base pair mismatch between the sensor immobilized hybridization probes and the ligated probes, will shift the T_m to lower temperatures. Furthermore, mutations in the target sequence that will not affect the ligation reaction can also be discriminated with the FO-SPR assay. This means that not all mutations in the target sequence have to be known. The two LCR reactions performed both for WT and the MM target were compared with a melting analysis of the same targets (as described previously in Chapter 4). Although the MM target clearly had a lower T_m value compared to the WT, as expected, it surprisingly showed better yield of the LCR reaction (Figure 6.8). This can be explained by a difference in hybridization yield. The MM ligation probes are hybridized at a temperature further below the melting point of probes and targets, which is known to give a good hybridization yield[23]. As for the WT ligation probes, the hybridization temperature is less optimal, explaining why there is a difference in ligation yield. Importantly, the T_m measured during the LCR reaction allowed discrimination of the SNP bearing target from the WT target. In comparison with the melting analysis performed at a lower ramping speed, the melting signal obtained from the LCR assay was considerably lower with wider melting peaks. However, the resolution of the fast melting cycles was better with a ΔT_m between WT and MM target of 4.3°C compared to 3.8°C in the slow melting analysis. Similar trends in T_m were also visible during the optimization experiments for thermal ramping speed. It can be speculated that the increased ramping speed results in the formation of less bonds between the Au NPs and the FO-SPR surface through the target DNA, which broadens the melting transition[14].

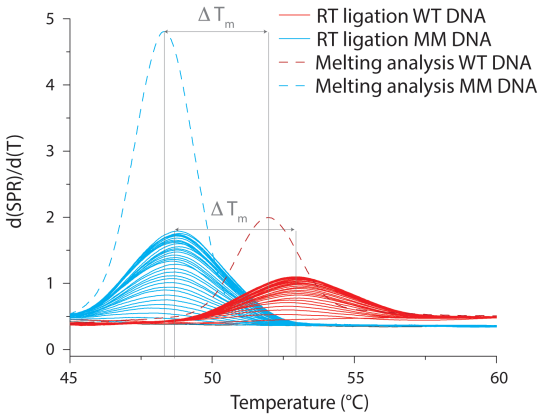

Figure 6.8: Obtained signals for the FO-SPR LCR assay using WT and MM target DNA (target [C]= 10nM). The mutant clearly has a higher yield but a lower melting point.

6.5 Conclusion

Integration of LCR with the FO-SPR melting assay considerably increased the value of both assays. The combined assay allowed quantifying and identifying DNA targets over a wide concentration range. Moreover, the assay could discriminate SNPs without any post reaction analysis. The integration of the two assays required initial optimization, especially buffer ionic strength and thermal ramping speed as these parameters both influence the ligation enzyme performance and the hybridization yield of the Au NPs on the FO-SPR sensor. Here, the higher temperature ramping speeds were selected for at the cost of melting resolution as the assay speed is an important factor for its future applications. Nonetheless, even at a ramping speed 10 times higher than classic FO-SPR DNA melting assays, the discrimination of SNP bearing targets was still feasible with high precision. The FO-SPR LCR assay had a LOD of 100 fM, which is only 1 order of magnitude higher than PCR. Better ligation probe design and selection of optimal ligation conditions could decrease the LOD even further to a similar level as PCR. Finally, in comparison with earlier described LCR assays, the FO-SPR implementation offered the advantage of cycle-to-cycle information on the amplified target strands, eliminating any time-consuming post reaction analysis steps. Therefore, the FO-SPR LCR assay represents a great improvement in development of fast POC assays.

References

1. L. Gervais, N. de Rooij and E. Delamarche, *Adv. Mater.*, 2011, **23**, H151-176.
2. E. M. Cornett, E. A. Campbell, G. Gulenay, E. Peterson, N. Bhaskar and D. M. Kolpashchikov, *Angew. Chem. Int. Ed. Engl.*, 2012, **51**, 9075-9077.
3. C. J. Murray and J. A. Salomon, *Proc. Natl. Acad. Sci. U. S. A.*, 1998, **95**, 13881-13886.
4. J. C. Cheng, C. L. Huang, C. C. Lin, C. C. Chen, Y. C. Chang, S. S. Chang and C. P. Tseng, *Clin. Chem.*, 2006, **52**, 1997-2004.
5. S. Sando, H. Abe and E. T. Kool, *J. Am. Chem. Soc.*, 2004, **126**, 1081-1087.
6. M. J. Espy*, et al.*, *Clin. Microbiol. Rev.*, 2006, **19**, 165-256.
7. C. Lodeiro, J. L. Capelo, J. C. Mejuto, E. Oliveira, H. M. Santos, B. Pedras and C. Nunez, *Chem. Soc. Rev.*, 2010, **39**, 2948-2976.
8. R. L. Phillips, O. R. Miranda, C. C. You, V. M. Rotello and U. H. Bunz, *Angew. Chem. Int. Ed. Engl.*, 2008, **47**, 2590-2594.
9. J. J. Storhoff, A. D. Lucas, V. Garimella, Y. P. Bao and U. R. Muller, *Nat. Biotechnol.*, 2004, **22**, 883-887.
10. H. Jans and Q. Huo, *Chem. Soc. Rev.*, 2012, **41**, 2849-2866.
11. W. Shen, H. Deng and Z. Gao, *J. Am. Chem. Soc.*, 2012, **134**, 14678-14681.
12. W. Shen, H. Deng, A. K. Teo and Z. Gao, *Chem. Commun. (Camb)*, 2012, **48**, 10225-10227.
13. L. A. Lyon, M. D. Musick and M. J. Natan, *Anal. Chem.*, 1998, **70**, 5177-5183.
14. R. Jin, G. Wu, Z. Li, C. A. Mirkin and G. C. Schatz, *J. Am. Chem. Soc.*, 2003, **125**, 1643-1654.
15. S. J. Hurst, A. K. Lytton-Jean and C. A. Mirkin, *Anal. Chem.*, 2006, **78**, 8313-8318.
16. C. Y. Lee, P. Gong, G. M. Harbers, D. W. Grainger, D. G. Castner and L. J. Gamble, *Anal. Chem.*, 2006, **78**, 3316-3325.
17. T. Stakenborg, S. Peeters, G. Reekmans, W. Laureyn, H. Jans, G. Borghs and H. Imberechts, *J. Nanopart. Res.*, 2008, **10**, 143-152.
18. K. P. Janssen, K. Knez, L. Vanysacker, J. Schrooten, D. Spasic and J. Lammertyn, *Nanotechnology*, 2012, **23**, 235503.
19. K. Kuwajima, M. Ikeguchi, T. Sugawara, Y. Hiraoka and S. Sugai, *Biochemistry*, 1990, **29**, 8240-8249.
20. H. Gudnason, M. Dufva, D. D. Bang and A. Wolff, *Nucleic Acids Res.*, 2007, **35**, e127.
21. M. Meyer*, et al.*, *Nucleic Acids Res.*, 2008, **36**, e5.
22. F. Barany, *PCR Methods Appl.*, 1991, **1**, 5-16.

23. W. Rychlik, W. J. Spencer and R. E. Rhoads, *Nucleic Acids Res.*, 1990, **18**, 6409-6412.

Chapter 7

Real-time FO-SPR PCR monitoring for multiplex DNA identification

7.1 Introduction

In the previous chapters, the FO-SPR assay was applied to identify and quantify single DNA target with high precision. However, current microbiological diagnostics have a need for microbiological tests capable of identifying the presence of multiple pathogens with even discriminating their particular phenotypes[1]. Although PCR is capable of multiplexing, the current generation of quantitative PCR (qPCR) devices is somewhat limited for diagnostic applications as the transducer, being fluorescence, makes them bulky, complex and expensive. Furthermore, the maximal number of dyes that can be used in one PCR reaction is limited because of spectral overlap between their emission spectra[2]. As a result, most qPCR assays detect simultaneously only 2-3 targets, although conventional PCR could support many more targets[3]. Recently this was proven by using the characteristic melting temperature (T_m) of PCR amplicons as a secondary label in qPCR allowing identification of 50 different DNA sequences in one sample[4].

Multiplex DNA detection by analyzing the T_m of the amplicons has already been applied multiple times in PCR assays[5]. Because the melting analysis is always applied post PCR, it does not allow monitoring specific targets during the PCR reaction and as a result cannot be used to quantitate DNA, but solely for identifying the presence of particular DNA targets. These limitations of DNA melting make the technology in practice only useful as a screening tool for the presence of mutations. However, the newly acquired resolution would also make T_m a good tool for multiplex quantification, surpassing thus the limitations of fluorescent dyes.

7.2 Aim of this chapter

The aim of this chapter is to study the potential of the FO-SPR technology for multiplex DNA identification. The FO-SPR melting assay, as described in the previous chapters, is used to monitor PCR based DNA amplification. Previously the FO-SPR was already applied for monitoring solid-phase PCR reactions[6], however in this chapter, a solution phase multiplex PCR will be evaluated. In comparison the new FO-SPR assay enables both quantification and cycle-to-cycle identification of the reaction products, which was not possible with the solid-phase variant. Hereto, two sets of hybridization probes are immobilized on the FO-SPR sensor and Au NPs are used to allow the detection of the two different target sequences (Figure 7.1). As a proof-of-concept, a multiplex PCR reaction will be used to amplify conserved regions of the genome of *Mycobacterium bovis* (*M. Bovis*) and *Mycobacterium avium* subsp. *Paratuberculosis* (MAP), two frequently encountered pathogens in life stock.

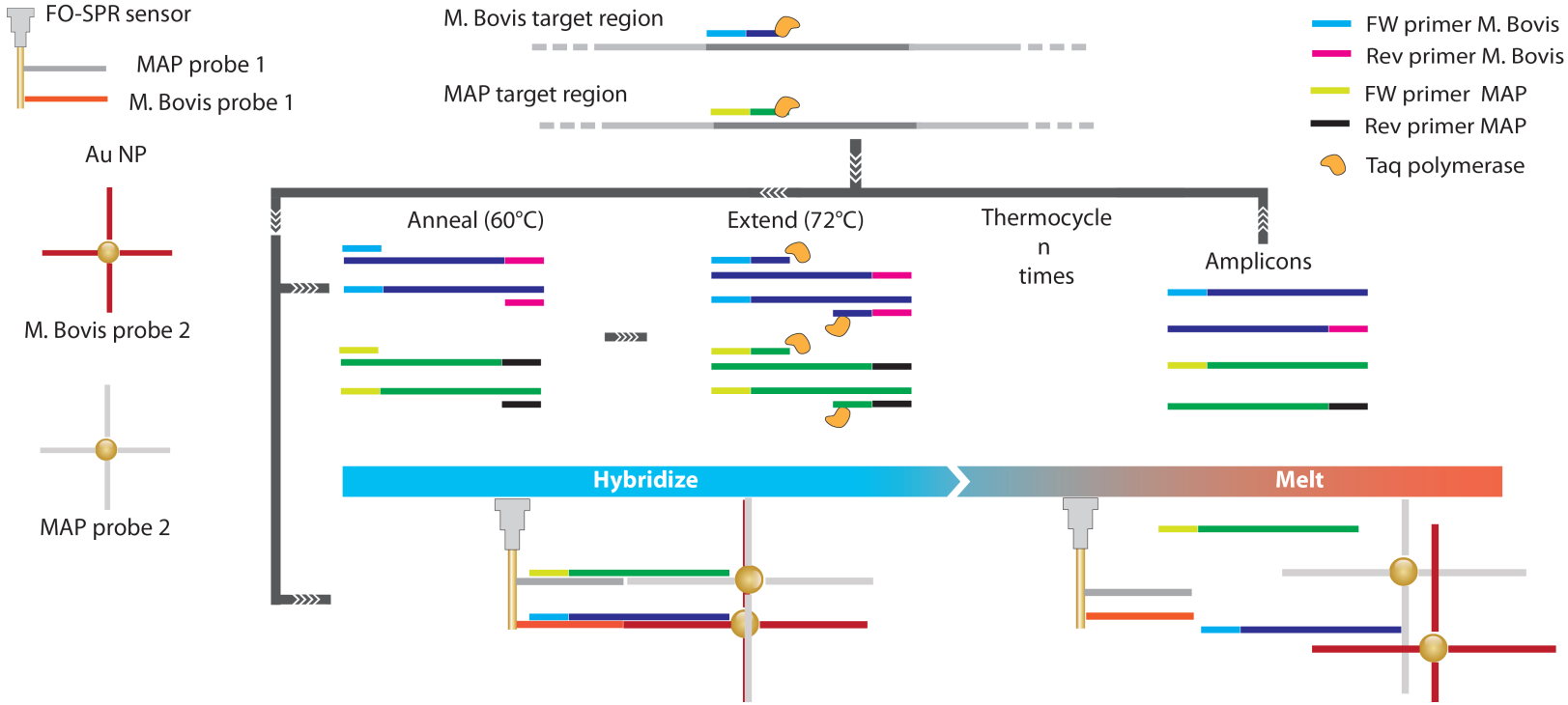

Figure 7.1: Conceptual overview of the FO-SPR quantitative multiplex PCR, the components used for FO-SPR are visualized on the left while all PCR components are visualized in the top right corner. The PCR primers specific for MAP and *M. Bovis* will be used to amplify a target region during a standard PCR reaction. The amplicons of both MAP and *M. Bovis* will be able to hybridize during the PCR reaction to complementary probes on the FO-SPR sensor and those on Au NPs. During the normal thermocycling used to denature the PCR amplicons for the PCR reaction, the FO-SPR sensor can register the T_m of the PCR amplicons and as a result perform n melting analyses, which can be used to identify different targets.

7.3 Materials and methods

7.3.1 Reagents

The chemically synthesized oligonucleotides were purchased from integrated DNA technologies (Haasrode, Belgium). An overview of the targets, capture probes and primer sequences can be found in Table 7.1. Both capture probes, used to capture the target sequence, are modified with a 3' C3 or 5' C6 thiol modifier (-SH) for immobilization of the oligonucleotides on the FO-SPR sensor and the Au NPs gold surfaces, respectively. The free 3' end of the hybridization probes was blocked from extension by the polymerase enzyme using a 3' phosphate modification. All chemicals were purchased from Sigma-Aldrich (Bornem, Belgium) unless stated otherwise.

Table 7.1: Overview of used oligonucleotides

Targets (5'→3')
M. Bovis Wild Type (WT), 76bp
GCA GAA GCG CAA CAC TCT TGG AGT GGC CTA CAA CGG CGCTCT CCG CGG CGC GGG CGT ACC GGA TAT CTT AGC TGGT
M. Bovis 5' Mismatch1 SNPs ($MM1_{BOV}$), 76bp
GCA GAA GCG CAA CAC TCT T**T**G AGT GGC CTA CAA CGG CGCTCT CCG CGG CGC GGG CGT ACC GGA TAT CTT AGC TGG T
M. Bovis 5' Mismatch 3 SNPs ($MM3_{BOV}$), 76 bp
GCA GAA GCG CAA CAC TCT T**T**G AG**C** G**T**C CTA CAA CGG CGCTCT CCG CGG CGC GGG CGT ACC GGATAT CTT AGC TGG T
MAP Wild Type (WT), 56 bp
TGG TCG TCT GCT GGGTTG ATC TGG ACA ATG ACG GTT ACG GAG GTG GTT GTG GC -3
MAP 5' Mismatch 1 SNPs ($MM1_{MAP}$), 56bp
TGG TCG TCT GCT GGG TTG AT**A** TGG ACA ATG ACG GTT ACG GAG GTG GTT GTG GC -3
MAP 5' Mismatch 3 SNPs ($MM3_{MAP}$), 56bp
TGG TCG TCT GCT GGG TTG AT**A** T**TA** ACA ATG ACG GTT ACG GAG GTG GTT GTG GC
Primers (5'→3')
M. Bovis primer forward, 19bp
GCA GAA GCG CAA CAC TCT T
M. Bovis primer reverse, 22bp
ACC AGC TAA GAT ATC CGG TAC G
MAP primer forward, 19bp
TGG TCG TCT GCT GGG TTG A

MAP primer reverse, 20bp
GCC ACA ACC ACC TCC GTA AC
Hybridization probes (5'→3')
M. Bovis probe 1, 48bp
CGC CGT TGT AGG CCA CTC CAA GAG TGT TGC GCT TCT GCT TTT TTT TTT - SH
M. Bovis probe 2, 48bp
SH- TTT TTT TTT TAC CAG CTA AGA TAT CCG GTA CGC CCG CGC CGC GGA GAG – Phos
MAP probe 1, 45bp
TGT CCA GAT CAA CCC AGC AGA CGA CCATTT TTT TTT TTT TTT TTT - SH
MAP probe 2, 44bp
SH - TTT TTT TTT TTT TTT TTT GCC ACA ACC ACCTCC GTA ACC GTC AT -Phos

Thiol-functionalized DNA was immobilized on the Au NPs by adding 1 µM of 5' thiol functionalized DNA oligo activated with dithiothreitol (DTT, 0.1 M in PB 0.18 mM, pH 8.3) to break up thiol dimers that could inhibit the DNA functionalization. DNA was first purified using a sephadex column (GE, Oslo, Norway) to remove any traces of active DTT before it was added to the concentrated nanoparticle solution. A fast salt maturation protocol[7] was used to maximize the DNA loading on the Au NPs. Afterwards, Au NPs were washed three times in phosphate buffer with 0.01 % SDS and stored at 4°C prior to use.

7.3.2 FO-SPR sensor fabrication and Au NP functionalization

The FO-SPR device and sensors were manufactured as described in the previous chapters. Citrate stabilized Au NPs with a mean diameter of 20 nm were purchased from BBI international (Cardiff, United Kingdom) and functionalized using the protocol described in Chapter 4. This standard protocol was adjusted for the simultaneous immobilization of two hybridization probes during the functionalization process. Both probes were added to the Au NPs in equal amounts (Figure 7.1).

7.3.3 Gold surface backfilling

Both the FO-SPR sensor and Au NPs were backfilled, as described in the material and methods section of Chapter 6 (a detailed description of the backfilling concept can be found in Chapter 1 section 1.6).

7.3.4 DNA melting analysis

The multiplex DNA melting analysis on the FO-SPR device was performed using a hybridization step at 55°C for 10 minutes, followed

by an increase in temperature to 90°C at 0.1°C/s. Experiments were performed in a 10 mM Tris HCl buffer with 2.5 mM $MgCl_2$ and 60 mM NaCl and 0.1% triton X-100. The target DNA concentration was 500 nM when individual DNA targets were analyzed and 250 nM when a multiplex target analysis was carried out.

7.3.5 Polymerase chain reaction (PCR)

PCR was performed to extend primers for a specific region of *M. Bovis* and MAP. Primers for MAP were adopted from Ravva et al.[8], who selected these primers using the insertion sequence IS900, a repetitive element present only in the MAP genome. Primers for *M. Bovis* were designed for the so-called regions of difference (RD), which contain sequence deletions in the genome of *M. Bovis* that are not present in other Mycobacteriacae[9].

A PCR mastermix (DimerEraser, Takara, Shiga, Japan) containing all necessary components for the PCR reaction, except primers, was used. The total reaction volume was 100 µL, this volume is considerably larger than for a standard PCR reaction, but was necessary to submerge the FO-SPR sensor completely in the PCR mixture. Future FO-SPR design improvements should allow reducing this volume considerably. The reaction mixture consisted of 50 µL Takara mastermix, 3 µL of each primer (300 nM final concentration), 20 µL Au NPs (1.0 nmol/L in distilled nuclease free H_2O), 4 µL $MgCl_2$ (50 mM), 4 µL NaCl, 10 µL target DNA. The reaction mixture was protected from evaporation during thermocycling by covering it with a layer of mineral oil (Immobiline DryStrip Cover Fluid, GE healthcare, Diegem, Belgium).

The sample temperature was cycled according to the following program:

1) Enzyme activation

- 30 s at 95°C

2) Three step PCR protocol (45 consecutive cycles):

- 30 s at 55°C (ramp speed = 5.0°C/s)
- 30 s at 72°C (ramp speed = 5.0°C/s)
- 5 s at 90°C (ramp speed = 1.0°C/s)

7.4 Results

7.4.1 Evaluation of multiplex FO-SPR performance

Simultaneous immobilization of different oligonucleotide probes on the FO-SPR sensor decreases the absolute number of each particular hybridization probe on the surface. Furthermore because the DNA sequence and length will influence immobilization efficiency, a particular hybridization probe can be favored during immobilization[10]. To study this possible effect, a FO-SPR melting analysis was performed with FO-SPR sensors functionalized with individual and multiplex hybridization probes.

The melting analysis of the individual probe-target complexes was performed identically to the protocol optimized in Chapter 4. A target concentration of 200nM was used as this is well above the detection limit of the FO-SPR biosensor and should result in a clear signal. In Figure 7.2A the results of the melting analysis are depicted. From this graph it can be observed that both bacterial targets can be easily identified, with the *M. Bovis* and MAP target having a T_m of 87°C and 80°C, respectively. A similar experiment was successfully performed in the multiplex FO-SPR setting, with a mixture of both target sequences. (Figure 7.2B).

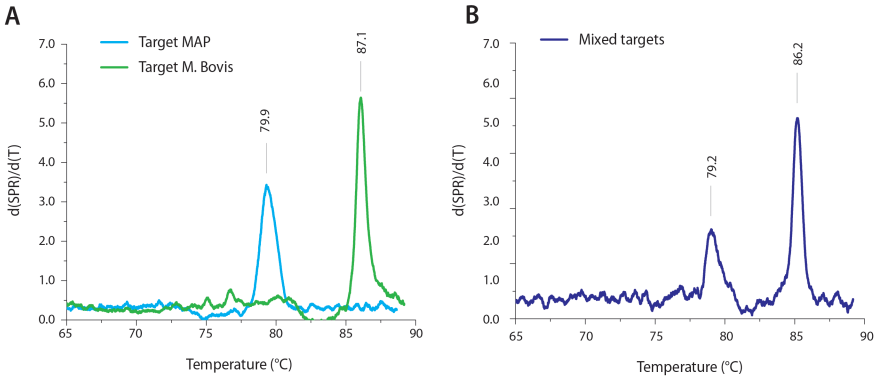

Figure 7.2: A) Individual and B) Multiplex FO-SPR melting analysis for the MAP and *M. Bovis* target sequences.

However, these results reveal a small difference in the melting profile of the multiplex FO-SPR melt analysis in comparison with the individual melting assay. The melting signal, has a slightly lower peak with the T_m being shifted to lower temperatures. This difference is most probably the result of the lower hybridization probe densities on the FO-SPR sensor and the Au NP surface. Similar trends of DNA melting assays are described in the literature when the densities of surface immobilized DNA probes are altered[11]. Nonetheless, the ΔT_m was only marginally different for individual and multiplex DNA melting analysis. The individual melting experiments resulted in a ΔT_m of 7.2 while for the multiplex experiments a window of 7.0 °C was obtained. It can be concluded from this experiment that the multiplex FO-SPR sensor can achieve a similar melting resolution as the single-plex FO-SPR melting analysis.

In a next experiment, the FO-SPR multiplex analysis was performed in a PCR master mix. Because the exact composition of this mixture is not known, an FO-SPR melting assay was performed to evaluate if a similar resolution could be obtained as in the previous experiment As can be seen from Figure 7.3, two peaks, corresponding to each of both targets, could be resolved when using PCR master mix. Peak height was considerably lower than in the previous experiments, which can probably be attributed to a lower ionic strength. Also, the ΔT_m was reduced from 7.0°C obtained in the previous experiments to 5.3°C for multiplex FO-SPR analysis in the PCR master mix. These results show that buffer ionic strength has a strong influence on the resolution of the FO-SPR melting analysis. However, to prevent PCR enzyme inhibition, the ionic strength cannot be substantially altered.

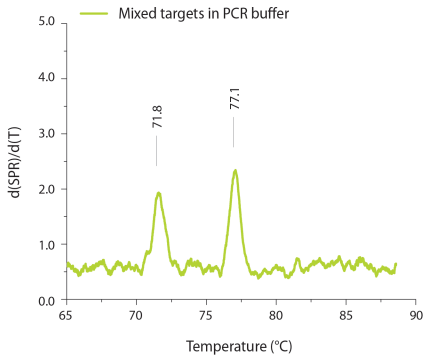

Figure 7.3: Multiplex FO-SPR melting analysis for the MAP and *M. Bovis* target sequence performed in PCR buffer.

7.4.2 FO-SPR PCR assay

The FO-SPR implementation of PCR resembles the LCR reaction described in the previous chapter. The main difference between both reactions is that in PCR primers are extended while in LCR, DNA probes are ligated. This makes that both reactions require different thermocycling conditions and different reaction mixtures. The buffer used for LCR is, as described above, not applicable for PCR as the PCR enzyme is very sensitive to changes in ionic strength.

In Figure 7.4 nine cycles of a PCR reaction are shown. Initially, the FO-SPR signal is the invers of the temperature change, which is continually monitored with a thermocouple. However, from the moment DNA target is amplified through PCR above the detection limit of the FO-SPR signal, the melting signal of the amplified DNA target will superimpose on the refraction index shift of the temperature measured with the FO-SPR sensor.

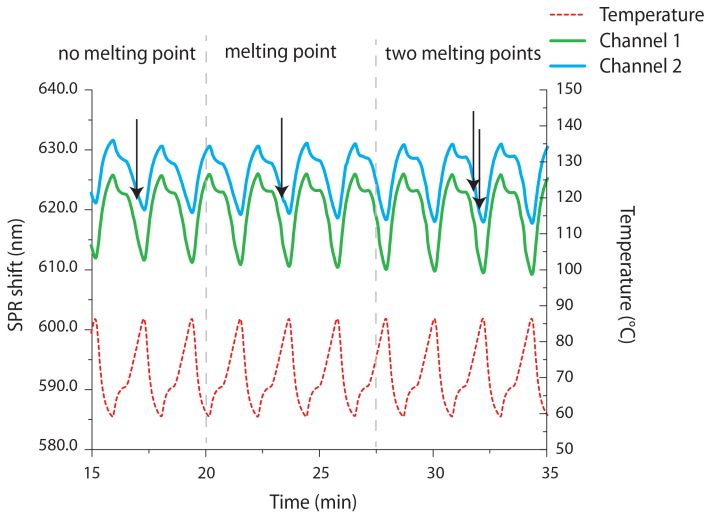

Figure 7.4: Raw data of an FO-SPR PCR measurement. Two measurement channels (channel 1 and channel 2) measure continuously changes in refractive index due to the thermocycling. As a result, the FO-SPR signal is the inverse of the temperature measured with a thermocouple. From the moment a target DNA species is present, the FO-SPR signal will obtain a characteristic melting point of the particular DNA target, which is superimposed on the FO-SPR signal of the temperature shift.

The effect of Au NP binding on the FO-SPR sensor through PCR products is clearly visible through the measurement of the individual cycles. In Figure 7.5, all cycles of a standard multiplex PCR reaction for both targets at a concentration of 1 nM are presented. Here, it is more clear that the SPR signal is initially the inverse of the temperature, with a melting point becoming visible after few reaction cycles. The melting point of *M. Bovis* becomes visible earlier due to the more efficient PCR. . Once both PCR reactions have reached the detection limit of the sensor, two clear melting points are visible.

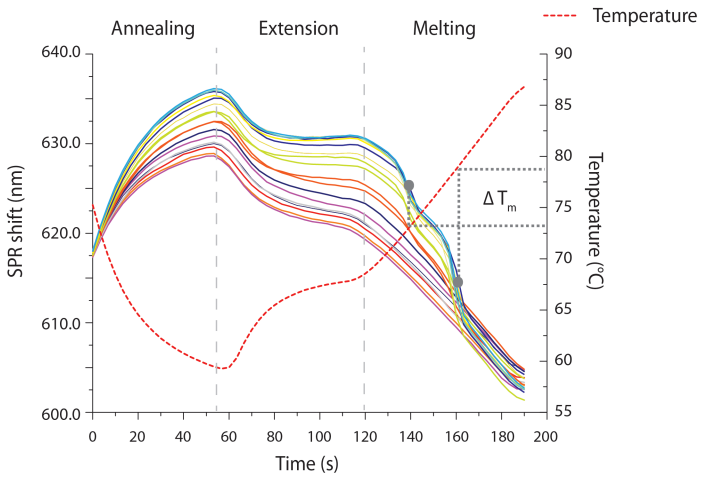

Figure 7.5: FO-SPR signal for each PCR cycle (represented with differently colored lines) in a multiplex PCR reaction containing bacterial DNA of both MAP and *M. Bovis* at a concentration of 1nM. Initially, the FO-SPR signal is the exact inverse of the temperature signal. When DNA reaches the detection limit of the FO-SPR sensor, a melting signal for each DNA target becomes visible.

By taking the first order derivative of the SPR signal and temperature signal, the T_m of each DNA target can be resolved very precisely, allowing an easy identification of both targets. In comparison with the earlier optimization reactions, the T_m of both targets is shifted approximately 3 °C. The shift in T_m is the result of a slightly higher ionic strength of buffer, necessary to stabilize the Au NPs in the PCR mixture. Use of increased ionic concentrations allowed keeping the Au NPs stable during the PCR reaction, as they appeared to be instable and prone to aggregation after extensive thermocycling (data not shown). The increased ionic strength was carefully optimized to prevent inhibition of the PCR reaction while having at the same time a stable Au NP solution capable of withstanding multiple thermal cycles.

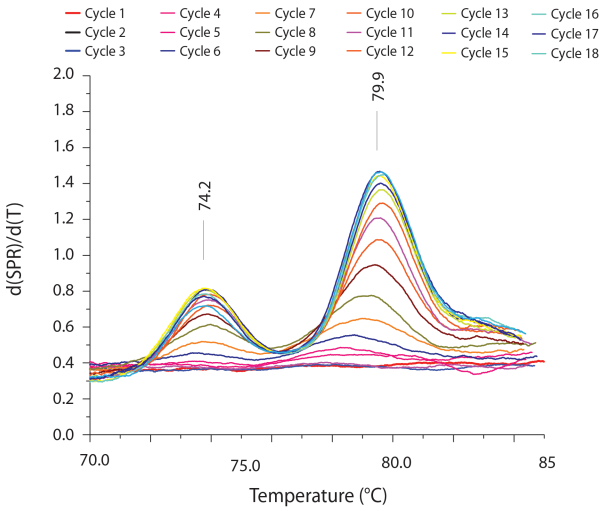

Figure 7.6: First order derivative of the FO-SPR signal and temperature, which allows resolving the melting point of the two target DNA types amplified with the multiplex PCR. The MAP sequence has a lower melting point, because it is considerably shorter. Both targets can easily be resolved as the signals are separated by 5.7°C. The different lines indicate the individual PCR cycles used to amplify the target DNA. From these curves the DNA quantity could potentially be derived.

7.4.3 FO SPR mutation analysis

Next, the FO-SPR assay was tested for its sensitivity towards SNP mutations when present in the target sequences (Figure 7.7). For this experiment, the FO-SPR PCR assay was used to amplify and analyze 6 different DNA targets. First, the wild type MAP and *M. Bovis* targets were analyzed at a concentration of 10 pM (versus 1 nM in the previous experiment). Both targets resulted in an almost identical T_m values as in Figure 7.6, suggesting that the technology is very robust.

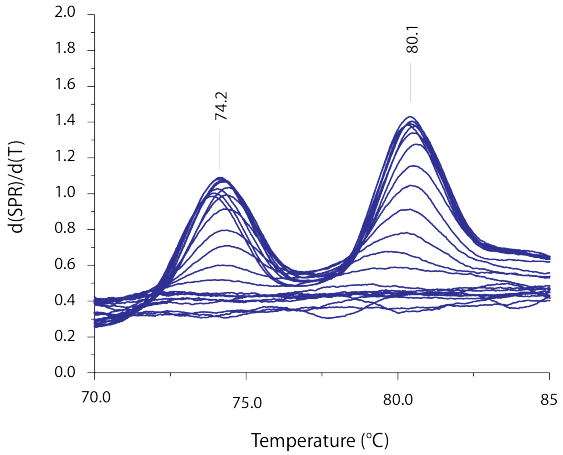

Figure 7.7: FO-SPR PCR analysis of the wild type MAP and *M. Bovis* target sequences at a concentration of 10 pM. Again the different curves represent the signal for each PCR cycle. With increasing numbers of PCR cycles a better melt signal is obtained.

Next, target sequences of MAP and *M. Bovis* bearing a single mutation ($MM1_{MAP}$ and $MM1_{BOV}$) were analyzed at the same concentrations of 10 pM. The mutation in the target sequence was located just outside the priming regions, in order to prevent PCR inhibition or loss of the mutation due to PCR amplification (see Chapter 5). The FO-SPR analysis of MM1 resulted in a clear melting signal with two melting points (Figure 7.8).

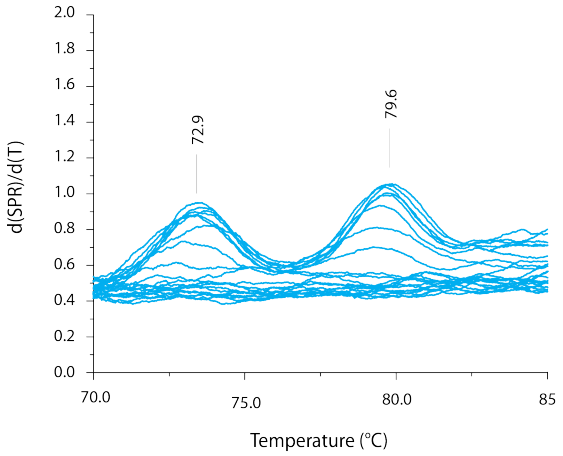

Figure 7.8: FO-SPR PCR melting analysis of MAP and *M. Bovis* sequences bearing a single SNP ($MM1_{MAP}$ and $MM1_{BOV}$).

The presence of a SNP in the *M. Bovis* target changes T_m value only for 0.5°C, while the change for MAP target T_m is 1.3°C. This difference is the result of the target length. Thus, SNP will have a bigger influence on hybridization and consequently melting of a shorter target, i.e. MAP sequence that is 55 bp long compared to M. Bovis, which is 76bp long.

To evaluate whether it is possible to differentiate targets with a single mutation from targets bearing multiple mutations, the FO-SPR PCR assay was applied to analyze both targets with three SNPs ($MM3_{MAP}$ and $MM3_{BOV}$). As can been seen from the results in Figure 7.9, the extra mutations resulted in a larger change of the T_m values for both targets compared to wild type sequences. The Δ T_m for the MAP target increased to 1.5°C and for M. Bovis to 1.0°C. Although these results need a further evaluation they give a first indication of the possibilities of the FO-SPR biosensor to discriminate between targets bearing single and multiple mutations.

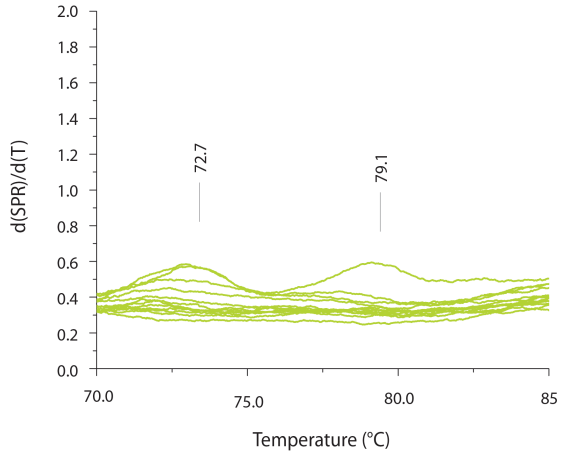

Figure 7.9: FO-SPR PCR melting analysis of MAP and *M. Bovis* sequences bearing triple mutations ($MM3_{MAP}$ and $MM3_{BOV}$).

Furthermore, it can be seen that also melting peak and cycle numbers are affected by the mutations present in the target sequences when the FO-SPR melting peak height is plotted versus the PCR cycle number for both WT and MM targets (Figure 7.10). When this signal for

the WT is compared with targets bearing either single or triple mutations, it is evident that more PCR cycles are needed for both mutated targets to reach the FO-SPR detection limit. Moreover, melting peaks are substantially smaller for both mutated targets in comparison with the melting signal of the WT target. Because mutations were not located in the priming regions and therefore could not influence PCR efficiency, these findings can only be explained by a lower hybridization efficiency of the two hybridization probes on FO-SPR sensor surface and Au NPs. The lower hybridization efficiency results from base pair mismatches between the target DNA with mutations and the immobilized hybridization probes on the FO-SPR biosensor and the gold nanoparticles. As a result the detection limit of the FO-SPR PCR biosensor for target sequences with mutations will always be slightly higher than for the wild type targets.

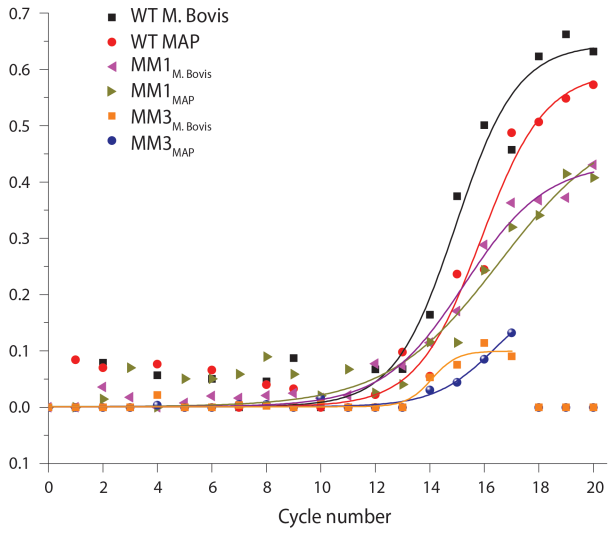

Figure 7.10: Plot of the height of the FO-SPR obtained melting peak versus the PCR cycle numbers. From this graph it can be seen that mismatches in the target sequence shift the cycle threshold to a higher value and that the final yield of the PCR reaction is lower. Full lines represent a sigmoidal fit of the corresponding colored data points.

7.5 Conclusion

In this chapter, it has been demonstrated that the FO-SPR assay is amenable to multiplex target analysis. The FO-SPR bioassay, used for real time monitoring of a multiplex PCR directed at detecting MAP and *M. Bovis* bacterial targets, was able to differentiate these two targets with the same resolution as the singleplex FO-SPR melting assay. This opens the possibility of developing a novel non-fluorescence based platform for quantitative multiplex PCR. Detecting the presence of mutations in the target sequences was possible as both a single SNP and multiple SNPs could be resolved. Shorter sequences were more sensitive to mutations, which is in agreement with the results of Chapter 4. The targets could be identified during thermocycling, which is in qPCR only possible when multiple fluorescence dyes are used. It can thus be concluded that the FO-SPR has some particular features, which could prove useful in POC biosensors such as the detection of multiple bacteria in real-time.

References

1. A. P. Malanoski, B. Lin, Z. Wang, J. M. Schnur and D. A. Stenger, *Nucleic Acids Res.*, 2006, **34**, 5300-5311.
2. C. T. Wittwer, M. G. Herrmann, C. N. Gundry and K. S. Elenitoba-Johnson, *Methods*, 2001, **25**, 430-442.
3. I. M. Mackay, K. E. Arden and A. Nitsche, *Nucleic Acids Res.*, 2002, **30**, 1292-1305.
4. Y. Liao, X. Wang, C. Sha, Z. Xia, Q. Huang and Q. Li, *Nucleic Acids Res.*, 2013, **41**, e76.
5. J. Li, R. Berbeco, R. J. Distel, P. A. Janne, L. Wang and G. M. Makrigiorgos, *Nucleic Acids Res.*, 2007, **35**, e84.
6. J. Pollet, K. P. Janssen, K. Knez and J. Lammertyn, *Small*, 2011, **7**, 1003-1006.
7. S. J. Hurst, A. K. Lytton-Jean and C. A. Mirkin, *Anal. Chem.*, 2006, **78**, 8313-8318.
8. S. V. Ravva and L. H. Stanker, *J. Microbiol. Methods*, 2005, **63**, 305-317.
9. B. A. Pinsky and N. Banaei, *J. Clin. Microbiol.*, 2008, **46**, 2241-2246.
10. L. K. Wolf, Y. Gao and R. M. Georgiadis, *Langmuir*, 2004, **20**, 3357-3361.
11. R. Jin, G. Wu, Z. Li, C. A. Mirkin and G. C. Schatz, *J. Am. Chem. Soc.*, 2003, **125**, 1643-1654.

Chapter 8

General conclusion and perspectives

8.1 General conclusions

In the last decade, a considerable amount of money and resources has been allocated to the development of the next generation detection methods for micro-organisms[1]. Despite these efforts, only a small number of new diagnostic assays have reached the market[2], often without being able to meet all the expectations and needs in medical diagnostics, industrial and environmental monitoring. As a result, technologies based on actual culturing of microorganisms or other time consuming and expensive laboratory tests have remained the gold standard[3]. Because of this, a pragmatic approach continues to be the preferred method of choice, where drastic, non-specific measures are practiced -such as use of broad-spectrum anti-bacterial agents- whenever the presence of micro-organisms is suspected[4,5]. This has resulted in antibiotic misuse over years and created a global problem of increased resistance in bacteria that can hardly be treated with any of the existing antibiotics. Therefore, the development of new diagnostic tests, which can rapidly and accurately identify patients truly needing antibiotics, is essential for changing the daily clinicians' practice from

groundless decision making to those being rational towards adequate use of antibiotics.

One of the problems in the development of applicable diagnostic tools in the field of micro-organism detection is that many new assays are built on very complex laboratory techniques such as mass spectroscopy[6] and sequencing technology[7]. Although these high-end technologies give us valuable new insights in the virulence, spread and biomarkers of micro-organisms, they are not the answer to the current diagnostic needs. The exact requirements for microbiological diagnostics are simple, fast, sensitive, selective and versatile assays that are portable and robust[8].

New developments in nanotechnology and molecular biology point towards new opportunities for development of desired diagnostics, as was extensively reviewed in **Chapter 2**. In general, the improvements in SNP detection have been achieved with technological advances in three domains, being an improved mutation discrimination, a better limit of detection and greater multiplexing capabilities. To achieve these improvements various strategies have been applied of which introduction of secondary structures in hybridization probes, enzymatic cascades and thermal denaturing have great potential in fast mutation detection. From this overview it can be concluded that the current limitations of diagnostics will not be resolved by implementing one of these new technologies, but by selecting the ideal combination of available technologies.

Therefore, this dissertation was devoted to the development of assays for detection of micro-organisms that could answer some of these unmet needs and thus become suited for integration in POC tests. More specifically, the assays were developed on an FO-SPR biosensor platform that was established in the biosensor group. This platform has several unique advantages that make it a very attractive technology for the next generation of microbiological diagnostics tests. First, SPR based transducers allow real-time monitoring of the assay flow with a high measurement sensitivity. Second, introducing the FO sensor tip into samples is simple and resembles a concept of one of the most straightforward diagnostic tools available to date: a ‘dipstick’ test. Third, due to the optical fibers, this platform offers a great cost advantage over

commercial SPR devices. Therefore, implementing improved bioassays for detecting micro-organisms on such platform could result in a diagnostic tool applicable even in resource limited environments.

In times when demands for sensitivity and specificity of biosensors are greater than ever, turning to multivalent bioreceptors is frequently becoming a strategy for improving the bioassay performance. This trend has also been witnessed by replacing bacteriophage affinity peptides with the entire phage as a receptor, despite scarce knowledge on the binding kinetics of complete phage particles. In **Chapter 3**, the FO-SPR sensor was used to study the affinity and binding kinetics of phages, displaying peptide libraries with affinity for eGFP. The eGFP was immobilized on the FO-SPR biosensor surface as a target protein of the viral particles, which allowed real-time monitoring of their interaction. Although the bioassay based on the detection of the entire viruses showed limited sensitivity, it proved to be a valuable tool for comparing binding kinetics of different viral particles, which expressed affinity peptides in different densities on the surface.

With a need for both detecting and identifying pathogens within the same POC test, a universal bioassay can be created by using the genetic material of micro-organisms[9]. However, the sensitivity of SPR towards DNA is poor, as this molecule has a limited impact on refractive index. Therefore, in **Chapter 4,** a new approach was described for improving the SPR sensitivity in DNA based bioassays. Here, thermal denaturation of DNA complexes was measured on the FO-SPR biosensor. These DNA complexes were formed between the target DNA and two probes, each complementary to one half of the target molecule and immobilized either on the Au NPs or the sensor surface. Application of Au NP labels resulted in a clear signal, which superimposed the SPR signal caused by temperature changes during DNA melting analysis. From the obtained melting curves, presence of SNPs was resolved in DNA targets with variable size (30, 56 and 80 bp long sequences) and for some of the used targets even further insight into the position of these SNPs was obtained.

This assay was further challenged in **Chapter 5** by directly screening PCR amplified DNA for mutations. The test case was built on the measurement of genetic variability in two genes of *L. pneumophila,*

which is a common human pathogen responsible for atypical pneumonia. Although the two selected genes are frequently used for the quantification of this bacteria, one of them is well documented as highly variable and therefore prone to introducing amplification bias in PCR based molecular diagnostic tests. Two different assays, being sequencing and qPCR DNA melting assay, were used in parallel with the FO-SPR DNA melting assay to determine the genetic variability in the bacterial qPCR priming regions. This cross platform comparison allowed assessing true POC potential of the FO-SPR bioassay. The sensor proved to be reliable for detecting mutations in those samples that previously displayed ambiguous qPCR quantification results. Moreover, it showed advantages as a high resolution and fast genetic screening tool that can compete with the current standard techniques for SNP detection. Additionally, this research identified a genetic region of *L. pneumophila* that should be avoided when selecting PCR primers for bacteria quantification.

In **Chapter 6,** the possibilities of the FO-SPR DNA biosensor were further explored. Here a quantification method was introduced for allowing not only identification of micro-organisms, but also their quantification. At the same time efforts were made to safeguard the assay sensitivity, as the quantification method required a shorter FO-SPR DNA melting assay time. Careful optimization of buffer and thermal ramping speed resulted in a level of SNP sensitivity similar to the FO-SPR melt assay described in Chapters 4 and 5. The new FO-SPR assay was able to monitor in real-time the quantitative ligation assay. The gradual increase in signal over multiple DNA ligation cycles was used to determine DNA concentrations over 7 orders of magnitude with a detection limit of 100 fM. Even more importantly, the obtained melting signal during each cycle of the ligation was accurate enough to discriminate a SNP in the amplified target molecule. Such resolution in melting assays has been demonstrated until now only when using a post amplification reaction HRM analysis.

In **Chapter 7,** two related bacteria, *Mycobacterium bovis* (*M. Bovis*) and *Mycobacterium avium* subspecies *paratuberculosis* (MAP) were detected simultanously using the FO-SPR biosensor. The FO-SPR sensor tip and the Au NP labels were therefore functionalized with two different sets of hybridization probes, each targeting a region of interest

in a different bacterial species. First experiments were done to evaluate if these alterations on the FO-SPR sensor DNA density had any significant effects on the performance of the FO-SPR biosensor. Next a multiplex assay was used, to improve the sensitivity of this assay by amplifying the target DNA. This also allowed FO-SPR to monitor in real-time the PCR reaction, which makes this multiplex FO-SPR also a quantitative assay. The assay was able to resolve presence of one or both bacteria and could even detect mutations in the target sequences.

8.2 Future research and perspectives

In this dissertation, the potential of FO-SPR as a biosensor for detection of micro-organisms was demonstrated. Nonetheless, several challenges remain before this technology finds its way to end–users. These will be addressed in the following sections.

8.2.1 Multiplexing

A useful biosensor for micro-organism detection should be capable of detecting simultaneously multiple pathogens or even multiple phenotypes within each pathogen. Therefore, the capacity of the FO-SPR biosensor as described in this thesis is insufficient and should be improved. However, SPR cannot be simply multiplexed by, for instance, using a different secondary label. In general, SPR is multiplexed using two different approaches. Most commercial SPR devices divide an SPR sensing surface in different regions, which are individually functionalized and addressed by using a complex microfluidic system. In this way, the SPR system can be multiplexed from 4 up to 20 channels in the high end products. A second approach, known as SPR imaging (SPRi), uses an entirely different SPR readout in order to enable multiplexing. As can be recalled from Section 1.4 of Chapter 1, a standard Kretchmann SPR configuration uses a goniometer with a diode array detector to determine the angle of the incident light at which the SPR signal is excited. In SPRi, a charge coupled device (CCD) is used to monitor the same effect on an array of 96 SPR sensitive spots at once. The only downside of this technology is that biomolecules need to be immobilized on the surface using a microspotter, which is time consuming and costly[10].

However, none of these approaches is applicable for the FO-SPR system. Introduction of microfluidics would compromise the simplicity of the dipstick sensor concept, while spotting would be technically challenging as a result of the fiber geometry. Thus, the creation of a multichannel FO-SPR sensor has to be approached differently. In one approach, two SPR sensitive zones are created on one sensor by depositing different metal layers or those of different thicknesses on the respective SPR sensitive regions, which will have an SPR adsorption band at different wavelengths. Depositing an SPR sensitive zone using another metal such as for example silver can shift the SPR dip to lower wavelengths[11] while a thicker gold layer will shift the SPR dip towards higher wavelengths[12] (Figure 8.1A). In practice this configuration results in two serially connected SPR sensors, which can be excited with a single light beam. The SPR signal has to have a clear wavelength division resulting in a multichannel FO-SPR biosensor that can detect simultaneously multiple analytes. From Section 1.4 of Chapter 1, it can be recalled that when a different SPR metal is used, light with the same angle of incidence can excite a surface plasmon wave (SPW) while with a different metal thickness, a different angle of incidence is needed to excite an SPW.

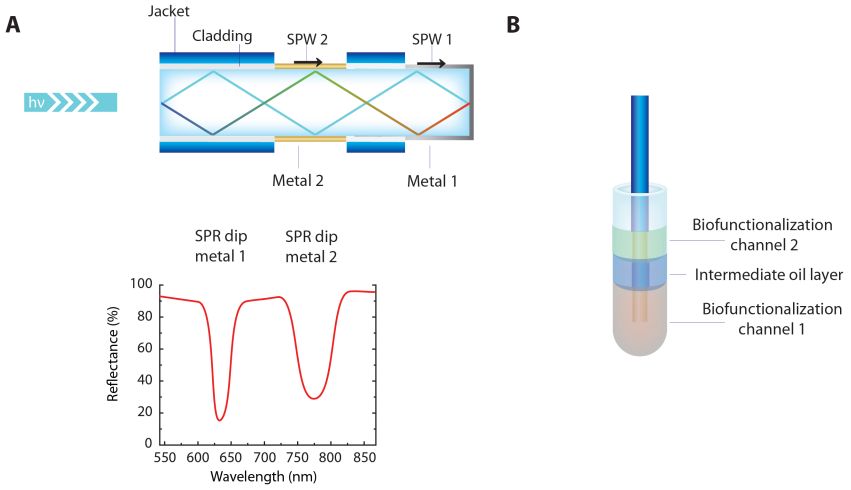

Figure 8.1: A) Schematic overview of the multichannel FO-SPR sensing concept, where coupling of the light with two different metals (metal 1 and metal 2) results in excitation of two SPR signals at different wavelengths. The expected sensor signal, is shown below. B) Biofunctionalization approach of the dual channel FO-SPR sensor to immobilize unique biomolecules on each channel.

The choice of the most appropriate metal and deposition layer thickness can be facilitated using mathematical models to theoretically determine the exact position of the SPR dip for each metal[11]. To allow comparison of measurements performed on different channels of the FO-SPR biosensors, sensitivity of the channels towards refractive index (RI) shifts should be similar. This can be achieved by including RI sensitivity in the mathematical modeling. When appropriate SPR applicable metals are applied, signals of multiple measurement channels can easily be differentiated using a normal visible light spectrometer (Figure 8.1, part A). The different metal layers can be deposited by using a mask to first cover sensing zone 2, while metal 1 is deposited and visa versa for the second metal. Functionalization of each channel with different biomolecules can be done without complex technologies by simply using an intermediary oil layer to separate the two solutions with different biomolecules (Figure 8.1, part B).

However, resolving each measurement accurately when using more than two channels would be challenging with this approach. Therefore, to further extend the number of measurement channels, multiple optical fiber sensors can be assembled in one connector, creating what is known in optics as a fiber bundle. Fiber bundles are widely used for bioanalytical purposes.[13]. The FO-SPR bundles would be simply a combination of different FO-SPR sensors in one optical connector, which is illuminated by a single light source and imaged by a single CCD (Figure 8.2). To resolve the SPR signal from the reflected light, the polychromatic light beam has to be split into the constituent wavelength components. This can be achieved with a grating. This step happens in the current FO-SPR device in the spectrophotometer, which also contains a CCD. Therefore in this new configuration each FO-SPR measurement channel would have, in comparison with the current FO-SPR configuration, a much smaller detector for the same reflected signal, which would result in a lower sensitivity. Another possible problem in this configuration could be that molecular diffusion would be limited by the close packing of FO-SPR sensors in one well. To exclude these effects of diffusion limitation and capillarity, the fiber bundles should contain a limited number of fibers, with 2-5 fibers in a standard PCR tube having a diameter of 6.4 mm.

Fibers could be manufactured and functionalized as described in this dissertation before being assembled in the fiber bundle. However, the bifurcated fiber, which is used in the current FO-SPR design to guide light from the light source to the FO-SPR sensor and back to the spectrophotometer, would become redundant when using the fiber bundle. This would allow further miniaturization of the entire FO-SPR biosensor and even more importantly would considerably shorten the light path, potentially eliminating loss in signal, which requires use of a powerful light source in the current FO-SPR setup. Combination of both multiplexing options would increase the number of measurement channels from two in the current FO-SPR biosensor to twenty individual measurement channels.

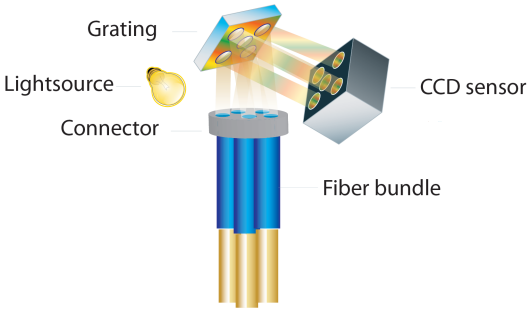

Figure 8.2: Fiber bundle concept to increase the number of measuring channels available on the FO-SPR biosensor.

8.2.2 Improving FO-SPR bioassay throughput and sensitivity

The longest DNA strands analyzed on the FO-SPR biosensor in this thesis had a length of 80bp. Increasing the length of targets would be of great interest for improving the throughput of the FO-SPR assay. However, the SPR sensitivity decays exponentially with increasing distance from the surface[14] (one third the wavelength of excitation as described in Section 1.4, Chapter 1). Therefore, targets exceeding 80bp cannot be analyzed with the same sensitivity as shorter targets. Excitation of long-range surface plasmon waves, allows extending the penetration depth of the SPR signal up to a few micrometers[15]. As can be seen in Figure 8.3, Long-range Surface Plasmon (LRSP) waves are typically first excited along a thin gold layer, by embedding it between

media with a similar refractive index (RI)[16]. This results in excitation of plasma waves on opposite sides of the thin metal, that are coupled and lead to an enhancement of the penetration depth of the surface plasmon wave (SPW). For biosensing implementations, this would require a material with a refractive index close to the sensing medium (typically 1.33), which has to be deposited underneath the gold layer. The polymer Teflon AF (Dupont, Wilmington, Delaware, U.S.) is a good candidate because of its refractive index of approximately 1.31 resembling many biologic buffering solutions. Using this approach, several groups were able to reach a sensitivity and resolution similar or even better than the best known commercial SPR devices[17].

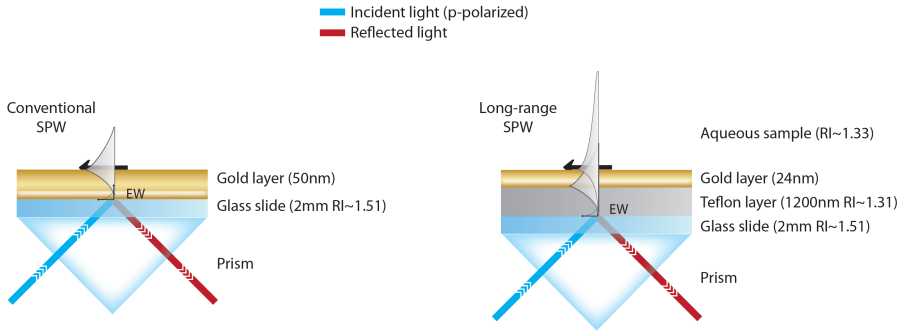

Figure 8.3: Comparison between conventional SPR and long range (LR) SPR, where the LR SPR penetrates the sample at a greater depth by introducing an intermediary Teflon layer (SPW: surface plasmon wave, EW: evanescent wave, RI: Refractive index)

Better sensitivity towards longer DNA target strands is also possible by increasing the density of Au NP labels per strand. This can be achieved by using shorter hybridization probes immobilized on the Au NP surface. Not only will this result in an improved sensitivity for the target strand, but it will also allow increasing mutation discrimination capabilities. As was discussed in Section 2.1 of Chapter 2, shorter hybridization probes are more sensitive towards mutations. However the organization of the Au NP labels when hybridized on the target DNA has to be carefully studied, such that Au NP labels will not influence the hybridization yield due to steric hindrance. Furthermore, location awareness can be obtained by choosing oligonucleotides of different length with distinctive melting temperatures, enabling to trace back the mutation by looking at T_m shifts of particular hybridization probes.

Another option to increase the sensitivity of the FO-SPR is an extensive optimization of the ionic components in the reaction buffer. The ionic concentration is crucial in any FO-SPR assay, because of the dependence of Au NP stability, enzyme performance and hybridization rate. Previous research reports already have shown that a thorough optimization of these components can result in a considerable increase in assay sensitivity[18]. Here a comparison was made between monovalent (NaCl) and divalent ($MgCl_2$) salts as components in hybridization buffers. The divalent salts consistently give a higher hybridization yields as a result of a better shielding of the negative charges of the DNA target molecule during hybridization on the negatively charged DNA coated surface, which also can be found on the FO-SPR sensor. This results in a better mutation discrimination and in a better stabilization of long DNA duplexes (>80bp) on the surface.

Finally, some types of mutations such as base pair neutral mutations, where a nucleotide is replaced with its complementary base and thus the G/C content remains the same, will result in only a very small shift in thermodynamic stability of the duplex[19]. To improve the mutation detection capabilities of the FO-SPR assay in these situations, short oligonucleotides that have a considerable influence on the T_m of the reaction products can be used. These oligonucleotide labels are known as temperature tags. In Chapter 2, an assay developed by Liao et al. used such to improve the multiplexing capacity of a DNA melting assay considerably[20]. In a similar fashion these tags could also be implemented on the FO-SPR melting assay. The temperature tags can be ligated on the target sequence when containing a particular mutation. Because the T_m tag will shift the melting temperature of the target-T_m tag complex to slightly higher or lower temperatures, closely related mutations can be more easily resolved (Figure 8.4).

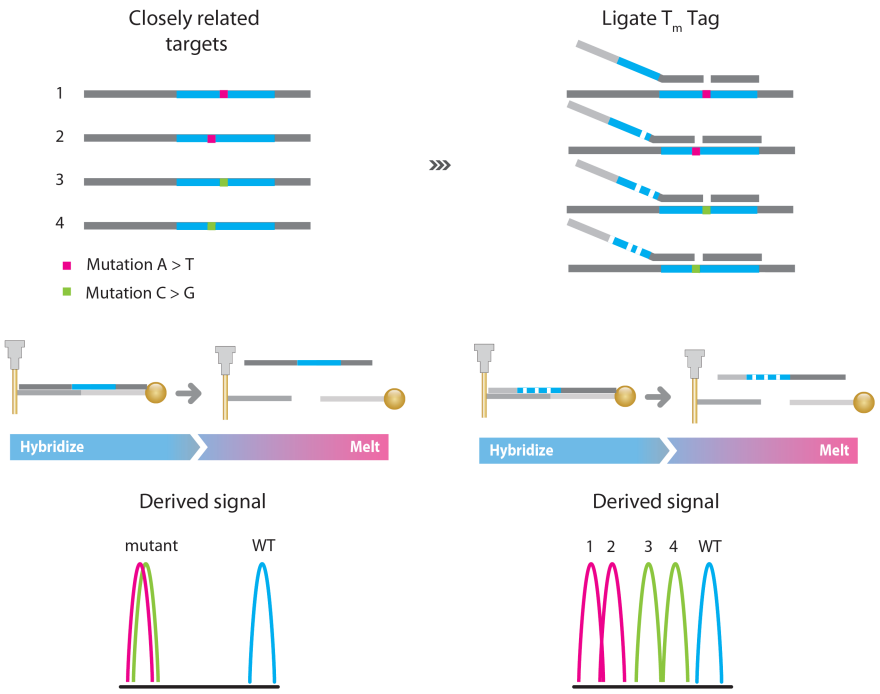

Figure 8.4: Improved FO-SPR DNA sensing of closely related targets with mutations that are normally very difficult to discriminate using DNA melting, but resolved much easier when using T_m tags.

The sensitivity of the FO-SPR assay can also be influenced by non-specific interactions of DNA probes, as is proven in Section 6.4.4 of Chapter 6. Here the detection limit of the ligation assay was limited by the generation of a non-specific signal due to probe interactions in absence of the target strands. Therefore, careful design of hybridization probes used in FO-SPR DNA assays and selection of target sequences could substantially improve the assay performance. In recent years, considerable efforts have been made to develop algorithms capable of screening primer sequences to be combined in PCR[21,22]. Although these large-scale primer design tools have been developed for sequencing, they could be adopted for FO-SPR probe design. Better probe design would also exclude sequences prone to secondary structures formation, as they are known to slow down surface hybridization[23]. However, as mentioned in Chapter 2, some secondary structures, such as a hairpins found in molecular beacons, are favorable for hybridization specificity and can even improve hybridization efficiency on secondary structure

containing targets[24]. Therefore the design of an algorithm both capable of eliminating non-specific interactions and unwanted secondary structures but at the same time allowing integration of desirable secondary structures, could further improve the robustness and performance of the FO-SPR.

8.2.3 Integration of FO-SPR in POC test

Current POC platforms for micro-organisms struggle mostly with a cost-benefit imbalance, especially for resource limited countries[25,26]. One of the main drivers in cost reduction is production scale. Consequently, dedicated instruments are very expensive as they are produced in relatively small numbers[27]. On the other hand, when using standard consumer electronic devices (CED) as a base for new POC biosensors, this problem could be overcome, which has been already proven by the development of several such functional platforms[28,29]. Additionally, these compact POC biosensors can thrive from the extensive features and continuously increasing capabilities of CEDs.

One of the most promising CED biosensor platforms is a smartphone, as this device has the most extensive number of features among all available CEDs[30]. Owing to these features, it was possible to implement complex analytical devices such as fluorescence microscopy on a smartphone[31]. In a similar engineering effort, Preechaburana *et al.* tried to integrate angle resolved SPR on a smartphone[32]. They designed a disposable optical coupling device, which could be attached to the smartphone screen and camera (Figure 8.5, part A). This optic coupler guided light from the smartphone screen to a gold sensor surface where an SPR signal was generated. Reflected light passed then through the optical coupler and was transported to the camera of the smartphone where the SPR adsorption angle was monitored (Figure 8.5, part B). The researchers noticed that existing smartphone components (such as light source and camera) are well suited for SPR and as a result require fewer adaptations than for fluorescence measurements. The created SPR biosensor reached a sensitivity of $11x10^{-3}$ refractive index units per degree change in angle (RIU/°), which was approximately 4 orders of magnitude lower than the best performing commercial devices. However, this sensitivity sufficed to perform an antibody based bioassay for the protein β_2-microglobulin, which is an unspecific

predictive biomarker used for evaluating disease state and progression in several pathologies such as cancer (lymphoma), inflammation and kidney disease, with a detection limit that is sufficient to discriminate a state of disease (0.1 µg/mL). Further improvements of the smartphone SPR implementation, by using the complete resolution capabilities of the standard smartphone Video Graphics Array camera, better known as VGA with a resolution of 640 pixels, would allow in theory to reach a sensitivity of 2.96×10^{-7} RIU/°, which approximates a table top SPR device[17]. A similar adaptation could be manufactured for the FO-SPR device with the most challenging part being the integration of a heating element for performing the melting analysis.

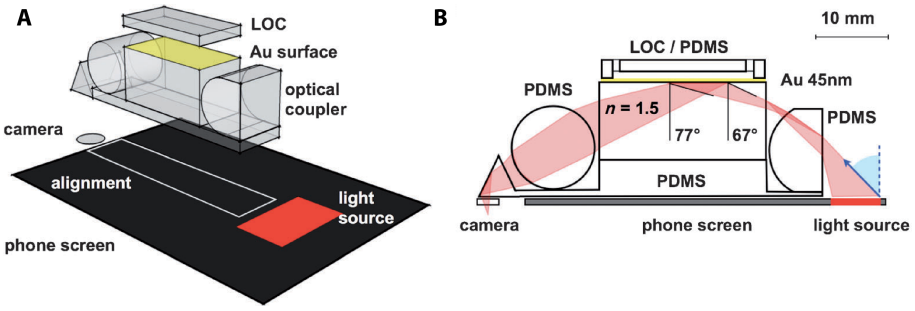

Figure 8.5: A) Smartphone implementation of angle-resolved SPR where the smartphone screen is used for illumination and the front camera as a detector optically coupled by disposable device with integrated lab on a chip (LOC) for sample handling. b) 2D drawing of the experimental arrangement showing the light path from screen to camera (from Preechaburana *et al.*[32])

In conclusion, numerous options are available to both improve the FO-SPR hardware and the implemented DNA melting assay. As a result, the FO-SPR DNA melting assay has great potential to become a valuable POC biosensor that combines a simple assay format with good specificity and sensitivity at an affordable price.

References

1. D. Mabey, R. W. Peeling, A. Ustianowski and M. D. Perkins, *Nat. Rev. Micro.*, 2004, **2**, 231-240.
2. R. S. Wallis, M. Pai, D. Menzies, T. M. Doherty, G. Walzl, M. D. Perkins and A. Zumla, *Lancet*, 2010, **375**, 1920-1937.
3. A. Niemz, T. M. Ferguson and D. S. Boyle, *Trends Biotechnol.*, 2011, **29**, 240-250.
4. F. Aarestrup, *Nature*, 2012, **486**, 465-466.
5. M. Blaser, *Nature*, 2011, **476**, 393-394.
6. S. Sauer and M. Kliem, *Nat. Rev. Microbiol.*, 2010, **8**, 74-82.
7. N. J. Loman*, et al.*, *Nat. Rev. Microbiol.*, 2012, **10**, 599-606.
8. D. A. Giljohann and C. A. Mirkin, *Nature*, 2009, **462**, 461-464.
9. H. J. Chung, C. M. Castro, H. Im, H. Lee and R. Weissleder, *Nat. Nanotechnol.*, 2013, **8**, 369-375.
10. G. J. Wegner, A. W. Wark, H. J. Lee, E. Codner, T. Saeki, S. Fang and R. M. Corn, *Anal. Chem.*, 2004, **76**, 5677-5684.
11. Y. Yuan, L. Wang and J. Huang, *Sens. Actuators, B*, 2012, **161**, 269-273.
12. A. D. Taylor, J. Ladd, Q. Yu, S. Chen, J. Homola and S. Jiang, *Biosens. Bioelectron.*, 2006, **22**, 752-758.
13. D. R. Walt, *Chem. Soc. Rev.*, 2010, **39**, 38-50.
14. M. Vala, S. Etheridge, J. A. Roach and J. Homola, *Sens. Actuators, B*, 2009, **139**, 59-63.
15. M. Vala, R. Robelek, M. Bockova, J. Wegener and J. Homola, *Biosens. Bioelectron.*, 2013, **40**, 417-421.
16. K. Matsubara, S. Kawata and S. Minami, *Opt. Lett.*, 1990, **15**, 75-77.
17. J. Homola, *Chem Rev*, 2008, **108**, 462-493.
18. T. Springer, H. Sipova, H. Vaisocherova, J. Stepanek and J. Homola, *Nucleic Acids Res.*, 2010, **38**, 7343-7351.
19. C. N. Gundry*, et al.*, *Nucleic Acids Res.*, 2008, **36**, 3401-3408.
20. Y. Liao, X. Wang, C. Sha, Z. Xia, Q. Huang and Q. Li, *Nucleic Acids Res.*, 2013.
21. S. Weckx, P. De Rijk, C. Van Broeckhoven and J. Del-Favero, *Bioinformatics*, 2005, **21**, 385-387.
22. K. Li*, et al.*, *BMC Bioinformatics*, 2008, **9**, 191.
23. Y. Gao, L. K. Wolf and R. M. Georgiadis, *Nucleic Acids Res.*, 2006, **34**, 3370-3377.
24. D. Y. Zhang, S. X. Chen and P. Yin, *Nat. Chem.*, 2012, **4**, 208-214.

25. C. C. Boehme*, et al.*, *N. Engl. J. Med.*, 2010, **363**, 1005-1015.
26. C. A. Evans, *PLoS Med*, 2011, **8**, e1001064.
27. D. Figeys and D. Pinto, *Anal. Chem.*, 2000, **72**, 330A-335A.
28. S. A. Lange*, et al.*, *Angew. Chem. Int. Ed. Engl.*, 2005, **45**, 270-273.
29. Y. Li, L. M. Ou and H. Z. Yu, *Anal. Chem.*, 2008, **80**, 8216-8223.
30. D. Gallegos*, et al.*, *Lab Chip*, 2013, **13**, 2124-2132.
31. I. Navruz*, et al.*, *Lab Chip*, 2013.
32. P. Preechaburana, M. C. Gonzalez, A. Suska and D. Filippini, *Angew. Chem. Int. Ed. Engl.*, 2012, **51**, 11585-11588.

Publications

1.1 Articles in internationally reviewed academic journals

Knez, K., Spasic, D., Janssen, K., Lammertyn, J. (2013), Emerging technologies for hybridization based single nucleotide polymorphism detection. *Analyst.* (in press)

Knez, K., Noppe, W., Geukens, N., Janssen, K., Spasic, D., Heyligen, J., Vriens, K., Thevissen, K., Cammue, B., Petrenko, V., Ulens, C., Deckmyn, H., Lammertyn, J. (2013). Affinity comparison of p3 and p8 peptide displaying bacteriophages using surface plasmon resonance. *Analytical Chemistry.* (in press)

Knez, K., Janssen, K., Spasic, D., Declerck, P., Vanysacker, L., Denis, C., Tran, T., Lammertyn, J. (2013). Spherical Nucleic Acid enhanced FO-SPR DNA melting for detection of mutations in Legionella pneumophila. *Analytical Chemistry,* 85 (3), 1734-1742.

Knez, K., Janssen, K., Pollet, J., Spasic, D., Lammertyn, J. (2012). Fiber optic high-resolution genetic screening using gold-labeled gene probes. *Small, 8* (6), 868-872.

Tran, T.*, **Knez, K.*,** Janssen, K., Pollet, J., Spasic, D., Lammertyn, J. (2013) Selection of aptamers against Ara h 1 protein for FO-SPR biosensing of peanut allergens in food matrices (* Tran T. and Knez K. are joint first author). *Biosensors & Bioelectronics, 43*, 245-251.

Janssen, K., **Knez, K.,** Spasic, D., Lammertyn, J. (2013). Nucleic acids for ultra-sensitive protein detection. *Sensors, 13*, 898-930.

Ceyssens, F., Witters, D., Van Grimbergen, T., **Knez, K.,** Lammertyn, J., Puers, B. (2013). Integrating optical waveguides in electrowetting-on-dielectric digital microfluidic chips. *Sensors and Actuators B, Chemical, 181*, 166-171.

Witters, D., **Knez, K.,** Ceyssens, F., Puers, B., Lammertyn, J. (2013). Digital microfluidics-enabled single-molecule detection by printing and sealing single magnetic beads in femtoliter droplets. *Lab on a Chip, 13* (11), 2047-2054.

Janssen, **K., Knez,** K., Spasic, D., Schrooten, J., Lammertyn, J. (2012). Multiplexed protein detection using an affinity aptamer amplification assay. *Analytical and Bioanalytical Chemistry, 404* (6-7), 2073-2081.

Delport, F., Pollet, J., Janssen, K., Verbruggen, B., **Knez, K.,** Spasic, D., Lammertyn, J. (2012). Real-time monitoring of DNA hybridization and melting processes using a fiber optic sensor. *Nanotechnology, 23* (6), 065503.

Janssen, K., **Knez, K.,** Vanysacker, L., Schrooten, J., Spasic, D., Lammertyn, J. (2012). Enabling fiber optic serotyping of pathogenic bacteria through improved anti-fouling functional surfaces. *Nanotechnology, 23* (23), art.nr.NANO/425045/PAP.

Janssen, K., **Knez, K.,** Pollet, J., Roberts, S., Schrooten, J., Lammertyn, J. (2011). Assay design considerations for use of affinity aptamer amplification in ultra-sensitive protein assays using capillary electrophoresis. *Analytical methods, 3*, 2156-2159.

Pollet, J., Janssen, K., **Knez, K.,** Lammertyn, J. (2011). Real-Time Monitoring of Solid-Phase PCR Using Fiber-Optic SPR. *Small, 7* (8), 1003-1006.

1.2 Papers at international scientific conferences and symposia, published in full in proceedings

Witters, D., **Knez, K.,** Janssen, K., Verbruggen, B., Puers, B., Lammertyn, J. (2012). High-Throughput Patterning of Single Magnetic Beads Using

Digital Microfluidic Technology. . MicroTAS 2012. Okinawa, Japan, 28 October-1 November 2012.

Vermeir, S., Witters, D., Vergauwe, N., **Knez, K.,** Gijs, M., Puers, B., Lammertyn, J. (2012). Ferromagnetic particles for an improved heterogeneous bioassay performance on a digital lab-on-a-chip. . Microtas2012. Okinawa, Japan, 28 October-1 November, 2012.

1.3 Meeting abstracts, presented at international scientific conferences and symposia, published or not published in proceedings or journals

Knez, K., Janssen, K., Spasic, D., Lammertyn, J. (2012). Real-time monitoring of solid-phase PCR and point mutation screening using fiber optic biosensor. Biosensors. Cancún, 15-18 may 2012, Abstract No. BIOS2012_054.

Arghir, I., **Knez, K.,** Janssen, K., Pollet, J., Lammertyn, J., Spasic, D. (2012). Nanostructuring Optical Surfaces towards FO–SPR Biosensors with Improved Performances. International Conference on Scientific and Clinical Applications of Magnetic Carriers. Minneapolis, MN, USA, 22-26 May 2012.

Pollet, J., **Knez, K.,** Janssen, K., Spasic, D., Lammertyn, J. (2012). Fiber optic SPR assay for enhanced real-time PCR analysis of non-transparent samples. ACS National Meeting. San Diego, March 25-29, 2012.

Janssen, K., Pollet, J., **Knez, K.,** Lammertyn, J. (2011). Real-Time Monitoring of Solid Phase PCR using Fiber-Optic SPR. International Conference on Bio-Sensing Technology 2011. Amsterdam, 10-12 October 2011, Abstract No. 0056.

Knez, K., Janssen, K., Pollet, J., Tran, T., Delport, F., Lammertyn, J. (2011). Improving solid phase PCR on gold surfaces by means of alkanethiol backfilling. Hybrid Materials 2011. Straßburg, 6-10 March 2011.

Delport, F., **Knez, K.,** Tran, T., Janssen, K., Pollet, J., Sels, B., Hofkens, J., Lammertyn, J. (2011). Binding Strategies to carboxyl nanoparticles for

high performance DNA hybridization bio-assays. Multifunctional, Hybrid and Nanomaterials. Strasbourg, 6-10 March 2011.